



**REACTIVITY ASSESSMENT  
AND SUBAQUEOUS OXIDATION  
RATE MODELLING FOR  
LOUVICOURT TAILINGS**

**MEND Project 2.12.1d**

**This work was done on behalf of MEND and sponsored by Aur Resources Inc.,  
Noranda Inc.,  
Teck Corporation, and  
le Ministère des Ressources naturelles du Québec and  
the Canada Centre for Mineral and Energy Technology (CANMET) through the CANADA/  
Québec Mineral Development Agreement**

**March 2001**

*Final Report*

---

**REACTIVITY ASSESSMENT  
AND SUBAQUEOUS  
OXIDATION RATE MODELLING  
FOR LOUVICOURT TAILINGS**

---

Submitted to

Aur Resources  
Noranda Inc.  
Teck Corporation  
MEND2000

by

M. Li and L. St-Arnaud  
Noranda Inc., Technology Centre  
Pointe-Claire, Québec

December 2000



## EXECUTIVE SUMMARY

This report documents the results of the NTC part of a MEND-coordinated, multi-participant research project. The project was designed to evaluate the effectiveness of shallow water covers in the prevention of acid mine drainage from reactive sulphidic tailings, using Louvicourt Mine as the experimental site. Laboratory tests conducted on Louvicourt tailings were used to derive the intrinsic oxidation rate necessary for perform mathematical modelling of submerged tailings oxidation.

In this study, various Louvicourt tailings samples were characterized for grain size distribution, quantitative mineralogy, geochemical whole-rock composition, and extended acid-base accounting (ABA). Flow-through cell leach tests were used to investigate the influences of four parameters on metal releases by tailings under simulated submergence. Eight humidity cells containing duplicates of four samples were tested for eighty weeks to determine the rates of sulphide oxidation and acid neutralization. Pre- and post-humidity cell analyses were performed to complete geochemical and mineralogical mass balances and to validate the humidity cell data interpretation. Data generated from these laboratory tests were used to predict field acid generation for a hypothetical field exposure. Mathematical modelling was used to evaluate the effects of four oxygen transport mechanisms on the degree of subaqueous sulphide oxidation.

ABA results indicate that the tailings are potentially net acid-generating. A four-month in-plant monitoring campaign conducted in 1994-1995 showed a variation of sulphide content from 11 to 49%. The sulphides in the tailings are dominated by pyrite, with minor or trace pyrrotite, sphalerite, and chalcopyrite. Carbonate mineral contents in the samples varied from nearly nil to as high as 24%. The main carbonate minerals are ankerite and siderite, both containing varying amounts of magnesium and manganese. The main silicate neutralising mineral is clinocllore.

Flow-through cell leach experiments with different leachant solutions using the Taguchi design approach suggest the following influence on metal releases: leachant  $\text{Fe}^{2+}$  concentration (strong) > leachant DO level (strong) > leachant pH (medium) > hydraulic gradient (weak). Presence of  $\text{Fe}^{2+}$  in the inflow increases metal releases likely through a one-time ion exchange process. High DO in the inflow promotes Zn releases through oxidation of sulphides whereas low DO facilitates the release of Mn. Lower pH favours

metal releases probably because of higher solubility of hydroxides and carbonates of most metals. The tailings were found to contain sufficient buffering capacity to maintain the pore water pH nearly neutral. Mechanisms controlling metal releases include solubility control and dissolution rate control. Overall metal releases are low throughout the experiments except during the initial flush-out of accumulated soluble constituents.

The humidity cell results show that the Louvicourt tailings have relatively high oxidative reactivity. The oxidation rate of the eight tests ranged 864-2143 (average 1449) mg CaCO<sub>3</sub> eq/kg/week, and the NP consumption rate ranged 955-2238 (average 1500) mg CaCO<sub>3</sub> eq/kg/week. All samples are potentially net acid-generating, with predicted humidity cell lag times ranging 0.56-2.5 (average 1.2) years. Predictions based on a hypothetical field exposure of the tailings indicate that, for a typical tailings, the lag time before acid generation is 4.5 years. For a worse-than-average case the lag time reduces to 2.6 years.

Sphalerite oxidation appeared to be accelerated by galvanic effects after the leachate pH dropped below about 3.0. Ankerite seemed to contribute fully to the total available NP. Siderite and clinocllore were less reactive and contributed less to the total available NP. Siderite dissolution seemed to be accelerated after onset of acid generation whereas clinocllore dissolution was relatively unaffected by acidification.

A new technique was employed to calculate the dissolution rates of individual neutralizing minerals and sulphide minerals from weekly leachate volume and chemical data. The validity of this technique appears to be acceptable judging from the independently measured mineralogical mass balances.

Due to the “non-ideality” of the humidity cell tests, not all particles placed in the cells were accessible for oxidation and neutralization reactions. This was probably attributable to the formation of impermeable particle aggregates as a result of cementation and coating. Methods for correcting for the non-ideality were proposed and demonstrated. It was found that, without agitation, on average only about 37% of the sample mass in the humidity cells was available for oxidation and neutralization reactions.

Four basic cases that may occur after reactive tailings are disposed of under a shallow, 0.3-m water cover were mathematically modelled based on typical tailings properties and other site conditions found at the Louvicourt Mine. The four cases are stagnant water cover, fully oxygenated and mixed water cover, fully oxygenated and mixed water



cover with downward infiltration, and tailings resuspension. The stagnant water cover through which oxygen must diffuse across transports the least amount of oxygen to the submerged tailings, with the flux being on the order of  $3 \text{ g O}_2/\text{m}^2 \text{ interface/year}$ . Although this is the most desirable condition, to date field data collected in other studies indicated that it is highly questionable that this condition exists in reality, since winds that are almost always present in the field naturally cause mixing, circulation, wave action, and aeration in shallow water bodies. The three other cases are more realistic scenarios, which increase the oxygen flux into the submerged tailings significantly. Modelling results suggest that, compared with the base case of stagnant water cover, mixing/oxygenation of the water cover and tailings resuspension each is capable of increasing the oxygen flux by one order of magnitude, whereas downward infiltration of fully-aerated water cover can enhance the oxygen flux by a factor of three. The range of oxygen fluxes seen in the modelling results suggest that for most sites, a simple, well-maintained water alone without additional measures is sufficient to suppress oxidation of sulphides in reactive tailings while maintaining the discharge from the water cover during wet seasons in compliance. Nevertheless, for exceptional circumstances where this is not achievable, supplemental measures, such as physical, chemical, and biological barriers/oxygen interceptors, are available to further reduce the oxygen flux and enhance the effectiveness of the water cover.

It is recommended that the findings of this laboratory/modelling study be compared with the results from the field experimental cell study (by INRS-Eau) and the laboratory column study (by Canmet) for consistency and corroboration. Any discrepancies among the three in basic findings should be addressed and ultimately resolved.

Future research opportunities on water covers should be taken advantage of to study factors controlling water cover aeration/mixing and factors controlling resuspension of tailings. The goal of such researches should be to establish the capability of quantitatively predicting the degree of aeration and resuspension in shallow water covers from basic information such as tailings properties, meteorological data, and physiography of the site.

## SOMMAIRE

Le présent rapport décrit les résultats obtenus dans la partie CTN d'un projet de recherche réalisé en collaboration avec plusieurs participants et coordonné par le NEDEM. Le projet a été conçu afin d'évaluer l'efficacité de couvertures aqueuses peu profondes à prévenir le drainage minier acide provenant de résidus sulfurés réactifs. On a utilisé à cette fin la mine Louvicourt comme site expérimental. Des essais en laboratoire sur les résidus de cette mine ont permis de déterminer la vitesse d'oxydation intrinsèque nécessaire pour procéder à une modélisation mathématique de l'oxydation des résidus submergés.

Au cours de la présente étude, divers échantillons de résidus de la mine Louvicourt ont été caractérisés afin d'en déterminer la distribution granulométrique, la composition minéralogique, la composition géochimique de la roche entière, ainsi que des essais statiques de prédiction de génération d'acide (essais ABA). Des essais de lixiviation en continu ont été réalisés pour analyser les effets de quatre paramètres sur le rejet de métaux par les résidus dans des conditions d'immersion simulée. Des essais cinétiques ont été réalisés sur une période de quatre-vingt semaines avec huit cellules d'humidité renfermant quatre échantillons en double, afin de déterminer les vitesses d'oxydation des sulfures et de neutralisation des acides. On a effectué des analyses avant et après passage dans les cellules d'humidité pour déterminer les bilans massiques géochimiques et minéralogiques et pour valider l'interprétation des données obtenues avec les cellules d'humidité. Les données obtenues lors de ces essais en laboratoire ont été utilisées pour prévoir la production acide sur le terrain lors d'une exposition hypothétique *in situ*. On a procédé à une modélisation mathématique pour évaluer les effets de quatre mécanismes de transport de l'oxygène sur le degré d'oxydation subaquatique des sulfures.

Les résultats des essais ABA indiquent que les résidus sont potentiellement des producteurs nets d'acide. Une campagne de surveillance de quatre mois menée en usine en 1994-1995 a mis en évidence une variation de 11 à 49 % de la teneur en sulfures. Les sulfures présents dans les résidus sont constitués principalement de pyrite et de quantités moindres ou de traces de pyrrhotine, de sphalérite et de chalcopyrite. La teneur en carbonates des minéraux dans les échantillons variait de pratiquement 0 % jusqu'à un maximum de 24 %. Les principaux carbonates sont l'ankérite et la sidérite qui, l'un et l'autre, renferment diverses quantités de magnésium et de manganèse. Le principal silicate neutralisant est le clinocllore.

Les essais de lixiviation en continu réalisés avec différentes solutions en appliquant l'approche conceptuelle de Taguchi permettent de supposer l'influence ci-après sur la libération d'espèces métalliques : concentration de  $\text{Fe}^{2+}$  dans la solution de lixiviation (forte) > niveau d'oxygène dissous dans la solution de lixiviation (forte) > pH de la solution de lixiviation (moyenne) > gradient hydraulique (faible). La présence d'ions  $\text{Fe}^{2+}$  dans le flux d'alimentation augmente la quantité de métaux libérés, probablement grâce à un processus unique d'échange d'ions. Une forte teneur en oxygène dissous dans le flux d'alimentation favorise la libération de Zn par l'intermédiaire de l'oxydation des sulfures, alors qu'une faible teneur en oxygène dissous favorise la libération de Mn. Des pH plus faibles favorisent la libération de métaux, probablement en raison de la plus grande solubilité des hydroxydes et des carbonates de la plupart des métaux. On a constaté que les résidus possédaient une capacité tampon suffisante pour maintenir l'eau interstitielle à un pH proche de la neutralité. Parmi les paramètres contrôlant la libération des métaux, on compte la solubilité et la vitesse de dissolution. Dans l'ensemble, la libération de métaux était faible au cours des expériences, sauf pendant le lessivage initial des éléments solubles accumulés.

Les essais réalisés avec les cellules d'humidité indiquent que les résidus de la mine Louvicourt sont relativement très oxydatifs. La vitesse d'oxydation mesurée lors des huit essais variait de 864 à 2143 (moyenne de 1449) mg d'équivalent de  $\text{CaCO}_3/\text{kg}/\text{semaine}$ , tandis que la vitesse de consommation de NP allait de 955 à 2238 (moyenne de 1500) mg d'équivalent de  $\text{CaCO}_3/\text{kg}/\text{semaine}$ . Tous les échantillons sont potentiellement des producteurs nets d'acide, le décalage prévu lors des essais en cellules d'humidité variant de 0,56 à 2,5 (moyenne de 1,2) ans. Les prévisions basées sur une exposition hypothétique des résidus sur le terrain indiquent que, pour des résidus typiques, le décalage précédant la production d'acide est de 4,5 ans. Pour un cas pire que la moyenne, ce décalage serait réduit à 2,6 ans.

L'oxydation de la sphalérite semblait être accélérée par des effets galvaniques après diminution du pH du lixiviat sous une valeur d'environ 3,0. L'ankérite semblait contribuer pleinement au NP total disponible. La sidérite et le clinocllore étaient moins réactifs et contribuaient moins au NP total disponible. La dissolution de la sidérite semblait s'accélérer après le début du processus acidogène, alors que la dissolution du clinocllore était relativement peu touché par le processus d'acidification.

On a utilisé une nouvelle technique pour calculer les vitesses de dissolution de chaque minéral neutralisant et de chaque minéral sulfuré à partir des volumes hebdomadaires de lixiviat et de données chimiques. Cette technique semble être valable, si on se base

sur les bilans massiques minéralogiques mesurés de manière indépendante.

En raison de la « non-idéalité » des essais réalisés en cellules d'humidité, toutes les particules placées dans les cellules n'étaient pas soumises aux processus d'oxydation et de neutralisation, probablement à cause de la formation d'agrégats imperméables de particules résultant de processus de cimentation et d'enrobage. On a proposé et on a fait la démonstration de méthodes permettant de tenir compte de cette « non-idéalité ». On a constaté que, sans agitation, seulement 37 % en moyenne de la masse de l'échantillon présent dans les cellules d'humidité était disponible pour les processus d'oxydation et de neutralisation.

En se basant sur les propriétés typiques des résidus miniers et sur d'autres conditions observées au site de la mine Louvicourt, on a procédé à la modélisation mathématique des quatre scénarios de base qui peuvent se présenter après la déposition des résidus réactifs sous une couverture aqueuse de 0,3 m. Ces quatre scénarios sont : couverture aqueuse stagnante; couverture aqueuse totalement oxygénée et mélangée; couverture aqueuse totalement oxygénée et mélangée avec infiltration vers le bas; et remise en suspension des résidus. La couverture aqueuse stagnante au travers de laquelle l'oxygène doit diffuser est celle qui transporte la plus faible quantité d'oxygène vers les résidus submergés, la vitesse de diffusion étant de l'ordre de 3 g de  $O_2/m^2$  d'interface/an. Bien que ce scénario corresponde aux conditions les plus souhaitables, les données obtenues jusqu'ici sur le terrain lors d'autres études indiquent qu'il est fort douteux que ces conditions existent réellement, car en situation réelle il y a presque toujours présence de vents qui provoquent le mélange, la circulation, le brassage par les vagues et l'aération des masses d'eau peu profondes. Les trois autres scénarios sont plus réalistes, la vitesse de diffusion de l'oxygène vers les résidus submergés étant alors nettement plus importante. Les résultats de la modélisation permettent de supposer que, comparativement au scénario de base comportant une couverture aqueuse stagnante, le mélange/oxygénation de la couverture aqueuse et la remise en suspension de résidus sont, l'un et l'autre, capables d'accroître la vitesse de diffusion de l'oxygène par un ordre de grandeur, alors que l'infiltration vers le bas de l'eau entièrement aérée peut accroître cette vitesse par un facteur de trois. La gamme de vitesses de diffusion de l'oxygène indiquée par les résultats de la modélisation permet de penser que, sur la plupart des sites, une simple couverture aqueuse bien entretenue, sans aucune autre mesure additionnelle, est suffisante pour éliminer l'oxydation des sulfures dans les résidus réactifs, tout en maintenant la conformité de la décharge à partir de la couverture aqueuse au cours des saisons humides. Néanmoins, en présence de circonstances exceptionnelles où cela n'est pas possible, des mesures supplémentaires, comme des barrières physiques, chimiques ou

biologiques ou des intercepteurs d'oxygène sont disponibles pour réduire encore plus la vitesse de diffusion de l'oxygène et ainsi améliorer l'efficacité de la couverture aqueuse.

On recommande que les résultats de la présente étude en laboratoire et des modélisations soient comparés aux résultats des essais en cellule réalisés sur le terrain (par l'INRS - Eau - MEND 2.12.1c) et aux résultats de l'étude en colonne réalisée en laboratoire (par CANMET - MEND 2.12.1e), afin d'en déterminer la cohérence et de voir s'ils peuvent être corroborés. Toute divergence des résultats de base de ces trois études devrait être étudiée et ultérieurement résolue.

On devrait exploiter les possibilités de recherches futures sur les couvertures aqueuses pour étudier les facteurs qui contrôlent l'aération/le mélange de la couverture aqueuse et la remise en suspension de résidus. Ces recherches devraient avoir comme objectif d'établir la capacité à prévoir quantitativement le degré d'aération et de remise en suspension dans des couvertures aqueuses peu profondes à partir de données de base comme les propriétés des résidus, les données météorologiques et la physiographie du site.

## TABLE OF CONTENTS

EXECUTIVE SUMMARY .....	i
LIST OF TABLES .....	vi
LIST OF FIGURES .....	vii
LIST OF APPENDICES .....	ix
1.0 INTRODUCTION .....	1
1.1 Site Description .....	1
1.2 Project History .....	1
1.3 Project Objectives and Approach .....	2
2.0 CHARACTERISTICS OF LOUVICOURT TAILINGS .....	3
2.1 Samples .....	3
2.2 Grain Size Distribution .....	3
2.3 Mineralogy .....	4
2.4 Whole-Rock Composition .....	5
2.5 Acid-Base Accounting .....	6
2.5.1 B.C. Research Initial and Confirmation Tests .....	6
2.5.2 Extended ABA .....	7
2.6 TCLP Test and Tailings Water Composition .....	10
2.7 In-Plant Monitoring of Tailings Composition Variation .....	10
3.0 FLOW-THROUGH CELL LEACH TESTS .....	12
3.1 Objectives .....	12
3.2 Sample, Test Apparatus, Procedure and Conditions .....	12
3.3 Results .....	14
3.4 Interpretation .....	14
3.4.1 Hydraulic Conductivity .....	14
3.4.2 Phases A and B .....	21
3.4.3 Phases C to I .....	23
3.4.4 Design of Experiment .....	26
3.5 Summary .....	26
4.0 HUMIDITY CELL TESTS .....	28

4.1	Objectives .....	28
4.2	Test Samples, Set-Up, and Procedure .....	28
4.3	Test Results .....	29
4.3.1	Leachate Chemistry .....	29
4.3.2	Post-Humidity Cell Solid Analyses .....	29
4.3.2.1	Post-Humidity Cell Leach .....	29
4.3.2.2	Acid-Base Accounting .....	31
4.3.2.3	Whole-Rock Composition .....	31
4.3.2.4	Mineralogy .....	32
4.4	Interpretation .....	38
4.4.1	Humidity Cells .....	38
4.4.1.1	Assumptions .....	38
4.4.1.2	Principles of Interpretive Calculation .....	39
4.4.1.3	Discussion .....	43
4.4.1.4	Correction of Lag Time Prediction .....	61
4.4.1.5	Hypothetical Predictions for the Field .....	65
4.4.2	Post-Humidity Cell Geochemical and Mineralogical Mass Balances .....	66
4.4.2.1	Acid Base Accounting .....	66
4.4.2.2	Geochemical Whole-Rock Mass Balance .....	68
4.4.2.3	Mineralogical Mass Changes .....	72
4.4.3	Comparisons between Humidity Cell and Post-Humidity Cell Data .....	72
4.5	Summary of Important Findings .....	77
5.0	SUBAQUEOUS TAILINGS OXIDATION RATE MODELLING .....	78
5.1	Stagnant Water Cover .....	79
5.2	Fully-Oxygenated Water Cover .....	83
5.2.1	Specific Surface Area .....	83
5.2.2	Oxidation Rate .....	84
5.2.3	Oxidation under Water Cover .....	85
5.3	Fully-Oxygenated Water Cover with Downward Infiltration .....	90
5.4	Tailings Resuspension .....	95
5.5	Comparison of Cases .....	96
5.6	General Field Implications .....	98
5.7	Summary .....	101
6.0	CONCLUSIONS AND RECOMMENDATIONS .....	103
6.1	Conclusions .....	103
6.2	Recommendations .....	105
7.0	CLOSURE .....	106
8.0	REFERENCES .....	107

## LIST OF TABLES

Table 2.1	Comparison of Modal Mineralogy between Samples L-1 and CRM . . . . .	4
Table 2.2	Mineralogy of Samples LVW-1 through LVW-4 Determined by Canmet . . . . .	5
Table 2.3	Whole-Rock Composition of Louvicourt Tailings Samples . . . . .	7
Table 2.4	Extended ABA Results for LVW Series of Samples . . . . .	9
Table 3.1	Leaching Conditions for Phases A and B . . . . .	14
Table 3.2	Leaching Conditions for Phases C to J . . . . .	14
Table 4.1	Post-Humidity Cell ABA . . . . .	30
Table 4.2	Whole-Rock Composition of Post-Humidity Cell Solids . . . . .	31
Table 4.3	Post-Humidity Cell Mineralogy . . . . .	34
Table 4.4	Summary of Interpretive Calculations of Humidity Cell Test Results . . . . .	42
Table 4.5	Uncorrected and Corrected Lag Time Prediction versus Observed Lag Time . . . . .	64
Table 4.6	Comparison between Mineral Depletions Calculated from Humidity Cell (HC) Test Data and Those Revealed by Mineralogical Mass Balance (mean $\pm$ s, %) . . . . .	75
Table 5.1	Idealized Cases for Subaqueous Tailings Oxidation . . . . .	79
Table 5.2	Comparison of Dissolved Oxygen Consumption for Four Cases . . . . .	97



## LIST OF FIGURES

Figure 2.1	Grain Size Distribution of Louvicourt Flotation Tailings . . . . .	3
Figure 2.2	Variation of Cu, Zn, and Fe Contents in Louvicourt Tailings . . . . .	11
Figure 3.1	Schematic Drawing of Flow-Through Leach Test Apparatus . . . . .	13
Figure 3.2	Correlation between Run Time, Pore Volumes Passed, and Phases . . . . .	15
Figure 3.3	Leaching Results for Phases A and B - $\text{SO}_4^-$ , K, and Na . . . . .	16
Figure 3.4	Leaching Results for Phases A and B - $\text{SO}_4^-$ , Ca, and Mg . . . . .	16
Figure 3.5	Leaching Results for Phases A and B - $\text{SO}_4^-$ , Al, and Mn . . . . .	17
Figure 3.6	Leaching Results for Phases A and B - $\text{SO}_4^-$ , $\text{Fe}^{2+}$ and $\text{Fe(T)}$ . . . . .	17
Figure 3.7	Leaching Results for Phases A and B - $\text{SO}_4^-$ , Cu, Ni, and Zn . . . . .	18
Figure 3.8	Leaching Results for Phases A to I - $\text{SO}_4^-$ , K, and Na . . . . .	18
Figure 3.9	Leaching Results for Phases A to I - $\text{SO}_4^-$ , Ca, and Mg . . . . .	19
Figure 3.10	Leaching Results for Phases A to I - $\text{SO}_4^-$ , Al, and Mn . . . . .	19
Figure 3.11	Leaching Results for Phases A to I - $\text{SO}_4^-$ , $\text{Fe}^{2+}$ and $\text{Fe(T)}$ . . . . .	20
Figure 3.12	Leaching Results for Phases A to I - $\text{SO}_4^-$ , Cu, Ni, and Zn . . . . .	20
Figure 4.1	Pre- and Post-Humidity Cell $\text{CO}_2$ and $\text{S}_\text{T}$ Concentrations . . . . .	33
Figure 4.2	Post-Humidity Cell Mineralogy - Photomicrographs of Sample LVW-1A . . . . .	35
Figure 4.3	Post-Humidity Cell Mineralogy - Photomicrographs of Samples LVW-2A, -3A, and -4A . . . . .	35
Figure 4.4	Charge Balance of Leachate from Humidity Cell Tests . . . . .	43
Figure 4.5	Change of Humidity Cell Leachate pH over Time . . . . .	44
Figure 4.6	Acidity Production, Acidity Neutralization, and Mineral Depletion . . . . .	47
Figure 4.7	NP Depletion/AP Depletion Ratio versus Acidity Production . . . . .	53
Figure 4.8	Total Acidity Production versus Acid Potential . . . . .	56
Figure 4.9	Partition of Total Acidity Production . . . . .	57
Figure 4.10	Time to AMD Onset versus NP . . . . .	58
Figure 4.11	Cumulative AP Depletion with Time . . . . .	59
Figure 4.12	Cumulative NP Depletion with Time . . . . .	60
Figure 4.13	Comparison of Average AP and NP Cumulative Depletion . . . . .	60
Figure 4.14	Paste pH versus $\text{SO}_4$ Content . . . . .	67
Figure 4.15	Post-Humidity Cell Elemental Mass Changes . . . . .	70
Figure 4.16	Post-Humidity Cell Total Mass Changes . . . . .	71
Figure 4.17	Pre- and Post-Humidity Cell $\text{CaO-CO}_2$ . . . . .	71
Figure 4.18	Correlation between Normative Mineralogy and Mineralogy by Direct Methods . . . . .	73
Figure 4.19	Mineral Depletion in Weathered Louvicourt Tailings . . . . .	74
Figure 4.20	Comparison of Mineral Depletions Calculated from Humidity Cell (HC) Leachate Chemistry with Those Revealed by Mineralogical Mass Balance . . . . .	76

Figure 5.1	DO Profiles in Stagnant Water Cover . . . . .	81
Figure 5.2	DO Flux into Tailings from Stagnant Water Cover . . . . .	82
Figure 5.3	DO Mass Transferred into Tailings from Stagnant Water Cover . . . . .	82
Figure 5.4	Tailings Porewater DO Profiles under Fully-Oxygenated Water Cover . . . . .	89
Figure 5.5	DO Flux into Tailings from Fully-Oxygenated Water Cover . . . . .	89
Figure 5.6	DO Mass Transfer into Tailings from Fully-Oxygenated Water Cover . . . . .	90
Figure 5.7	Tailings Porewater DO Profiles under Fully-Oxygenated, Infiltrating Water Cover . . . . .	93
Figure 5.8	DO Flux into Tailings from Fully-Oxygenated, Infiltrating Water Cover . . . . .	93
Figure 5.9	DO Mass Transferred into Tailings from Fully-Oxygenated, Infiltrating Water Cover . . . . .	94
Figure 5.10	Dissolved Oxygen Consumption by Oxidation of Resuspended Tailings . . . . .	96
Figure 5.11	Comparison of Dissolved Oxygen Consumption among Four Cases . . . . .	98

## LIST OF APPENDICES

APPENDIX II-1	ANALYTICAL CERTIFICATES
APPENDIX II-2	MINERALOGY REPORTS
APPENDIX II-3	IN-PLANT MONITORING DATA OF TAILINGS COMPOSITION VARIATION
APPENDIX III-1	INTERPRETATION OF FLOW-THROUGH CELL LEACH TESTS USING TAGUCHI METHODOLOGY
APPENDIX IV-1	WEEKLY HUMIDITY CELL LEACHATE CHEMISTRY
APPENDIX IV-2	INTERPRETIVE CALCULATIONS FOR WEEKLY HUMIDITY CELL LEACHATE CHEMISTRY
APPENDIX IV-3	POST-HUMIDITY CELL LEACH DATA
APPENDIX IV-4	POST-HUMIDITY CELL ABA
APPENDIX IV-5	POST-HUMIDITY CELL WHOLE-ROCK GEOCHEMISTRY
APPENDIX IV-6	POST-HUMIDITY CELL MINERALOGY
APPENDIX IV-7	POST-HUMIDITY CELL GEOCHEMICAL MASS BALANCE CALCULATIONS
APPENDIX IV-8	POST-HUMIDITY CELL MINERALOGICAL MASS BALANCE CALCULATIONS
APPENDIX V-1	30-YEAR HISTORIC WEATHER RECORDS AT THE VAL D'OR METEOROLOGICAL STATION

## 1.0 INTRODUCTION

### 1.1 Site Description

The Louvicourt deposit, located about 20 km east of Val d'Or, Québec, is a copper-zinc massive sulphide ore body discovered by Aur Resources in 1989. The project is a joint venture of three partners: AUR Resources Inc. (30%), Teck (25%), and Nouvicourt (60% owned by Noranda) (45%). Mine production commenced in mid 1994. The ore reserve as of mid 1999 is about 8 million t at an estimated average grade of 3.5% Cu, 1.7% Zn, and 1 oz/t Ag.

The tailings area is 9 km from the mine site. The east cell, covering an area of about 100 hectares, has been receiving tailings from the beginning. It has enough capacity to provide tailings storage for the life of the mine. All dams were built with a low permeability glacial till core to reduce seepage. All slopes were lined with a geotextile and quarried inert rock cover for erosion control. The tailings basin is underlain by low-permeability clay and bedrock, which limits the rates of ground water flows.

The tailings are discharged underwater through a floating pipeline extending from the dam to the basin. Presently, about 20% of the mill production is discharged to the tailings basin; 20% reports to the concentrate; and 60% is used in paste backfill. The water cover depth was 3.0 m at start-up of the mine; this will gradually decrease as the basin fills with tailings. A minimum water cover depth of 1.0 m will be maintained throughout operation and after closure, except at a few discrete locations in some years of operation during the coldest two months (December and January, with average temperature of -13EC and -17EC, respectively). These short, cold exposures are not expected to cause any acid generation (Filion et al., 1994). Experience of the past several years has shown that underwater tailings disposal at this site is safe and relatively easy to operate.

### 1.2 Project History

During permitting of the Louvicourt project, several ARD characterization tests were done on the tailings. These included the B.C. Research Initial Test and the Confirmation Test, grain size distribution, TCLP leach test, mineralogy, liquid phase chemistry, and flow-through cell leach tests (Lakefield Research, 1993; Centre de Recherche Minerale, 1992; Noranda Technology Centre, 1993).

The Mine Environment Neutral Drainage (MEND) program by 1993 had set a high priority on the research of the effectiveness of subaqueous tailings disposal in artificial containment structures under shallow water covers. The Louvicourt project presented an ideal opportunity for this research from the very beginning of a mine. Golder Associés submitted a draft proposal to MEND in March 1994 (Golder Associés Ltée., March 1994). The draft proposal was reviewed by MEND and the co-funders of the project (Noranda, Teck, and Aur) in a meeting at NTC on May 27, 1994. As a result of this review, the original scope of work was modified

and the proposed budget reduced (St-Arnaud, June 29, 1994). Golder submitted the revised proposal in November 1994 (Golder Associés Ltée., November 1994), which after review was accepted by MEND and the co-funders in January 1995.

The project contract specified Golder Associés as the lead consultants, with Aur, Canmet, INRS-EAU, Senes, UBC, and NTC as collaborators. As a participant, NTC submitted a proposal (NTC, 1994) to MEND and the co-funders, which was approved on a reduced scope of work and incorporated into Golder's revised proposal.

### 1.3 Project Objectives and Approach

The general objectives of the project were two-fold (Golder Associés, 1994):

- < To demonstrate the effectiveness of shallow water covers as a permanent means of preventing the oxidation of sulphide minerals and the consequent formation of acid rock drainage; and
- < to examine the effectiveness, cost, and method of placement of wet organic barriers as an alternative (or supplemental) technology to very shallow water covers.

The objectives of NTC's involvement in the project were as follows:

- < To characterize the Louvicourt tailings' reactivity through humidity cell tests and associated pre- and post-analyses;
- < Using the oxidation rate obtained from humidity cell tests, to model subaqueous tailings oxidation rate;
- < To evaluate the feasibility of a biologically-supported water cover and recommend for a "go/no go" decision for a field test; and
- < To be responsible for the implementation of the field tests if a "go" decision is made for the field tests on a biologically-supported cover.

The project approach was to carry out the perceived work in three phases as follows:

- < Phase I: Proposal formulation, conceptual design, project costing, and approval by the funding partners (completed as of January 1995).
- < Phase II: Integrated laboratory and field studies (now completed).
- < Phase III: Field tests of biologically-supported shallow water covers (not started).

Phase III of the project is outside the time frame for MEND and would only be undertaken based on a future decision of the funding partners. It would involve the placement of organic and inorganic covers and/or establishment of an aquatic vegetation, as well as monitoring and evaluation of their performance.

## 2.0 CHARACTERISTICS OF LOUVICOURT TAILINGS

### 2.1 Samples

The samples used for physical and chemical characteristics are as follows:

- < Sample L-1, produced from bench-scale flotation tests using Comp-6, which was a composite of core samples representing 65% of the mineralization and used in all the tests conducted by Lakefield in 1993 (before this project).
- < A sample used by Aur Resources for analyses at CRM, designated as “CRM”.
- < Four weekly composite samples taken at the backfill plant at Louvicourt during a continuous one-month period in May-June, 1995. These four samples are considered representative of the total tailings at that time. They were consecutively labelled as LVW-1, LVW-2, LVW-3, and LVW-4 and used for humidity cell tests and other chemical analyses at NTC.

### 2.2 Grain Size Distribution

Grain size distribution is available for samples L-1 and CRM (Figure 2.1), both of which are flotation tailings produced by metallurgical tests before the opening of the mine. The materials contain mainly silt to fine sand sized particles.

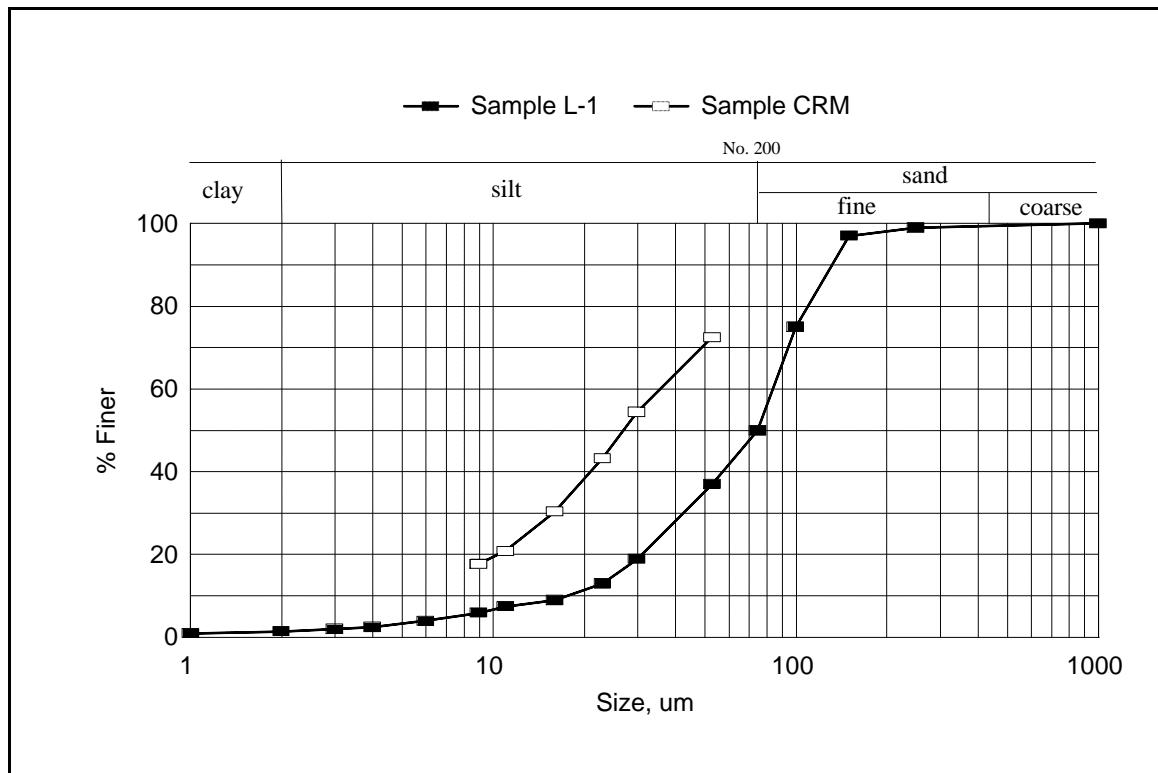


Figure 2.1 Grain Size Distribution of Louvicourt Flotation Tailings

## 2.3 Mineralogy

Mineralogical studies provide crucial information for understanding ABA results, interpreting kinetic test results, predicting future acid-generation, and mathematical modelling. Mineralogy was performed on sample L-1 by Lakefield, on sample CRM by CRM, and on LVW-1, LVW-2, LVW-3, and LVW-4 by Canmet. The mineralogy reports are found in Appendix II-2.

At both Lakefield and CRM, the mineralogy was determined by a combination of XRD (X-ray diffraction), optical microscopy, and bulk chemical analyses. A “modal” mineralogy was computed from the bulk chemical analyses with guidance of the information obtained from optical microscopy and XRD. The two modal mineralogy compositions are compared in Table 2.1.

Table 2.1 Comparison of Modal Mineralogy between Samples L-1 and CRM

Mineral	L-1 (Lakefield)	CRM (CRM)
	% of Total Mass	
Pyrite	46.0	30-45
Pyrrhotite	< 0.1	< 2
Chalcopyrite	0.7	0.8
Arsenopyrite	0.2	-
Sphalerite	0.4	0.6
Galena	< 0.1	-
Silicate (mainly chlorite)	major	26-53
Quartz	11.0	-
Magnetite	1.7	1
Hematite	< 0.1	< 0.5
Carbonates	minor	12-24

The mineralogy of these two samples is similar except the content of carbonates, which was between 12-24% according to CRM but only minor according to Lakefield.

The Lakefield report gave a description of the morphology and mineral associations in L-1:

*Pyrite was the dominant sulphide mineral and occurred as angular liberated grains, as small rounded inclusions within sulphide, oxide, and gangue, and as a binary phase with chalcopyrite, gangue and other sulphide and oxide grains. Trace chalcopyrite occurred as small inclusions and rims on pyrite grains, binaries with gangue and magnetite, small inclusions within gangue and as rare liberated grains... Trace sphalerite was present as a binary phase with pyrite, chalcopyrite, magnetite and gangue and as rare liberated grains. No pyrrhotite was observed...*

Since copper (as chalcopyrite) and zinc (as sphalerite) are mostly associated with pyrite, it is likely that the oxidation of pyrite could mobilize these metals, although in small amounts due to their low contents. Pyrrhotite is not a major phase in either case. The abundant liberated pyrite grains imply plenty of pyrite surfaces for oxidation to take place.

The mineralogy determined by Canmet (Appendix II-2) was most relevant to this study because it was done on the same samples as those used later in the humidity cell tests. The results are summarized in Table 2.2. The technique used by Canmet is a combination of x-ray microanalysis, SEM, and image analysis. Mineral abundances were determined by an integrated image analyzer (microprobe-SEM-IPS) based on their gray levels in the SEM images. Minerals having similar gray levels were distinguished by means of x-ray dot mapping. About 3,000 grains in each polished section were scanned at a magnification of 200x for the abundance determination.

Table 2.2 Mineralogy of Samples LVW-1 through LVW-4 Determined by Canmet

Minerals	Mineral Abundances (% by wt)			
	LVW-1	LVW-2	LVW-3	LVW-4
Quartz	15.4	23.6	27.0	28.3
Muscovite <sup>1</sup>	18.0	10.8	5.7	8.7
Clinocllore	8.3	6.4	4.0	8.0
Mg-Siderite	13.0	9.5	6.0	8.8
Ankerite <sup>2</sup>	14.5	7.2	4.8	3.3
Rutile <sup>3</sup>	trace	1.6	0.9	1.5
Pyrite	29.2	39.9	50.4	41.7
Pyrrhotite	0.6	trace	0.6	0.7
Chalcopyrite	1.0	trace	trace	trace
Sphalerite	trace	1.0	0.6	trace
Galena	trace	trace	trace	trace
1	Also includes K-feldspar and Na-plagioclase			
2	Mg-Mn-containing ankerite and calcite (if any)			
3	Also includes ilmenite and goethite			

There are large variations among the samples shown in Table 2.2 and between the samples in Table 2.2 and those in Table 2.1. This reflects the fluctuation in the ore feed to the concentrator over time.

## 2.4 Whole-Rock Composition

Whole-rock compositions are available for samples L-1 (by Lakefield), CRM (by CRM), and LVW-1 to LVW-4 (by NTC). These analyses have been recalculated to a comparable form and are shown in Table 2.3. Relevant certificates of analyses are in Appendix II-1.

Table 2.3 shows that, whereas sample CRM is similar to samples LVW-1 to LVW-4 in whole-rock composition, sample L-1 is quite different at 26.5% sulphur content, or approximately



50% pyrite, compared with sulphur content of CRM at 19.5 (about 37% pyrite), and of LVW-1 to LVW-4 ranging from 15.0-17.4% (about 28-33% pyrite). Among the LVW series, there are large variations in CO<sub>2</sub> content and moderate variations in sulphur content.

## 2.5 Acid-Base Accounting

### 2.5.1 B.C. Research Initial and Confirmation Tests

In 1993, Lakefield Research conducted B.C. Research Initial and Confirmation Tests on sample L-1. The analytical certificates and a brief description of the two procedures can be found in Appendix II-1. The B.C. Research Initial Test is a form of acid-base accounting (ABA) where the Acid Production Potential (APP) is calculated the same way as the standard (Sobek) procedure using total sulphur, whereas the Acid Consuming Ability (ACA) is determined differently, by titrating the solids with sulphuric acid to a stable end pH of 3.5. The B.C. Research (Biological) Confirmation Test is a simple microbial oxidation test attempting to predict whether the tailings are able to self-sustain a significant bacterial population.

The B.C. Research Initial Test showed an APP of 759 kg H<sub>2</sub>SO<sub>4</sub>/t sample and an ACA of 24.8 kg H<sub>2</sub>SO<sub>4</sub>/t sample, giving an Net Acid Consuming Ability (NACA) of -734.1 kg H<sub>2</sub>SO<sub>4</sub>/t sample. This indicates a high potential for acid generation.

The B.C. Confirmation Test returned a negative result. The sample was unable to sustain continued bacterial growth despite the high acid-generating potential. The meaning of this result is that the test failed to confirm that the sample can sustain bacterially-catalyzed acid generation. It however cannot be interpreted as a confirmation that the sample will not actually generate acid. The most probable reason for the negative confirmation results is the presence of high contents of carbonate neutralization minerals.

Table 2.3 Whole-Rock Composition of Louvicourt Tailings Samples

Components	Content in Samples (%)					
	L-1	CRM	LVW-1	LVW-2	LVW-3	LVW-4
CaO	1.76	2.06	4.40	2.69	2.07	2.10
MgO	-	4.64	5.50	4.48	3.95	4.31
K <sub>2</sub> O	-	-	0.46	0.55	0.62	0.71
Na <sub>2</sub> O	-	0.51	0.37	0.43	0.43	0.33
Al <sub>2</sub> O <sub>3</sub>	-	-	5.20	6.69	7.13	7.56
SiO <sub>2</sub>	-	40.0	28.55	35.25	40.02	38.11
BaO	-	0.12	-	-	-	-
Fe	28.3	22.8	20.40	22.50	20.15	20.96
Mn	-	0.30	0.31	0.20	0.15	0.18
S(total)	26.5	19.5	15.19	17.42	15.86	15.00
S <sup>2-</sup>	-	18.2	-	-	-	-
P <sub>2</sub> O <sub>5</sub>	0.07	0.16	-	-	-	-
CO <sub>2</sub>	6.25	-	11.80	6.79	5.09	5.60
LOI	22.7	-	-	-	-	-
Cu	0.25	0.60	0.14	0.11	0.10	0.11
Pb	0.03	0.08	0.014	0.011	0.010	0.003
Zn	0.23	0.92	0.32	0.48	0.40	0.23
As	0.11	0.16	0.05	0.09	0.08	0.04
Ni	-	0.006	0.005	0.006	0.006	0.007
Cd	-	0.004	0.0006	0.0013	0.0012	0.0003
Co	-	0.04	0.036	0.023	0.023	0.028
Cr	-	0.008	0.0019	0.0045	0.0049	0.0046
Mo	-	<0.01	-	-	-	-
Se	-	-	0.015	0.013	0.012	0.015
Te	-	-	0.0046	0.0046	0.0046	0.0036
Tl	-	-	0.0022	0.0024	0.0022	0.0026
Total*	63.50	91.91	92.75	97.73	96.10	95.28

\*Excluding S<sup>2-</sup> and LOI (loss on ignition) from the summation.

### 2.5.2 Extended ABA

The standard Sobek (EPA) ABA procedure, the modified ABA procedure, and the B.C. Research Initial Test differentiate neither between sulphur species nor between carbonate NP and other NP (i.e., silicate NP). This information is very important in interpreting the ABA results correctly. To overcome this deficiency, samples were analyzed for “extended ABA”. Extended ABA is simply the standard (or modified) ABA complemented with information about the carbonate content and sulphur speciation. Extended ABA was performed on the LVW series of samples. The analytical certificate is attached in Appendix II-1; and the results are shown in Table 2.4 together with those of sample L-1 for comparison. Acronyms used for reporting extended ABA results are as follows: AP = acid potential, SAP = sulphide acid potential, NP = neutralization potential, CNP = carbonate neutralization potential, NNP = net

neutralization potential (= NP - AP), NCNP = net carbonate neutralization potential (= CNP - SAP).

Table 2.4 reveals the following points:

- < Sample L-1 has a much higher acid-generation potential than the LVW series.
- < All the LVW series of samples are highly potentially net acid-generating, with SAPs of about 500 kg CaCO<sub>3</sub> eq/t and NCNPs about -400 kg CaCO<sub>3</sub> eq/t.
- < The average distribution of sulphide S in the LVW samples is 95.6% in pyrite, 2.6% in pyrrhotite, 1.1% in sphalerite, and 0.7% in chalcopyrite. Thus we could expect potential releases of mainly Fe, Zn and perhaps some Cu upon oxidation.
- < For the LVW samples, the CNPs calculated from CO<sub>2</sub>% account for about 150-170% of the NPs determined by the conventional standard (Sobek) ABA procedure (HCl hot digestion followed by back titration of residual acid). These discrepancies suggest the presence of siderite (FeCO<sub>3</sub>) and rhodochrosite (MnCO<sub>3</sub>), which contribute to CNP but not to NP.
- < The LVW samples showed a large variation in CNP but only a modest variation in SAP. The calcium carbonate equivalent of the CNPs ranged from 12 to 27% of the sample mass, which is in good agreement with the mineralogical determinations (Tables 2.1 and 2.2). The significant percentages of carbonates in the Louvicourt tailings provide readily available neutralizing capacity during the initial stages of the acidification process, resulting in a relatively long lag period.

Table 2.4 Extended ABA Results for LVW Series of Samples

Conventional ABA							Extended ABA											Analysed by
Sample ID	paste pH	S(T) %	AP kg/t*	NP kg/t*	NNP kg/t*	NP/AP Ratio	S(pyr) %	S(pyrrh) %	S(sphl) %	S(chlcp) %	Inorg CO2 %	SAP kg/t*	% of AP	CNP kg/t*	% of NP	NCNP kg/t*	CNP/SAP Ratio	
LVW-1	7.64	15.21	475	181.5	-294	0.38	14.43	0.48	0.16	0.14	11.8	475	100.0	268	148	-207	0.56	NTC
LVW-2	7.55	17.45	545	101.5	-444	0.19	16.45	0.65	0.24	0.11	6.8	545	100.0	154	152	-391	0.28	NTC
LVW-3	7.60	16.31	510	75.0	-435	0.15	15.65	0.36	0.20	0.10	5.1	510	100.0	116	154	-394	0.23	NTC
LVW-4	7.50	15.57	487	74.0	-413	0.15	15.16	0.20	0.11	0.11	5.6	487	100.0	127	172	-359	0.26	NTC
L-1	N/A	24.55	767	24.8	-742	0.03	N/A	N/A	N/A	N/A	N/A	N/A	N/A	N/A	N/A	N/A	N/A	Lakefield
<b>Mean</b>	<b>7.57</b>	<b>17.82</b>	<b>557</b>	<b>91</b>	<b>-465</b>	<b>0.18</b>	<b>15.42</b>	<b>0.42</b>	<b>0.17</b>	<b>0.12</b>	<b>7.3</b>	<b>504.21</b>	<b>100.0</b>	<b>166</b>	<b>157</b>	<b>-338</b>	<b>0.33</b>	
<b>Median</b>	<b>7.58</b>	<b>16.31</b>	<b>510</b>	<b>75</b>	<b>-435</b>	<b>0.15</b>	<b>15.41</b>	<b>0.42</b>	<b>0.18</b>	<b>0.11</b>	<b>6.2</b>	<b>498.14</b>	<b>100.0</b>	<b>141</b>	<b>153</b>	<b>-375</b>	<b>0.27</b>	
Std. Dev.	0.06	3.86	121	58	166	0.13	0.85	0.19	0.06	0.02	3.1	30.83	0.0	70	11	89	0.16	
Max	7.64	24.55	767	182	-294	0.38	16.45	0.65	0.24	0.14	11.8	545.22	100.0	268	172	-207	0.56	
Min	7.50	15.21	475	25	-742	0.03	14.43	0.20	0.11	0.10	5.1	475.34	100.0	116	148	-394	0.23	

\* kg CaCO3 equivalent per t of material

## 2.6 TCLP Test and Tailings Water Composition

TCLP (Toxicity Classification Leach Protocol) is an USEPA procedure used to classify industrial wastes into different toxic classes. A TCLP test was conducted on sample L-1. The analytical certificate is included in Appendix II-1. In summary, all metals but Zn and Mn have negligible or extremely low releases. The sample would not be classified as “special waste”, although the leachate concentration of Zn approaches the classification limit for “special waste”. In Canada and particularly in Québec, similar procedures exist (MENVIQ Test in Quebec); relevant legislation however excludes application of such classifications to mill tailings.

The process water associated with sample CRM was analyzed and the results are attached in Appendix II-1. The process water chemistry is relevant to evaluation of the stability of the Louvicourt tailings because the it will become the initial pore water upon disposal of the tailings. The process water has a high pH and contains appreciable levels of sulphate and thiosalts and moderate levels of Ca and Na. All other metals and semi-metals are either very low or below detection.

The presence of thiosalts in the process water is a concern. Oxidation of thiosalts could lower the water cover pH, which in turn could lead to the release of some metals from tailings disposed of under water. Chapter 3.0 addresses the effects of pH on the dissolution of submerged fresh tailings. The generation of acid from thiosalts oxidation is, however, only an operational problem and thus can be managed by addition of lime to control the pH of the water cover. Thiosalts would not cause long-term water quality problems after the mine’s closure.

## 2.7 In-Plant Monitoring of Tailings Composition Variation

To study the in-plant variation of the tailings properties over time, Cu, Zn, and Fe contents were monitored from December 1, 1994 to April 5, 1995 (125 days) at the backfill plant, at a frequency of 4-5 times a week. The tailings at the backfill plant were representative of the total tailings produced at the Louvicourt mill. The samples analyzed were daily composites. The monitoring data appear in Appendix II-3 and are plotted in Figure 2.2.

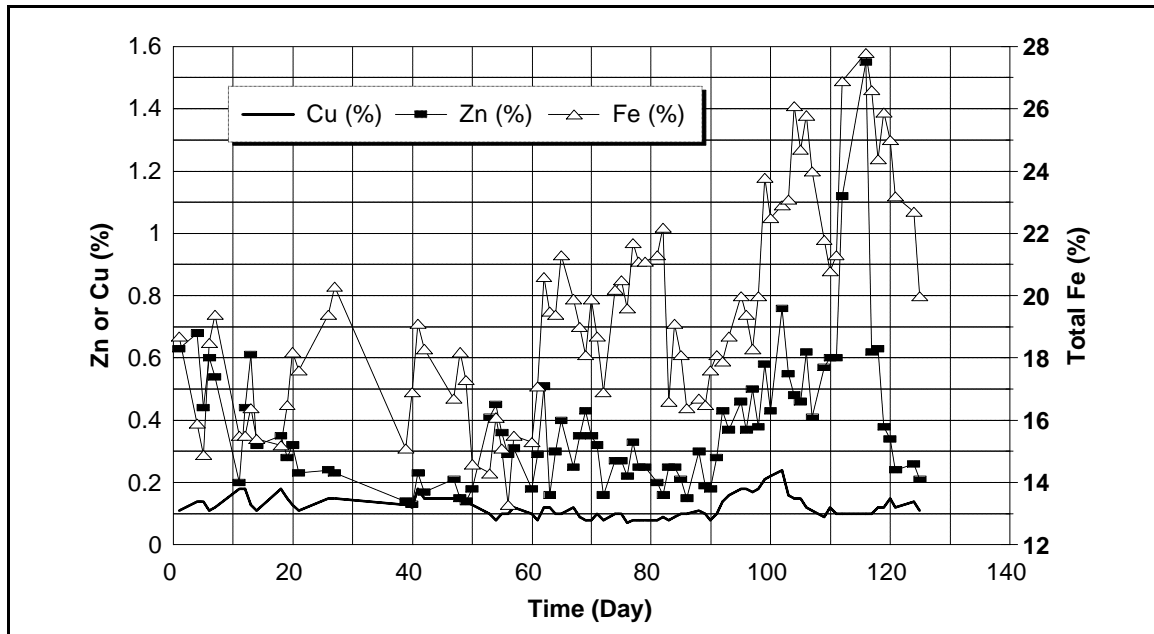


Figure 2.2 Variation of Cu, Zn, and Fe Contents in Louvicourt Tailings

Figure 2.2 shows that the Cu content had little variation (from 0.1-0.2%), whereas the Fe and Zn contents exhibited great variations: Fe from 14 to 28%, and Zn from 0.2 to 1.6%. The spike in Zn at about 110 days was apparently the result of a process upset, as it returned quickly to the normal range of variation (about 0.2-0.6%).

Since the sulphides in the tailings are predominantly pyrite (see Table 2.4), the sulphide content may be estimated from the Fe content. Using a regression equation derived from the sulphide speciation information of the four LVW samples,

$$[\text{Fe}\% \text{ in Sulphide}] = \{[\text{Total Fe}\%] - 9.76\}/0.798$$

and the stoichiometric conversion

$$[\% \text{ Sulphide}] = [\text{Fe}\% \text{ in Sulphide}] / 56 \times 120$$

the sulphide content variation was calculated between 11.4% and 49.0%. The average total Fe content during the monitored period is 19.4, which translates to a sulphide content of about 26%. The variation in sulphide content is therefore -56% and +88% around the mean.

### 3.0 FLOW-THROUGH CELL LEACH TESTS

#### 3.1 Objectives

The objectives of the flow-through cell leach tests were to determine the release rates of dissolved metals and anions, if any, under a simulated water cover as a function of leachant pH, dissolved oxygen (DO) concentration, dissolved  $\text{Fe}^{2+}$  concentration, and flow rate.

#### 3.2 Sample, Test Apparatus, Procedure and Conditions

The sample used in the flow-through leach tests was L-1. The test apparatus was a standard triaxial loading cell for soil testing, specially modified for this study. The tailings sample was wrapped into a cylindrical shape with an impervious elastic membrane, then immersed in an enclosed acrylic cylinder. The swelling and shrinking of the tailings sample were monitored on a buret connected to the water inside the acrylic cylinder. The inflow leachant with controlled hydraulic pressure was introduced at the top of the tailings sample, inside the elastic membrane. The outflow leachate pressure at the bottom of the tailings sample, also inside the elastic membrane, was monitored. The hydraulic gradient across the tailings was calculated as the difference in the hydraulic pressure between the top and the bottom of the sample divided by the height of the sample. The inflow leachant pH was adjusted with solutions of NaOH or HCl. A high DO level was achieved by bubbling air into the leachant and a low DO level by bubbling nitrogen gas into the leachant. The inflow DO levels were monitored.  $\text{Fe}^{2+}$  concentration in the leachant was adjusted by adding  $\text{FeSO}_4 \cdot 7\text{H}_2\text{O}$ . The pore volume in the tailings sample was calculated from the dry mass, the average solid density, and the cylinder volume. The amounts of leachant passed through the cell are expressed as “pore volumes”. A schematic drawing of the leach apparatus is given in Figure 3.1.

The test procedure involved passing the prescribed leachant solution at specified hydraulic gradients, recording the volume change of the sample, and monitoring the leachate solution collected at the bottom of the cell, over time, for volume, pH, and elemental concentrations (with ICP).

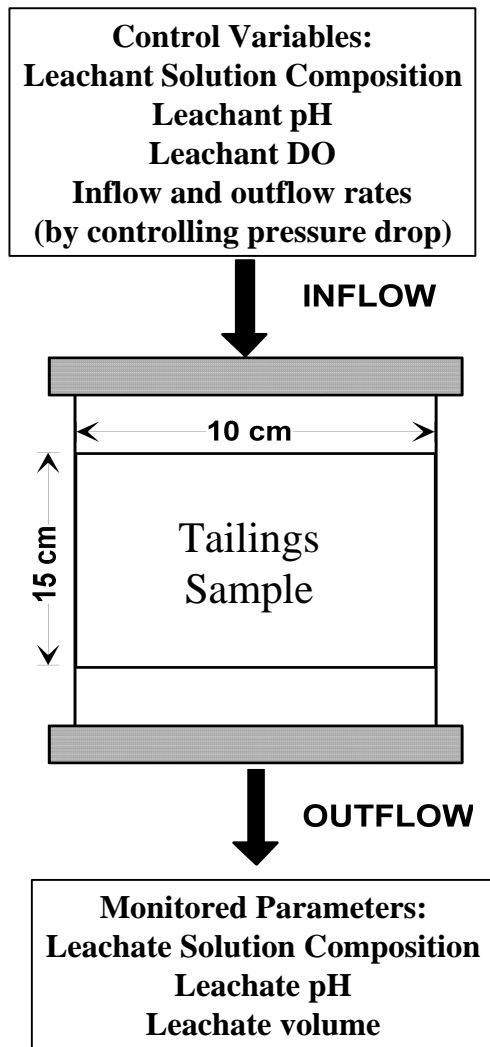


Figure 3.1 Schematic Drawing of Flow-Through Leach Test Apparatus

The test conditions were derived as follows. The leaching sequence was divided into ten phases, designated with letters from A to J. Phases A and B were designed to measure the metal releases at high (10.0) and neutral (7.0) pHs. The test conditions for phases A and B are shown in Table 3.1. Note that the hydraulic gradient  $I$  is unitless, since it is expressed as the ratio of the hydraulic head drop (dimension  $L$ ) across the sample to the height of the sample (dimension  $L$ ).

Table 3.1 Leaching Conditions for Phases A and B

Phase	Leaching Conditions				
	pH	DO (mg/L)	Fe <sup>2+</sup> (mg/L)	I	Temperature
A	10	8	0	5	23-25 EC
B	7	8	0	5	23-25 EC



Phases C through J formed a sequence of experiments constituting a Taguchi experimental design (for details refer to Appendix III-1), aimed at evaluating simultaneously and quantitatively the effects of the four parameters on metal releases. The leaching conditions for these phases are recorded in Table 3.2. However, due to equipment malfunction and sample shortage, phase J failed to generate data.

Table 3.2 Leaching Conditions for Phases C to J

Phase	Conditions				
	pH	DO (mg/L)	Fe <sup>2+</sup> (mg/L)	I	Temperature
D	5	8	0	2.5	23-25 EC
J	5	8	100	5	23-25 EC
C	5	<1	0	5	23-25 EC
E	5	<1	100	2.5	23-25 EC
G	3	8	0	5	23-25 EC
I	3	8	100	2.5	23-25 EC
F	3	<1	0	2.5	23-25 EC
H	3	<1	100	5	23-25 EC

### 3.3 Results

Figure 3.2 shows the correspondence between pore volumes and run time for phases A through I. Figures 3.3 through 3.7 present the results for phases A and B. Figures 3.8 through 3.12 show the results of phases C through I (phase J data missing), which are parts of the Taguchi experiments, along with those of phases A and B for comparison.

### 3.4 Interpretation

#### 3.4.1 Hydraulic Conductivity

The slope in Figure 3.2,  $d[\text{pore volume}]/d[\text{run time}]$ , is equivalent to flow rate,  $Q$ . According to Darcy's law

$$Q = k \cdot I \cdot A$$

where  $k$  = hydraulic conductivity,  
 $I$  = hydraulic gradient, and  
 $A$  = cross-sectional area of the tailings sample,

if  $A$  and  $I$  are kept constant (as is the case in each phase of the experiment),  $Q$  is directly proportional to  $k$ , the hydraulic conductivity. Any change in  $Q$  (i.e., the slope of the curve in Figure 3.2) indicates a change in hydraulic conductivity  $I$ .

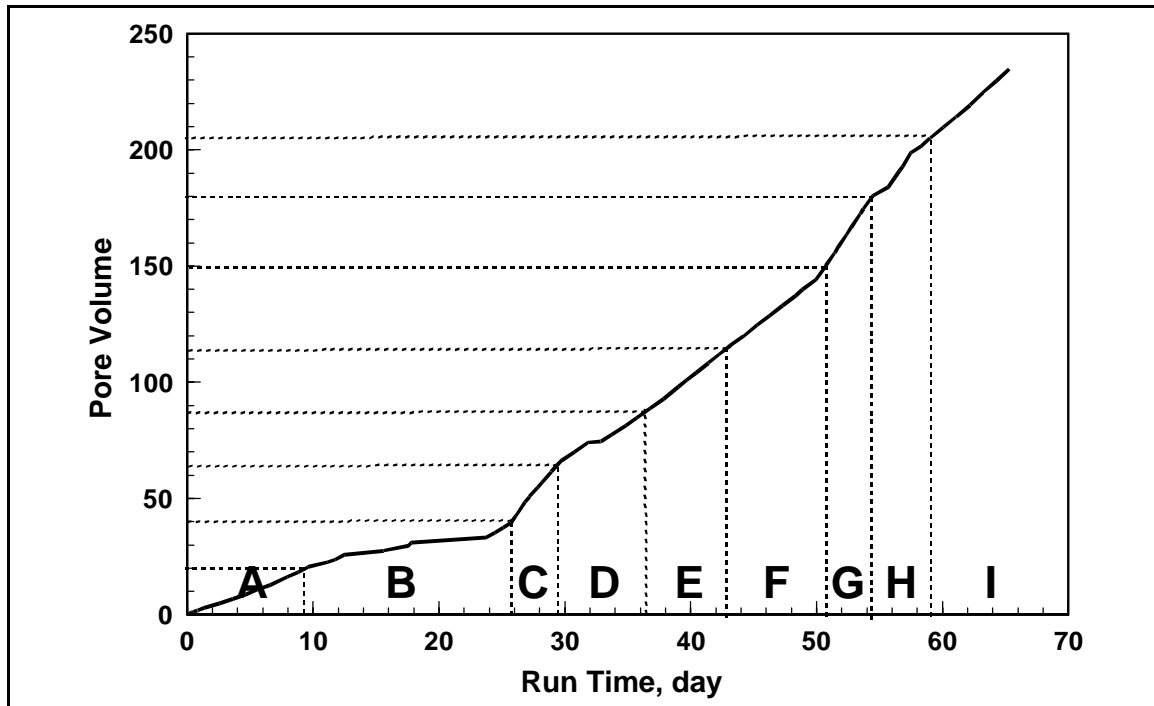


Figure 3.2 Correlation between Run Time, Pore Volumes Passed, and Phases

Figure 3.2 shows that the slopes in phases A, C, E, F, G, and I are constant, indicating invariant flow rates and hydraulic conductivity in these phases. In contrast, the slopes in phases B, D and H showed obvious changes, suggesting changes in flow rates and hence changes in hydraulic conductivity. These changes reflect the combined effects of the changes in influent chemistry (including pH and chemical composition) and hydraulic gradient.

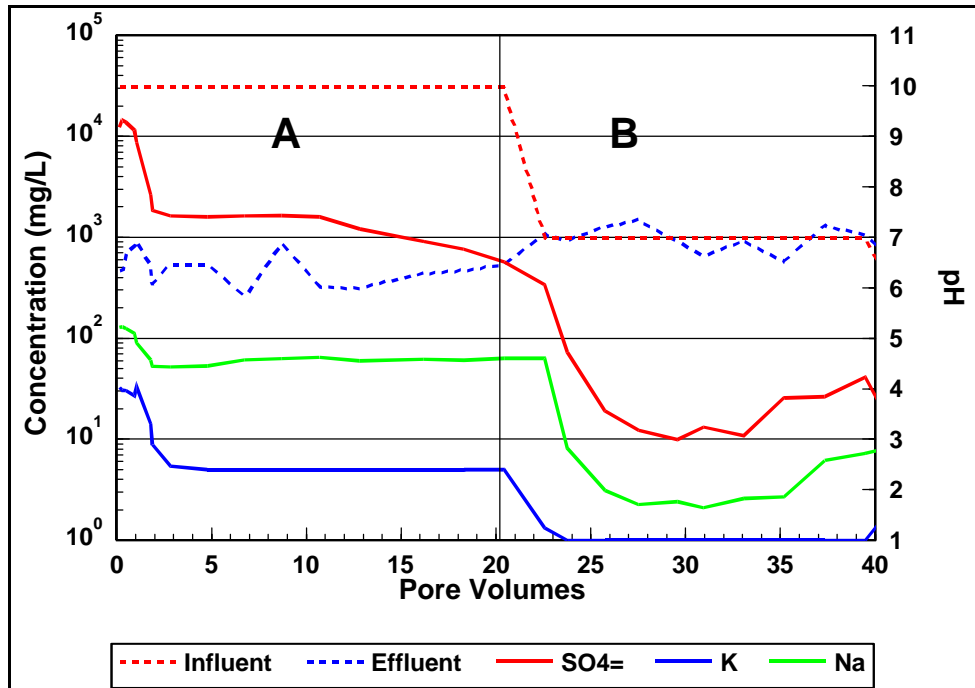


Figure 3.3 Leaching Results for Phases A and B -  $\text{SO}_4^-$ , K, and Na (dotted line indicate pH, others as marked)

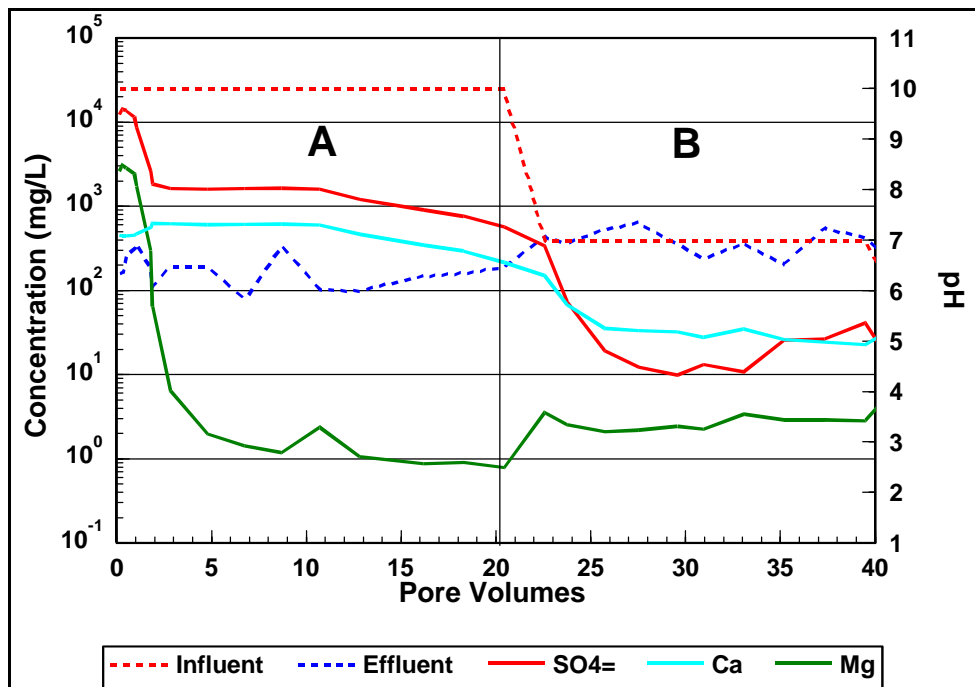


Figure 3.4 Leaching Results for Phases A and B -  $\text{SO}_4^-$ , Ca, and Mg (dotted line indicate pH, others as marked)

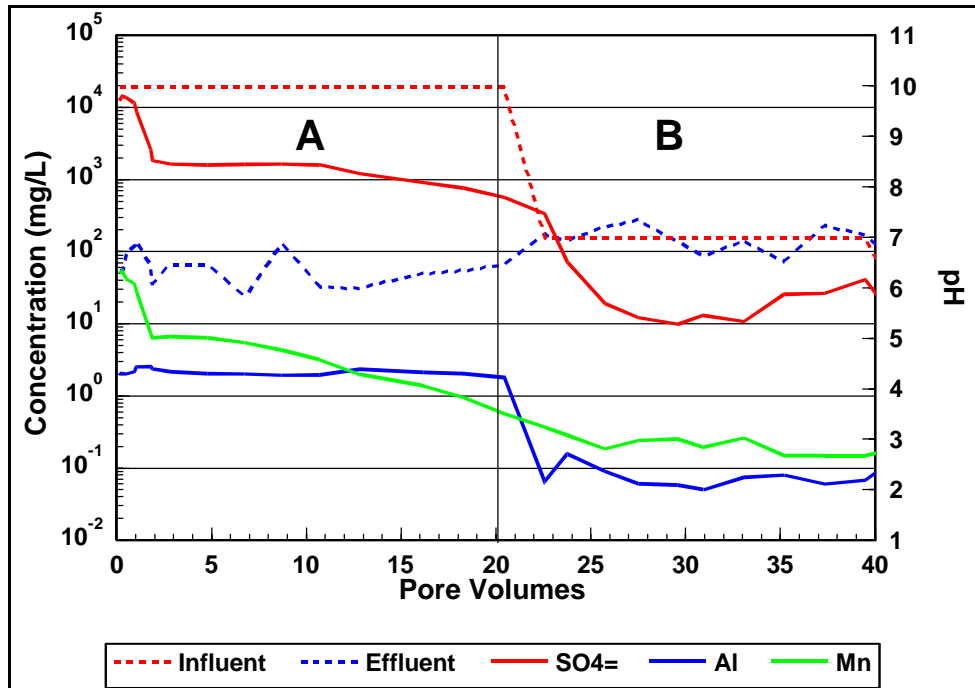


Figure 3.5 Leaching Results for Phases A and B -  $\text{SO}_4^-$ , Al, and Mn (dotted line indicate pH, others as marked)

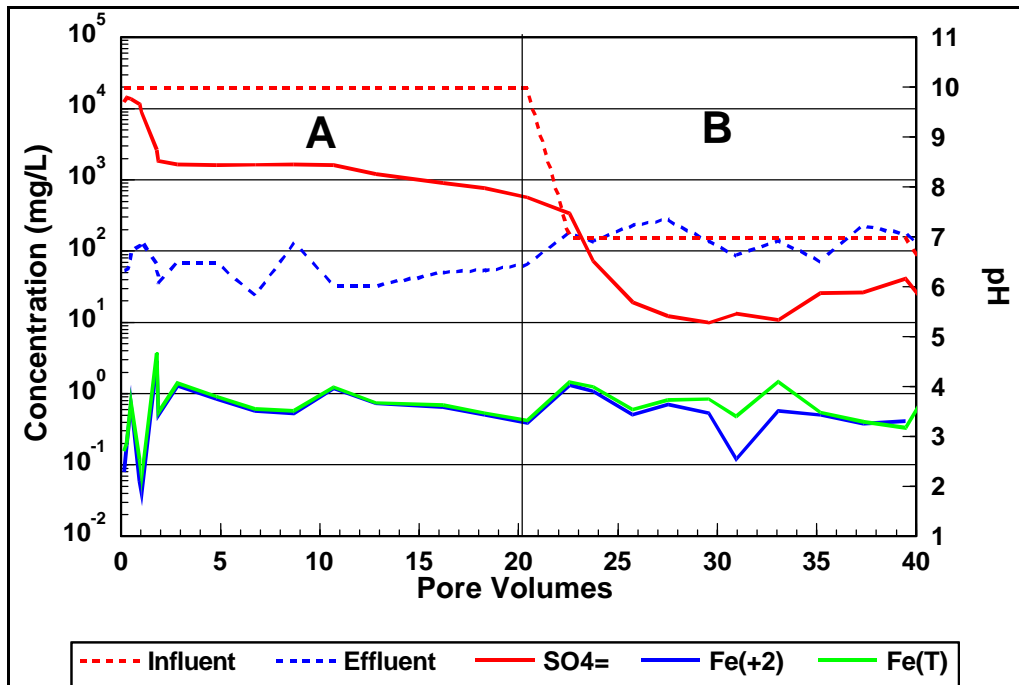


Figure 3.6 Leaching Results for Phases A and B -  $\text{SO}_4^-$ ,  $\text{Fe}^{2+}$  and Fe(T) (dotted line indicate pH, others as marked)

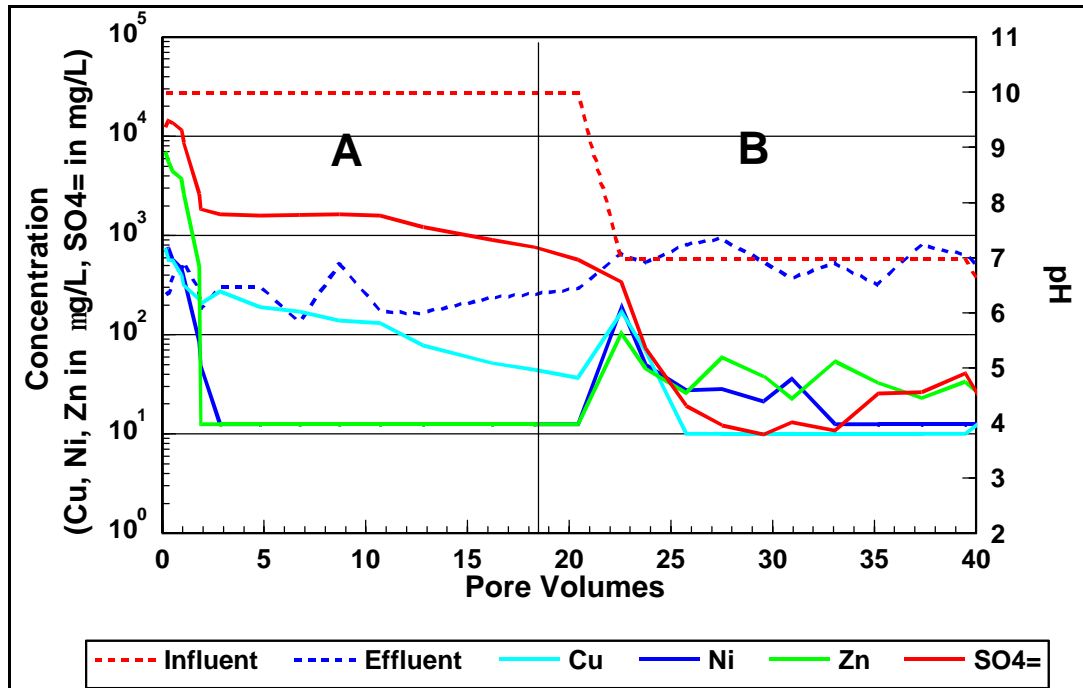


Figure 3.7 Leaching Results for Phases A and B -  $\text{SO}_4^-$ , Cu, Ni, and Zn (dotted line indicate pH, others as marked)

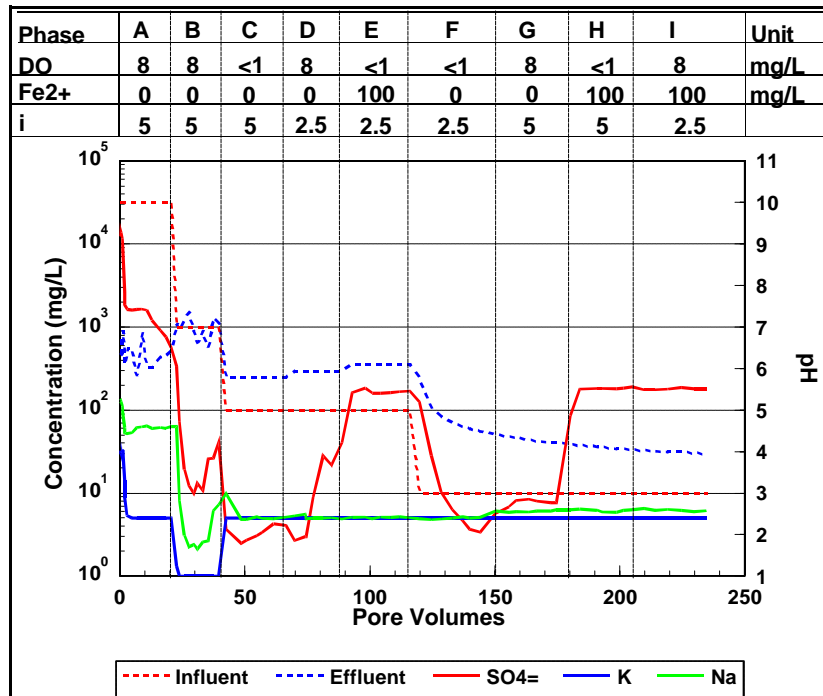


Figure 3.8 Leaching Results for Phases A to I -  $\text{SO}_4^-$ , K, and Na (dotted line indicate pH, others as marked)

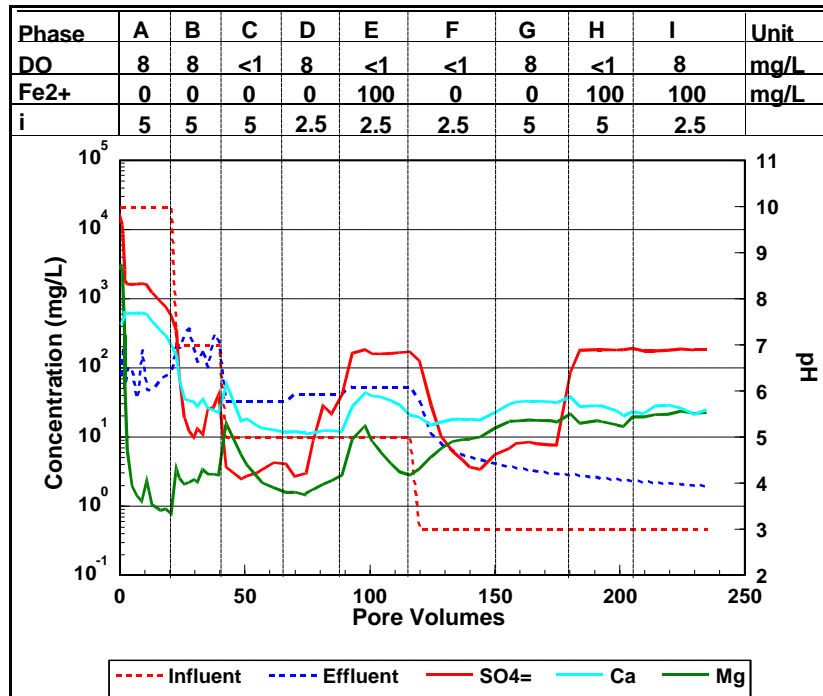


Figure 3.9 Leaching Results for Phases A to I -  $\text{SO}_4^-$ , Ca, and Mg (dotted line indicate pH, others as marked)

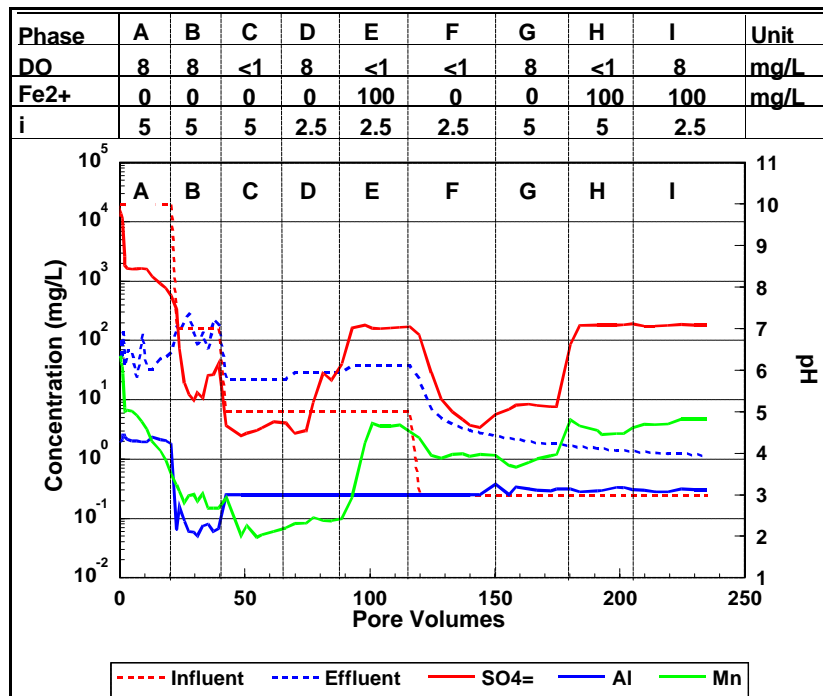


Figure 3.10 Leaching Results for Phases A to I -  $\text{SO}_4^-$ , Al, and Mn (dotted line indicate pH, others as marked)

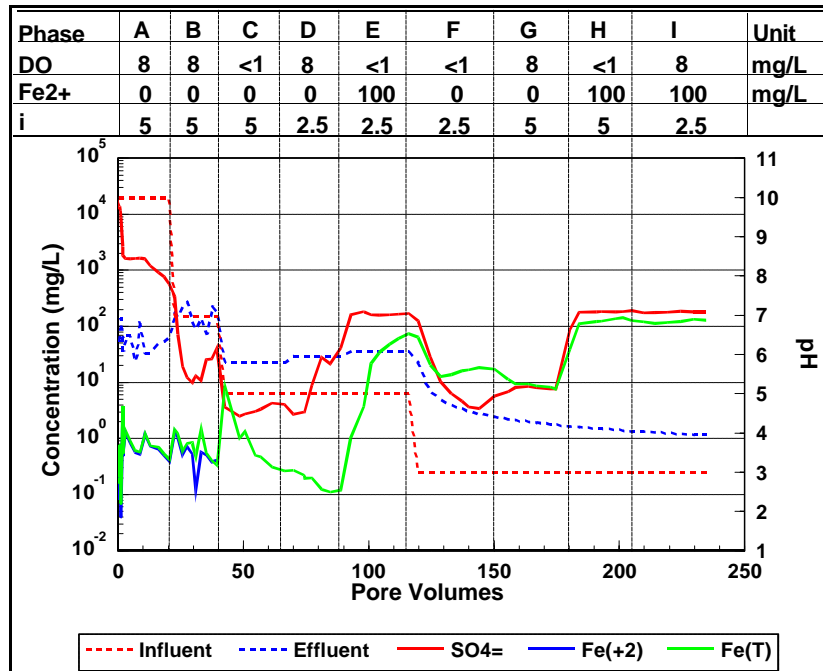


Figure 3.11 Leaching Results for Phases A to I -  $\text{SO}_4^-$ ,  $\text{Fe}^{2+}$  and  $\text{Fe(T)}$   
(dotted line indicate pH, others as marked)

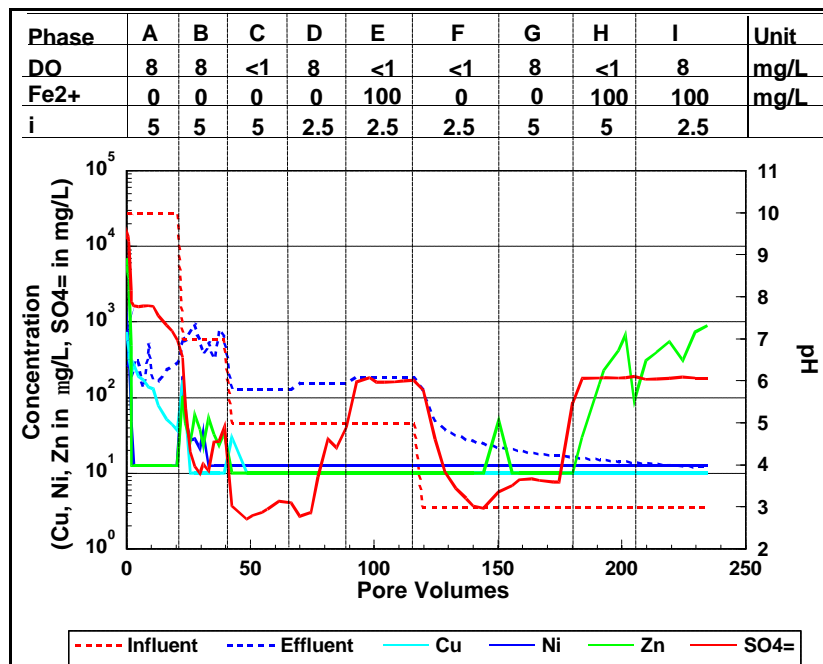


Figure 3.12 Leaching Results for Phases A to I -  $\text{SO}_4^-$ , Cu, Ni, and Zn  
(dotted line indicate pH, others as marked)

### 3.4.2 Phases A and B

#### *Prior Oxidation of Tailings Sample*

The tailings sample used in the flow-through leach tests had undergone some oxidation during the sample handling process. This is reflected by the high dissolved constituents in the leachate during the first 2-3 pore volumes of leaching:  $\text{SO}_4^-$ , up to about 15,000 mg/L; Mn, up to 50 mg/L; Zn, up to 7 mg/L; Cu and Ni, up to about 1 mg/L.

#### *Flushing of Soluble Constituents*

Figures 3.3-3.7 indicate that the readily soluble constituents, present either as dissolved matter in the pore water or as secondary minerals on the tailings particles, are flushed out after 2-3 pore volumes of leachant pass through the cell. Such constituents include Zn, Ni, Mg, K, and Na. In the leachate of the initial 2-3 pore volumes, these constituents exhibit a concentration drop by at least an order of magnitude: Zn by three orders of magnitude, Ni by two, Mg by three, K and Na both by one order. After 2-3 pore volumes, the concentrations of these constituents normally fall below their analytical detection limits. The concentrations of Na and K did not fall below their detection limits because they were added in the inflow for pH adjustment to 10.0 as NaOH (with K as an impurity).

Constituents which are not completely flushed out after 2-3 pore volumes are involved in one or more of the follow processes:

- < The concentration of the constituent is regulated by the solubility of a sparingly soluble mineral, e.g., gypsum ( $\text{CaSO}_4 \cdot 2\text{H}_2\text{O}$ ), jurbanite ( $\text{AlOHSO}_4 \cdot 5\text{H}_2\text{O}$ ), and anglesite ( $\text{PbSO}_4$ );
- < The release of the constituent is controlled by the dissolution rate of its secondary mineral(s), e.g., Ca by  $\text{CaSO}_4 \cdot 2\text{H}_2\text{O}$  (gypsum), Al by  $\text{AlOHSO}_4 \cdot 5\text{H}_2\text{O}$  (jurbanite), and Mn perhaps by  $\text{MnCO}_3$  (rhodochrosite); and
- < The constituent is continuously being released by chemical reactions, e.g.,  $\text{Fe}^{2+}$  and  $\text{SO}_4^-$  by pyrite oxidation.

#### *Solubility Control on Constituent Release*

Figure 3.4 demonstrates features which suggest that the concentration of  $\text{SO}_4^-$  and Ca into the leachate is controlled, from the beginning of the experiment to about 11 pore volumes, by the solubility of gypsum: as sulphate concentration decreased, Ca concentration increased (pore volumes 1-2); as sulphate concentration stabilized at around 1600 mg/L, Ca concentration stabilized at 600 mg/L (pore volumes 2-11). After pore volume 11, both sulphate and Ca decreased in concentration, signalling the end of gypsum saturation. However, they did not drop to very low levels in 2-3 pore volumes (the amount of leachant required to completely flush out a soluble constituent); but rather, they decreased gradually from pore volume 11 to about 25. During this period the concentrations of both seem to be controlled by the slow rate of gypsum dissolution. After pore volume 25, the dissolution of gypsum stored in the tailings



was completed. Sulphate and Ca concentrations were maintained at around 10 mg/L and 30 mg/L, respectively. This is achieved primarily by ongoing pyrite oxidation by DO, neutralization of acid generated by calcite ( $\text{CaCO}_3$ ), and calcite dissolution itself, as indicated by the following calculations.

If we assume that all 8 mg/L DO in the inflow is used to oxidize pyrite, the sulphate generated in the leachate should be 14 mg/L, in agreement with the observed sulphate level. Meanwhile, if we further assume that the acid generated from the above oxidation is fully neutralized by calcite to form  $\text{HCO}_3^-$ , the Ca concentration generated is about 6 mg/L, which suggests that about 24 mg/L Ca comes from the non-reactive dissolution of calcite itself. Equilibrium calculation with MINTEQA2 shows that dissolution of calcite in pure water at 1 atm, 25 EC and in contact with air gives rise to 25 mg/L Ca in the solution.

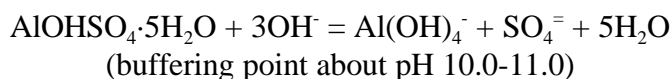
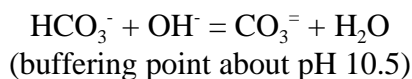
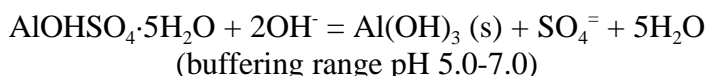
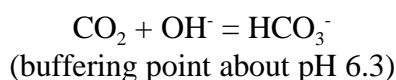
Similarly, release of Al could also be controlled by the solubility of jurbanite ( $\text{AlOHSO}_4 \cdot 5\text{H}_2\text{O}$ ): for pore volumes 0 to 2, as sulphate concentration decreased, Al concentration increased; for pore volumes 2 to about 11, leachate sulphate concentration stabilized at about 1600 mg/L, as did Al concentration at around 2 mg/L; when sulphate concentration declined again from 11 to about 13 pore volumes, Al concentration rose to about 3 mg/L, at which point the solubility-controlled release of Al ended. From 13 to about 20 pore volumes, both sulphate and Al concentrations decreased gradually, suggesting a control on Al release by the slow dissolution rate of  $\text{AlOHSO}_4 \cdot 5\text{H}_2\text{O}$ . From 20 to 22 pore volumes, Al concentration dropped abruptly by more than an order of magnitude, concurrent with the drop in inflow pH. This drop may indicate the depletion of  $\text{AlOHSO}_4 \cdot 5\text{H}_2\text{O}$  stock. Despite the decrease in the influent pH from 10.0 to 7.0 at approximately 20 pore volumes, the effluent pH showed an increase at the same time. This pH rise may have contributed to the drop in Al concentration in the leachate by means of solubility control. After pore volume 22, Al concentration in the leachate stabilized at about 0.1 mg/L, which appears to be sustained by active Al dissolution (probably from aluminosilicates) at the inflow pH of 7.0.

#### *Control on Release of Mn and Cu*

The releases of Mn and Cu seem to follow the same pattern: both had a quick, initial decrease from 0 to 2 pore volumes, consistent with the volume required to wash out the dissolved species in the initial pore water. From 2 to about 25 (20 for Cu) pore volumes, the concentration of Mn (Cu) decreased steadily, from 6 mg/L (200  $\mu\text{g/L}$  for Cu) to 0.2 mg/L (40  $\mu\text{g/L}$  for Cu). During this period, the release of Mn (Cu) seems to have been controlled by the dissolution rate of Mn- (Cu-) containing minerals, which may be in the form of carbonates, hydroxides, or oxides.

### *pH Buffering of Tailings Pore Water*

The leachate (thus the tailings pore water) was apparently buffered against pH rises: although the inflow pH was as high as 10.0 in phase A, the outflow pH was always between 6.0 and 7.0. In the present system, possible buffering reactions, in decreasing order of importance, are as follows:



All these reactions bind up  $\text{OH}^-$ , preventing the pH of the pore water from rising thus providing the buffering action. Since the outflow pH was generally between 6.0 and 7.0, the major buffering capacity must have been provided by the first two reactions above, i.e., the major buffering species were dissolved  $\text{CO}_2$  and aluminum hydroxy sulphate.

Buffering of the pore water from an inflow pH of 10.0 to an outflow pH of 6.0-7.0 is equivalent to eliminating  $10^{-4}$  mol  $\text{OH}^-/\text{L}$  from the solution. Assuming that all 8 mg/L inflow DO reacts with pyrite to generate acid, half of which reacts with calcite to form dissolved  $\text{CO}_2$  (the other half reacts with calcite to form  $\text{HCO}_3^-$ ), the amount of dissolved  $\text{CO}_2$  so formed in the leachate would be  $0.36 \times 10^{-4}$  mol/L. Since the cell is a closed system, all this dissolved  $\text{CO}_2$  would be available to react with  $\text{OH}^-$  according to the first reaction above, eliminating  $0.36 \times 10^{-4}$  mol/L  $\text{OH}^-$ , or 36%, of the  $10^{-4}$  mol/L  $\text{OH}^-$ . The remaining 64% would be eliminated by the second reaction above, requiring  $0.32 \times 10^{-4}$  mol/L of  $\text{AlOHSO}_4 \cdot 5\text{H}_2\text{O}$  to take part in reaction. This amount could easily be satisfied by the  $\text{AlOHSO}_4 \cdot 5\text{H}_2\text{O}$  already in stock at the beginning of the leach tests.

#### 3.4.3 Phases C to I

By the end of phase B, nearly all accumulated oxidation products (dissolved constituents in pore water and secondary minerals on tailings particles) had been flushed out after 40 pore volumes of leaching. Therefore, starting from phase C, the concentrations of various constituents in the leachate reflect the active on-going geochemical processes.

### *Sulphide Oxidation and Sulphate Release*

As stated earlier, from phase C on, the release of sulphate into the leachate reflects the active, on-going geochemical reactions. The elevated sulphate concentration in phases E, H, and I is primarily a result of the addition of  $\text{FeSO}_4 \cdot 7\text{H}_2\text{O}$  for adjusting the dissolved  $\text{Fe}^{2+}$  concentration in the leachant, thus is not comparable to the sulphate levels in other phases.

Comparison of sulphate releases in phases C and D reveals the effect of DO on sulphide oxidation (Figure 3.9). In phase C, the sulphate concentration in the leachate is extremely low, around 3 mg/L, indicating a total lack of sulphate generation from sulphide oxidation due to unavailability of DO. In phase D, in contrast, the sulphate level jumped by roughly an order of magnitude, to 20-30 mg/L. This sulphate level is in approximate agreement with the total consumption of inflow DO by pyrite oxidation, which would yield a sulphate concentration of 14 mg/L. The comparison of phases F and G reveals the same pattern, although less pronounced, due to the residual influence of the high sulphate addition in phase E.

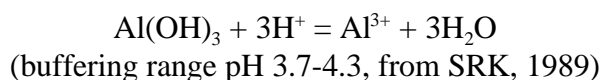
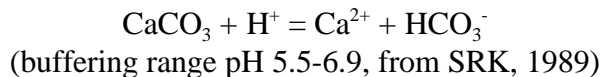
### *Effects of $\text{Fe}^{2+}$ Addition*

There is an interesting lag of  $\text{Fe}^{2+}$  concentration (as measured by  $\text{Fe(T)}$ ) behind that of  $\text{SO}_4^-$  when  $\text{FeSO}_4 \cdot 7\text{H}_2\text{O}$  was added the first time (phase E, Figure 3.11). The  $\text{SO}_4^-$  concentration in the outflow leachate rose instantly to the inflow level and stabilized at that level, the outflow  $\text{Fe}^{2+}$  concentration however rose only gradually in phase E, achieving the inflow level only toward the end of phase E (taking about 20 pore volumes). This means that there was a net accumulation of  $\text{Fe}^{2+}$  on the tailings particles. This accumulation cannot have occurred in the pore water because it had been flushed 20 times. At the same time, Mn, Ca, and Mg concentrations in the outflow exhibited sudden, large rises. These observations suggest that Mn, Ca, and Mg originally adsorbed on the tailings particle surfaces were displaced by  $\text{Fe}^{2+}$  through ion exchange, due to the large  $\text{Fe}^{2+}$  concentration in the inflow. After  $\text{Fe}^{2+}$  was removed from the inflow (phase F), a fraction of the adsorbed  $\text{Fe}^{2+}$  started to desorb, causing the outflow  $\text{Fe}^{2+}$  concentration to hang above that of sulphate. When 100 mg/L  $\text{Fe}^{2+}$  was re-introduced in the inflow in phase H,  $\text{Fe}^{2+}$  adsorbed again on the tailings particles; but this time the lag of  $\text{Fe}^{2+}$  concentration behind that of sulphate in the outflow was much less pronounced, because some of the tailings surface sites were still occupied by the  $\text{Fe}^{2+}$  which adsorbed in the last round (i.e., the desorption of  $\text{Fe}^{2+}$  in phases F and G was incomplete); meanwhile, due to the lower pore water (outflow) pH, the surface charges on the tailings particles were less negative, causing less  $\text{Fe}^{2+}$  ions to be adsorbed at equilibrium.

Addition of  $\text{Fe}^{2+}$  did not seem to cause other changes in the outflow chemistry than those accounted by simple ion exchange.

*pH Buffering*

As the inflow pH dropped to 5.0 in phases C to E and further to 3.0 in phases F to I, the outflow pH was buffered at about 6.0 and between 4.0-5.0, respectively. The pH buffering was most probably afforded by two minerals: calcite ( $\text{CaCO}_3$ ) and gibbsite ( $\text{Al}(\text{OH})_3$ ):



Experimental evidences for these buffering reactions taking place are as follows:

- < For phases C, D, and E, there is continued release of Ca; the leachate pH is consistent with the buffered range of calcite; and
- < For phase G, H, and I, there is continued release of Al; the leachate pH falls within the buffering range of gibbsite.

Other possible buffering minerals include Mg- and Mn-containing minerals, such as dolomite,  $\text{CaMg}(\text{CO}_3)_2$ ; rhodochrosite,  $\text{MnCO}_3$ ; kutnohorite,  $\text{Ca}(\text{Mn,Mg,Fe})(\text{CO}_3)_2$ , and manganese oxide,  $\text{MnO}_2$ . Experimental evidences for these buffering reactions are constantly elevated levels of Mg and Mn throughout phases C to I.

#### *Silicate Dissolution*

Dissolution of primary silicate minerals seems to be minimal, as K and Na concentrations were barely detectable throughout phases C to I.

#### *Release of Metals*

Only Mn and Zn exhibited significant release when the outflow pH dropped below 4.0 and when 100 mg/L  $\text{Fe}^{2+}$  was introduced in the inflow (Figures 3.10 and 3.12): Mn rose to about 5 mg/L (end of phase I) and Zn to 1 mg/L (end of phase I). These concentrations, in any case, are still quite low compare to levels that can be found in acid mine drainage.

It is difficult to figure out which caused the releases of Mn and Zn in phases H and I: low leachate pH or high inflow  $\text{Fe}^{2+}$ . Data interpretation on the basis of Taguchi experimental design sheds some light on this (Appendix III-1), which seems to indicate that the high  $\text{Fe}^{2+}$  concentration in the inflow plays a somewhat more important role.

### 3.4.4 Design of Experiments Using the Taguchi Approach

Details on the results and interpretation of the Taguchi experiments are contained in Appendix III-1. The following is a summary of conclusions and recommendations.

For the conditions tested, the order of influence of the parameters on metal releases is observed as follows:  $\text{Fe}^{2+}$  (strong) > DO (strong) > pH (medium) > I (weak). The directions of influences are that higher  $\text{Fe}^{2+}$ , lower DO (surprisingly), lower pH, and perhaps smaller I are conducive to higher metal concentrations in the leachate. Nevertheless, the absolute quantities of metals released are quite small.

These experiments suggest that, to curb metal releases in the field, flow of AMD containing mainly  $\text{Fe}^{2+}$  through the submerged tailings should be avoided and a neutral pH should be maintained in the water cover. Although anoxic conditions (nearly zero DO) appear to increase the total metal release, particularly that of dissolved Mn, it is not advisable to increase the oxygenation of the water cover to curb Mn release, since this would, in the long term, cause aqueous oxidation of sulphides in the submerged tailings, which could lead to release of other metals, such as dissolved  $\text{Fe}^{2+}$  and Zn.

### 3.5 Summary

Analyses of metal release curves appear to indicate the following: Presence of  $\text{Fe}^{2+}$  in the inflow appears to increase metal releases primarily through a one-time ion exchange process. DO in the inflow seems to promote the release of  $\text{SO}_4$ , Ca and Al through oxidation of sulphides in the tailings. Lower influent pH favours metal releases probably because of the higher solubility of hydroxides and carbonates of most metals at lower pHs; however the influence of inflow pH ranks behind  $\text{Fe}^{2+}$  and DO, since the tailings have sufficient buffering capacity to maintain the pore water pH at nearly neutral levels. Lower hydraulic gradient increases metal concentrations in the outflow mainly through prolonging the contact time between the passing-through water and the tailings; it does not necessarily increase metal fluxes from the solid phase to the leach solution.

Taguchi experiments suggest the following influence on metal releases:  $\text{Fe}^{2+}$  (strong) > DO (strong) > pH (medium) > I (weak). Higher  $\text{Fe}^{2+}$ , lower pH, and smaller I are all conducive to higher metal concentrations in the leachate. Lower DO is conducive to the release of Mn.

It takes only 2-3 pore volumes of leachant to completely flush out the readily-soluble oxidation products accumulated in the tailings. Mechanisms controlling metal releases include solubility control on  $\text{SO}_4^-$ , Ca, and Al by gypsum and aluminum hydroxy sulphate (jurbanite) in the early phases, and dissolution rate control on  $\text{SO}_4^-$ , Ca, Al, and Mn by gypsum, aluminum hydroxy sulphate (jurbanite), and unidentified Mn minerals in the later phases. A complete rinse-out of the slowly-dissolving minerals (gypsum and aluminum hydroxy sulphate or jurbanite) accumulated in the tailings as oxidation products took about 20 pore volumes of leaching.

The tailings pore water and the leachate are buffered in the nearly neutral range against both pH rise and pH drop - by dissolved  $\text{CO}_2$ , aluminum hydroxy sulphate, calcite, and unidentified Mn minerals. Primary silicate minerals do not seem to dissolve appreciably.

Overall metal releases are quite low throughout the experiments except during the initial flush-out of accumulated soluble constituents due to prior oxidation. Sustained low-pH inflow seems to be able to depress the pH of the pore water after many pore volumes, causing the release of Mn and Zn.

The leach test results imply some field measures that can be used to control metal releases: maintenance of a neutral-pH water cover and avoidance of AMD flow through the submerged tailings. They also suggest that the tailings have natural buffering capacity and thus can withstand short periods of acidic pH in the water cover without releasing metals.

## 4.0 HUMIDITY CELL TESTS

Humidity cell test is a kinetic test which employs a three-day wet, a three-day dry, and a one-day rest-leaching period in each seven-day cycle. In the wet period, air saturated with water vapour is passed over the test material; in the dry period, dehumidified air is passed. In the rest-leaching period, the sample is soaked with distilled or deionized water and then the water (leachate) is drained and filtered. The filtrate is measured for pH, conductivity, redox potential, acidity, alkalinity, and dissolved metals and anions. The data collected are interpreted to determine the primary rates of oxidation, and acid neutralization. The humidity cell test procedure followed in this study is a hybrid of those given in Sobek et al. (1978) and Coastech (1990).

### 4.1 Objectives

The objectives of the humidity cell tests in this study are as follows:

- < to characterize the reactivity of tailings samples by determining their primary oxidation rates under a favourable oxidizing environment, i.e., dry and moist cycles, room temperature, and periodic leaching to wash away oxidation products thereby exposing fresh sulphide surfaces;
- < to determine the in-situ rates and efficiency of neutralization by naturally-present buffering minerals;
- < to compare the rates of acid generation and neutralization, thereby empirically determining the deficiency or surplus of neutralization minerals (i.e. whether acid generation would occur) and predicting the length of the lag period (i.e., the period before the onset of acid generation) if the tailings were to be exposed to atmosphere and eventually become net acid-generating; and
- < To provide a laboratory-determined oxidation rate for Louvicourt tailings, which will allow to evaluate the water cover efficiency in preventing tailings oxidation, by comparing the humidity cell test oxygen consumption rate with the *in situ* measured rate of the submerged tailings (made by INRS-Eau).

### 4.2 Test Samples, Set-Up, and Procedure

The four test samples used were LVW-1, LVW-2, LVW-3 and LVW-4, as described in section 2.1. These four samples are alternatively also labelled as LV-1 through LV-4.

The humidity cell tests began on September 1, 1995 and ended on March 6, 1997. Each sample was tested in duplicate cells, identified by the letters A and B following the sample designations. Leachate samples were taken weekly on Thursdays except during the two Christmas periods when the leaching cycles were skipped.



Into each cell was put a 200 g dry tailings sample. The volume of leaching water added each week was 200 mL. Leachate samples were recovered and measured for volume, pH, conductivity, redox potential, acidity, and alkalinity. A 40-mL filtered (0.45 µm cellulose nitrate filter) leachate sub-sample was preserved with HCl and later sent for ICP (21 elements) and Fe(III) analyses at the NTC lab. The sample bed was stirred when required. The eight humidity cells were operated for a duration of eighty weeks.

After the humidity cell tests were terminated, solid sub-samples were collected from each cell and sent for post-humidity cell extended ABA analysis at Chemex Laboratories. Four cells (one from each duplicate set, i.e., LV-1A, LV-2A, LV-3A and LV-4A) were selected for post-humidity cell leach, mineralogy, and geochemical whole-rock analysis.

For post analyses, the four humidity cells were emptied and all the solids were collected and dried. The dry solids were homogenized and sub-sampled. The leach was conducted by NTC using 10 g of solids in 1.5 L of deionized water. The mixture was sealed in a 2-L bottle and agitated in an end-over-end fashion for 24 hours. The supernatant was sampled, filtered, and analyzed. For geochemical whole-rock analysis, trace metal contents and sulphur speciation (into total, soluble and elemental sulphur) were determined by NTC, whereas major oxides, total sulphur and CO<sub>2</sub> contents were analyzed by CRM. For mineralogical determinations, polished thin sections were made from dry solids for optical microscopy, electron microprobe analysis, and x-ray diffractometry (XRD).

### 4.3 Test Results

The comprehensive humidity test results include pre-humidity cell solid characterization (presented in Chapter 2.0), weekly leachate chemistry data, and post-humidity cell solid analyses.

#### 4.3.1 Leachate Chemistry

The weekly humidity cell leachate chemistry raw data are documented in Appendix IV-1 and the results of interpretative calculations are given in Appendix IV-2.

#### 4.3.2 Post-Humidity Cell Solid Analyses

Post-humidity cell test data, including final leach, ABA, whole-rock geochemistry, and mineralogy, have been compiled as Appendices IV-3 to IV-6.

##### 4.3.2.1 Post-Humidity Cell Leach

The purpose of this test is two-fold: (1) to dissolve all possible soluble secondary minerals, such as gypsum and acid iron sulphates, in the test samples which have not been completely

Table 4.1 Post-Humidity Cell ABA

Sample ID	Paste pH	S (T) %	S (Sulfide) %	S (Sulfate) %	inorg CO2 %	AP kg CaCO3/t	NP kg CaCO3/t	NNP kg CaCO3/t	NP/AP	SAP kg CaCO3/t	CNP kg CaCO3/t	NCNP kg CaCO3/t	CNP/SAP
LVW-1A	6.7	17.5	16.4	0.32	7.1	547	83	-464	0.15	513	161	-351	0.31
LVW-1B	6.9	17.5	16.45	0.22	9	547	33	-514	0.06	514	204	-310	0.40
LVW-2A	5.4	17.4	16.49	0.25	2.8	544	28	-516	0.05	515	64	-452	0.12
LVW-2B	5.5	18.4	17.42	0.27	1.6	575	22	-553	0.04	544	36	-508	0.07
LVW-3A	2.7	16.8	15.23	1.15	0.6	525	-13	-538	-0.02	476	14	-462	0.03
LVW-3B	2.7	16.4	14.75	1.07	0.7	513	-16	-529	-0.03	461	16	-445	0.03
LVW-4A	2.8	15.3	13.84	0.9	1.2	478	-8	-486	-0.02	433	27	-405	0.06
LVW-4B	3.9	15.3	14.37	0.55	1.4	478	4	-474	0.01	449	32	-417	0.07

removed through weekly flushing; and (2) to dissolve all possible soluble secondary minerals formed by sulphide oxidation during the period from the termination of the humidity cell tests to the time of sampling the solids in the cells for post-humidity cell solid analyses. The information gathered in this test is used to complete a closed-circle mass balance calculation. The leach procedure followed was that given in Morin and Hutt (1997), with minor modifications. The results are documented in Appendix IV-3.

#### 4.3.2.2 Acid-Base Accounting

The analytical certificates for post-humidity cell ABA's are attached in Appendix IV-4 and a summary is shown in Table 4.1. Acronyms used for reporting are the same as in Table 2.4 and have been explained in Section 2.5.

#### 4.3.2.3 Whole-Rock Composition

Post-humidity cell whole-rock geochemical data are in Appendix IV-5. The results are summarized in Table 4.2.

Table 4.2 Whole-Rock Composition of Post-Humidity Cell Solids

Components	Content in samples (wt%)			
	LVW-1A	LVW-2A	LVW-3A	LVW-4A
CaO	3.77	0.78	0.59	0.35
MgO	5.17	3.24	2.31	3.32
K <sub>2</sub> O	0.53	0.65	0.75	0.76
Na <sub>2</sub> O	0.34	0.62	0.42	0.36
Al <sub>2</sub> O <sub>3</sub>	6.37	7.86	7.56	9.26
SiO <sub>2</sub>	26.70	37.50	39.00	38.80
Fe(t)	22.94	21.05	18.67	20.70
MnO	0.47	0.15	0.12	0.10
TiO <sub>2</sub>	0.35	0.41	0.48	0.50
S(total)	15.50	15.70	12.70	12.10
SO <sub>4</sub>	1.94	1.45	7.60	2.39
S <sup>o</sup>	0.79	0.32	0.47	0.59
P <sub>2</sub> O <sub>5</sub>	0.12	0.15	0.13	0.17
CO <sub>2</sub>	8.40	2.60	1.17	1.39
LOI	19.70	16.10	19.80	15.30
Cu	0.12	0.08	0.08	0.09
Pb	0.04	0.04	0.02	0.00
Zn	0.32	0.58	0.15	0.12
As	0.07	0.10	0.07	0.03
Total*	92.50	92.48	89.29	89.65

\*Excluding LOI (loss on ignition) from summation.

Table 4.2 should be read in comparison with Table 2.3 (pre-humidity cell whole-rock analyses). Table 4.2 shows that the tailings in cell LVW-1A are less siliceous than those in the other cells, which is consistent with the data in Table 2.3. The sulphide sulphur contents range 9.7-14.9% (or approximately 18-28% pyrite), which is considerably less than in the unoxidized tailings (Table 2.3). The inorganic CO<sub>2</sub>% ranges 1.2-8.4% (or about 2.7-19% carbonate in CaCO<sub>3</sub> equivalence), which is less than those of the pre-humidity cell solids. The pre- and post-humidity cell CO<sub>2</sub> and total sulphur concentrations are compared in Figure 4.1.

#### 4.3.2.4 Mineralogy

The post-humidity cell mineralogy was determined by a combination of XRD, electron microprobe analysis, and optical microscopy. Mineral abundances were obtained from point counting and electron microprobe analyses on polished thin sections. A modal interpretation was calculated using the identified minerals and the whole-rock composition. The results are found in Appendix IV-6. A summary of the post-humidity cell mineralogy and the specific gravity of the weathered tailings is shown in Table 4.3. Illustrative photomicrographs of some of the minerals observed are presented in Figures 4.2 and 4.3.

##### *Primary Minerals*

The dominant silicates are quartz, chlorite, andalusite, chloritoid, muscovite, albite and orthoclase. Andalusite and chloritoid have not been reported in the pre-humidity cell mineralogy. These are primary silicates frequently found in Fe-rich aluminous alteration zone that have undergone upper-greenschist metamorphism. Andalusite has no acid neutralization capacity whereas Mg-chloritoid is most likely slow-reacting and probably possesses a neutralization potential similar to that of clinocllore.

Carbonates are much more abundant in cell LVW-1A than in the other cells. The carbonates identified in these weathered solids are Mg-Mn ankerite and Mg-Mn siderite, similar to those found in the pre-humidity cell mineralogy. The total carbonate content ranges 0.8-19% by mass, which is in good agreement with the inorganic CO<sub>2</sub> content of the solids (Table 4.2).

Magnetite is the dominant primary iron-oxide mineral. Accessory ilmenite accounts for most of the TiO<sub>2</sub>, with the remainder accounted for by minor rutile.

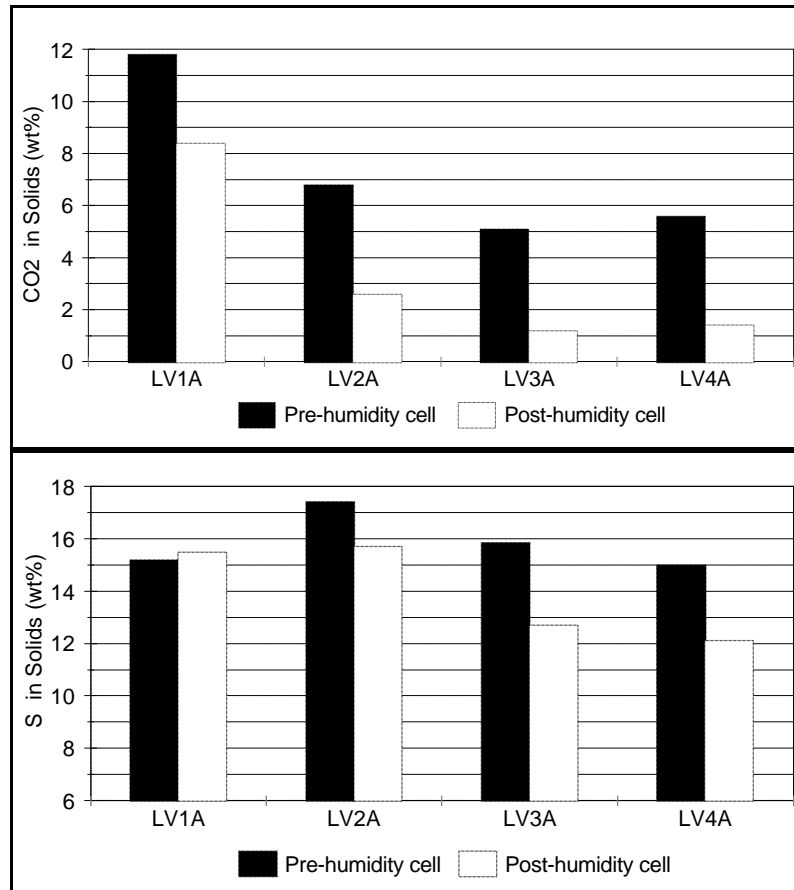


Figure 4.1 Pre- and Post-Humidity Cell CO<sub>2</sub> and S<sub>T</sub> Concentrations

The dominant sulphide mineral is pyrite, which occurs in two liberated grain size populations (Figure 4.2 a, b). The pyrite content ranges 20-32% by mass, which is consistent with the whole-rock geochemistry (Table 4.2). There is about 5% pyrrhotite in the weathered solids from LVW-1A, but less than 1% in the other cells. Sphalerite is a trace component in LVW-1A, 2A and 4A. Chalcopyrite was observed in LVW-1A and 2A as small inclusions in pyrite. Arsenopyrite was only observed in LVW-1A as liberated grains. Galena was seen only in LVW-2A rimming pyrite and as liberated grains.

### Secondary Minerals

The secondary minerals are gypsum and trace amounts of unidentified Mg-sulfate (hexahydrate?); unidentified Fe-sulfate (rozenite? melanterite?), iron hydroxide (goethite?) and probable chlorite-smectite interlayering each other. The iron hydroxide often causes a reddish stain to the matrix and to some fragments, as shown in Figure 4.3. Some fragments appear to have been impermeable and are stainless.

Table 4.3 Post-Humidity Cell Mineralogy

Mineral	Post-Humidity Cell Sample No.			
	LVW-1A	LVW-2A	LVW-3A	LVW-4A
Quartz	18.0	31.5	26.5	35.1
Andalusite	0.5	1.2	1.4	2.2
Orthoclase	0.9	4.0	1.1	2.4
Albite	1.8	0.5	4.0	2.4
Chlorite	8.1	9.8	16.4	11.7
Chloritoid	0	0.7	0	2.5
Anthophyllite	0	1.2	0	0
Muscovite	1.0	1.1	9.2	3.9
Mg-Ankerite	9.5	0.6	0	0
Mg-Siderite	11.9	12.3	0.8	5.7
Magnetite	7.1	2.0	3.4	1.2
Ilmenite	0.8	0.9	1.0	3.3
Rutile	0.7	2.5	0	1.0
Pyrite	31.6	27.4	19.6	24.5
Pyrrhotite	4.7	0.9	1.0	0
Sphalerite	0.7	0.8	0	1.0
Arsenopyrite	1.0	0	0	0
Chalcopyrite	0.7	0.8	0	0
Galena	0	0	3.3	0
Gypsum*	0.3	1.4	8.1	2.2
Goethite	0.7	0	3.7	0
Specific Gravity	3.61	3.31	3.15	3.21
* Including other sulphates such as those of iron				

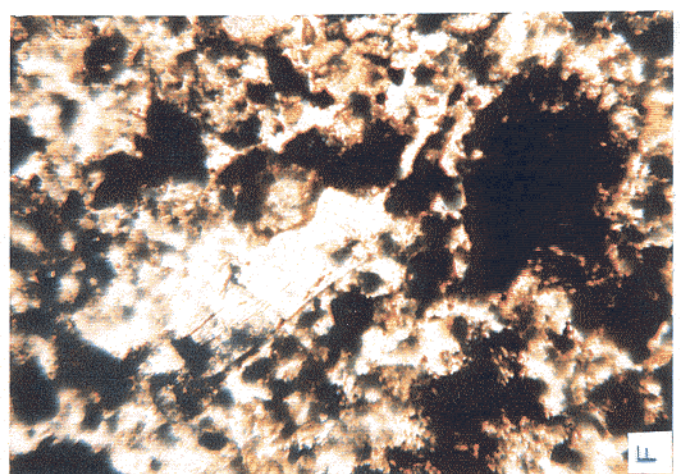
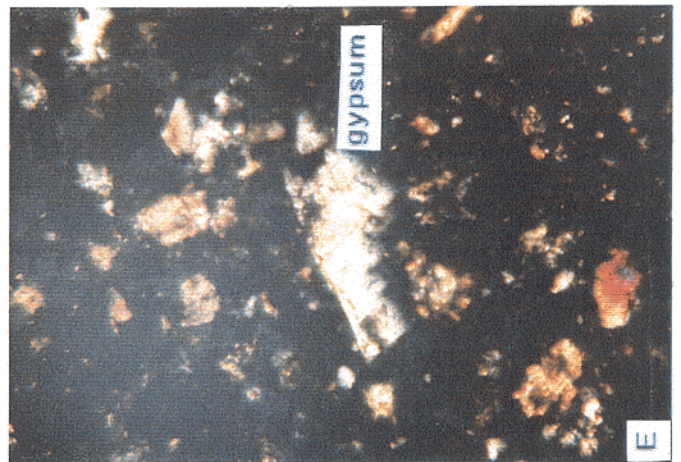
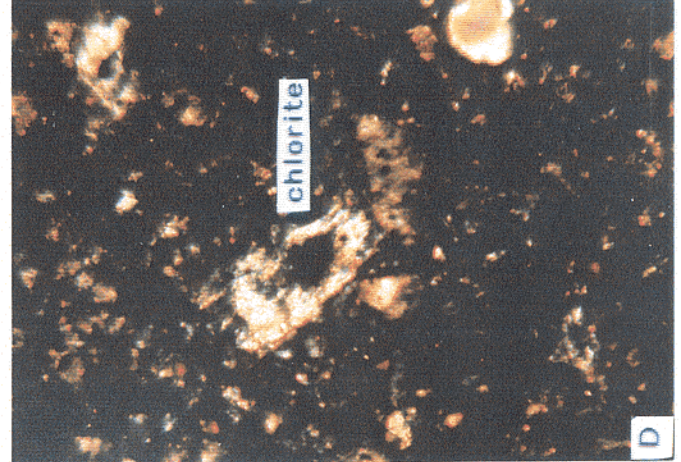
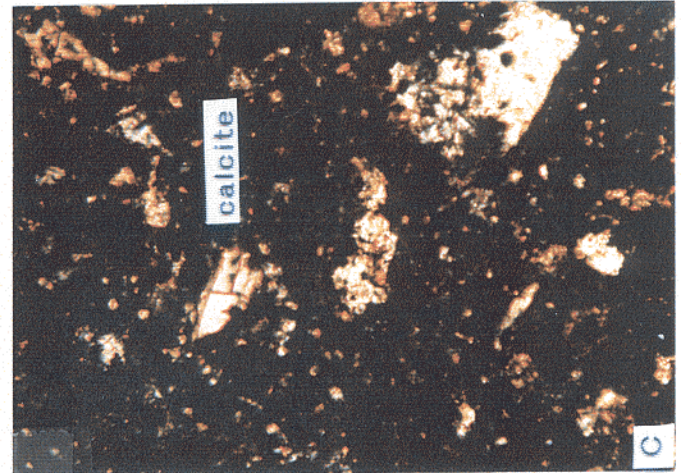
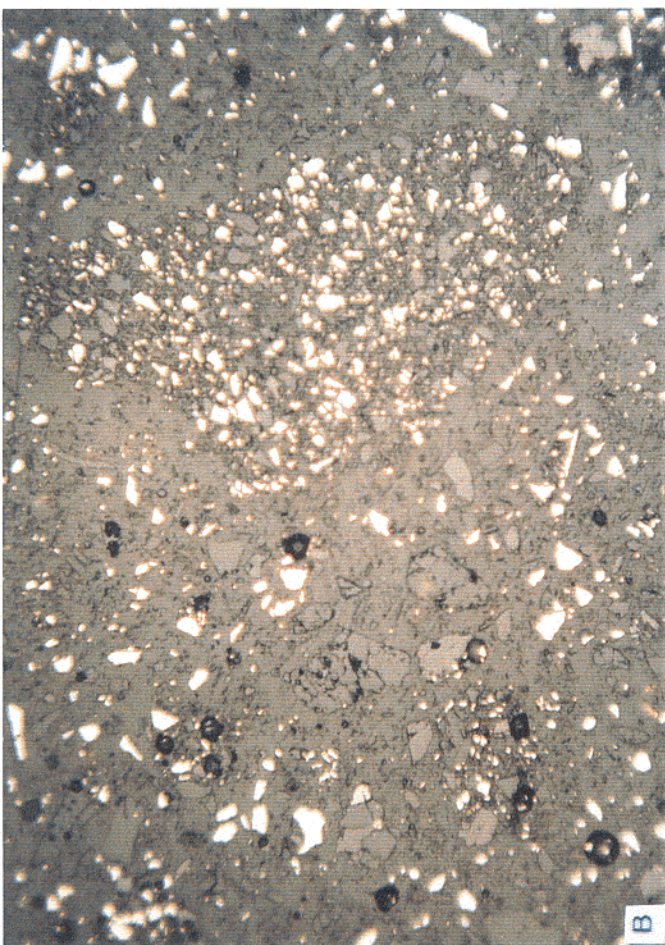
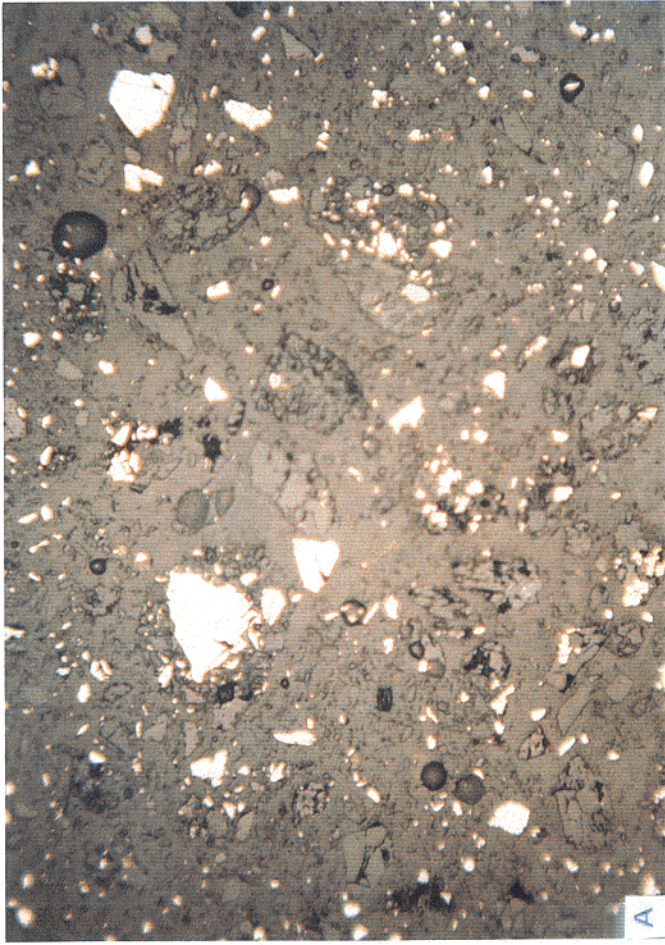
Figure 4.2 Post-Humidity Cell Mineralogy - Photomicrographs of Sample LVW-1A

- a) This view shows the two grain size populations of pyrite. Note that the pyrite grains are anhedral to subhedral and are largely liberated. Reflected light, 80X.
- b) Large aggregates rich in fine-grain pyrite. Reflected light, 80X.
- c) Carbonate fragments showing the rhombohedral cleavage. Polarized light and crossed nichols, 80X.
- d) Weathered grain of chlorite (smectite?). Polarized light and crossed nichols, 132X.
- e) Large grain of gypsum showing the characteristic low birefringence (grayish-white). Polarized light and crossed nichols, 132X.
- f) Same as e) but in polarized light only. Note the cleavage traces.

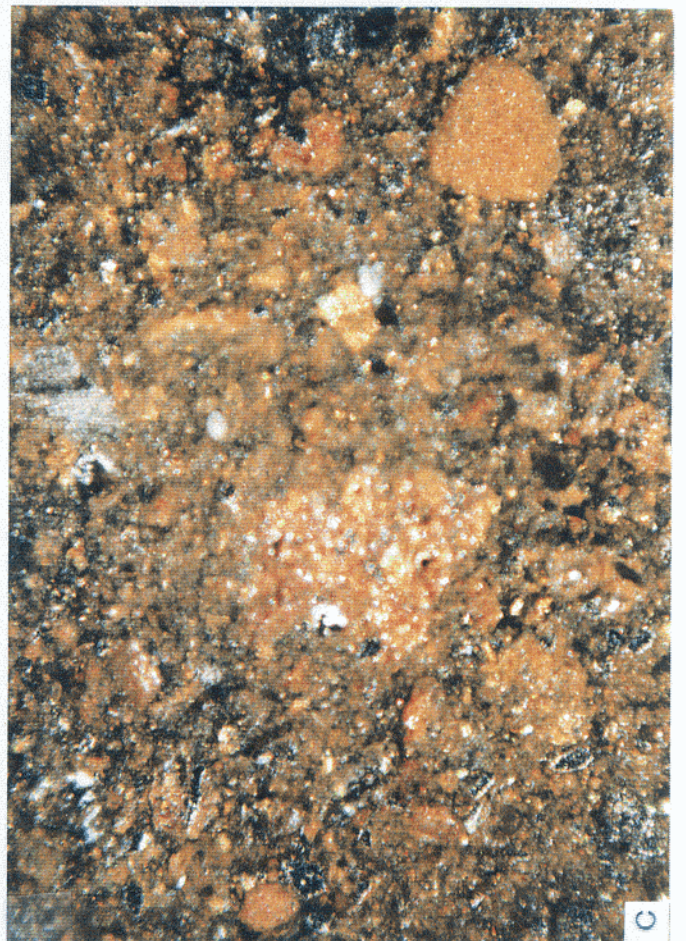
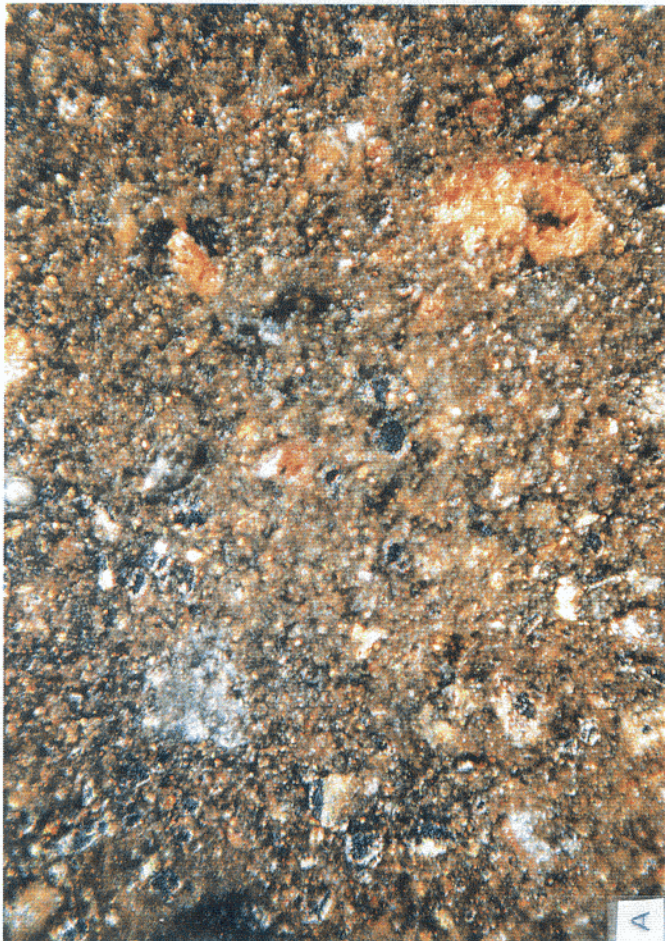
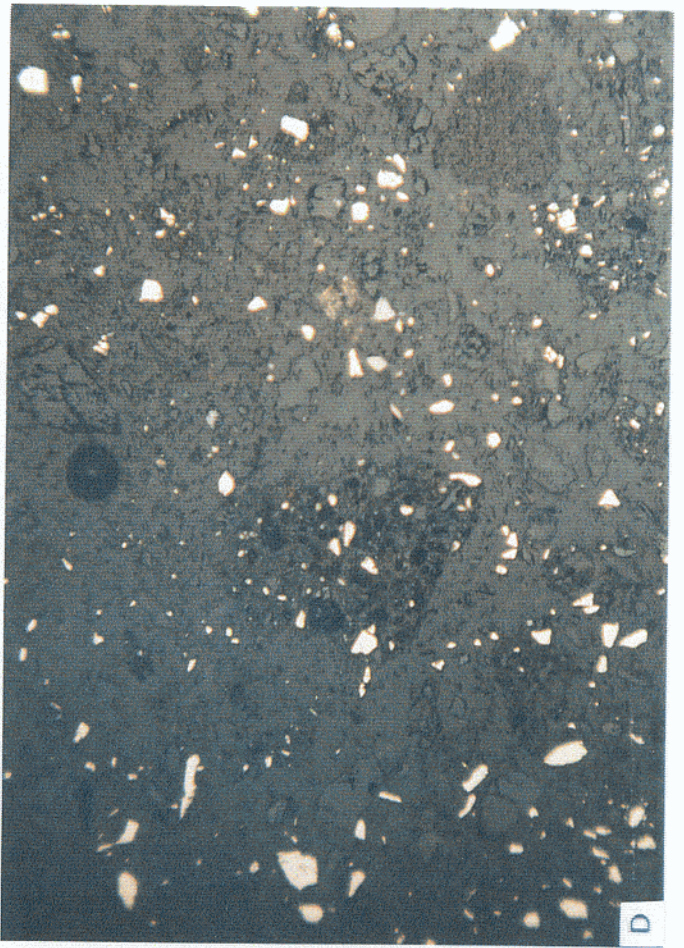
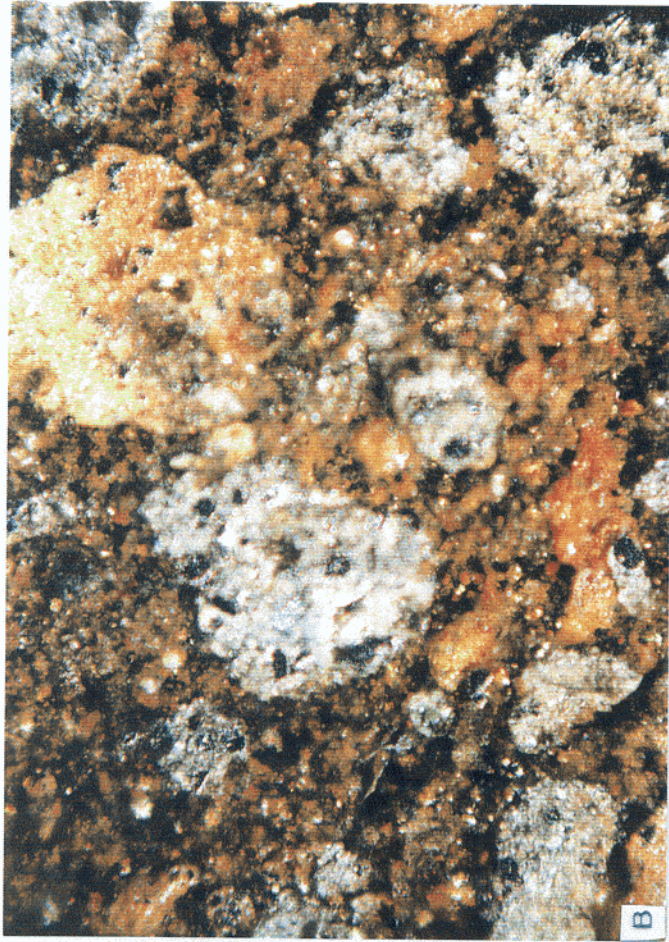
Figure 4.3 Post-Humidity Cell Mineralogy - Photomicrographs of Samples LVW-2A, -3A, and -4A

- a) View showing the red staining on some fragments caused by secondary iron hydroxide minerals. Note that some fragments appear to have been impermeable and are stainless. Inclined light, 80X. LVW-2A.
- b) Same as a) but for LVW-3A.
- c) Same as a) but for LVW-4A. Note the increase in stained fragments compared with A.
- d) Same field as in c) but taken in reflected light. Both magnetite (gray) and pyrite (pale-yellow) grains are present.











## 4.4 Interpretation

### 4.4.1 Humidity Cells

#### 4.4.1.1 Assumptions

As pointed out by Morin and Hutt (1999), there are two types of humidity cells: the “Sobek cells” and the “non-Sobek cells”. The Sobek cells attempt to measure the primary (or intrinsic) oxidation and neutralization rates by flushing out all reaction products in each leaching cycle using measures such as large quantities of flushing water, long leachant-solid contact time, and sample bed disturbance. The “non-Sobek cells” in general attempt to simulate the field weathering conditions in the laboratory and do not make special efforts to remove reaction products. The Sobek cell conditions may be approached to various degrees in the lab, but rarely completely achieved. This is because under most circumstances removal of secondary mineral precipitates from humidity cells cannot be 100% efficient. Nevertheless, Sobek cells are one of the best means for measuring the empirical primary oxidation and neutralization rates for tailings exposed to air. The humidity cells in this study were intended to be operated as Sobek cells.

The basic interpretation of the humidity cell test results is to calculate the rate of sulphide oxidation, the rate of acid neutralization, and to predict the lag period. The following assumptions were necessary for the interpretation of the Sobek humidity cell test results.

1. *After the initial flush-out of accumulated sulphate and prior to onset of acid generation in the cell, no sulphate accumulation occurs in the humidity cell as solid precipitates; all newly-generated sulphate is flushed out at the end of each cycle. In addition, after the initial flush-out, sulphide oxidation is the only source of sulphate; the samples contain no other sulphate-releasing minerals.*

This assumption paves the road for using leachate  $\text{SO}_4^{2-}$  concentrations for the calculation of sulphide oxidation rates. It will be shown later that sulphate accumulation in the solid phase did occur - especially after the humidity cell had turned acidic and sulphide oxidation rate was very high. However, this assumption is reasonable when the humidity cell is still neutral and when the sulphide oxidation is relatively slow. As only the pre-acid generation period is used in computing the sulphide oxidation rate for the purpose of lag time prediction, this assumption should essentially hold true. The assumption of sulphide oxidation being the sole sulphate source is true for the present study as the pre-humidity cell mineralogy shows no sulphate minerals in the fresh tailings.

2. *For the period prior to the onset of acid generation, the alkalinity in the leachate is comprised of bicarbonate alkalinity only.*

The assumption is necessary for using the measured alkalinity concentrations for calculating  $\text{HCO}_3^-$  concentrations, which are necessary to complete the ionic charge balance loop. This assumption is supported by the pre-humidity cell mineralogy, which indicates a lack of sources of amphoteric anions other than carbonates, such as phosphate minerals.

3. *The only sources of dissolved Ca and Mg in the leachate are carbonates.*

This assumption is necessary for using leachate Ca and Mg concentrations to calculate carbonate mineral dissolution rate. This is only an approximation as the dissolution of clinocllore (chlorite) also contributes Mg to the leachate.

4. *Dissolved Na and K come from dissolution of silicate minerals.*

This assumption is necessary for using leachate Na and K concentrations to calculate silicate mineral dissolution rates. This is only an approximation and likely results in under-estimation of silicate dissolution rates, as silicate minerals also contribute other cations such as  $\text{Ca}^{2+}$ ,  $\text{Mg}^{2+}$ ,  $\text{Mn}^{2+}$  to the leachate when they dissolve.

In summary, the above assumptions are necessary for interpretive calculations of the humidity cell results. Some of these assumptions can be checked against post-humidity cell solid analyses for proof of their correctness. This is done in later sections.

#### 4.4.1.2 Principles of Interpretive Calculation

The interpretive calculations are performed entirely on the basis of leachate chemistry. In each leachate, the electrical neutrality of the solution must be obeyed. In our present case, this translates approximately to the equation:

$$2\{\text{SO}_4^{2-}\} + \{\text{HCO}_3^-\} = 2\{\text{Ca}^{2+}\} + 2\{\text{Mg}^{2+}\} + \{\text{K}^+\} + \{\text{Na}^+\} + 3\{\text{Al}^{3+}\} + 3\{\text{Fe}^{3+}\} + 2\{\text{Fe}^{2+}\} + 2\{\text{Mn}^{2+}\} + 2\{\text{Cu}^{2+}\} + 2\{\text{Zn}^{2+}\} \quad (4.1)$$

where the braces “{ }” indicate unspicated concentrations in mmol/L. If we convert the concentrations to mg  $\text{CaCO}_3$  eq/L (which is equal to meq/L times 50), apply a constant factor to all concentration terms to transform from a per L of leachate to a per kg of sample basis, and neglect the ferric contribution, Equation (4.1) can be rewritten as

$$[\text{SO}_4^{2-}] + [\text{HCO}_3^-] = [\text{Ca}^{2+}] + [\text{Mg}^{2+}] + [\text{K}^+] + [\text{Na}^+] + [\text{Al}^{3+}] + [\text{Fe}^{2+}] + [\text{Mn}^{2+}] + [\text{Cu}^{2+}] + [\text{Zn}^{2+}] \quad (4.2)$$

where the square brackets “[ ]” indicate loadings in the weekly leachate expressed in mg  $\text{CaCO}_3$  eq/kg/week. The loading terms in Equation (4.2) can be interpreted as follows:

$$[\text{SO}_4^{2-}] = \text{total acidity produced from sulphide oxidation};$$

$[\text{HCO}_3^-]$  = residual alkalinity in leachate;  
 $[\text{Ca}^{2+}] + [\text{Mg}^{2+}]$  = total alkalinity production from carbonate dissolution;  
 $[\text{K}^+] + [\text{Na}^+]$  = total alkalinity production from silicate dissolution; and  
 $[\text{Al}^{3+}] + [\text{Fe}^{3+}] + [\text{Mn}^{2+}] + [\text{Cu}^{2+}] + [\text{Zn}^{2+}]$  = residual acidity in leachate.

Thus (4.2) can be written as

$$\text{Total acidity production} + \text{residual alkalinity} = \text{total alkalinity production} + \text{residual acidity} \quad (4.3)$$

or

$$\text{Total acidity production} - \text{residual acidity} = \text{total alkalinity production} - \text{residual alkalinity} \quad (4.4)$$

where *total alkalinity production* is the sum of alkalinity production from carbonate dissolution and silicate dissolution. The left side in Equation (4.4) is in fact acidity neutralized; the right side is alkalinity used to neutralize acidity. Therefore (4.4) becomes

$$\text{Acidity neutralized} = \text{alkalinity used to neutralize acidity} \quad (4.5)$$

In the above equations, the residual alkalinity is taken as that measured by titration of the leachate to an end pH of 4.5 with HCl; the residual acidity is the acidity measured by titration of the leachate to an end pH of 8.3 with NaOH. The acidity neutralized by silicate minerals was calculated from the dissolved K and Na concentrations in the leachate. The acidity neutralized by carbonates was calculated from the dissolved Ca and Mg concentrations. The total acidity neutralized is the sum of acidity neutralized by carbonates and that neutralized by silicates. The total acidity production was calculated from dissolved sulphur analyses. AP depletion rate was calculated from the total acidity produced from oxidation. Finally NP depletion rate was calculated by summing the alkalinity used to neutralize acidity and residual alkalinity in the leachate.

The mean AP and NP depletion rates for each humidity cell were calculated by averaging their weekly rates after cycle 5 but before onset of acid generation (defined as the time when the leachate pH drops below 5.0). Since in cycles 1 to 5 the accumulated oxidation products in the test samples were being flushed, the AP and NP depletion rates calculated for this period would be biased. This is why the first five cycles were excluded from mean rate calculations. Since one cannot use the AP and NP depletion rates after the onset of acid generation for prediction of the lag time, data for cycles after the onset of acid generation were also excluded from mean rate calculations. For LVW-1A, -1B, -2A and -2B, the above calculation was performed for weeks 6-65. For LVW-3A, and -3B, the calculation was done using data from weeks 6-27, and for LVW-4A and -4B, the weeks used were 6-41. The calculations for LVW-1A, -1B, -2A and -2B excluded weeks 66-80 because during this period the experimental conditions underwent a major change as a result of the commencement of weekly sample bed

disturbances as part of the experimental design. Predictions based on the mean AP and NP depletion rates are calculated as follows:

- < The “years before NP depletion” were calculated for each test by dividing the total available NP with the mean NP depletion rate and applying necessary unit conversion factors.. (The concept of *total available NP* is further discussed later.)
  
- < The “years before AP depletion” were calculated for each test by dividing the SAP with the mean AP depletion rate and applying necessary unit conversion factors. For non-potentially net acid generating materials this provides a true measure of the length of sulphide oxidation. However for potentially net acid generating materials, this is only a reference number, because after the onset of acid generation the sulphide oxidation rate will be higher and consequently the true duration of sulphide oxidation will be shorter than predicted with this figure.
  
- < The “safe NP/AP ratio”, defined as the ratio of available NP/SAP above which the sample would not generate an acidic leachate, was calculated as (mean NP depletion rate)/(SAP depletion rate).

Results of the calculation for each individual humidity cell are presented in Appendix IV-2. A summary of the results for all eight tests is given in Table 4.4.

Table 4.4 Summary of Interpretive Calculations of Humidity Cell Test Results

Humidity Cell No. LVW-	S(T) %	AP	NP from ABA	Total Avail. NP*	NNP	NP*/AP Ratio	Mean Values for All Weeks after the Week 5 but before Onset of Acid Generation								Yrs before NP Depl or AMD Onset	Res S(T) at NP Depl or AMD Onset	Safe NP/AP Ratio
							Tot Acidity Prod'n	Acid. Neut. by Carb	Acid Neut. by Silicates	Tot Acidity Neut'd	Res. Alk	Res Acidity	AP Depl Rate	NP Depl Rate			
							mg CaCO3/kg/wk										
1A	15.21	475	182	121	-355	0.25	301	306	11	317	28	8	301	334	7.0	10.0	1.11
1B	15.21	475	182	123	-352	0.26	311	312	11	323	32	5	311	344	6.9	9.9	1.10
2A	17.45	545	101	64	-481	0.12	397	389	11	400	22	8	397	411	3.0	14.3	1.03
2B	17.45	545	101	66	-479	0.12	534	526	11	537	17	11	534	543	2.3	14.3	1.02
3A	16.31	510	75	66	-443	0.13	536	521	13	534	15	12	536	536	2.4	13.9	1.00
3B	16.31	510	75	66	-443	0.13	607	609	13	621	18	12	607	627	2.0	14.0	1.03
4A	15.57	487	74	63	-423	0.13	628	621	10	631	15	11	628	636	1.9	13.2	1.01
4B	15.57	487	74	63	-423	0.13	756	750	11	760	19	11	756	769	1.6	13.2	1.02
<b>Mean</b>	<b>16.14</b>	<b>504</b>	<b>108</b>	<b>79</b>	<b>-425</b>	<b>0.16</b>	<b>509</b>	<b>504</b>	<b>11</b>	<b>515</b>	<b>21</b>	<b>10</b>	<b>509</b>	<b>525</b>	<b>3.4</b>	<b>12.9</b>	<b>1.04</b>
Median	15.94	498	88	66	-433	0.13	535	523	11	535	19	11	535	539	2.4	13.6	1.03
Std. Dev.	0.92	29	47	26	49	0.06	161	158	1	158	6	3	161	154	2.2	1.8	0.04
Max	17.45	545	182	123	-352	0.26	756	750	13	760	32	12	756	769	7.0	14.3	1.11
Min	15.21	475	74	63	-481	0.12	301	306	10	317	15	5	301	334	1.6	9.9	1.00

\* Calculated from leachate chemistry based on Mg-ankerite and Mg-Mn-siderite abundances.

4.4.1.3 Discussion

*Leachate Charge Balance*

It is clear from the last section's discussion that the foundation of the present interpretive calculation is a charge-balanced leachate chemistry data. If the total positive and total negative charges are not equal, Equations (4.1)-(4.5) will break down, and the calculations would be meaningless.

The unspicated electrical charge balance of the leachate from every humidity cell was monitored every week. Whenever the charge imbalance became appreciable, an investigation was made to find and correct the causes. The leachate charge balance for the eight humidity cell tests over the 80-week period is shown in Figure 4.4. In the graph, % cation surplus, defined as  $(\text{total cationic charge} - \text{total anionic charge}) / (\text{average of total cationic charge and total anionic charge})$  where all charges are expressed in absolute values, is plotted against the week number. It reveals that, for most of the time, the cation surplus is within  $\pm 10\%$ . A charge imbalance within  $\pm 15\%$  indicates a reasonable analytical data quality. It is impractical and impossible (without enormous effort) to control the charge imbalance to a smaller range due to various errors in the entire sample processing and analysis chain, and due to the error propagation, magnification, and summation in that chain.

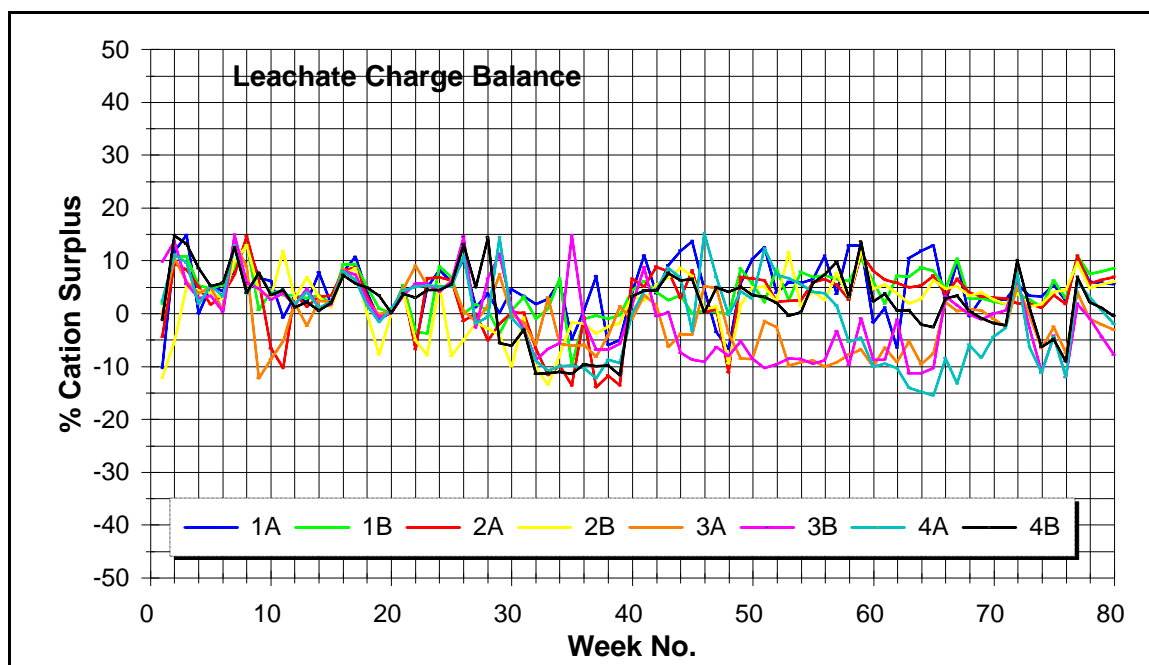


Figure 4.4 Charge Balance of Leachate from Humidity Cell Tests

*pH Evolution*

Figure 4.5 plots the evolution of pH with time for the four samples (LVW-1, -2, -3, and -4) in duplicate humidity cells (designated as A and B), for a total of eight humidity cells and a duration of 80 weeks. Conductivity is also included in the graph to show the evolution of total dissolved solids concentration in the acidification process. Generally, the figure shows good replication of pH between the duplicate cells for most of the time.

Samples LVW-1 and -2 remained neutral to the end of the test, whereas LVW-3 and -4 had acidified. The acidification of LVW-3 started around week 22 and reached a pH of 2.5 during weeks 50-65. LVW-4 started acidification a little later - at week 30; the pH dropped below 3.0 in the last 10 weeks of test.

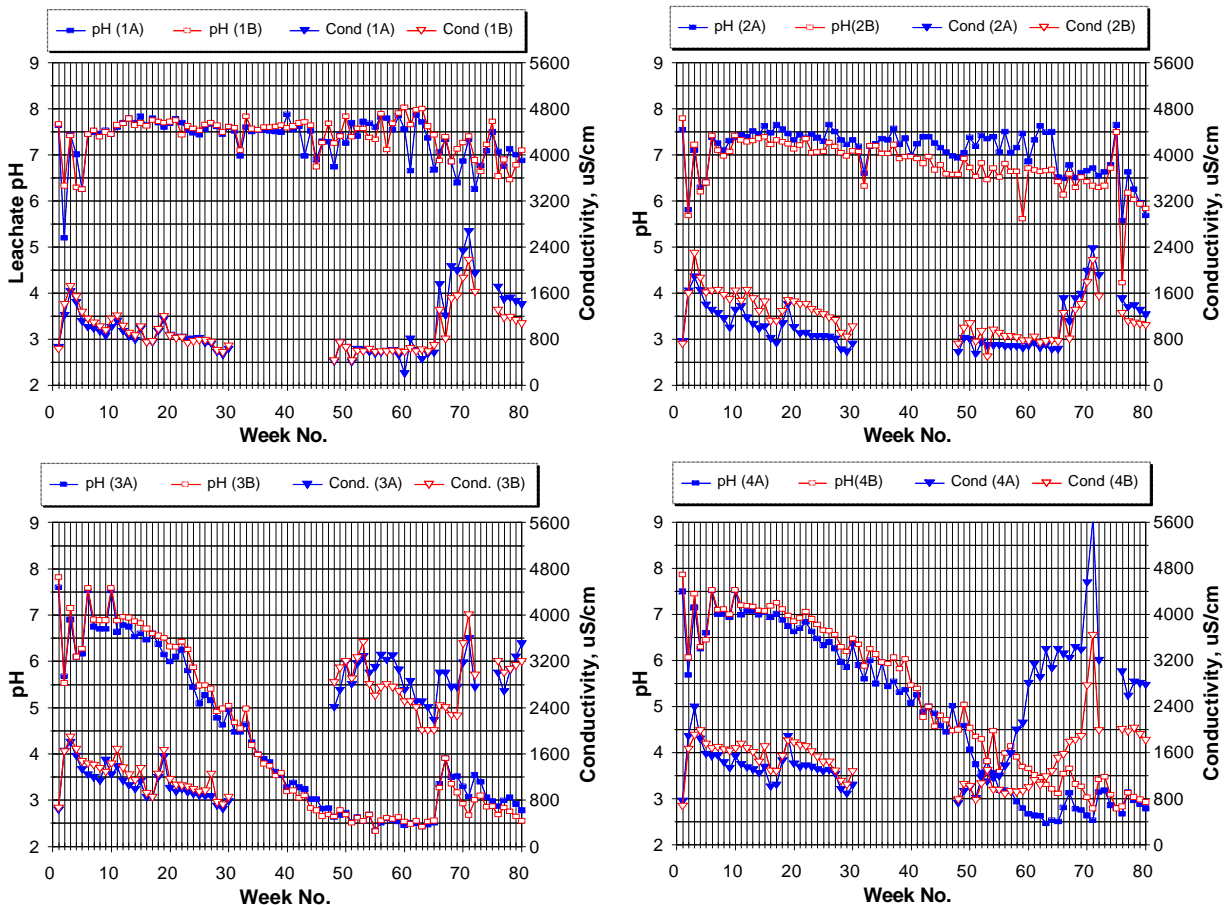


Figure 4.5 Change of Humidity Cell Leachate pH over Time (above and left, LVM-1, above and right, LVM-2, below and left, LVM-3 and below and right, LVM-4)



### *Acidity Production, Acidity Neutralization, and Mineral Depletion*

Figure 4.6 shows the variations in acidity production and neutralization over time for the eight humidity cells. It also shows AP and NP depletion, as well as the depletion of important sulphide, carbonate, and silicate minerals.

Generally, individual mineral depletion cannot be calculated from leachate chemistry. In the present study, the depletion of minerals can be calculated from the leachate chemistry because of the simple mineralogy of neutralizing minerals. The assumed compositions of the minerals consumed is given in the CANMET mineralogical report, appendix II-2, section 3, p.i. As revealed by the mineralogical studies, there are basically three minerals in the tailings providing neutralizing potential: Mg-ankerite, Mg-Mn-siderite, and clinocllore. Mg-ankerite is a carbonate of Fe, Ca, and Mg; Mg-Mn-siderite is a carbonate of Fe, Mn, and Mg; and clinocllore is a mafic silicate. Since Mg-ankerite is the only neutralizing mineral that contains Ca, all Ca in the leachate is attributed to the dissolution of ankerite, and thus ankerite depletion can be calculated from leachate Ca concentrations. Next, only two neutralizing minerals - Mg-ankerite and Mg-Mn-siderite - contain Mn; hence all Mn in the leachate is attributed to the dissolution of these two minerals. To calculate the depletion of siderite, the leachate Mn concentrations, after correcting for the contribution from ankerite (depletion already known), are employed. For calculating the depletion of clinocllore, the leachate Mg concentrations, after correcting for contributions by ankerite and siderite dissolution (both now known), are utilized.

The calculation of sulphide depletion is straight-forward. Sphalerite depletion is calculated from leachate Zn concentrations assuming that all dissolved Zn is attributable to sphalerite dissolution. The depletion of pyrite is calculated from total dissolved sulphur concentrations in the leachate after correction for contributions from sphalerite and chalcopyrite, which are usually very small. In the depletion calculation, pyrrhotite is lumped together with pyrite as pyrrhotite contents are generally small in the tailings.

The accuracy of these individual mineral depletion calculations is verified by the post-humidity cell mineralogical examinations in a later section. It suffices to say here that the depletion calculation described above is in reasonable agreement with the post-humidity cell mineralogy.

Some common features in Figure 4.6 are noted as follows:

- < All eight humidity cells show a common pattern: an initial spike in acidity production, which is believed to reflect the flush-out of the accumulated oxidation products, followed by a phase characterized by a gradual decline of acidity production rate, then followed again by a phase characterized by stabilized acidity production rate. The initial flush-out is seen to last five weeks for all cells. This is why the first five weeks were excluded from the calculation of average AP and NP depletion rates.
- < For LVW-3A, -3B, -4A, and -4B, the acidity production accelerated at the onset of acid generation, signified by leachate pH dropping below 4.0-5.0. This phenomenon

has long been realized: when the tailings become acidic, the acidophilic bacteria, mainly *thiobacillus ferrooxidans*, thrive and accelerate the acid generation. Estimating from the slope changes of the AP depletion curves, the acceleration factor is between 2 and 3, in agreement with the range reported in the literature.

- < There is another spike in acidity generation for all eight humidity cells in the period from week 66 to week 80. The explanation for this is the following change of experimental conditions. From week 1 to week 65, the humidity cell tests were operated with an undisturbed sample bed. Starting with week 66, the sample bed was disturbed manually every week to expose fresh surfaces. Theoretically, if the sample bed is reasonably dried during the dry cycle, it should allow full access of oxygen throughout the sample bed, and thus whether the sample bed is disturbed or not should not affect the rate of acidity production and neutralization. The intention in disturbing the sample bed was to see if this argument holds true for this study. Obviously, it does not, as the sample disturbance drastically elevated the acidity production. This can be explained by the fine nature of the tailings and by the observation that the tailings retained moisture quite well even during the dry cycles, preventing oxygen from fully accessing the interior of sample bed. Coinciding with the disturbance of the sample beds, acceleration of sulphide oxidation occurred in all cells, suggesting exposure of new sulphide surfaces. The pH exhibited an up-surge in LVW-3A and -3B, indicating exposure of new neutralizing mineral surfaces.
  
- < The acidity neutralized by carbonates (this includes the contribution from clinocllore in the present case because of the way the carbonate alkalinity production was calculated) followed closely the acidity produced, indicating that carbonate minerals (including clinocllore) react with the acidity produced quickly. In contrast, the portion of acidity neutralized by silicates (K- and Na-containing feldspars and possibly clay minerals) was small, indicating slow rates of dissolution, and did not vary appreciably with acidity production rates.

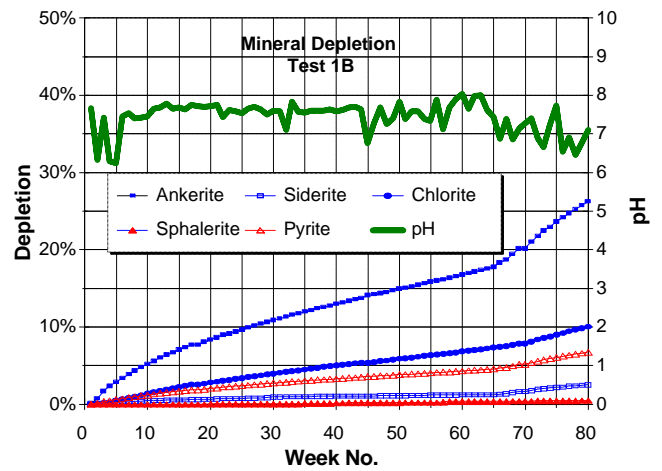
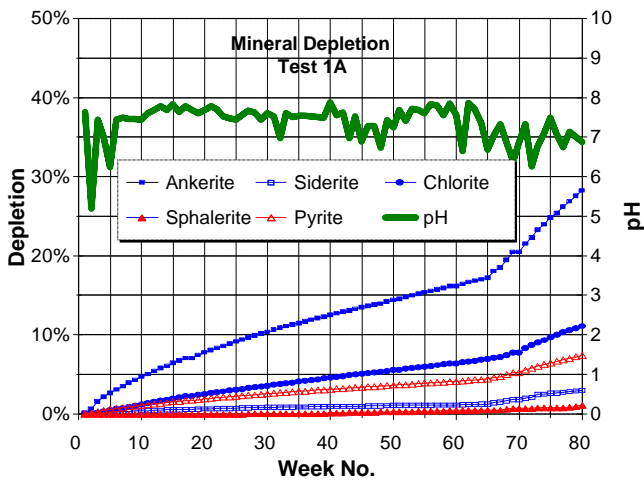
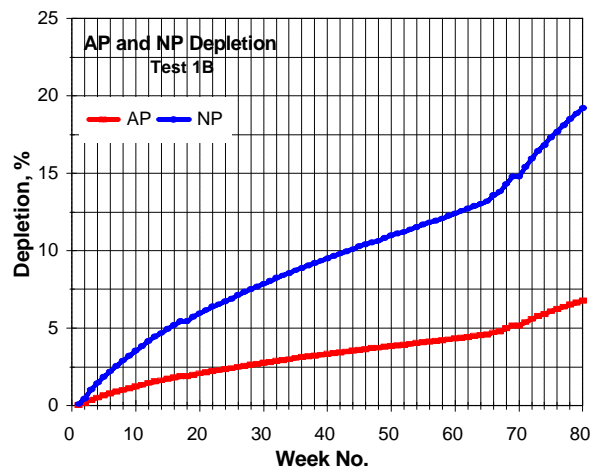
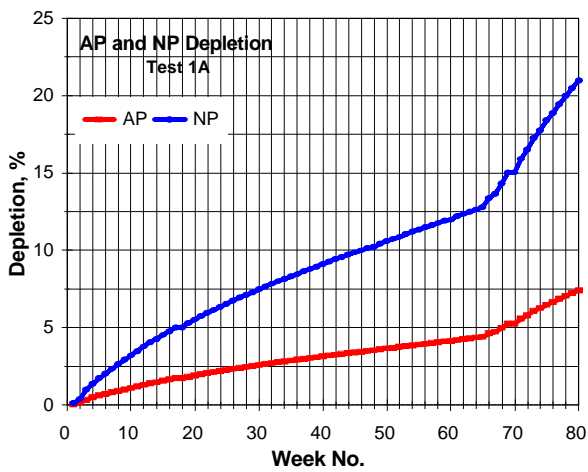
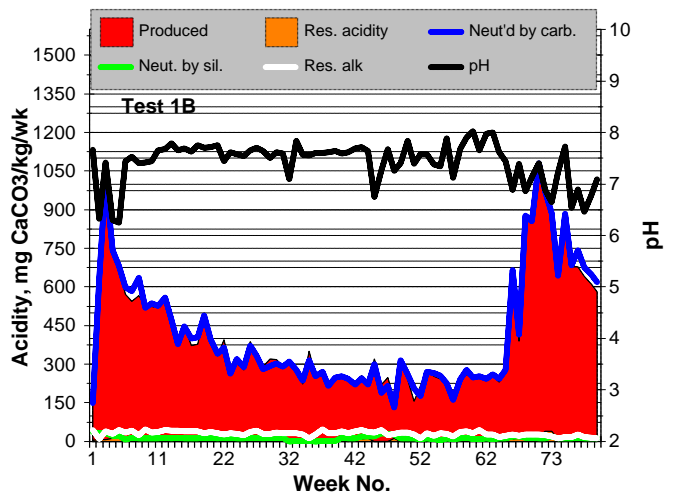
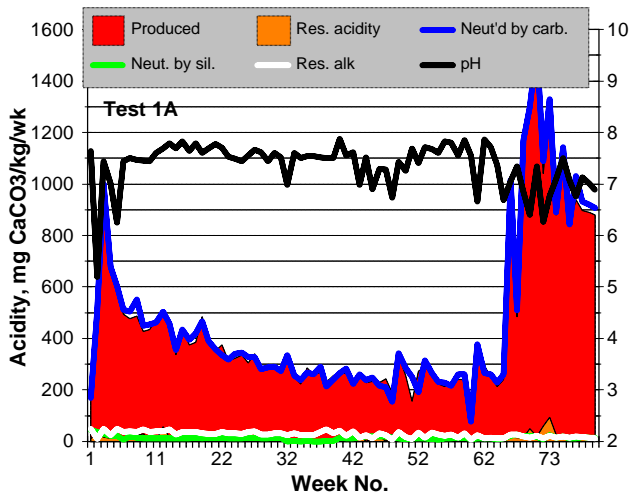


Figure 4.6 Acidity Production, Acidity Neutralization, and Mineral Depletion

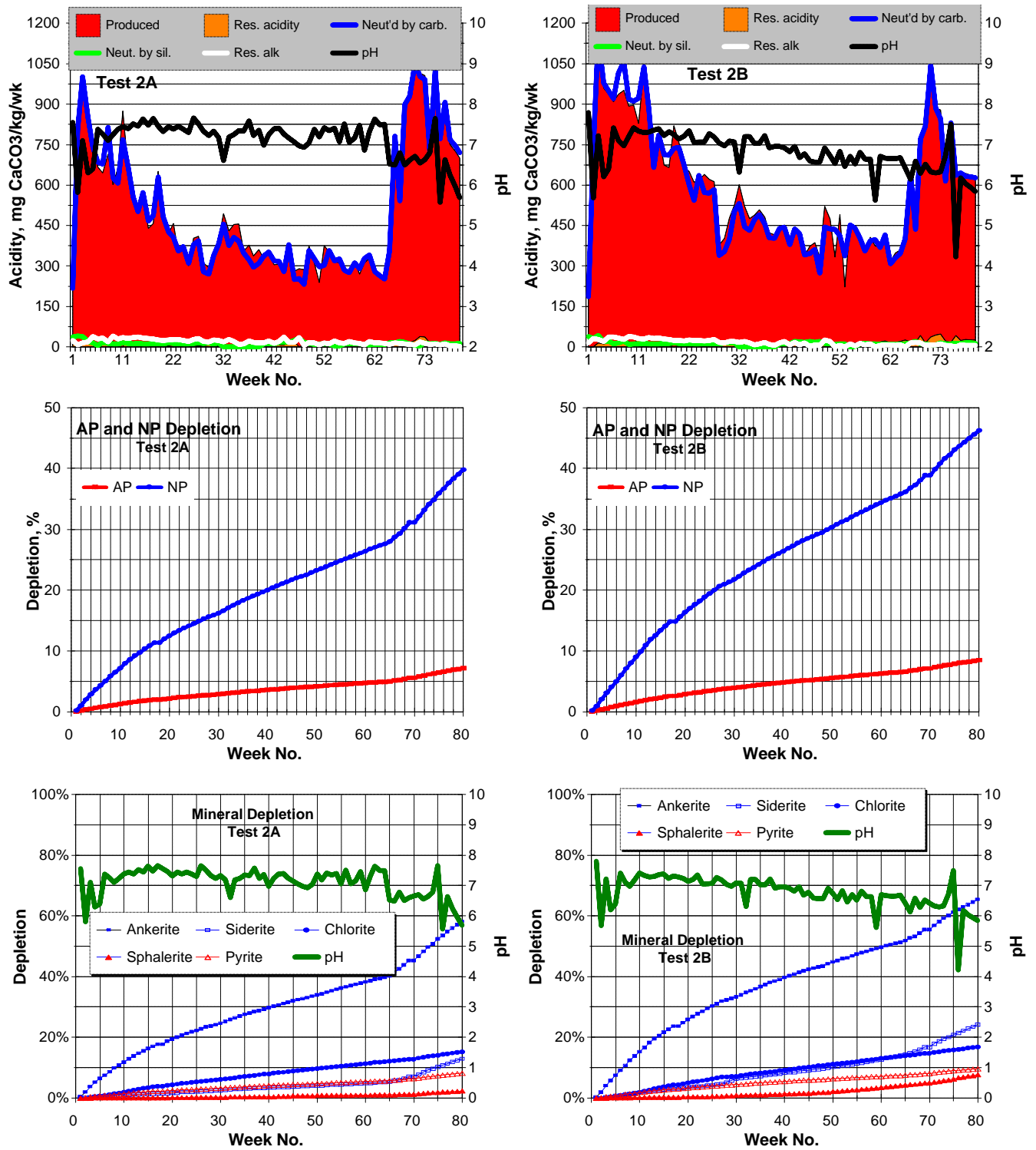


Figure 4.6 Acidity Production, Acidity Neutralization, and Mineral Depletion (Continued)

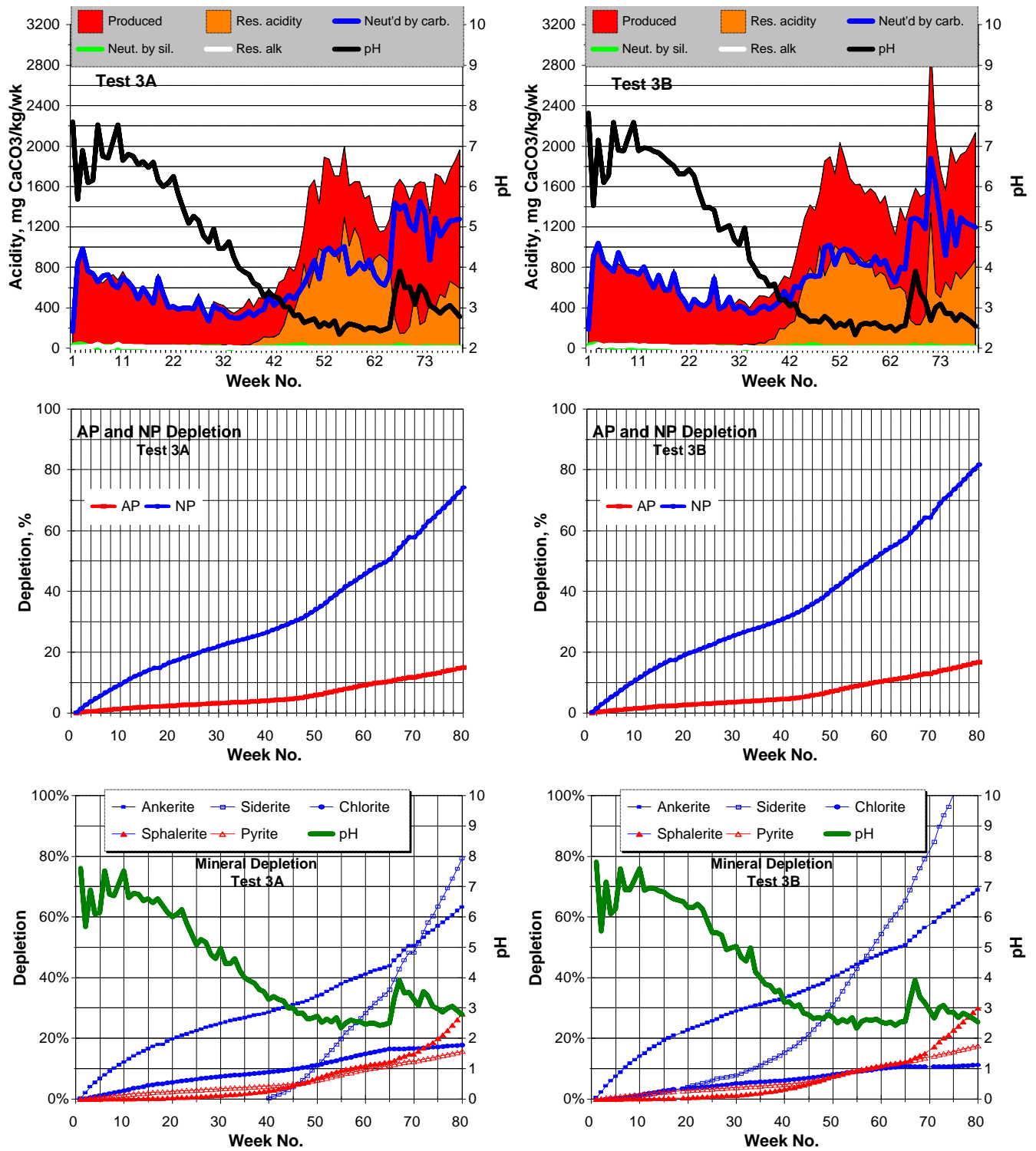


Figure 4.6 Acidity Production, Acidity Neutralization, and Mineral Depletion (Continued)

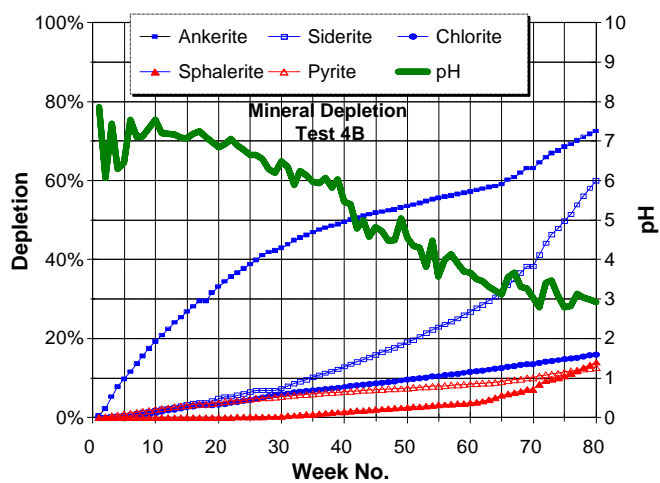
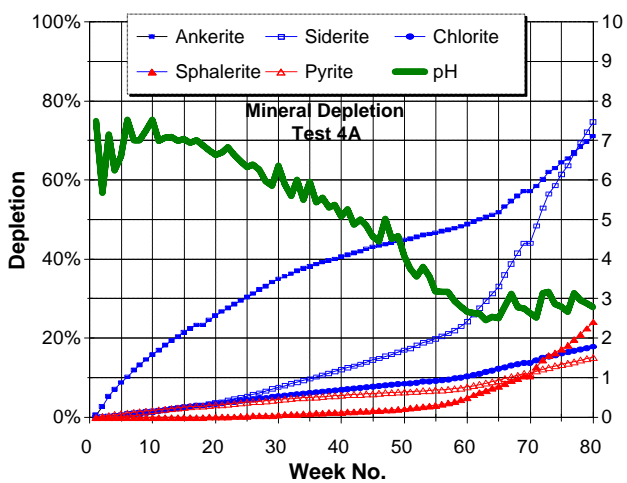
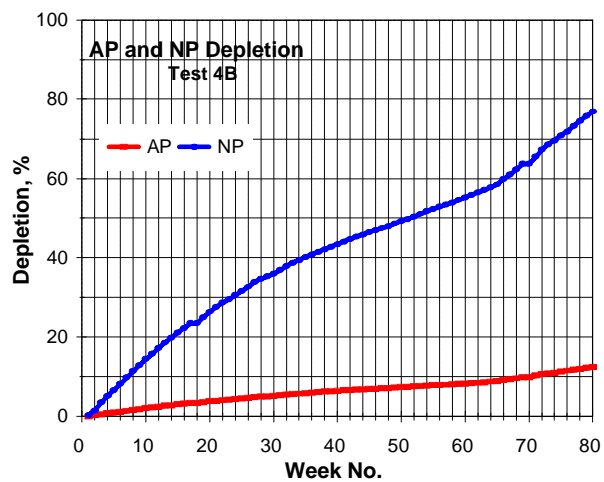
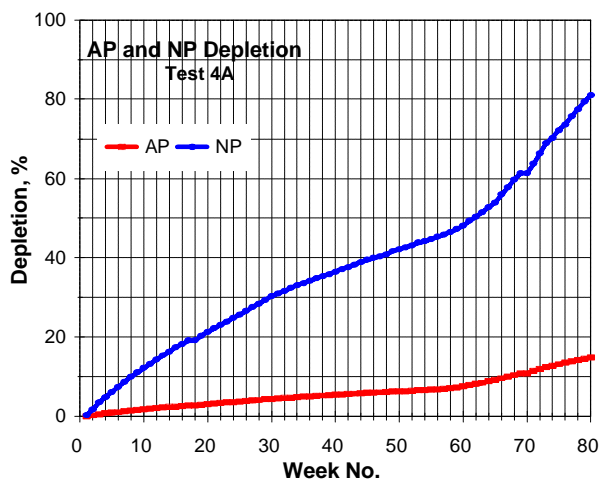
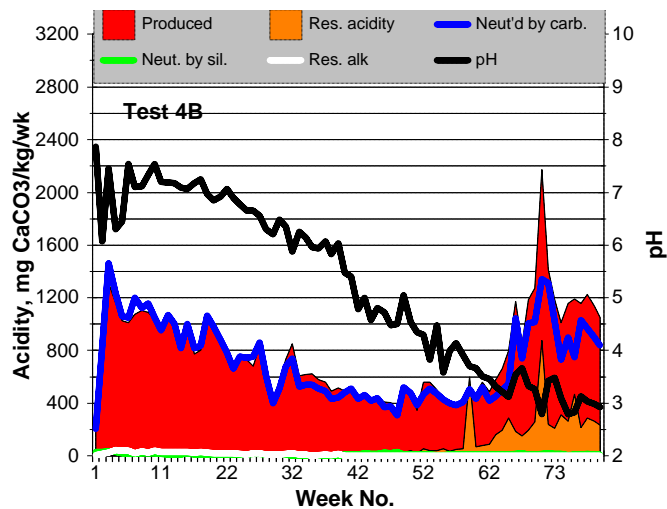
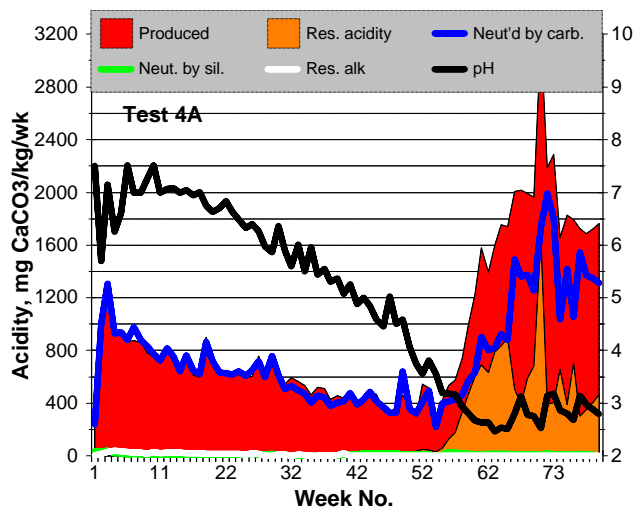


Figure 4.6 Acidity Production, Acidity Neutralization, and Mineral Depletion (Continued)

### *Neutralizing Mineral Depletion*

The order of depletion rate (i.e., slope of the depletion curve) for the three neutralizing minerals when the leachate pH is neutral is ankerite > clinochlore > siderite (Figure 4.6, third graphs). However, as soon as the leachate pH became acidic, i.e., below approximately 5.0, the rate of siderite depletion started to exceed that of ankerite. When the leachate pH dropped below 3.0 (at which time the micro-environment pH in the humidity cells, which is normally about 0.5 pH unit lower than the leachate pH, would have approached pH 2.5), there is a large increase in the dissolution rate of siderite, as seen in Figure 4.6 (Tests LVW-3A, -3B, -4A, and 4B). The effect of leachate pH dropping below 3.0 on the dissolution rate of ankerite was much less dramatic.

Another noticeable pattern in Figure 4.6 is that at neutral pH, the depletion rate of clinochlore (chlorite) is greater than that of siderite, indicating its relatively soluble nature (among silicates). Besides, the dissolution rate of clinochlore is little affected by lowering of leachate pH. These two observations are in agreement with most studies on silicate dissolution rates reported in the literature.

### *Sulphide Mineral Depletion*

The depletion of two sulphides - sphalerite and pyrite - is depicted in Figure 4.6 as well. A common observation among all cells is that sphalerite depletion rate is slower than that of pyrite when the leachate pH is greater than about 3.0, but exceeds it when the pH decreases below 3.0. This can be explained by the galvanic effect (Li, 1997). As pH decreases, the electrode potential difference between sphalerite and pyrite widens, promoting the galvanic coupling of sphalerite and pyrite particles. In the mean time, increases in ionic strength of the pore water due to acidification would enhance the conductivity of the “electrolyte” (the pore water in contact with both sphalerite and pyrite particles), also promoting galvanic reactions. The galvanic effect influences sphalerite depletion rate much more than pyrite depletion rate, because pyrite is much more abundant than sphalerite in the samples. For each sphalerite particle, there are many pyrite particles nearby to form a galvanic cell; on the contrary, for each pyrite particle, it is rare to find a sphalerite particle in the vicinity.

### *Safe NP/AP Ratio*

The “years before NP depletion” and “years before AP depletion” are simple extrapolations on the assumption that (1) the average AP and NP depletion rates calculated are valid for the future; (2) the “total available NPs” and the SAPs are available for reaction; and (3) the neutralizing materials react virtually instantly with the acid produced from sulphide oxidation. Under these assumptions, if the “years before NP depletion” are equal to the “years before AP depletion”, the neutralizing material would last just as long as would the acid-producing material; and the tailings would not generate acid. If the former is shorter than the latter, the tailings will eventually turn acidic once the total available NP is exhausted. Conversely, if the former is longer than the latter, the AP will be depleted first and the tailings will never generate

acid. The relative magnitudes of these two quantities thus provide a criterion for distinguishing net acid-generating from non-net acid generating materials. This criteria can be simply expressed as a *safe NP/AP ratio* and can be calculated as (mean NP depletion rate) / (mean AP depletion rate).

The overall average safe NP/AP ratio of the eight humidity cells is calculated according to the following formula. Note that this calculation is directly applicable only to the conditions present in the humidity cells and only for the tailings represented by the average of the eight humidity cell samples.

$$[\text{Safe NP/AP Ratio}] = \frac{\left[ \frac{1}{8} \sum_{\text{Cell}1}^{\text{Cell}8} \left( \frac{1}{n-5} \sum_{\text{Week } 6}^{\text{Week } n} \text{NP Depletion Rate} \right) \right]}{\left[ \frac{1}{8} \sum_{\text{Cell}1}^{\text{Cell}8} \left( \frac{1}{n-5} \sum_{\text{Week } 6}^{\text{Week } n} \text{AP Depletion Rate} \right) \right]}$$

where n = 65 for LVW-1A, -1B, -2A and -2B;  
 n = 27 for LVW-3A and -3B;  
 n = 41 for LVW-4A and -4B.

The number n corresponds to the week of the start of acidification (i.e., pH dropping below 5.0) or to the last week before the start of sample bed disturbances.

With the “safe NP/AP ratio” determined, the criteria for prediction of acid generation is as follows: If the total available NP/SAP ratio is equal or greater than the safe NP/AP ratio, the material is not expected to generate acid; otherwise, the material will eventually generate acid.

Figure 4.7 plots the ratio (NP depletion rate)/(AP depletion rate) individually calculated for each cell and for each week against acidity production rates. As the acidity production rate varied in the wide range of 100 to 1500 mg CaCO<sub>3</sub> eq/kg sample/week, the ratio was basically in the range of 0.8 to 1.2. If the weeks after the start of acidification for LVW-3A, -3B, -4A and -4B are excluded from the graph, the variation in the ratio reduces to the range of 0.95 to 1.2, with individual cell averages varying between 1.0 and 1.1. The eight red squares in Figure 4.7 represent the average (NP depletion rate)/(AP depletion rate) ratios for the eight individual cells. The overall average NP/AP ratio for the eight humidity cells is 1.035 at an overall average acidity production rate of about 600 mg CaCO<sub>3</sub> eq/kg/week. This overall average ratio indicates that, stoichiometrically, slightly more neutralization material (mostly carbonates) dissolved than acid was produced from sulphide oxidation, with the residual alkalinity present in the leachate as bicarbonate.



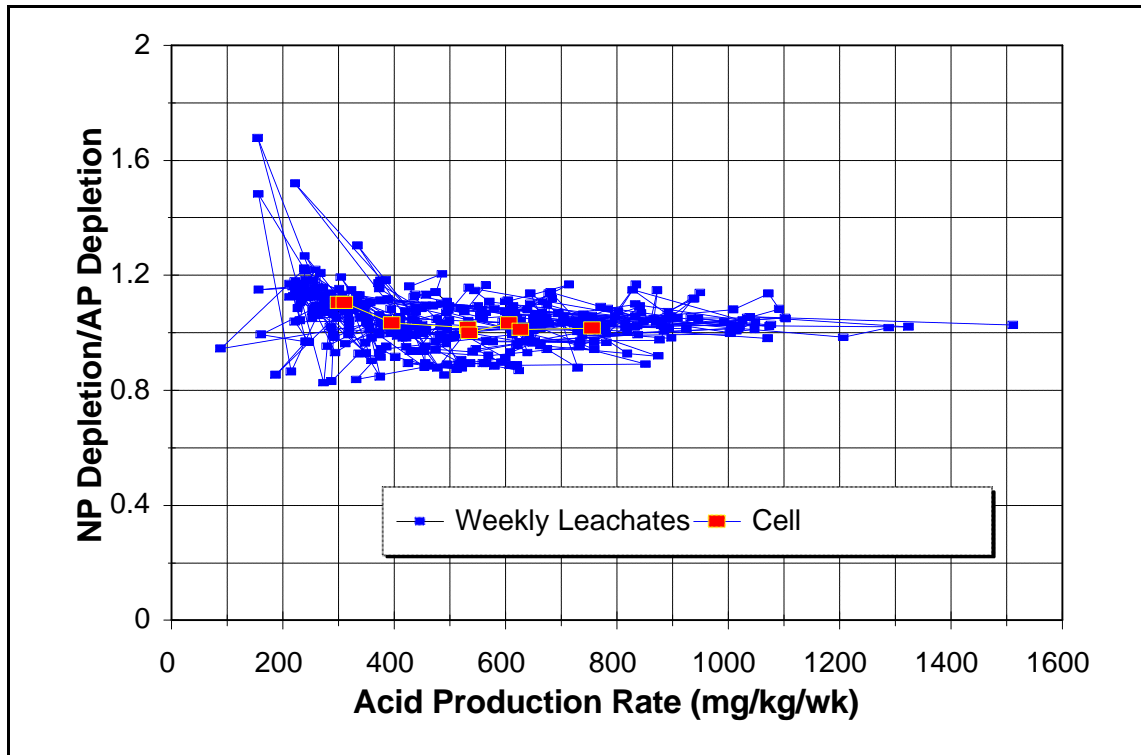


Figure 4.7 NP Depletion/AP Depletion Ratio versus Acidity Production

#### *Total Available NP before Acid Generation*

As mentioned previously, “total available NP” is a very important concept, especially crucial in predicting the lag period length. Why is one interested in predicting the lag period? The interest arises from the need in the planning of waste management strategies. Although exposition of the tailings to the atmosphere should be avoided as much as possible to prevent the formation of soluble alteration products, temporary exposure to the atmosphere could be unavoidable at times in term of operation logistic. If this is the case, effort should be made so that the exposure occurs only at low temperatures, preferably freezing temperatures. For example, waste rock stripped from an open pit may need to be stored temporarily on land before being finally disposed of underwater in the mined-out, flooded pit. For another example, a tailings beach may need to be exposed before the water elevation rises to submerge it. It is crucial in these instances to know in advance the length of time the waste can be exposed without causing acid generation.

The total available NP to be used in association with the measured NP depletion rate for lag time prediction is, ideally, that which is available for neutralizing acidity before the onset of acid generation (defined as leachate pH dropping below, for example, pH 5.0). This is not the NP measured by the original Sobek, or the Modified, or any other similar variational NP procedures, because these procedures invariably subject the sample to acid attacks much stronger than the attack of the acid produced by sulphide oxidation when the pore water pH

is still above 5.0 (i.e., before onset of acid generation). A portion of the NP determined in ABA procedures will never be available to prevent onset of acid generation, although some of that portion may be usable in neutralizing acid once acid generation has become severe and the pore water pH has decreased to a low value, such as below 3.0. Thus it is evident that the NP determined by the ABA procedures is unsuitable for use in the prediction of lag period. To correct this drawback, Morin (1996) takes advantage of field experiences which often pointed to the fact that about 10-15 kg CaCO<sub>3</sub> eq/t of the ABA-derived NP are unavailable for neutralizing acid before onset of acid generation. To do so, The NP determined by the usual ABA procedures is decreased by 10-15 before being used for lag time prediction. Li (1997) discussed alternatives to this approach and concluded that the direct determination of the total available NP cannot be achieved by existing measurement methods. A proposition by the author of this report is the measurement of neutralization curves, in which the sample is titrated very slowly to selected equilibrium endpoint pHs spaced 0.5 (or smaller) unit apart in a range of interest, such as 7.0-2.5. A curve of available NP versus equilibrium pH can then be generated, and the total available NP can be read off the curve at a desired equilibrium pH, such as 5.0. The NP so derived would be a reasonable approximation to the total available NP required for the lag time prediction. The biggest difficulty of this method, of course, is the lengthiness of the titration procedure as equilibrium at every endpoint pH is prescribed.

To further clarify the concept of total available NP, let us consider several illustrative cases. First, if the ABA-derived NP consists of only carbonate minerals which are readily and quickly soluble above pH 5.0, such as calcite, araganite, and ankerite, all that NP counts as total available NP.

Next, consider the case where the ABA-derived NP consists of partly carbonate minerals readily soluble above pH 5.0 and partly silicate minerals which are partially soluble above pH 5.0 but at a very slow dissolution rate. As in the last case, all the readily-soluble carbonate NP counts as total available NP. But only a part of the silicate NP (or SNP) - that part which would have dissolved by the onset of acid generation - can be counted toward the total available NP. For ease of discussion let us call this portion of the SNP "available SNP", meaning that this part of the SNP can be used for acid neutralization prior to the onset of acid generation. The available SNP is normally far from 100% of the SNP measured by usual ABA procedures, as only a small fraction would have dissolved by the time of onset of acid generation. The magnitude of available SNP varies with the length of the lag period, making its determination even more uncertain. This is because silicate dissolution rates are normally slow and relatively constant, with little variation with changes in pore water pH. Consequently, the longer the lag period, the more SNP would dissolve, thus the larger the available SNP.

The above discussion makes the determination of total available NP seem out of reach. This is primarily due to the presence of slow-dissolving NPs, mainly those of silicates. In practice, we can often ignore the available SNP from the calculation of total available NP and incur little error when the sulphide oxidation rate is large, the carbonate NP is large, and the SNP is small. However, when the sulphide oxidation rate is moderate or slow, the carbonate NP is small, and the SNP is relatively large, the determination of total available NP becomes more complex.

A notable special case is when the sulphide oxidation is slow, the carbonate NP is virtually zero, and the SNP is moderate to large. In this situation, it is possible that nearly 100% of the SNP is available NP, as the SNP dissolution rate could be faster than the sulphide oxidation rate on a per unit mass basis, making onset of acid generation impossible before depletion of all SNP.

The approach used in this report to arrive at the total available NP is that given by Equation (1) in Li (1997), i.e., to calculate from the abundances and compositions of Mg-Mn-ankerite and Mg-Mn-siderite (both are carbonate minerals). Since the sulphide oxidation rates are relatively high and the abundances of clinocllore are relatively low, clinocllore (a mafic silicate) is excluded from the total available NP calculation. Other silicates have very low dissolution rates and thus are also excluded. The results of the total available NP calculations are given in Table 4.4 in the column labelled "total available NP". The total available NPs are less than the ABA-determined NPs (also shown in Table 4.4) by 60, 36, 11, and 11 kg CaCO<sub>3</sub> eq/t, respectively, for samples LVW-1, -2, -3, and -4. Therefore, subtracting 10-15 from the ABA-derived NP to obtain the total available NP is only a rough measure, usable when information necessary to do a better evaluation is missing.

#### *Acidity Production Rate and AP Depletion Rate*

These are the same measures expressed in two different terms because of different perspectives. The mean acidity production rates of individual humidity cells fall in the range of 300 to 750 mg CaCO<sub>3</sub> eq/kg/week, with an overall mean value of about 510 mg CaCO<sub>3</sub> eq/kg/week (Table 4.4). These oxidation rates are considered medium to high. Recall that these rates are pre-acid generation rates. The post-acid generation rates for LVW-3A, -3B, -4A, and 4B are higher - greater than 1000 mg CaCO<sub>3</sub> eq/kg/week - presumably due to bacterial catalysis. Figure 4.8 plots the mean acidity production rates of individual humidity cells against their APs. No correlation is visible between these two parameters.

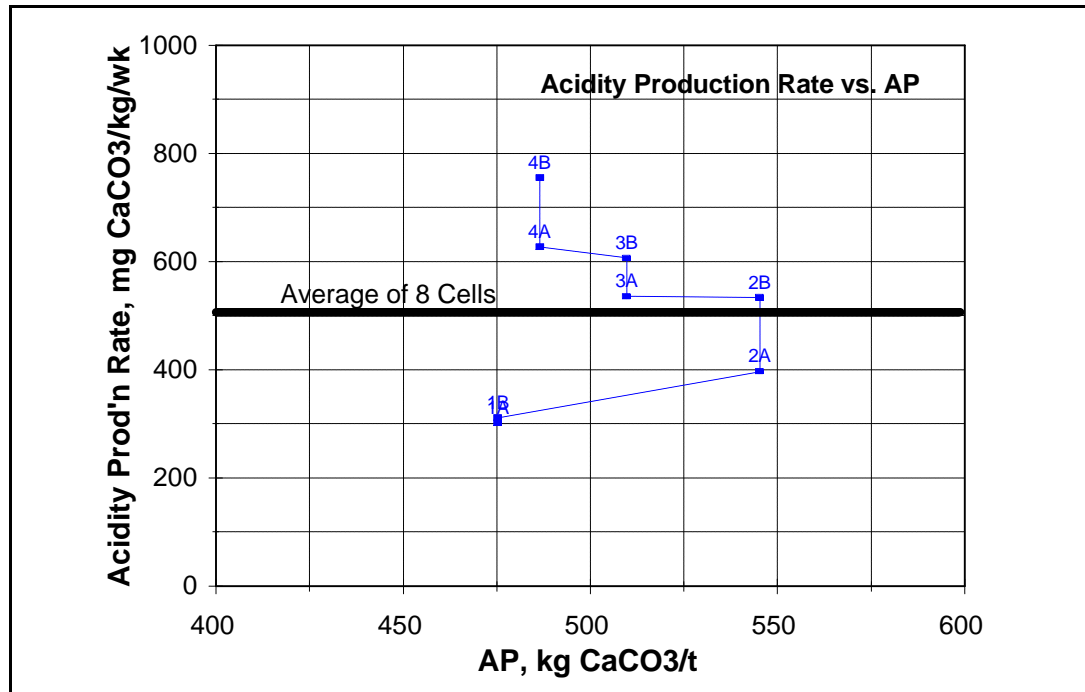


Figure 4.8 Total Acidity Production versus Acid Potential

#### NP Depletion Rate

The mean NP depletion rates of individual humidity cells fall in the range from about 330 to 770 mg CaCO<sub>3</sub> eq/kg/week, with an overall mean of 525 mg CaCO<sub>3</sub> eq/kg/week (Table 4.4).

Figure 4.9 decomposes the average total acidity into three components: that neutralized by carbonates, that neutralized by silicates, and that unneutralized (residual acidity). These components are plotted against average total acidity produced. The acidity neutralized by silicates remains nearly constant at about 11 mg CaCO<sub>3</sub> eq/kg/week. The amount of silicates dissolved in each cycle seem to only depend on the cycle length and temperature, independent of the amount of produced acidity available for neutralization. Similarly, the levels of residual acidity present in the leachate are also roughly constant. Residual acidity normally depends on pH and the kinds of dissolved metals in the leachate. Since these were also relatively constant throughout the tests, the residual acidity did not change significantly, and is independent of acidity production.

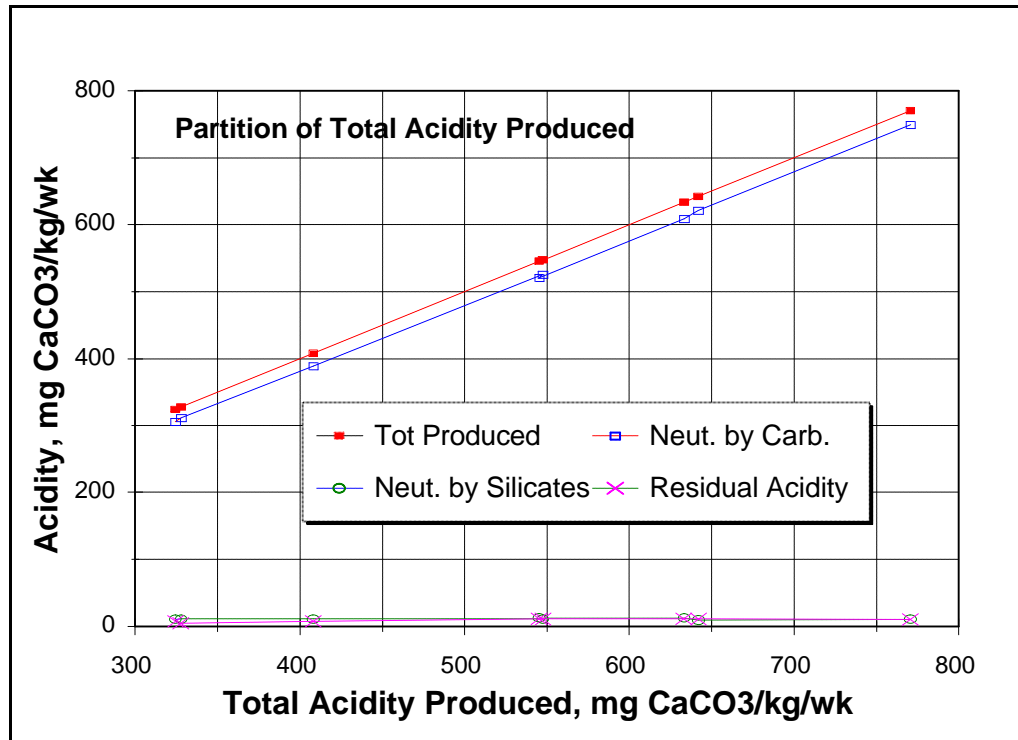


Figure 4.9 Partition of Total Acidity Production

In contrast, the amount of acidity neutralized by carbonates is almost perfectly correlated with the amount of acidity produced. The explanation for this observation is as follows: the dissolution of carbonate minerals is relatively fast and the amount of carbonates dissolved is usually controlled by equilibrium reactions. The more acidity produced, the more carbonate minerals would dissolve to bring the solution pH to nearly neutral levels, as dictated by the equilibrium between water and carbonate minerals.

#### *Years before AMD Onset (Lag Time)*

The number of years before onset of acid generation (i.e., the number of years before NP is exhausted) was predicted to vary in the range of 1.6 to 7.0 years, with a mean of 3.4 years. The sulphide sulphur content at the time of NP exhaustion was predicted to vary between 9.9 and 14.3%, with a mean of 12.9%. The predicted number of years before onset of acid generation, or the lag time, tends to increase with the NP of the sample (Figure 4.10).

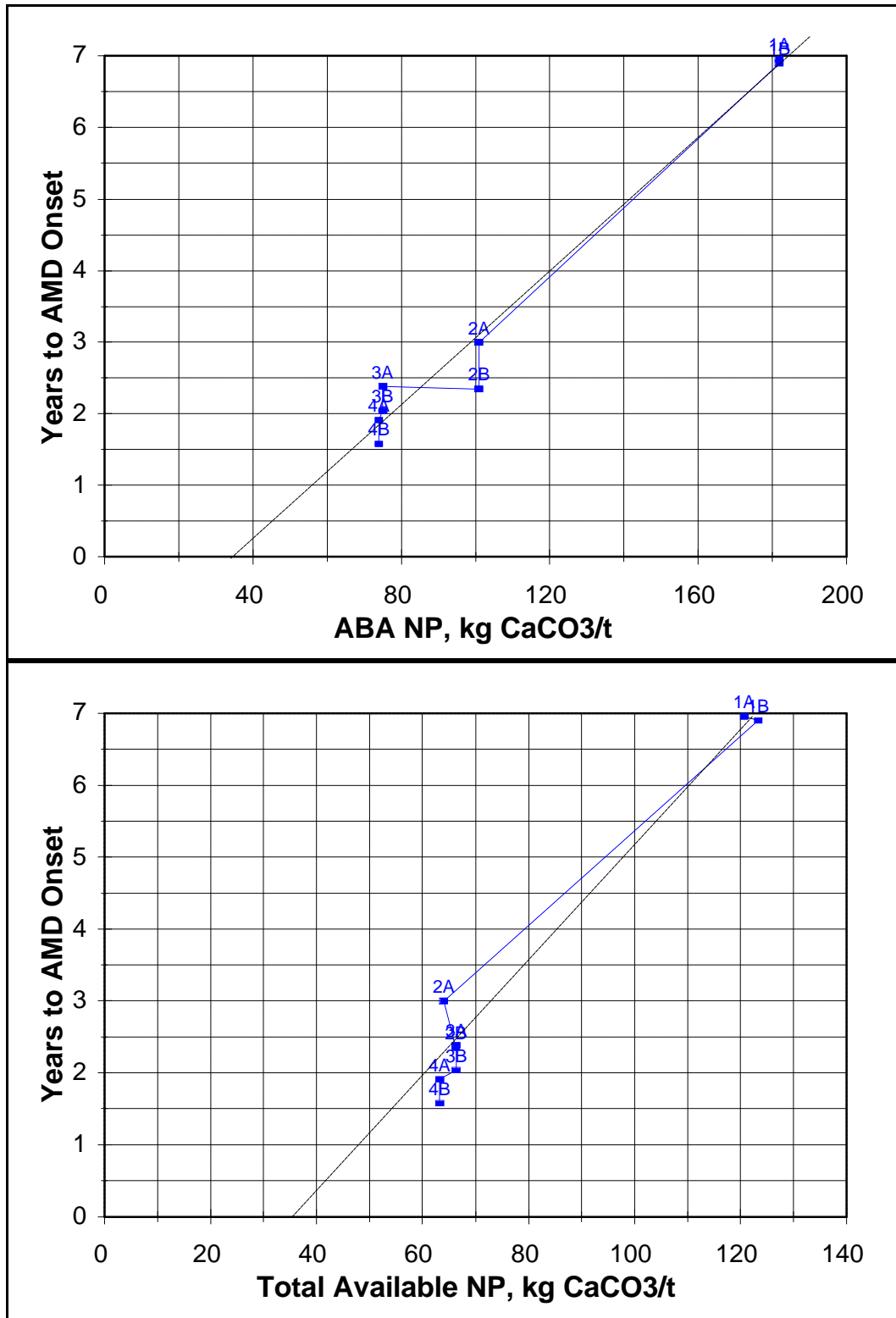


Figure 4.10 Time to AMD Onset versus NP

*Comparison between AP Depletion and NP Depletion*

The AP depletion and NP depletion of individual humidity cells are compared in Figures 4.11 and 4.12. The average depletions are shown in Figure 4.13.

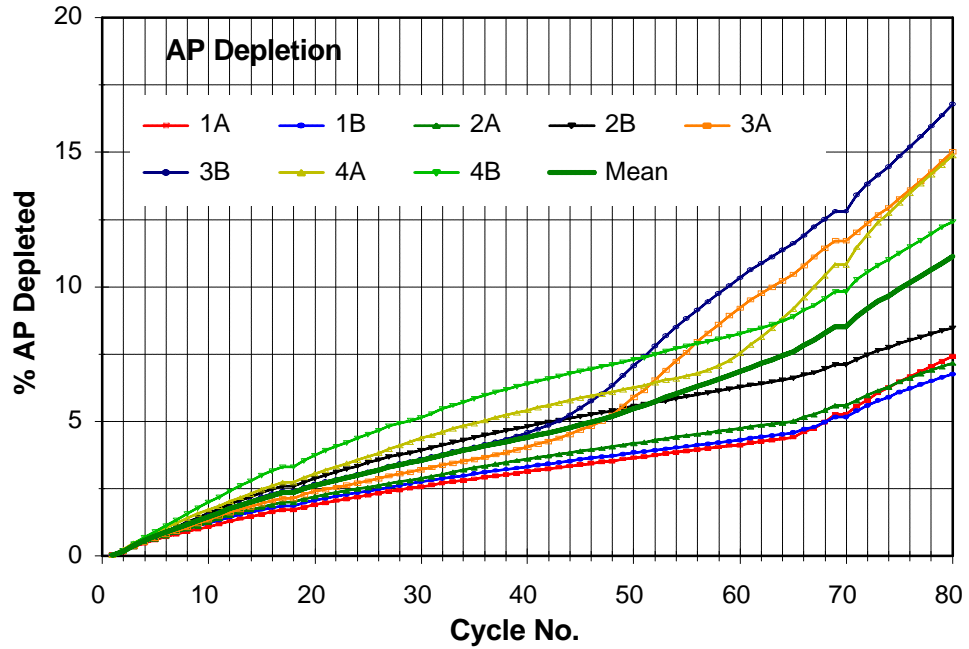


Figure 4.11 Cumulative AP Depletion with Time

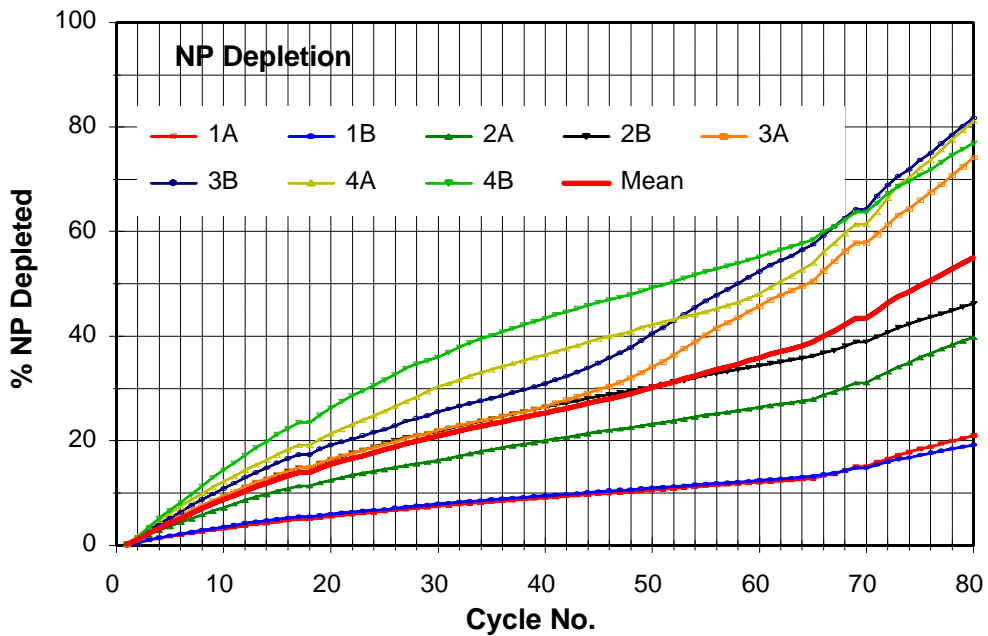


Figure 4.12 Cumulative NP Depletion with Time

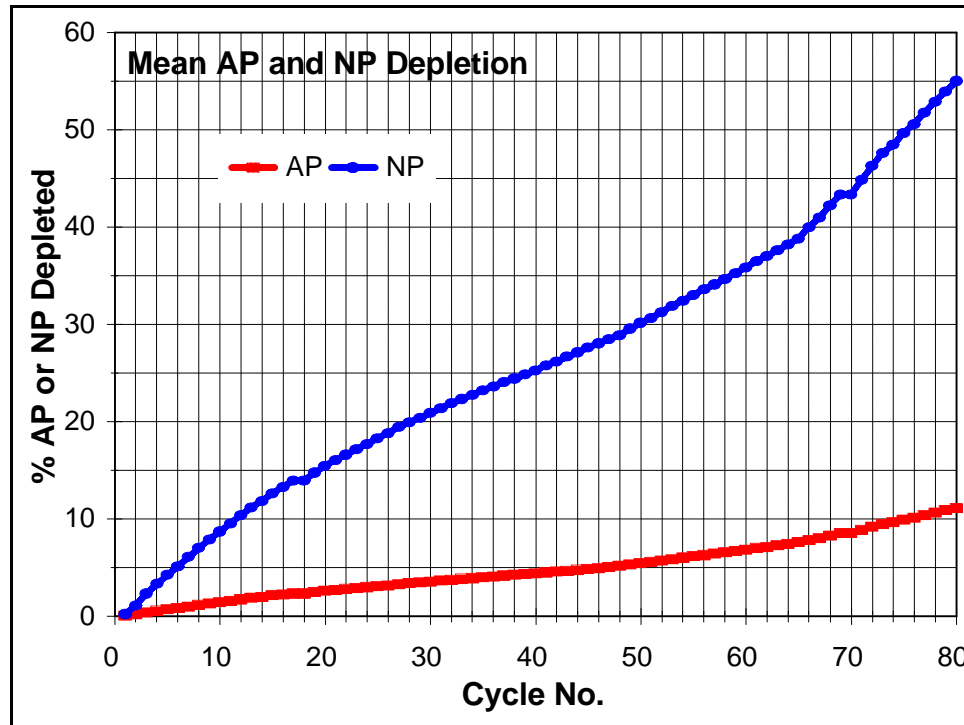


Figure 4.13 Comparison of Average AP and NP Cumulative Depletion

#### AMD Prediction for Humidity Cells

It is apparent from Table 4.4 that all four tailings samples are highly potentially net acid-generating, because their total available NP/SAP ratios are far less than the mean safe NP/AP ratios (also shown in Table 4.4), which fall within the range of 1.0 to 1.1. Given that all will eventually generate acid, the next question is how long the materials can be exposed before acid generation actually takes place. This is the lag time prediction described next.

To generalize the humidity cell test results to the field, the first step is to predict the acid generation from the humidity cells themselves. Taking the eight samples as a whole and using average conditions, we can make the following prediction. The fresh tailings would have 16% sulphide sulphur and 79 kg CaCO<sub>3</sub> eq/t total available NP at the beginning. The oxidation of sulphides would produce 509 mg CaCO<sub>3</sub> eq/kg/week acidity, which is neutralized in situ. During this period the drainage from the tailings would have nearly zero acidity and a neutral pH. The NP will be consumed at a rate of 525 mg CaCO<sub>3</sub> eq/kg/week. This process would continue for 3.4 years, after which the available NP in the tailings will have been exhausted. At that time, there is still 12.9% sulphide sulphur unoxidized. This sulphur will continue to oxidize and produce acidity. A small part of the acidity produced will continue to be neutralized by silicate minerals; but the majority will not. As a result, pH will decrease and dissolved metals will elevate. As the pH drops below 4.0, bacterial activities would pick up to catalyze the acid producing reactions, accelerating the acidity production. This accelerated acidity



production will continue until sulphide sulphur is nearly depleted, at which time acidity production will stop.

#### 4.4.1.4 Correction of Lag Time Prediction

The lag time predictions presented above have been based on simple linear extrapolation. Correct application of this technique requires the following two basic conditions to be met:

- < The average of the sulphide oxidation rates measured in the humidity cells for weeks 6 to n (where n corresponds to the last week before onset of acid generation, or to the last week of test with undisturbed sample bed; see previous explanation for the reason to choose n this way) is applicable to the future until the onset of acid generation.
- < The total available NP reacts quickly with acid generated from sulphide oxidation to maintain the porewater and leachate pH at near-neutral levels until it is totally depleted.

These two conditions would be satisfied in an “ideal humidity cell” demonstrating the following features prior to the onset of acid generation: (1) All sulphides in the humidity cell must have full access to oxygen, and (2) the total available NP in the humidity cell must be available to react at all times. These two features can be achieved if the sample in the humidity cell (1) is dried sufficiently during each drying cycle to allow air to penetrate, (2) does not form impermeable aggregates due to cementing or coating of sulphide and carbonate particles, and (3) is rinsed well each week so that all secondary soluble products are flushed out.

Generally speaking, some humidity cell tests conducted on mining wastes can approach the “ideal humidity cell”, but most can't. As a rule of thumb, tests using tailings that are relatively coarse and that contain relatively low amounts of sulphides are likely to be close to “ideality”. Tailings that are fine-grained and highly sulphidic (as is the Louvicourt tailings) are likely to deviate more from the “ideal humidity cell”. Because of the common occurrence of “non-ideal” humidity cells, predictions based on the simple linear extrapolation approach often require correction when necessary information is available. There are no accepted rules for such corrections; the method used below can serve as an illustration.

The humidity cells in this study did not possess all the features of the “ideal humidity cell”, as suggested by the following observations. First, at week 66 when the sample bed was first disturbed, the newly-exposed material from breakage of lumps exhibited colors different from those seen without the disturbance. The contrast was especially strong for LVW-3A, -3B, -4A, and -4B, all of which had gone acidic. Second, the post-humidity cell microscopic examinations revealed patches appearing to be impermeable to staining by iron precipitates (Figure 4.2 and 4.3). Third, all the cells showed a remarkable increase in sulphate production rate after week 66 (Figure 4.6), indicating large amounts of new sulphide surfaces were exposed as a result of sample bed disturbance. Fourth, like sulphate production rates, rates of alkalinity release also jumped significantly in all cells following the disturbance, suggesting the availability of new NP mineral surfaces (Figure 4.6).

The deviation of these humidity cells from “ideality” causes the lag time predictions based on simple linear extrapolation (Table 4.4) to be inaccurate. For example, Table 4.4 predicts LVW-3A, -3B, -4A, and -4B to go acidic after 2.4, 2.0, 1.9, and 1.6 years, respectively, whereas in fact they became net acid-generating in 0.5, 0.5, 0.8 and 0.8 years, respectively. To correct for the non-ideality of the humidity cells, we first introduce the following term:

- < Apparent mean SO<sub>4</sub> production rate, R<sub>SO<sub>4</sub>,app</sub>, mg SO<sub>4</sub>/kg/week, calculated by dividing the mean weekly SO<sub>4</sub> production by the sample mass in the cell.
- < Corrected SO<sub>4</sub> production rate, R<sub>SO<sub>4</sub>,cor</sub>, mg SO<sub>4</sub>/kg/week, calculated by dividing the mean weekly SO<sub>4</sub> production by the mass of the fractional sample participating in oxidation reactions, not by the mass of the whole sample in the cell.
- < Percentage of the sulphides in the sample participating in oxidation (i.e., not locked up in the interior of aggregates), %S.
- < Apparent mean NP consumption rate, R<sub>NP,app</sub>, mg CaCO<sub>3</sub>/kg/week, calculated by dividing the mean weekly NP consumption by the sample mass in the cell.
- < Corrected NP consumption rate, R<sub>NP,cor</sub>, mg CaCO<sub>3</sub>/kg/week, calculated by dividing the mean weekly NP consumption by the mass of the fractional sample participating in neutralization reactions, not by the mass of the whole sample in the cell.
- < Percentage of the total available NP in the cell participating in neutralization (i.e., not locked up in the interior of aggregates), %NP.
- < Ratio of moles of NP consumed to moles of SO<sub>4</sub> produced, r.
- < Total available NP in the sample, denoted by “NP”.
- < NP participating in neutralization reactions, denoted by NP<sub>free</sub>.

The following relationships exist among the above quantities:

$$\begin{aligned}
 R_{SO4,cor} &= R_{SO4,app} / \%S \\
 R_{NP,cor} &= R_{NP,app} / \%NP \\
 R_{NP,app} &= 1.042 \times r \times R_{SO4,app} \\
 NP_{free} &= NP \times \%NP
 \end{aligned}$$

Using the definitions given above, the uncorrected lag time (in years) was previously calculated by linear extrapolation with the following formula:

$$T = \frac{NP \times 1000}{R_{NP,app} \times 52} \tag{4.6}$$

The corrected lag time is given by

$$T_c = \frac{NP_{free} \times 1000}{R_{NP,app} \times 52} \quad (4.7)$$

Equation (4.7) can also be expressed in terms of the apparent sulphate production rate,  $R_{SO_4,app}$ :

$$T_c = \frac{NP_{free}}{1.042 \times r \times R_{SO_4,app}} \times \frac{1000}{52} \quad (4.8)$$

To illustrate, a numerical value is given as follows. Suppose that the mean weekly sulphate production is 100 mg SO<sub>4</sub> eq, that there are 0.2 kg of tailings in the cell, and that the total available NP is 100 kg CaCO<sub>3</sub> eq/t sample. The apparent SO<sub>4</sub> production rate  $R_{SO_4,app}$  is thus (100/0.2) = 500 mg SO<sub>4</sub> eq/kg/week. The uncorrected lag time by Equation (4.6) is then  $T = (NP \times 1000) / (R_{NP,app} \times 52) = (100 \times 1000) / (1.042 \times 1.04 \times 500 \times 52) = 3.55$  years<sup>1</sup>. Now assume that only 50% the sulphides and 50% of the total available NP participate in reactions due to non-ideality of the humidity cell. That is, %S = 50% and %NP = 50%. The corrected lag time using (4.8) becomes  $T_c = (NP_{free} \times 1000) / (R_{NP,app} \times 52) = (50 \times 1000) / (1.042 \times 1.04 \times 500 \times 52) = 1.77$  years. The corrected lag time is only one half of the uncorrected lag time.

Equation (4.8) is the general formula for calculating the corrected lag time by linear extrapolation. Notice that it is independent of %S. Obviously, for “ideal” humidity cells, %NP equals 100%, whereas for “non-ideal” humidity cells, %NP is less than 100%.

The lag time predictions shown in Table 4.4 are overestimates due to the non-ideality. They can be corrected using Equation (4.8). To use this formula, %NP, the percentage of the sample’s total available NP participating in neutralization reactions prior to the onset of acid generation, must be estimated for each of the eight humidity cells. This was done in the following ways.

For cells LVW-1A, -1B, -2A and -2B, the slopes of the NP depletion curves in Figure 4.6 were measured before and after week 66, designated as SLOPE1 and SLOPE2, respectively. Assuming that after week 66 the humidity cell tests were “ideal”, namely %NP = 100%, then [SLOPE1/SLOPE2] × 100% is the %NP prior to week 66. For cells LVW-3A, -3B, -4A, and -4B, %NP is read off the depletion axis (y axis) corresponding to the point on the ankerite depletion curve at the time when the leachate pH first dropped below 5.0 (i.e., onset of acid generation). For example, in LVW-3A, the leachate pH dropped below 5.0 at week 27, at

---

<sup>1</sup>The value of  $r = 1.04$  is taken from Table 4.4, the average safe NP/AP ratio for all cells.

which time the ankerite depletion was about 25%, which is the %NP value. The reasons behind this graphical technique is this: since ankerite is a fast-reacting carbonate mineral, at the onset of acid generation, all ankerite that is available to react must have reacted. Since the ankerite depletion curves in Figure 4.6 are calculated as  $[\text{ankerite dissolved}]/[\text{total amount of ankerite in sample}] \times 100\%$ , the depletion at the onset of acid generation has the meaning of “the fraction of ankerite in the sample available to react”, which can be used to approximate %NP. The results of %NP determination and corrected lag time predictions for all the cells are presented in Table 4.5, along with the observed lag time for comparison.

Table 4.5 shows reasonable agreement between the corrected lag time predictions and the observed lag times. The table also reveals that, on average, only 37% of the samples put in the humidity cells participated in oxidation and neutralization reactions before the onset of acid generation or before the sample bed was disturbed.

Table 4.5 also shows the corrected AP and NP depletion rates, which will be used to make field lag time predictions later. It can be seen that the corrected AP and NP depletion rates are quite large, indicating that the Louvicourt tailings are highly reactive.

Table 4.5 Uncorrected and Corrected Lag Time Prediction versus Observed Lag Time

Cell No.	Uncorrected Lag Time, T (yr)	%NP <sup>1</sup>	Corrected Lag Time, T <sub>c</sub> (yr)	Observed Lag Time (yr)	Corrected AP Depletion Rate <sup>4</sup> , $1.042 \times R_{\text{SO}_4, \text{cor}}$ (mg CaCO <sub>3</sub> /kg/wk)	Corrected NP Depletion Rate <sup>5</sup> , R <sub>NP, cor</sub> (mg CaCO <sub>3</sub> /kg/wk)
1A	7.0	23%	1.6	>1.3	1311	1451
1B	6.9	36%	2.5	>1.3	864	955
2A	3	42%	1.3	>1.3	945	978
2B	2.3	46%	1.1	>1.3	1160	1180
3A	2.4	25%	0.60	0.53	2143 <sup>2</sup>	2143
3B	2.0	28%	0.56	0.52	2166	2238
4A	1.9	42%	0.80	0.79	1494	1514
4B	1.6	50%	0.80	0.81	1511	1537
Mean	3.4	37%	1.15	N/A	1449 <sup>3</sup>	1500

<sup>1</sup>Percent of total NP available to react.  
<sup>2</sup>This value is used for the “worse-than-average” case.  
<sup>3</sup>This value is used for hypothetical field lag time prediction for the “average” case.  
<sup>4</sup>Assumed %S = %NP.  
<sup>5</sup>The r values were taken from Table 4.4.

#### 4.4.1.5 Hypothetical Predictions for the Field

Since the Louvicourt tailings have been disposed of under a water cover from the outset, the discussion that follows is entirely hypothetical. It predicts what would happen if the tailings had been deposited on-land in exposed tailings beaches.

To generalize the predictions made for the humidity cells to the field, several factors must be considered. Lower temperature, freezing-thawing, less frequent flushing, and lower humidity all tend to reduce the rate of sulphide oxidation and delay the onset of AMD. There are many uncertainties associated with generalization of lab results to the field, because many factors influencing acidity generation and neutralization are beyond our control and some of the rate-limiting processes involved are still poorly understood. Realizing these uncertainties, we can nevertheless estimate the AMD generation in the field under some simplified assumptions.

Assuming that

- < oxidation of sulphides ceases during the five coldest months (November to March inclusive) when the monthly mean air temperature is below 0EC (i.e., freezing conditions);
- < the mean monthly temperatures for the remaining seven months of the year are 0.8EC, 8.9EC, 14.2EC, 17.1EC, 15.5EC, 10.4EC, and 4.4EC (based on 30 years of records at the Val d'Or weather station, see Appendix V-1), respectively;
- < each 10EC drop in temperature causes the oxidation rate to half;
- < the residual acidity in the drainage does not change from the lab to the field;
- < the (NP depletion rate)/(AP depletion rate) ratio of 1.035 also applies in the field;
- < the neutralization reactions are the same in the field as in the lab; and
- < all other aspects of the lab test can be transferred directly to apply to the field;

we can make the following calculations.

For a typical case based on the average parameters derived from the eight humidity cell samples (Tables 4.4 and 4.5):

- < SAP (which equals AP for Louvicourt tailings) = 504 kg CaCO<sub>3</sub> eq/t
- < Total available NP = 79 kg CaCO<sub>3</sub> eq/t
- < Corrected acidity production rate adjusted for the lower temperature of 10EC = 1449\*0.384 = 556 mg CaCO<sub>3</sub> eq/kg/week, 0.384 being the temperature adjustment factor
- < NP depletion rate = 556\*1.035 = 575 mg CaCO<sub>3</sub> eq/kg/week
- < Years before NP depletion = (79/573)\*(1000/30.33<sup>2</sup>) = 4.5 years
- < Residual AP at NP depletion = 504 - 556\*4.5\*30.33/1000 = 428 kg CaCO<sub>3</sub> eq/t
- < Residual unoxidized S at NP depletion = 428/31.25 = 13.7%

For a worse-than-average case (fast oxidation rate), as represented by humidity cells LVW-3A and -3B (Tables 4.4 and 4.5):

- < SAP = AP = 510 kg CaCO<sub>3</sub> eq/t
- < Total available NP = 66 kg CaCO<sub>3</sub> eq/t
- < Corrected acidity production rate adjusted for 10EC = 2143\*0.384 = 823 mg CaCO<sub>3</sub> eq/kg/week

---

<sup>2</sup>The number 30.33 is derived by 365\*(7/12), the number of non-freezing weeks in a year.

- < NP depletion rate =  $823 \times 1.00 = 823$  mg CaCO<sub>3</sub> eq/kg/week
- < Years before NP depletion =  $66 \times 1000 / 823 / 30.33 = 2.6$  years
- < Residual AP at NP depletion =  $510 - 823 \times 2.6 \times 30.33 / 1000 = 445$  kg CaCO<sub>3</sub> eq/t
- < Residual unoxidized S at NP depletion =  $445 / 31.25 = 14.2\%$

In the typical case, the fresh tailings would become net acid-generating in the field after 4.5 years of exposure. At the onset of AMD, there would be 13.7% sulphide sulphur remaining unoxidized. In the worse-than-average case, the fresh tailings would become net acid-generating in the field after 2.6 years of exposure. At the onset of AMD, there would be 14.2% sulphide sulphur remaining unoxidized.

The above empirical prediction based on simple linear extrapolation applies only to the surface layer of exposed tailings where atmospheric oxygen supply is unlimited. The oxidation of subsurface tailings is restricted because oxygen must diffuse through the voids to reach reaction sites. Molecular diffusion of oxygen is a slow process and normally exert a control over the overall subsurface oxidation rate. The rate of oxygen intake by subsurface tailings depends on many factors including the gas diffusivity, oxygen concentration gradient, presence of hardpan, and so on. The depth of oxygen penetration and the rate of oxygen supply can be mathematically modelled if the size distribution, mineralogy, water content, and hydrological parameters of the tailings are known.

#### 4.4.2 Post-Humidity Cell Geochemical and Mineralogical Mass Balances

##### 4.4.2.1 Acid Base Accounting

The post-humidity cell extended ABA (Table 4.1) can be compared with the pre-humidity cell ABA (Table 2.4) to assess the changes in AP and NP owing to oxidation and neutralization processes. Table 4.1 reveals the following points:

- < Cells 3A, 3B, 4A, and 4B have no NP left, whereas Cells 1A, 1B, 2A, and 2B retained some NP. All cells still show a strong potential for acid generation, as indicated by the high SAP values. This corroborates with the fact that the paste pHs of Cells 3A, 3B, 4A and 4B indicate acidic conditions whereas those of 1A, 1B, 2A, and 2B indicate near-neutral conditions.
- < There is a tendency for the paste pH to decrease with increasing SO<sub>4</sub> concentration in the solids (Figure 4.14). This suggests that the more advanced a humidity cell is in the acidification process, the more sulphate is retained in the cell, and thus the less efficient the weekly rinses are in removing oxidation and neutralization products. A corrective measure would be to increase the rinse volume and the leach time as acid generation intensifies.
- < The amounts of carbonates remaining in the solids vary between 1.4 and 20.5% of the sample mass. This reveals that substantial acid neutralization by carbonates has

occurred when compared with the initial ABA data (Table 2.4). The CNPs calculated from inorganic CO<sub>2</sub> account for 164% to 621% of the NPs determined by the Sobek method in Cells 1A, 1B, 2A and 2B; and between 800% to almost infinity (!) of the Sobek NP for Cells 3A, 3B, 4A, and 4B. This suggests that the remaining carbonates in Cells 3A, 3B, 4A and 4B are essentially those of Fe and, less importantly, of Mn, neither of which contributes to NP. It also suggests that the most effective neutralizing carbonate (ankerite) was exhausted.

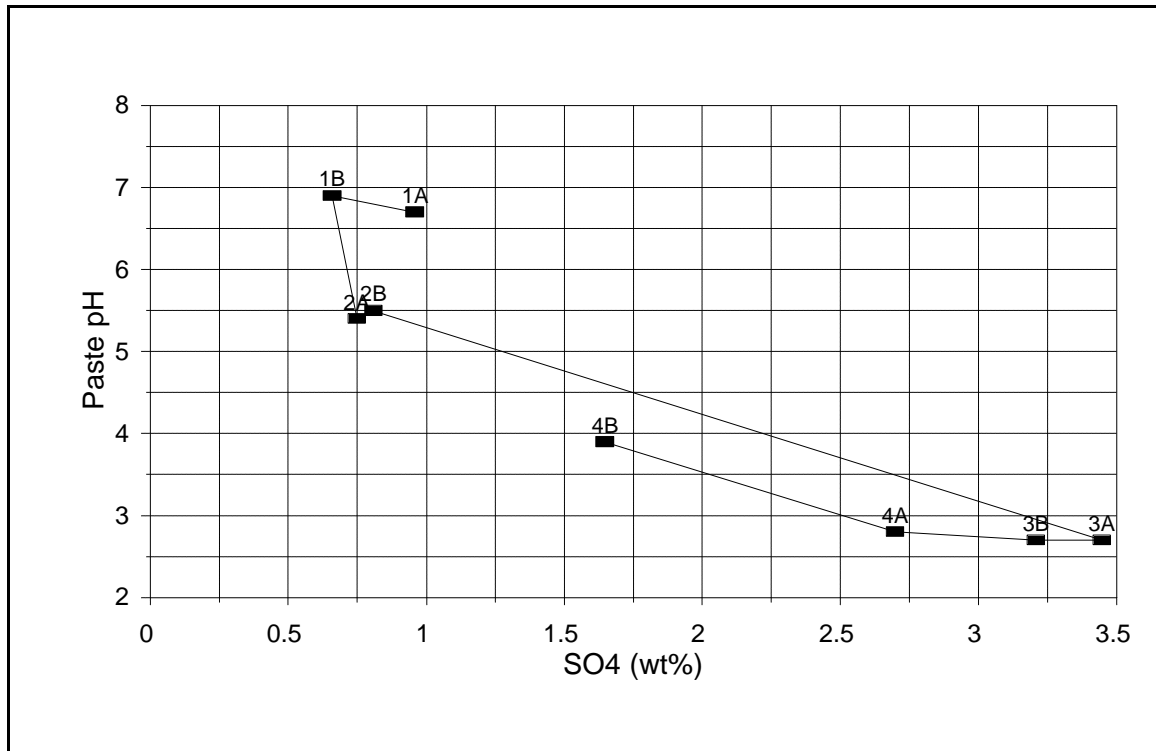


Figure 4.14 Paste pH versus SO<sub>4</sub> Content

#### 4.4.2.2 Geochemical Whole-Rock Mass Balance

The whole-rock geochemical analyses of the fresh tailings and their weathered counterparts allow us to calculate a mass balance to assess elemental changes during the weathering process if certain assumptions are made:

- < The mass balance calculation is made on the assumption of constant SiO<sub>2</sub>. This assumption is justifiable because quartz is the dominant silica bearing mineral and has a very low dissolution rate under the experimental conditions. This assumption is also supported by weekly leachate analyses showing very low Si concentrations (<2 mg/L).
- < The mass balance calculation is done on an anhydrous basis. To do so, it is assumed that the difference between the sum of the whole-rock contents and 100% represents water content. The whole-rock composition takes into account the redistribution of

total iron as Fe (in pyrite) and FeO (in carbonates, oxides and silicates), the sulphur speciation, and inorganic CO<sub>2</sub> content

Details of the mass balance calculation are given in Appendix IV-7. Figures 4.15 and 4.16 present the elemental mass changes and total mass changes in g per 100 g sample. The major elemental mass changes occurred in Cells LVW-3A and -4A. All cells have lost sulphide S, CO<sub>2</sub>, CaO and MgO, indicating that these components were released to the leachate as a result of sulphide oxidation and acid neutralization. All solids have gained elemental sulphur and sulphate. The reason for the mass gain in aluminum shown in Figure 4.15 is unclear and may be attributable to analytical error. The mass of K<sub>2</sub>O, Na<sub>2</sub>O and MnO appears to be relatively constant. Note that Cells LVW-3A and 4A gained significant FeO and SO<sub>4</sub>, but lost sulphide Fe and sulphide S. This could mean that large amounts of iron were kept in the system by precipitation as iron hydroxide and perhaps also sulphates. The mass gain in SO<sub>4</sub> could be a result of gypsum and iron sulphate precipitation, which accumulated because of insufficient rinsing during the humidity cell tests or because of the long rest time before the solids were sampled for analyses. Copper was released by all solids whereas Zn and As were lost only from cells 3A and 4A. Finally, it is interesting to note that the total mass changes (Figure 4.16) are the lowest in LVW-3A and -4A, which had the highest reactivity.

Figure 4.17 shows a CaO-CO<sub>2</sub> binary diagram correlating the pre- and post-humidity cell whole-rock CaO and CO<sub>2</sub> in molar percentages. In such a diagram, the line connecting the pre-humidity cell point to the post-humidity cell point (upper right to lower left direction) indicates carbonate dissolution. The slope of this line, representing  $\Delta \text{CaO} / \Delta \text{CO}_2$ , is indicative of the nature of the carbonate(s) being dissolved. If only calcite is dissolving, the slope would be 1; if only ankerite or dolomite is dissolving, the slope would be 0.5; and if only siderite or magnesite is dissolving, the slope would be zero. The intercept obtained by extrapolating this line indicates the CaO in the sample unassociated with carbonates. If the intercept is zero, all CaO is hosted by carbonates; if the intercept is significantly larger than zero, it normally indicates the presence of Ca-containing silicates, such as Ca-plagioclase and epidote.

In Figure 4.17, the eight points appear to fall on a straight line having a slope between those characteristics of ankerite and siderite. A linear regression line ( $R=0.98$ ) has a slope of 0.32 and an intercept of zero. From the slope of the regression, the proportions of carbonates being dissolved were calculated as 75% ankerite and 25% siderite. The zero intercept of the regression line suggests that basically the vast majority of Ca in the sample was present as carbonates. These figures compare favourably with the humidity cell test findings (discussed previously) and also with the mineralogical balances (discussed below).



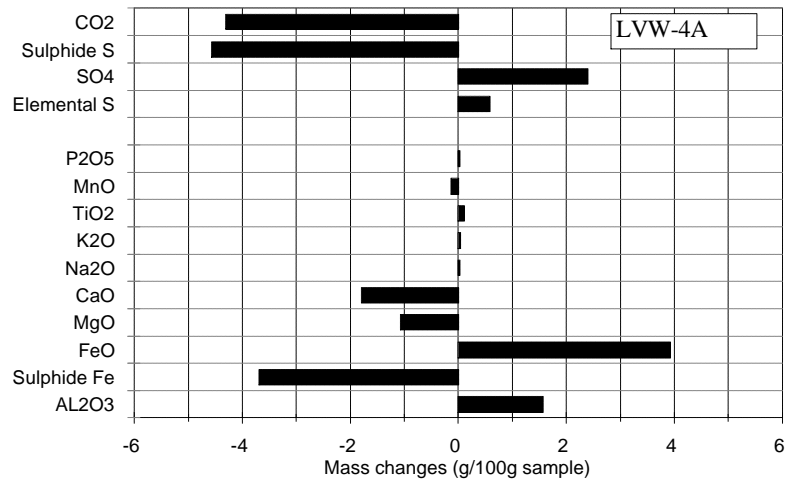
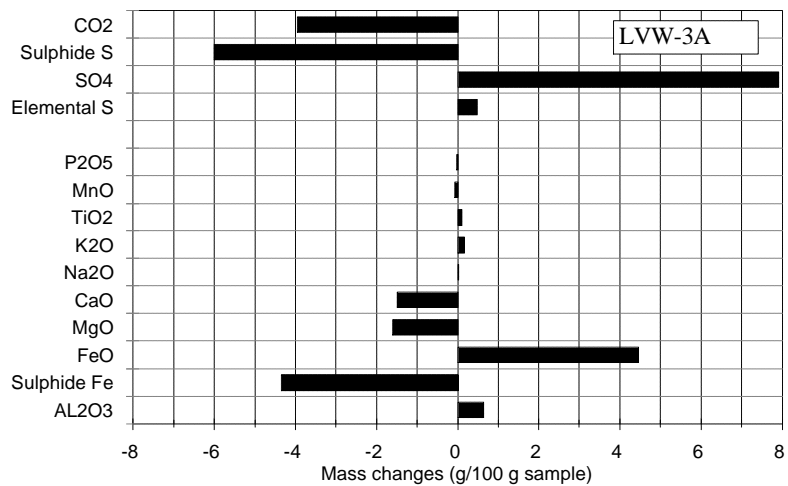
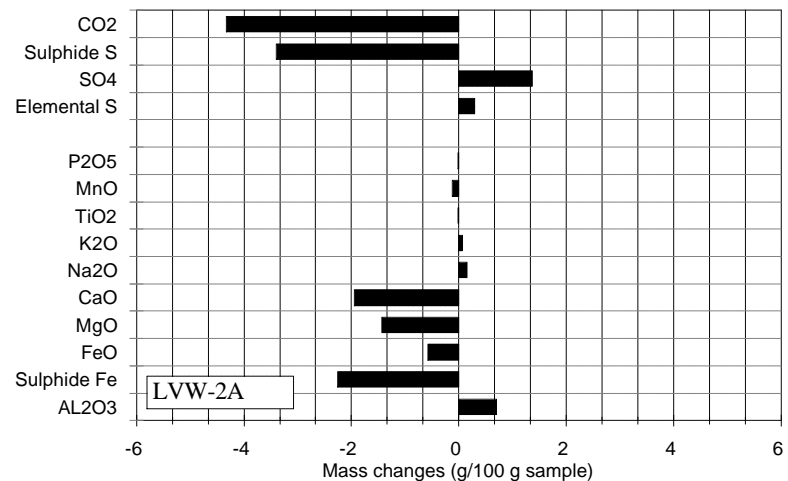
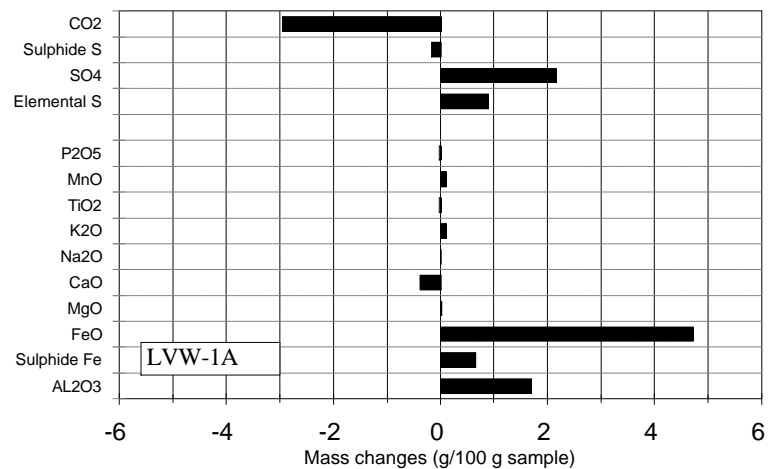


Figure 4.15 Post-Humidity Cell Elemental Mass Changes

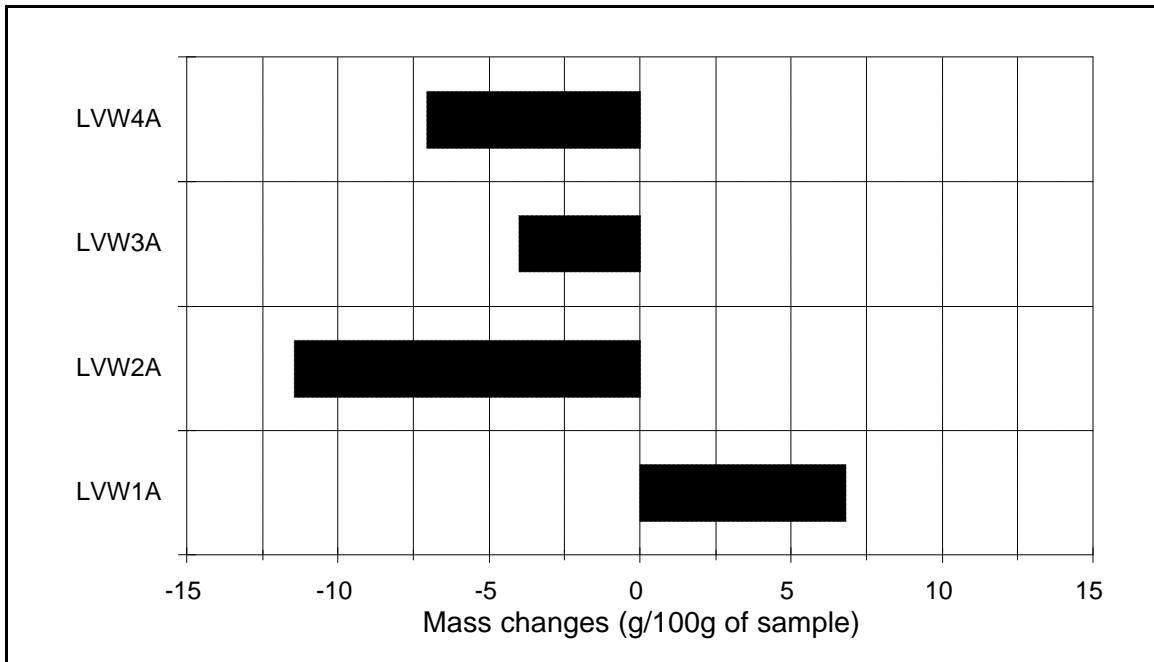


Figure 4.16 Post-Humidity Cell Total Mass Changes

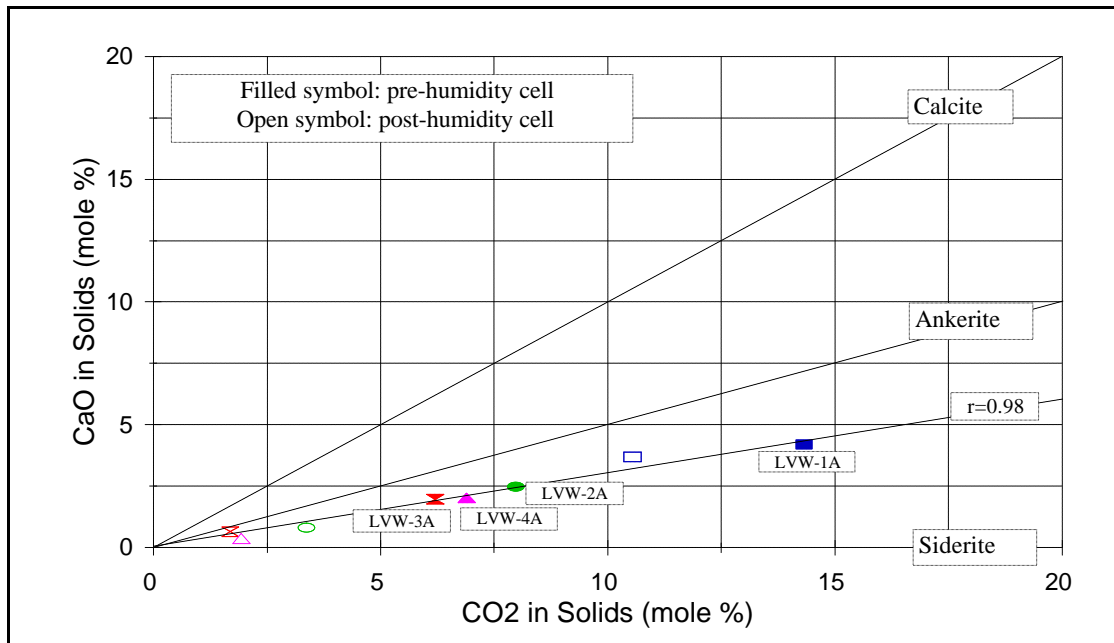


Figure 4.17 Pre- and Post-Humidity Cell CaO-CO<sub>2</sub> Binary Diagram

#### 4.4.2.3 Mineralogical Mass Changes

The mineralogical mass changes can be assessed if both pre- and post-humidity cell mineralogy is available. Because of the inherently large uncertainties in the quantitative determination of minor phases by direct mineralogical methods (optical microscopy and XRD), a normative mineralogy was considered better and thus used for the mineralogical mass balance calculations. The normative mineralogy was obtained by reconciling mineralogical compositions and whole-rock analyses of the solids. Details of the calculations and results are given in Appendix IV-8. To assess the validity of the normative mineralogy technique, the post-humidity cell normative mineralogy was correlated with the post-humidity cell mineralogy obtained by direct methods (point counting and electron microprobe). Reasonably good correlations ( $r=0.92$  to  $0.98$ ) are found (Figure 4.18).

The pre- and post-humidity cell normative mineralogy was used to calculate mineralogical mass changes in terms of percent mineral depletion (Figure 4.19). Ankerite dissolution was complete in Cell LVW-4A, 27% in 1A, 88% in 2A, and 72% in 3A. Siderite did not dissolve greatly in 1A but showed substantial dissolution in 2A (18% depletion), 3A (82% depletion) and 4A (62% depletion). Pyrite depletion was ~0% in 1A, 13% in 2A, 29% in 3A, and 27% in 4A.

The mineralogical mass change calculations also indicate that gypsum, rozenite, goethite and elemental sulphur were gained during weathering of the tailings. It should be mentioned that rozenite was assumed present for the reconciliation of the normative mineralogy. Other possible candidates are melanterite, bilinite, römerite, copiapite, coquimbite and fibroferrite (Jambor, 1994).

#### 4.4.3 Comparisons between Humidity Cell and Post-Humidity Cell Data

A number of comparisons can be made between the data generated from the humidity cell tests and the data from the post-humidity cell studies. Such comparisons serve to validate (or negate) the assumptions and techniques used in the interpretation of the humidity cell results, mainly the weekly leachate chemistry data. The highlights of these comparisons are presented below:

- < The humidity cell tests showed that Cells 3 (A, B) and 4 (A, B) became net acid-generating during the test term. This is consistent with the post-humidity cell ABA data, which showed acidic conditions for these cells with paste pH values as low as 2.7-2.8.
- < The small changes in Na and K in the solids chemistry suggests very little silicate dissolution (except clinocllore), which is in agreement with the very slow silicate neutralization rates obtained during the humidity cell experiments.

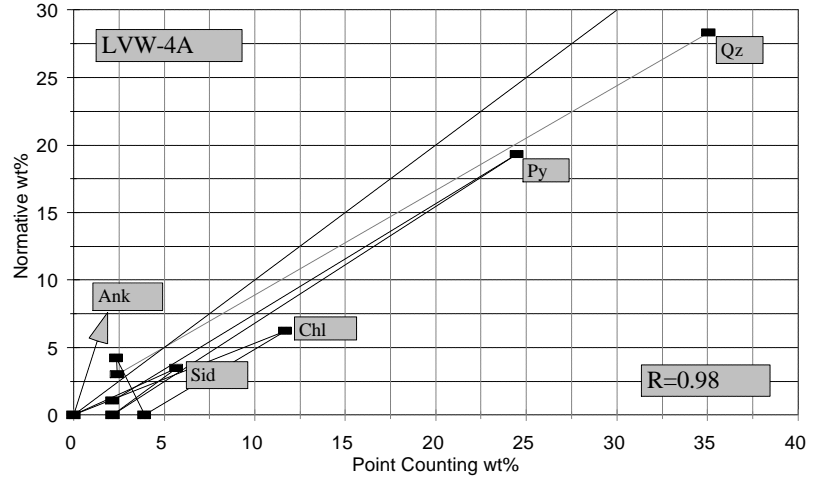
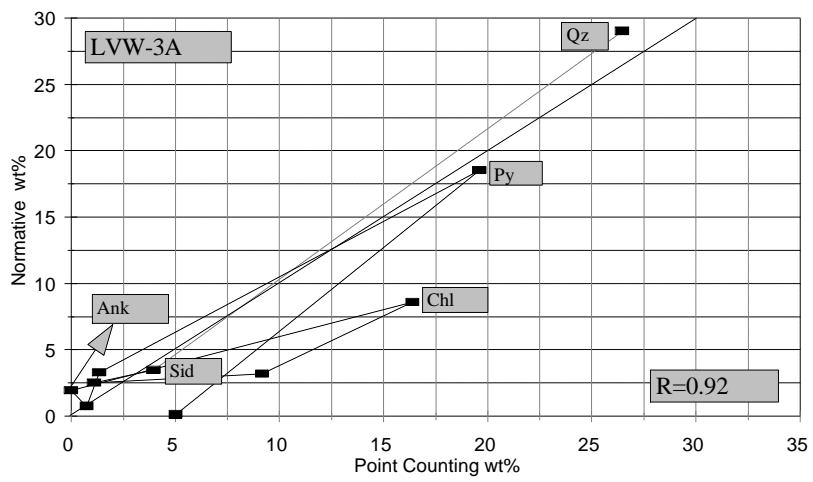
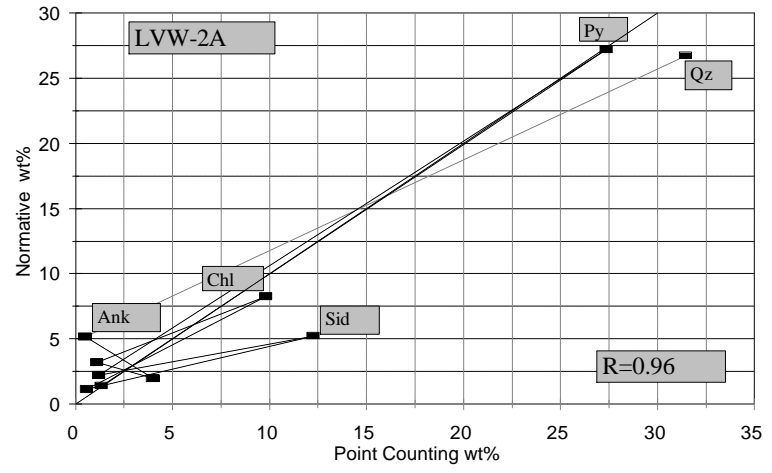
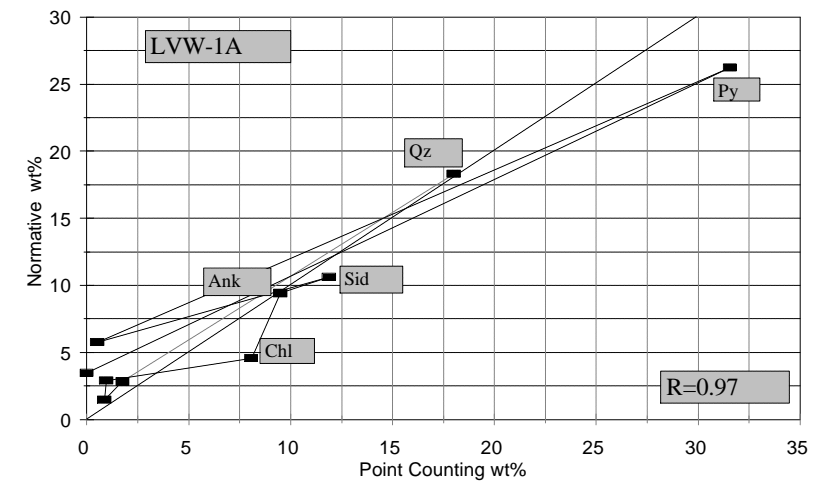


Figure 4.18 Correlation between Normative Mineralogy and Mineralogy by Direct Methods

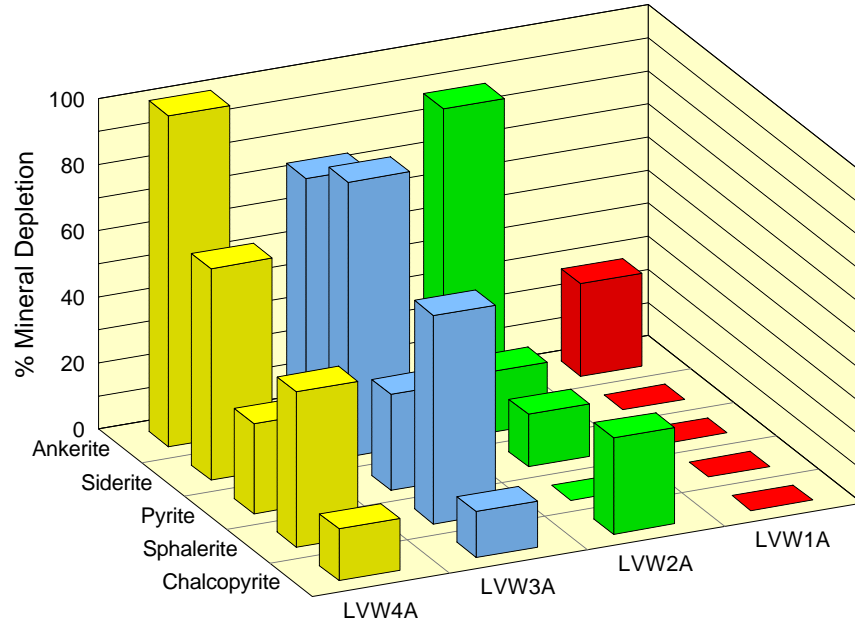


Figure 4.19 Mineral Depletion in Weathered Louvicourt Tailings

- < The percent carbonate and sulphide mineral depletions calculated from the mineralogical mass changes agree well with those calculated from weekly leachate chemistry (Table 4.6). This lends a strong support to the methodology used for calculating mineral depletions from weekly leachate chemical data. For most cases, the depletion figures from the two different sources agree with each other within the range of their error bars (Figure 4.20).
- < The post-humidity cell mineralogy shows that there is 20-30% pyrite, or 10-16% sulphide sulphur, left in the weathered solids. These figures are in agreement with the amounts of sulphide sulphur remaining, as calculated by subtracting the sulphide sulphur that has oxidized and been flushed out as sulphate from the initial total sulphide sulphur.

Table 4.6 Comparison between Mineral Depletions Calculated from Humidity Cell (HC) Test Data and Those Revealed by Mineralogical Mass Balance (mean  $\pm$  s, %)

Mineral	LVW-1A	LVW-2A	LVW-3A	LVW-4A
<b>Ankerite</b>				
from HC test data	56.0 $\pm$ 5.6	74.9 $\pm$ 7.5	78.2 $\pm$ 7.8	76.3 $\pm$ 7.6
from mineralogy	26.7 $\pm$ 8.4	88.2 $\pm$ 1.2	72.0 $\pm$ 2.8	100 $\pm$ 10
<b>Siderite</b>				
from HC test data	3.5 $\pm$ 0.4	26.1 $\pm$ 2.6	100 $\pm$ 10	88.2 $\pm$ 8.2
from mineralogy	0	18.4 $\pm$ 8.1	81.7 $\pm$ 1.8	62.1 $\pm$ 6.2
<b>Pyrite</b>				
from HC test data	11.8 $\pm$ 1.2	11.1 $\pm$ 1.1	30.1 $\pm$ 3.0	18.4 $\pm$ 1.8
from mineralogy	0	12.8 $\pm$ 4.3	28.7 $\pm$ 3.6	26.7 $\pm$ 1.3
<b>Sphalerite</b>				
from HC test data	1.6 $\pm$ 0.2	11.6 $\pm$ 1.6	49.7 $\pm$ 5.0	32.7 $\pm$ 3.3
from mineralogy	0	0	63.0 $\pm$ 8.0	44.1 $\pm$ 5.9

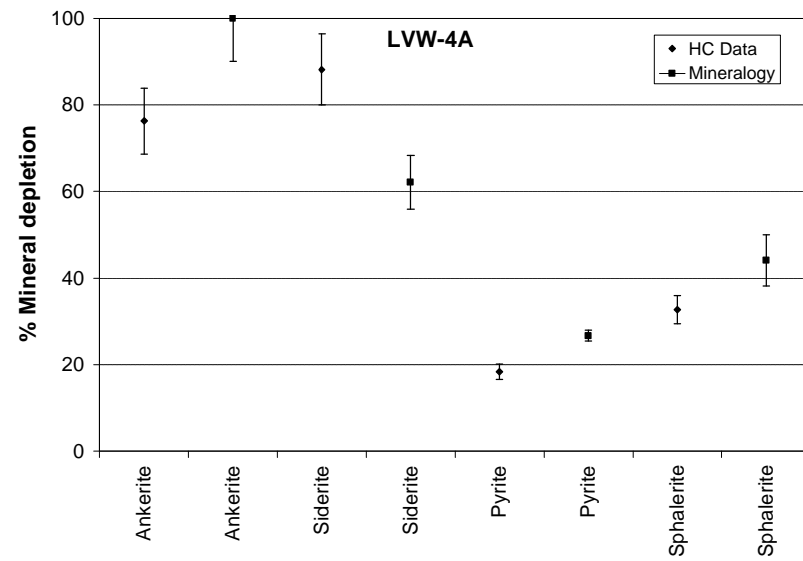
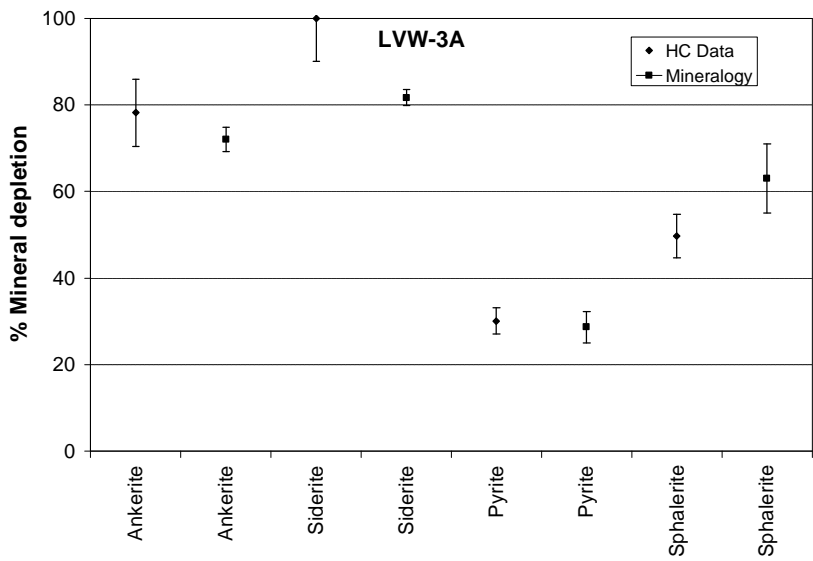
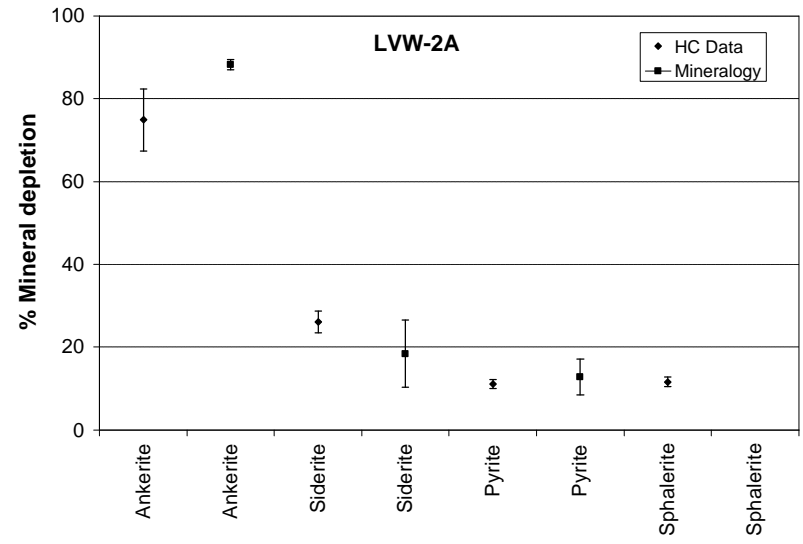
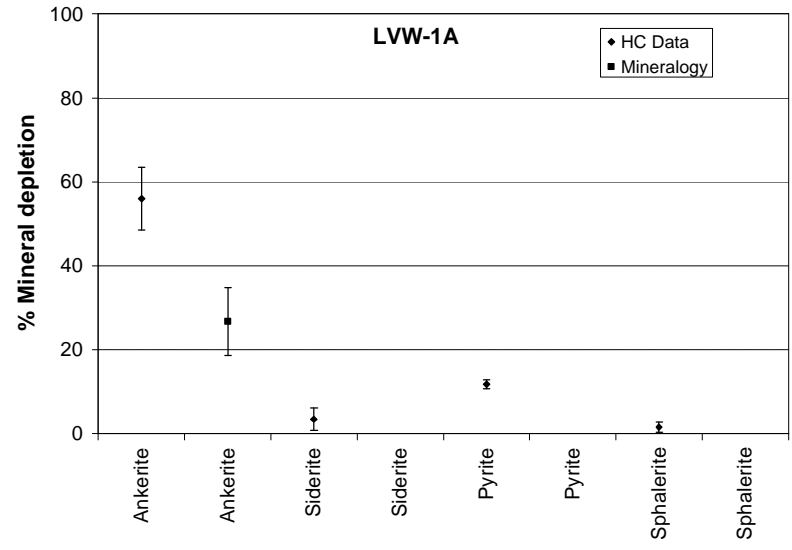


Figure 4.20 Comparison of Mineral Depletions Calculated from Humidity Cell (HC) Leachate Chemistry with Those Revealed by Mineralogical Mass Balance (error bars show  $\pm s$ )

#### 4.5 Summary of Important Findings

To characterize the oxidative reactivity of Louvicourt tailings, four composite samples were tested in duplicates in eight humidity cells for 80 weeks. Pre- and post-humidity cell solid analyses were also performed. Major findings from these tests are summarized as follows.

- < The humidity cell results show that the Louvicourt tailings have relatively high oxidative reactivity. The oxidation rate of the eight tests ranged 864-2143 (average 1449) mg CaCO<sub>3</sub> eq/kg/week, and the NP consumption rate ranged 955-2238 (average 1500) mg CaCO<sub>3</sub> eq/kg/week. All samples are potentially net acid-generating, with predicted humidity cell lag times ranging 0.56-2.5 (average 1.2) years.
- < Predictions based on hypothetical field exposure of the tailings indicate that, for a typical tailings composition as represented by the average of the four samples tested, the lag time before acid generation is 4.5 years. For a worse-than-average case as represented by the sample LVW-3, the lag time reduces to 2.6 years.
- < The main sulphide mineral in the tailings is pyrite with minor sphalerite and the main neutralizers are ankerite, siderite, and clinocllore. Sphalerite oxidation appeared to be accelerated by galvanic effects after the leachate pH dropped below about 3.0. The ankerite was readily available and contributed fully to the total available NP. The siderite and the clinocllore were less reactive and contributed less to the total available NP. Siderite dissolution seemed to be accelerated after onset of acid generation whereas clinocllore dissolution were relatively unaffected by acidification.
- < A new technique was employed to calculate the dissolution rates of individual neutralizing minerals and sulphide minerals from weekly leachate volume and chemical data. The validity of this technique proves to be acceptable, as the mineralogical mass balances predicted with this technique compare favourably with the mass balances computed from pre- and post-humidity cell solid analysis data that were obtained independently from the leachate chemistry data.
- < Due to the “non-ideality” of the humidity cell tests conducted in this study, not all particles placed in the cells were accessible for oxidation and neutralization reactions. This was probably attributable to the formation of impermeable particle aggregates as a result of cementation and coating. Methods for correcting for the non-ideality were proposed and demonstrated. It was found that, without agitation, on average only about 37% of the sample mass in the humidity cells was available for oxidation and neutralization reactions. To minimize the deviation of future humidity cell tests from ideality, it is recommended that the test sample be stirred weekly to expose “hidden” particles and that the weekly sample leach be carried out at a greater water to solids ratio and for a longer duration.



## 5.0 SUBAQUEOUS TAILINGS OXIDATION RATE MODELLING

Whereas it is known that the oxidation rate of water-covered sulphidic tailings is greatly reduced when compared with exposed tailings, it is also known that oxidation nevertheless occurs at the interface of water and submerged sulphidic tailings when oxygen interception or consumption layers are absent. The purpose of this chapter is to quantify the oxidation rate of subaqueous tailings, however slow it may be, using the tool of mathematical modelling. The simple models are developed from first principles of physics and chemistry and solved using realistically assumed initial/boundary conditions and parameter values. Whenever possible, parameter values suitable for the Louvicourt site is used. Both transient and steady-state solutions are given. The outputs from these models are dissolved oxygen profiles in the water or the tailings column and oxygen fluxes into submerged tailings. The fluxes can be combined with hydrologic and hydrogeologic information to predict the quality of the water cover. An example of this is given in Li et al., 1997.

In this chapter, the degree of subaqueous tailings oxidation is compared for four simplified and idealized cases: (1) a stagnant water cover, (2) a fully-oxygenated water cover without downward infiltration, (3) a fully-oxygenated water cover with downward infiltration, and (4) resuspension of tailings. In all cases, the water cover depth is assumed to be 0.3 m.

Historical meteorological records for the last 30 years at the Val d'Or station (Appendix V-1) show that seven months (April to October) of each calendar year have above-zero average monthly temperatures; the remaining five months (November to March) are, on average, frozen. Thus, as far as the calculations in this chapter are concerned, one year is treated as having exactly seven months (213 days) during which the overall mean temperature is 10EC. Oxidation and oxygen transport via either diffusion or convection are considered to cease during the five frozen months.

The idealized conditions for the four cases are listed in Table 5.1. Actual field conditions may be predominantly one of the cases or a combination of them. Field conditions may also change from time to time.

Table 5.1 Idealized Cases for Subaqueous Tailings Oxidation

Case No.	Water Cover Description	Conditions*				
		Water Aeration	O <sub>2</sub> Conc. in mg/L		Downward Infiltration	Tailings Resuspension
			Surface	Interface		
1	Stagnant	No	11.3	0	No	No
2	Fully oxygenated	Yes	11.3	11.3	No	No
3	Fully oxygenated + infiltration	Yes	11.3	11.3	1 m/year	No
4	Tailings resuspension alone	Yes	11.3	11.3	N/A	Yes

\*Water cover is assumed to be 0.3 m for all cases.

### 5.1 Stagnant Water Cover

In this case, we idealize the conditions as follows: the water cover (constantly 0.3 m deep) is saturated throughout its entire depth with dissolved oxygen (DO) at time zero (the moment of tailings deposition), and is in equilibrium with atmosphere at surface at all times. The ambient temperature is 10EC; thus the saturated dissolved oxygen concentration is 11.3 mg/L. The oxygen transport through the water cover is entirely through molecular diffusion. No convection exists. Oxygen is neither consumed nor generated within the water column. The water/tailings interface is situated at 0.3 m below water surface and oxidizes fast enough to maintain a zero oxygen concentration at and below the interface. This last assumption is a reasonable one, because at steady state the dissolved oxygen only penetrates a few mm below the water/tailings interface.

Under these conditions, the oxygen diffusion through the water column to the tailings, with the tailings acting as an oxygen sink, can be mathematically described by a one-dimensional, second order, partial differential equation(PDE):

$$D \frac{\partial^2 C}{\partial z^2} = \frac{\partial C}{\partial t} \quad (5.1)$$

- where D = diffusion coefficient of oxygen in water,  $1.3 \times 10^{-9} \text{ m}^2 \text{ s}^{-1}$  at 10EC and 1 bar and  $2.0 \times 10^{-9} \text{ m}^2 \text{ s}^{-1}$  at 25EC and 1 bar (Luckner et. al., 1991);
- C = C(z,t), dissolved oxygen concentration as a function of depth and time, g/m<sup>3</sup> (numerically equal to concentration expressed in mg/L);
- z = depth below water surface, m,  $0 \leq z \leq 0.3$ ; and
- t = time after deposition, s,  $t \geq 0$ ;

with the following initial and boundary conditions:

$$\begin{aligned} C(z, 0) &= C_0 \\ C(0, t) &= C_0 \\ C(h, t) &= 0 \end{aligned} \tag{5.2}$$

where  $C_0$  = saturated dissolved oxygen concentration in water, 11.3 g/m<sup>3</sup> at 10EC; and  
 $h$  = depth of the shallow water cover, 0.3 m in the present case.

Equation (5.1) with the initial and boundary conditions (5.2) has the following analytical solution (Crank, 1956, p. 47):

$$\begin{aligned} C(z,t) = C_0 \left( 1 - \frac{z}{h} \right) &+ \frac{2C_0}{\pi} \sum_{n=1}^{\infty} \frac{\sin \frac{npz}{h}}{n} \exp\left(-\frac{Dn^2 \pi^2 t}{h^2}\right) \\ &+ \frac{4C_0}{\pi} \sum_{m=0}^{\infty} \frac{1}{2m+1} \sin \frac{(2m+1)pz}{h} \exp\left(-\frac{D(2m+1)^2 \pi^2 t}{h^2}\right) \end{aligned} \tag{5.3}$$

The expression for dissolved oxygen profile at steady state can be obtained by simply setting  $t \rightarrow \infty$  in Equation (5.3), which causes the summations to disappear:

$$C(z, \infty) = C_0 \left( 1 - \frac{z}{h} \right) \tag{5.4}$$

The variation of the flux of dissolved oxygen from the water cover into the tailings over time,  $F(h,t)$ , can be calculated by Fick's first law

$$F(h,t) = -D \left( \frac{\partial C}{\partial z} \right)_{z=h} \tag{5.5}$$

where the term  $(\partial C / \partial z)_{z=h}$  is obtained by taking the partial derivative of Equation (5.3) with respect to  $z$  and then setting  $z=h$ . The resulting expression is as follows:

$$\begin{aligned} F(h,t) = -D \left( \frac{\partial C}{\partial z} \right)_{z=h} &= \frac{2C_0}{h} \sum_{n=1}^{\infty} \cos \frac{np}{h} \exp\left(-\frac{Dn^2 \pi^2 t}{h^2}\right) \\ &+ \frac{4C_0}{h} \sum_{m=0}^{\infty} \cos((2m+1)\pi) \exp\left(-\frac{D(2m+1)^2 \pi^2 t}{h^2}\right) \end{aligned} \tag{5.6}$$

Again, the steady state flux into the tailings can be calculated by substituting  $t \rightarrow \infty$  into Equation (5.6):

$$F(h, \infty) = D \frac{C_0}{h} \tag{5.7}$$

Substituting the values of  $D$ ,  $C_0$ , and  $h$  into Equation (5.7) gives a steady-state flux of  $4.90 \times 10^{-8} \text{ g/m}^2/\text{s}$ , or  $0.90 \text{ g/m}^2/\text{year}$  (recall that 1 year = 213 days).

The cumulative oxygen mass transfer into the tailings,  $M(h,t)$ , is obtained by integrating Equation (5.6) with respect to time from  $t=0$  to  $t=t$ :

$$\begin{aligned}
 M(h,t) &= \int_0^t F(h,t) dt \\
 &= \frac{DC_0}{h} t + \sum_{n=1}^{\infty} \frac{2hC_0}{n^2 p^2} \cos(np) \left[ 1 - \exp\left(-\frac{Dn^2 p^2 t}{h^2}\right) \right] + \\
 &\quad \sum_{m=0}^{\infty} \frac{4hC_0}{(2m+1)^2 p^2} \cos[(2m+1)p] \left[ 1 - \exp\left(-\frac{D(2m+1)^2 p^2 t}{h^2}\right) \right]
 \end{aligned} \tag{5.8}$$

The expressions in Equations (5.3), (5.6), and (5.8) are evaluated numerically and the results are plotted in Figures 5.1, 5.2 and 5.3.

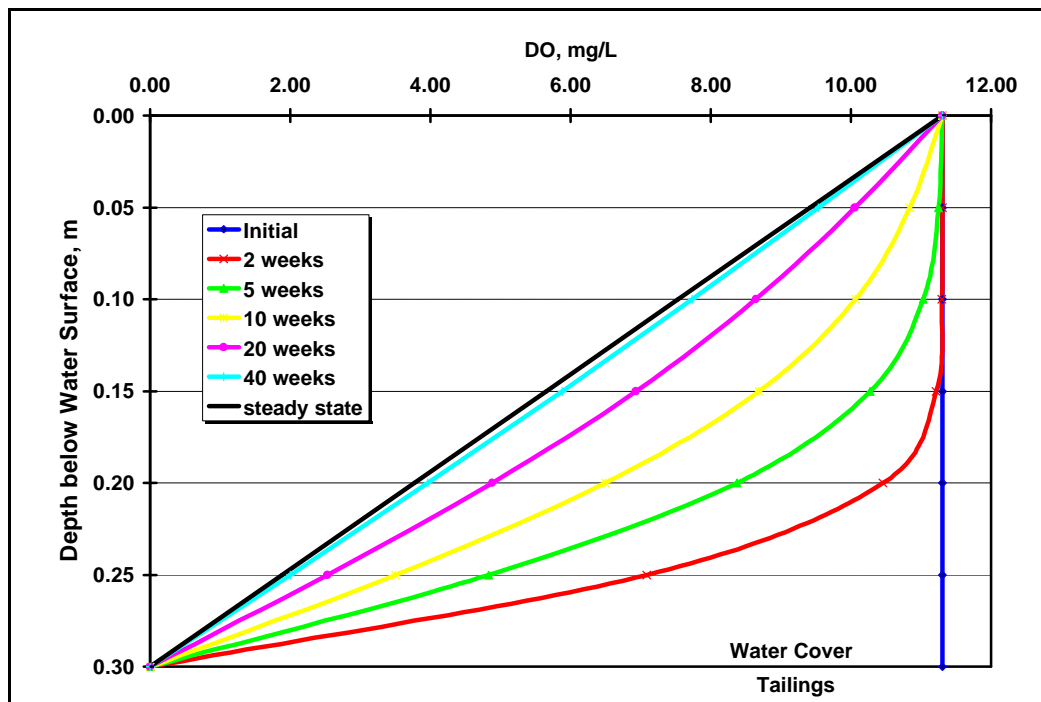


Figure 5.1 DO Profiles in Stagnant Water Cover

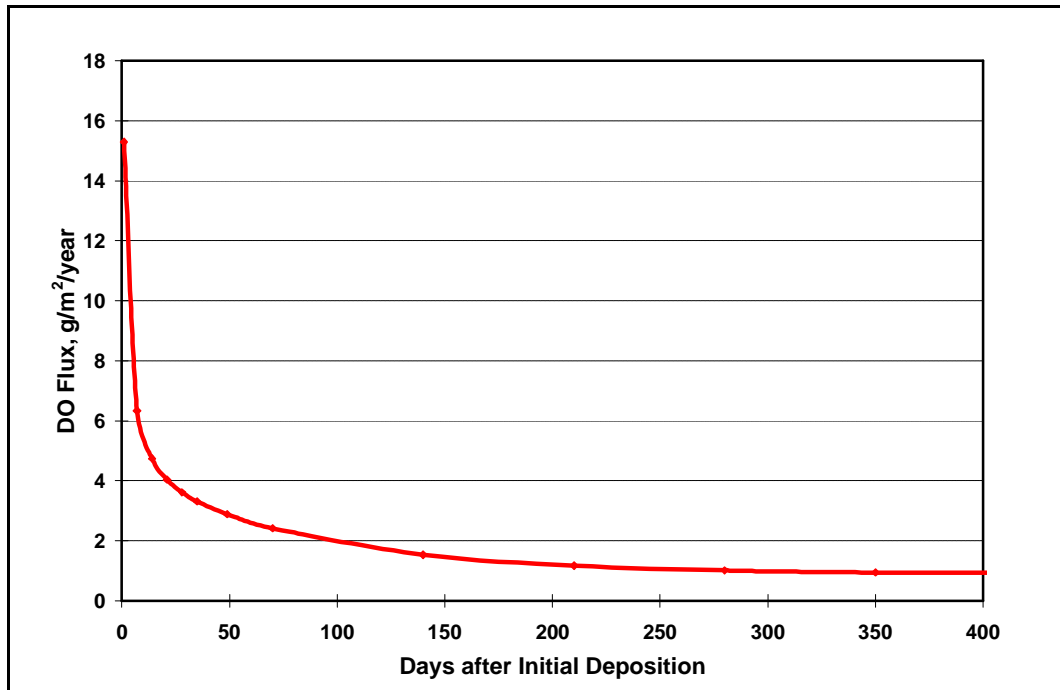


Figure 5.2 DO Flux into Tailings from Stagnant Water Cover

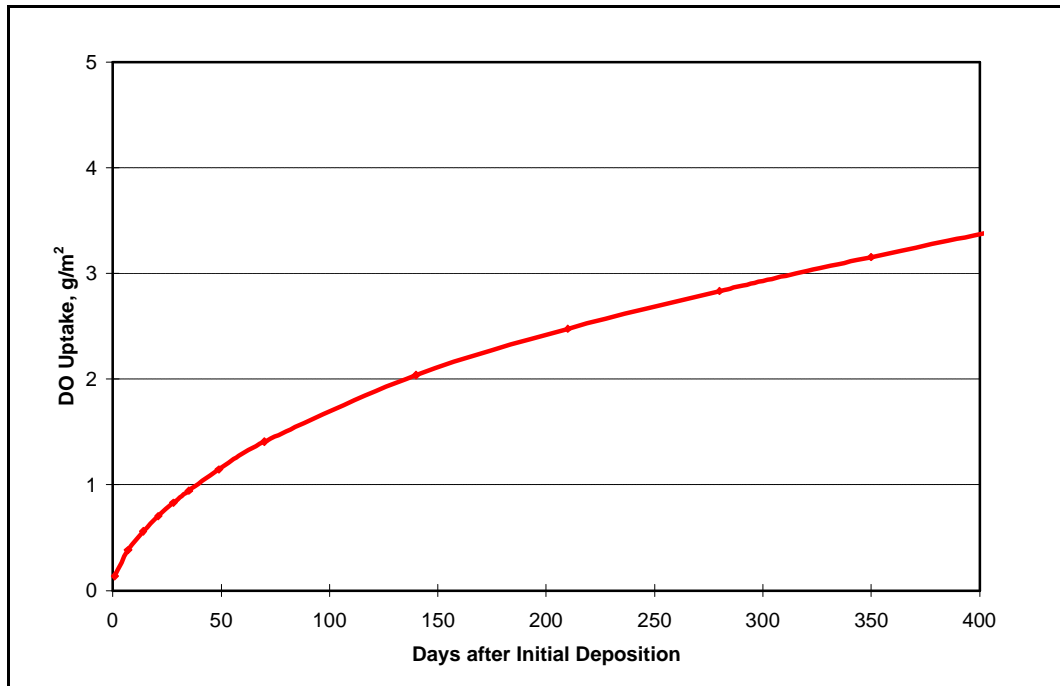


Figure 5.3 DO Mass Transferred into Tailings from Stagnant Water Cover

Figures 5.1 - 5.3 reveal the following points:

- < The transient period (time from initial tailings deposition to establishment of a steady state) is about 40 weeks (Figure 5.1). The slope  $(\text{MC}/\text{Mz})_{z=h}$  continuously decreases during the transient period until it reaches  $-C_0/h = - (11.3 \text{ g m}^{-3}) / (0.3 \text{ m}) = -37.7 \text{ g m}^{-4}$  and is everywhere equal throughout the water cover at the steady state.
- < The dissolved oxygen flux into the tailings initially decreases very quickly and then more slowly until a constant value of  $0.9 \text{ g m}^{-2} \text{ year}^{-1}$  is attained at steady state (Figure 5.2).
- < The total dissolved oxygen uptake by the tailings initially increases quickly during the transient period when the dissolved oxygen gradient is high; the increase becomes linear after about 40 weeks as a steady state is reached (Figure 5.3).

## 5.2 Fully-Oxygenated Water Cover

In this case, the 0.3 m water cover is assumed to be fully oxygenated and well mixed, therefore containing 11.3 mg/L dissolved oxygen (at 10EC). To calculate the rate of sulphide oxidation, we need to begin with the calculation of specific surface area of the tailings.

### 5.2.1 Specific Surface Area

Lacking direct measurement of the specific surface area (the total surface area per unit mass of tailings), it was calculated from the cumulative size distribution curve (Figure 2.1). The size distribution curve of sample L-1 was chosen because it covered a wider size range.

The specific surface area,  $a_{tail}$ , of the Louvicourt tailings is given by

$$a_{tail} = \frac{6\gamma}{\rho_p} \int_0^1 \frac{1}{d_p} df \quad (5.9)$$

where  $a_{tail}$  = specific surface area of tailings,  $\text{m}^2/\text{kg}$  of tailings;  
 $\gamma$  = shape factor, equals 1.0 for cubes and spheres and 1.75 for most other shapes;  
 $\rho_p$  = density of tailings particles;  
 $f$  = cumulative size fraction greater than size  $d_p$ ; and  
 $d_p$  = size of tailings particles.

The integral in the above equation was evaluated by graphically determining the area under the curve in a plot of  $1/d_p$  (y-axis) versus  $f$  (x-axis) and was found to be  $47.0 \text{ mm}^{-1}$ , or  $470 \text{ cm}^{-1}$ . Therefore,

$$\begin{aligned}a_{tail} &= (6)(1.75)(470)/(3.8) \\ &= 1299 \text{ cm}^2/\text{g} \\ &= 129.9 \text{ m}^2/\text{kg}\end{aligned}$$

where  $3.8 \text{ g/cm}^3$  is the estimated average particle density of the tailings.

### 5.2.2 Oxidation Rate

Recent literature on pyrite oxidation rate in a solid suspension suggests an oxidation rate of about  $0.5 \text{ nmol FeS}_2/\text{m}^2$  pyrite surface/s (Morin, 1993). This rate applies when the water is not in shortage of oxygen supply and has a nearly neutral pH. It has also been demonstrated that in the absence of dissolved oxygen, no sustainable sulphide oxidation takes place, even when ferric iron is present as an oxidant, unless external ferric iron is continuously added to the system.

The dominant sulphide in the Louvicourt tailings is pyrite. The pH of the water cover over the tailings is for most time of the year neutral or alkaline. Therefore, the above rate should be close to the actual underwater oxidation rate of the Louvicourt tailings.

Now let us compare the submerged oxidation rate found in the literature with the oxidation rate determined in the humidity cells. To do this the specific pyrite surface area of the Louvicourt tailings is required. This is calculated as follows. The average pyrite (including minor pyrrhotite) content in the Louvicourt tailings is about 29.5% by mass; adjusting this percentage by the average specific gravity of the tailings particles, 3.8, and the specific gravity of pyrite, 5.0, we obtain the percent pyrite content by volume:  $(29.5\%)/(5.0)*(3.8) = 22.4\%$ . Assuming that the average pyrite particle size is the same as that of the tailings, the percentage of pyrite surface area relative to the total tailings surface area would be the same as the pyrite content by volume: 22.4%; i.e., 22.4% of the total tailings surface area in the Louvicourt tailings are on pyrite. The specific pyrite surface area is then  $(129.9 \text{ m}^2/\text{kg tailings}) \times 22.4\% = 29.1 \text{ m}^2$  pyrite surface/kg tailings.

The average rate of oxidation measured in the humidity cell tests of the Louvicourt tailings at 25 EC is that which generated  $1449 \text{ mg CaCO}_3$  eq/kg/week acidity (Table 4.5), or  $870 \text{ mg FeS}_2/\text{kg/week}$ . Normalizing this mass-based oxidation rate by pyrite surface area gives an oxidation rate of  $870 \text{ mg FeS}_2/29.1 \text{ m}^2$  of pyrite surface/week, or  $0.42 \text{ nmol FeS}_2 \text{ m}^{-2} \text{ s}^{-1}$ , which is in excellent agreement with the rate reported in literature ( $0.5 \text{ nmol FeS}_2 \text{ m}^{-2} \text{ s}^{-1}$ ). To apply this rate to the field, it must be adjusted for the colder field temperatures. Using the average monthly temperatures for the seven unfrozen months at Louvicourt and assuming the oxidation rate to decrease with temperature exponentially, the average oxidation rate applicable to the Louvicourt site for the seven unfrozen months is found to be  $0.16 \text{ nmol FeS}_2 \text{ m}^{-2} \text{ s}^{-1}$ , or 38.4% of the laboratory-determined rate at 25EC. This rate will be used below for the calculation of underwater oxidation of the Louvicourt tailings.

### 5.2.3 Oxidation under Water Cover

It is assumed that the 0.3 m water cover above the tailings is fully oxygenated and well mixed for the seven unfrozen months of the year. The dissolved oxygen at the average temperature for the seven months (10EC) is 11.3 g/m<sup>3</sup>. It is also assumed that there is no downward water flow through the submerged tailings and thus the tailings pore water is stagnant.

Under these assumptions, dissolved oxygen will be readily available at the water/tailings interface at a concentration of 11.3 g/m<sup>3</sup>. However, since the tailings pore water is stagnant, this dissolved oxygen must diffuse through the pore water to reach sulphide particles before any oxidation can take place. This diffusion transports dissolved oxygen into the stagnant pore water, which is consumed by sulphide oxidation reactions. Dissolved oxygen concentration decreases with depth below the water/tailings interface until it is depleted at a certain depth.

The above process is described by the PDE

$$\frac{\partial C}{\partial t} = D_e \frac{\partial^2 C}{\partial z^2} - [MC/Mt]_{ox} \quad (5.10)$$

where C = C(z,t), dissolved oxygen concentration in the tailings pore water;  
 D<sub>e</sub> = effective diffusion coefficient through the tailings pore water for dissolved oxygen, dimensionless;  
 z = depth below the tailings/water interface, m;  
 t = time after initial deposition of the tailings; and  
 [MC/Mt]<sub>ox</sub> = change in dissolved oxygen concentration with time due to consumption of oxygen by sulphide oxidation.

Assuming a first-order reaction for oxygen consumption due to sulphide oxidation with respect to dissolved oxygen concentration, we have

$$\frac{\partial C}{\partial t} = -kC \quad (5.11)$$

where k is the rate constant, s<sup>-1</sup>; and the negative sign indicates that the term [MC/Mt]<sub>ox</sub> is a negative quantity in Equation (5.11) (i.e., C decreases because of oxygen consumption).

Substituting Equation (5.11) into (5.10), we obtain



$$\frac{MC}{Mt} = D_e \frac{M^2C}{Mz^2} + kC \quad (5.12)$$

The initial and boundary conditions for our present system are  $C=0$  for  $t = 0$  and  $z > 0$  (i.e., the dissolved oxygen concentration at time 0 is 0 below the water/tailings interface); and  $C=C_0$  for  $t > 0$  and  $z = 0$  (i.e., the dissolved oxygen concentration at the water/tailings interface is at all times equal to  $C_0$ , the saturated dissolved oxygen concentration at the temperature of concern). Equation (5.12) with the boundary conditions just stated has the following analytical solution (Crank, 1956, pp.129-131):

$$C(z,t) = C_0 \left[ \frac{1}{2} \exp\left(\frac{kz}{D_e}\right) \operatorname{erfc}\left(\frac{z}{2\sqrt{D_e t}} + \sqrt{kt}\right) + \frac{1}{2} \exp\left(\frac{kz}{D_e}\right) \operatorname{erfc}\left(\frac{z}{2\sqrt{D_e t}} - \sqrt{kt}\right) \right] \quad (5.13)$$

where  $\operatorname{erfc}$  is the complementary error function. The flux,  $F(0,t)$ , across the water/tailings interface at any time  $t$  is given by

$$F(0,t) = C_0 \sqrt{D_e k} \left[ \operatorname{erf}(\sqrt{kt}) + \frac{\exp(-kt)}{\sqrt{kt}} \right] \quad (5.14)$$

and the total mass of dissolved oxygen diffused across the water/tailings boundary,  $M(0,t)$ , from  $t=0$  to  $t=t$  is obtained by integrating the flux  $F(0,t)$  over the time interval  $[0, t]$  and has the form

$$M(0,t) = C_0 \sqrt{\frac{D_e}{k}} \left[ \left(kt + \frac{1}{2}\right) \operatorname{erf}(\sqrt{kt}) + \sqrt{\frac{kt}{\pi}} \exp(-kt) \right] \quad (5.15)$$

When enough time has passed and diffusion and sulphide oxidation have reached a *steady state*, Solutions (5.13) and (5.14) are reduced, by setting  $t \rightarrow \infty$ , to the following, much simpler forms:

$$C(z,\infty) = C_0 \exp\left(\frac{kz}{D_e}\right) \quad (5.16)$$

$$F(0,\infty) = C_0 \sqrt{D_e k} \quad (5.17)$$

Equations (5.16) and (5.17) indicate that to fully describe the steady state behaviour of the system, only two parameters are required:  $D_e$  and  $k$ .

The effective diffusion coefficient of dissolved oxygen in tailings pore water,  $D_e$ , can be calculated by the following formula:

$$D_e = \frac{Dn}{t} \quad (5.18)$$

where  $D$  = diffusion coefficient of oxygen in water,  $1.3 \times 10^{-9} \text{ m}^2 \text{ s}^{-1}$  at 10EC and 1 bar;  
 $n$  = porosity of the tailings, dimensionless; and  
 $t$  = tortuosity, dimensionless.

Using an assumed porosity of  $n=0.4$  and a tortuosity of  $t=5$ , we arrive at an effective diffusion coefficient of  $D_e = 1.04 \times 10^{-10} \text{ m}^2 \text{ s}^{-1}$ .

The first-order reaction rate constant,  $k$ , can be calculated from the tailings oxidation rate, determined to be  $0.16 \text{ nmol FeS}_2 \text{ m}^{-2} \text{ s}^{-1}$  for the field conditions at the Louvicourt site (see last section), as follows.

The stoichiometry of pyrite oxidation in submerged tailings, assuming the main terminal form of iron to be ferrous, is that every mole of pyrite oxidized consumes 3.5 moles of dissolved oxygen. Therefore, the term  $[\text{MC/Mt}]_{\text{ox}}$  in Equation (5.11) can be expressed as

$$\frac{\text{MC}}{-\text{Mt} \dot{I}_{\text{ox}}} = \frac{3.5}{V_p} \frac{dQ_{\text{py}}}{dt} = kC \quad (5.19)$$

where  $V_p$  = volume of the pore water associated with the reacting pyrite,  $\text{m}^3$ ; and  
 $Q_{\text{py}}$  = quantity of reactive pyrite, mol.

Dividing both sides of the above equation by the total surface area of pyrite,  $A_{\text{py}}$ , and rearranging gives

$$\frac{1}{A_{\text{py}}} \frac{dQ_{\text{py}}}{dt} = \frac{k}{3.5} \frac{V_p}{A_{\text{py}}} C \quad (5.20)$$

where the quantity  $[(dQ_{\text{py}})/(A_{\text{py}} dt)]$ , in  $\text{mol m}^{-2} \text{ s}^{-1}$ , is the same as that measured in the humidity cell tests. Re-writing  $[(dQ_{\text{py}})/(A_{\text{py}} dt)]$  as  $R$ , and solving for  $k$  gives

$$k = 3.5 \frac{A_{\text{py}}}{V_p} \frac{R}{C} \quad (5.21)$$

Since  $A_{\text{py}} = (1-n)V_{\text{tot}} \rho_{\text{tail}} a_{\text{py}}$  where  $V_{\text{tot}}$  is the total bulk volume of tailings,  $\rho_{\text{tail}}$  the average density of tailings particles, and  $a_{\text{py}}$  the specific pyrite surface ( $\text{m}^2$  pyrite surface area per kg of tailings), and since  $V_p = nV_{\text{tot}}$ , we have

$$\frac{A_{py}}{V_p} = \frac{(1+n)^2 a_{py}}{n} \quad (5.22)$$

Substitute this expression into Equation (5.21), we obtain

$$k = 3.5 \frac{(1+n)^2 a_{py} R}{n C} \quad (5.23)$$

Now we can use the humidity cell-determined oxidation rate,  $R_o$ , at saturated dissolved oxygen concentration,  $C_o$ , to calculate the first-order constant  $k$ . Substituting the following values into Equation (5.23):

$$\begin{aligned} n &= 0.4 \text{ (assumed)} \\ \rho_{tail} &= 3800 \text{ kg/m}^3 \text{ (assumed)} \\ a_{py} &= 29.1 \text{ m}^2/\text{kg} \\ R_o &= 1.6 \times 10^{-10} \text{ mol/m}^2/\text{s} \\ C_o &= 0.353 \text{ mol/m}^3 \end{aligned}$$

we obtain a  $k$  value of  $2.6 \times 10^{-4} \text{ s}^{-1}$ .

With the values of  $D_e$  and  $k$  known, we evaluated  $C(z,t)$ ,  $F(0,t)$ , and  $M(0,t)$  according to Equations (5.13), (5.14), and (5.15); corresponding results are graphically presented in Figures 5.4, 5.5, and 5.6. The following observations can be made of these figures:

- < Theoretically, the transient period lasts only about 10 hours (0.4 day, Figure 5.4). This is virtually equivalent to saying that the oxidation of tailings would be at steady state as soon as they are deposited under the water cover. This is in sharp contrast with the last case examined - stagnant water cover, where it requires about 40 weeks to reach a steady state. Of course the difference in the time to reach a steady state reflects the different rate-limiting mechanisms in operation - in the stagnant water cover case, it is the diffusion of oxygen; in the fully-oxygenated water cover case, it is the rate of tailings oxidation which consumes oxygen.

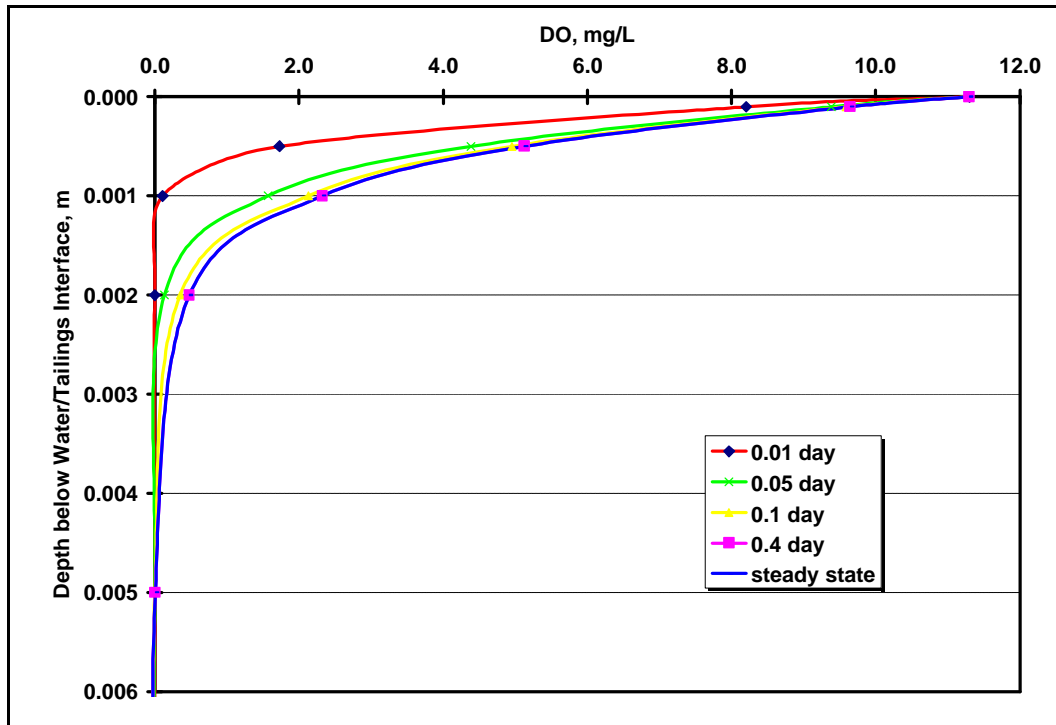


Figure 5.4 Tailings Porewater DO Profiles under Fully-Oxygenated Water Cover

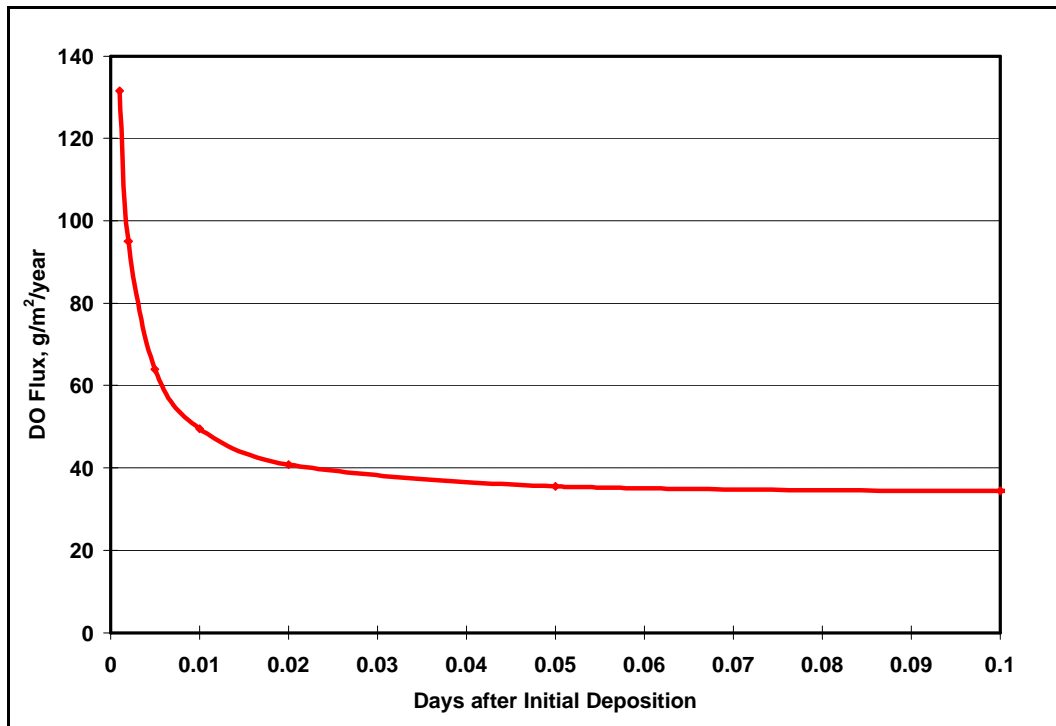


Figure 5.5 DO Flux into Tailings from Fully-Oxygenated Water Cover

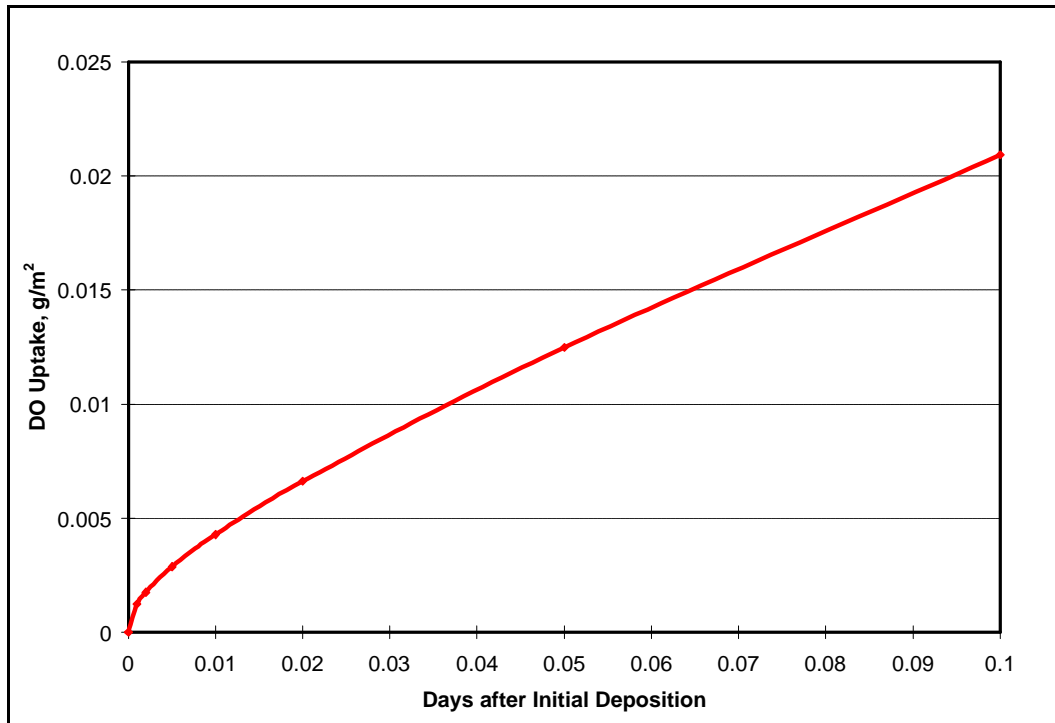


Figure 5.6 DO Mass Transfer into Tailings from Fully-Oxygenated Water Cover

- < At steady state, the dissolved oxygen concentration gradient is found the highest (in absolute value) at the water/tailings interface; it decreases with depth below the interface until it becomes zero at about 6 mm. As a result, the vertical dissolved oxygen flux decreases with depth below the interface as it is consumed by sulphide oxidation; it becomes zero at about 6 mm below which sulphide oxidation ceases. Since the oxidation rate is directly proportional to dissolved oxygen concentration (first order kinetics), it too decreases with depth below the interface and becomes zero at about 6 mm where dissolved oxygen concentration reduces to zero. The depth of dissolved oxygen penetration is therefore around 6 mm, limiting the tailings oxidation to a very thin layer of tailings just below the water/tailings interface.
- < The dissolved oxygen flux decreases very quickly with time and reaches a steady state value of 34.2 g/m<sup>3</sup>/year in 0.4 day (Figure 5.5).
- < The total dissolved oxygen uptake by the tailings increases quickly and non-linearly initially; however the increase soon becomes linear as a steady state is reached (Figure 5.6).

### 5.3 Fully-Oxygenated Water Cover with Downward Infiltration

This case is identical to the last case except that now the water cover infiltrates down into the tailings. It is assumed that the water cover depth will still be maintained (by adding enough water to compensate the downward infiltration) at 0.3 m and the down-flowing pore water

in the tailings has a linear velocity of 1 m/year ( $5.43 \times 10^{-8}$  m/s). Compared with the last case, this case facilitates more dissolved oxygen to be delivered to the reactive tailings by addition of convective transport of dissolved oxygen.

The present system is described by the PDE

$$\frac{\partial C}{\partial t} = D_e \frac{\partial^2 C}{\partial z^2} + v_z \frac{\partial C}{\partial z} - kC \quad (5.24)$$

with the initial and boundary conditions

$$\begin{aligned} C &= C_0 \quad \text{for } z=0 \text{ and } t \geq 0 \\ C &= 0 \quad \text{for } z \geq 0 \text{ and } t=0 \end{aligned} \quad (5.25)$$

where  $v_z$  is the downward linear velocity of the pore water infiltrating the tailings. The analytical solution for Equation (5.24) with boundary conditions (5.25) is as follows (Jost, 1960; Domenico et. al., 1990):

$$C(z,t) = \frac{C_0}{2} \exp\left[-\frac{v_z z}{2D_e} \left(1 + \sqrt{1 + \frac{4kD_e}{v_z^2}}\right)\right] \operatorname{erfc}\left[\frac{z + v_z t \sqrt{1 + \frac{4kD_e}{v_z^2}}}{2\sqrt{D_e t}}\right] \quad (5.26)$$

The flux of dissolved oxygen into the tailings as a function of time,  $F(0,t)$ , during the transient period is given by

$$F(0,t) = D_e \left. \frac{\partial C(z,t)}{\partial z} \right|_{z=0} + v_z C(0,t) \quad (5.27)$$

Substituting  $C(z,t)$  from (5.26) into (5.27) gives

$$\begin{aligned} F(0,t) &= \frac{C_0 v_z}{2} \left[ 1 + \frac{1}{2} \left( 1 + \sqrt{1 + \frac{4kD_e}{v_z^2}} \right) \right] \operatorname{erf}\left[\frac{v_z}{2\sqrt{D_e}} \sqrt{\left(1 + \frac{4kD_e}{v_z^2}\right)t}\right] \\ &\quad + \frac{C_0}{2} \sqrt{\frac{D_e}{\pi t}} \exp\left[-\frac{v_z^2}{4D_e} \left(1 + \frac{4kD_e}{v_z^2}\right)t\right] \end{aligned} \quad (5.28)$$

Integrating (5.28) from  $t=0$  to  $t=t$  gives us the total mass uptake of dissolved oxygen by the tailings from time 0 to time  $t$ , symbolled by  $M(0,t)$ :

$$\begin{aligned}
 M(0,t) &= \int_0^t F(0,t) dt \\
 &= k_1 t + \frac{k_1}{2k_2^2 k_3} \frac{k_4}{k_2} \sqrt{\frac{p}{k_3}} \operatorname{erf}(k_2 \sqrt{k_3} t) + \frac{k_1}{k_2} \sqrt{\frac{t}{pk_3}} \exp(-k_2^2 k_3 t)
 \end{aligned} \tag{5.29}$$

where  $k_1$ ,  $k_2$ ,  $k_3$ , and  $k_4$  are constants defined as follows:

$$\begin{aligned}
 k_1 &= \frac{C_0 v_z}{2} \left[ 1 + \frac{1}{2} (1 + \sqrt{1 + 4kD_e/v_z^2}) \right] \\
 k_2 &= \frac{v_z}{2\sqrt{D_e}} \\
 k_3 &= 1 + 4kD_e/v_z^2 \\
 k_4 &= \frac{C_0}{2} \sqrt{\frac{D_e}{p}}
 \end{aligned} \tag{5.30}$$

The steady state equations corresponding to (5.26) and (5.28) are obtained by setting  $t=4$ :

$$C(z,4) = C_0 \exp\left(\frac{v_z}{-2D_e} z\right) \left[ 1 + \sqrt{1 + 4kD_e/v_z^2} \right] \tag{5.31}$$

$$F(0,4) = C_0 v_z \left[ 1 + \frac{1}{2} (1 + \sqrt{1 + 4kD_e/v_z^2}) \right] \tag{5.32}$$

With  $v_z$ ,  $D_e$ , and  $k$  known, Equations (5.26), (5.28), and (5.29) are evaluated; the results are shown in Figures 5.7, 5.8, and 5.9, respectively. The following observations can be made from these graphs:

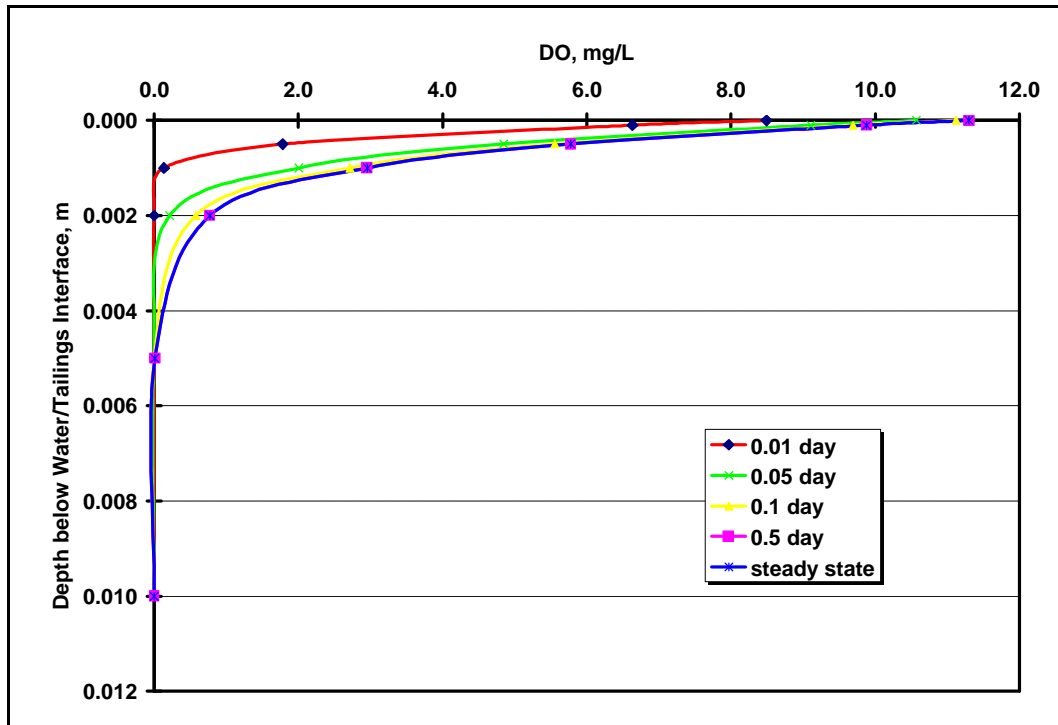


Figure 5.7 Tailings Porewater DO Profiles under Fully-Oxygenated, Infiltrating Water Cover

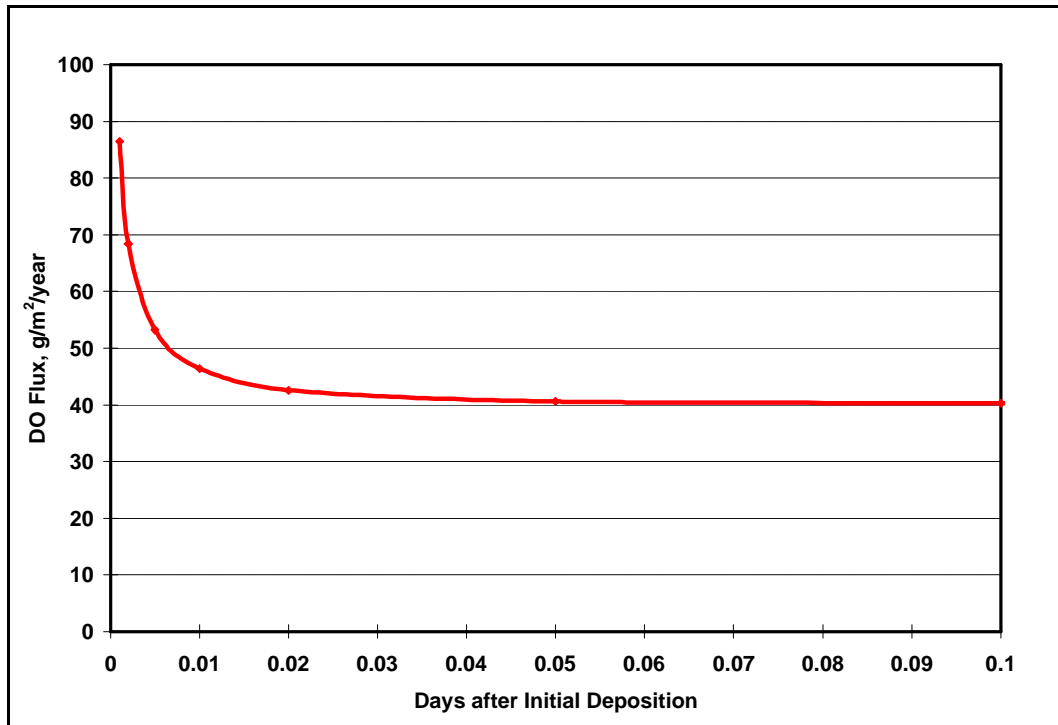


Figure 5.8 DO Flux into Tailings from Fully-Oxygenated, Infiltrating Water Cover



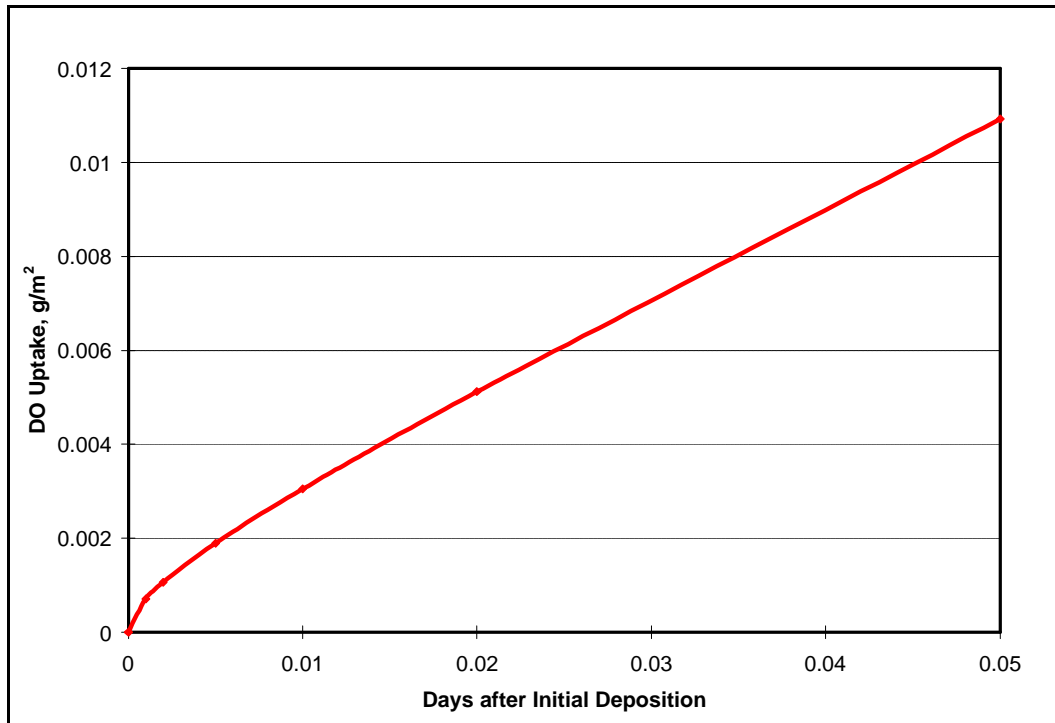


Figure 5.9 DO Mass Transferred into Tailings from Fully-Oxygenated, Infiltrating Water Cover

- < The transient period lasts about 10 hours (0.5 day, Figure 5.7), only marginally longer than the last case (without infiltration). The oxidation of tailings would virtually be at steady state once it is deposited under water.
- < As in the last case, at steady state, the dissolved oxygen concentration gradient is found the highest (in absolute value) at the water/tailings interface; it decreases with depth below the interface until it becomes zero at about 8 mm (which is 2 mm deeper than the last case without downward infiltration). Consequently, the vertical dissolved oxygen flux decreases with depth below the interface as it is consumed by sulphide oxidation; it becomes zero at about 8 mm below which sulphide oxidation ceases. Since the oxidation rate is directly proportional to dissolved oxygen concentration (first order kinetics), it too decreases with depth below the interface and becomes zero at about 8 mm where dissolved oxygen concentration reduces to zero. The depth of dissolved oxygen penetration is therefore around 8 mm, limiting the tailings oxidation to a very thin layer of tailings just below the water/tailings interface.
- < The dissolved oxygen flux decreases very quickly with time and reaches a steady state value of 40.3 g/m<sup>2</sup>/year in about 12 hours (Figure 5.8). Recall that the steady state flux for the last case is 34.2 g/m<sup>2</sup>/year, thus the contribution to steady state flux by the downward water movement is 6.1 g/m<sup>2</sup>/year, a 18% increase.

- < As in the last case, the total dissolved oxygen uptake by the tailings increases quickly and non-linearly initially, but the increase soon becomes linear as the steady state is reached (Figure 5.9).

#### 5.4 Tailings Resuspension

This case is different from the last three in that the last three cases all involve the transport of dissolved oxygen to the reactive sulphides in the settled and undisturbed tailings, whereas this case involves the transport of reactive sulphides, through resuspension of tailings, to the overlying water cover to access dissolved oxygen. The science for predicting the degree of tailings resuspension from variables such as wind speed, thermal stratification, pond geometry, properties of the pond water and of the tailings, etc. is still immature, and is the focus of some scientific research. Therefore we will not attempt predicting the amount of tailings suspended but rather, we will assume different amounts of tailings suspended (in terms of the thickness of the layer, assumed uniform, which goes into suspension) and calculate the corresponding amounts of oxidation taking place.

The following assumptions are made in calculating the degrees of oxidation associated with tailings resuspension:

- < Tailings resuspension occurs uniformly and the amount of resuspension is specified by the thickness of settled tailings which become resuspended.
- < The resuspended tailings oxidize at the average rate as determined by the humidity cell tests, adjusted for the field conditions (i.e.  $1.6 \times 10^{-10}$  mol FeS<sub>2</sub> m<sup>-2</sup> s<sup>-1</sup>). This is equivalent to saying that there is unlimited supply of dissolved oxygen and, as a result, the oxidation rate is limited only by the rate of chemical reaction.
- < The upper constraint for the amount of oxidation of suspended solids is the total amount of sulphides resuspended. Oxidation cannot proceed any further once all the sulphides in the resuspended tailings is depleted. Normally this upper constraint is not reached for the duration of tailings resuspension, as shown by the simple calculation below. At an oxidation rate of  $1.6 \times 10^{-10}$  mol FeS<sub>2</sub> m<sup>-2</sup> s<sup>-1</sup> or 0.337 g pyrite/kg tailings/week and a total amount of resuspended tailings (assuming 2 mm tailings resuspension) of 4.56 kg tailings/m<sup>2</sup> interface<sup>3</sup>, the total amount of tailings oxidized would be 1.54 g pyrite/m<sup>2</sup> interface/week. Since 29.5% of the 4.56 kg/m<sup>2</sup> interface, or 1.34 kg/m<sup>2</sup> interface, is pyrite, there is enough pyrite in the resuspended tailings for oxidation for  $1340/1.54 = 870$  weeks.

---

<sup>3</sup>Here the word “interface” refers to the tailings/water cover interface. The volume of tailings resuspended per m<sup>2</sup> of interface is numerically equal to the thickness of resuspension expressed in m. For example, if 2 mm, or 0.002 m of submerged tailings are resuspended, the volume resuspended would be  $0.002 \text{ m} \times 1 \text{ m}^2 = 0.002 \text{ m}^3$  per m<sup>2</sup> of interface.

- < For the calculation of oxidation associated with tailings resuspension, it is assumed, as in the previous cases, that one year equals the seven unfrozen months (213 days). During the remaining five months, the water cover would be frozen solid; neither resuspension nor oxidation would occur.

Under the foregoing assumptions, the oxidation associated with tailings resuspension is calculated and the results presented in Figure 5.10. For ease of comparison with previous cases, the degree of oxidation has been expressed in terms of dissolved oxygen consumption by oxidation. It is easy to see that the amount of oxidation due to tailings resuspension is directly proportional to the duration of resuspension and to the thickness of tailings resuspended.

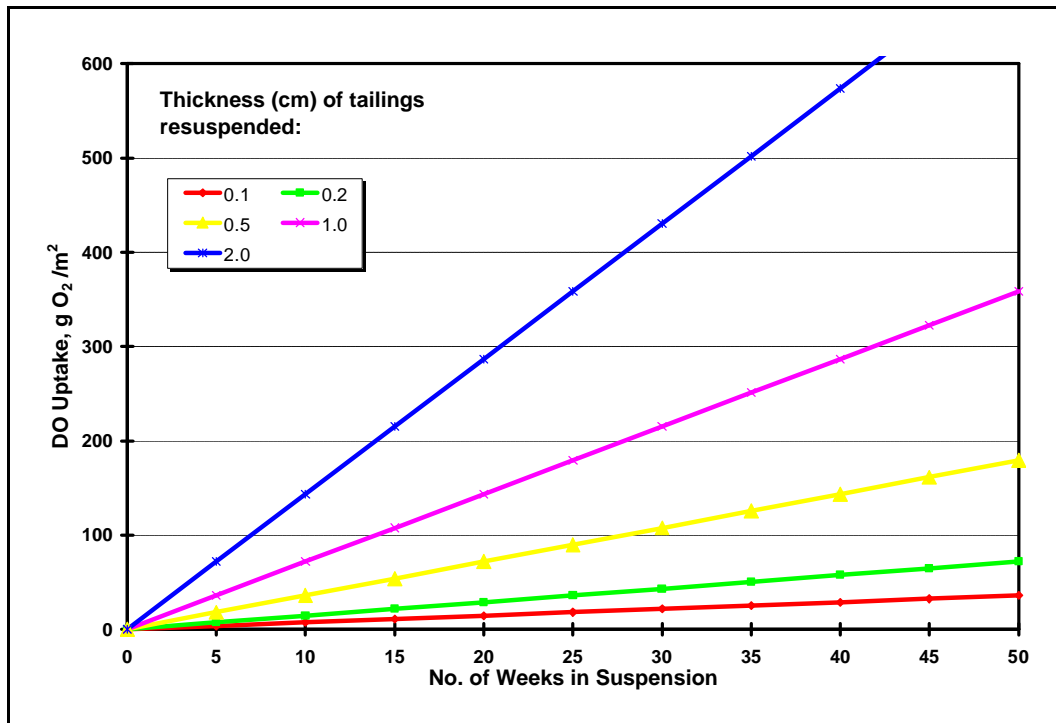


Figure 5.10 Dissolved Oxygen Consumption by Oxidation of Resuspended Tailings

### 5.5 Comparison of Cases

The four cases discussed are compared in Table 5.2 and Figure 5.11.

**Table 5.2 Comparison of Dissolved Oxygen Consumption for Four Cases**

Days	Cumulative Mass of DO Uptake by Tailings (g/m <sup>2</sup> interface)			
	Stagnant 0.3 m water cover	Fully oxygenated 0.3 m water cover	Fully oxygen. 0.3 m water cover with 1 m/y infiltration	Resuspension of 2 mm layer of tailings
0	0.00	0.00	0.00	0.00
1	0.14	0.16	0.19	0.20
7	0.38	1.13	1.33	1.43
14	0.56	2.25	2.65	2.87
21	0.70	3.38	3.98	4.30
28	0.83	4.50	5.30	5.74
35	0.94	5.62	6.63	7.17
49	1.15	7.89	9.28	10.04
70	1.41	11.24	13.25	14.34
140	2.04	22.48	26.50	28.69
210	2.48	33.78	39.75	43.03
280	2.83	44.97	53.00	57.37
350	3.15	56.19	66.24	71.71
700	4.65	112.38	132.47	143.43
Ratio	1.00	24.15	28.47	30.83

The dissolved oxygen consumptions by cases 2, 3, and 4 are in the same order of magnitude; the order of consumption is (resuspension of 2 mm layer of tailings<sup>4</sup>) . (fully oxygenated 0.3 m water cover with infiltration) > (fully oxygenated 0.3 m water cover without infiltration). All of the last three cases have an oxidation rate more about 30 times the pure diffusion case (stagnant 0.3 water cover). Table 5.2 shows that, if we take the dissolved oxygen consumption at the end of 700 days in the pure diffusion case as a base of 1.0, the oxygen consumptions in cases 2, 3, and 4 are approximately 24, 28, and 30, respectively.

---

<sup>4</sup>It is unlikely that in the field any tailings would remain continuously resuspended for any extended period of time. It is more likely that tailings would be resuspended briefly during high winds and then would resettle once the high winds subsides. In this case the oxygen consumption by resuspended tailings would be reduced proportionally.

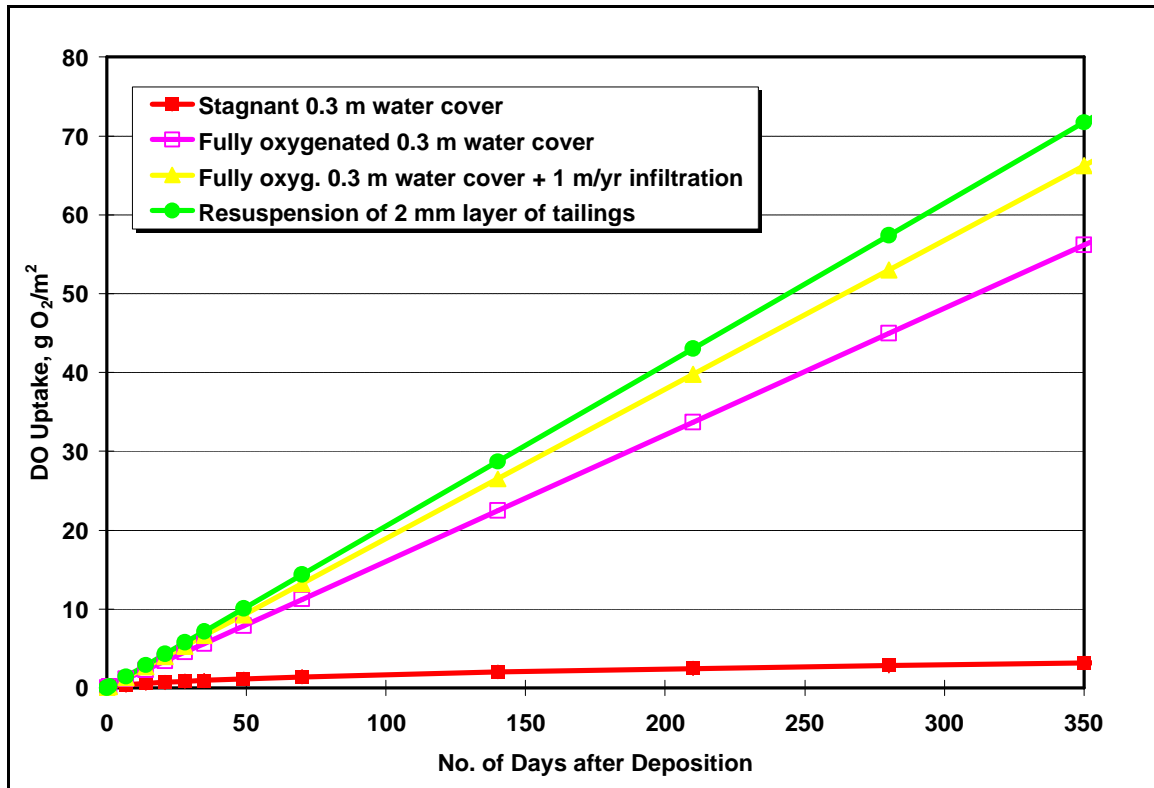


Figure 5.11 Comparison of Dissolved Oxygen Consumption among Four Cases

The above comparison is subject to the assumptions made in deriving these figures, especially the thickness of the layer of tailings resuspended (assumed to be 2 mm) and the infiltration velocity (assumed 1 m/year). If the assumptions change, the relative positions of the lines in Figure 5.11 as well as the ratios in Table 5.2 also change. Nevertheless, the calculations demonstrate the relative magnitudes of oxidation incurred by different mechanisms.

## 5.6 General Field Implications

It is clear that the effects of different mechanisms of increasing oxygen transport to reactive sulphides are approximately additive. In the field, the cases normally do not occur in isolation but rather occur in combination. To reduce the oxidation of submerged tailings, a stagnant water cover without aeration is the most desirable case. All of the mechanisms that increase the transport of oxygen into the submerged tailings should be minimized or eliminated, as discussed below. It must be pointed out that it is highly questionable whether the idealized stagnant water cover exists in the field at all. Field evidence collected so far indicates that shallow water covers are usually thoroughly mixed and fully saturated with dissolved oxygen. It is unrealistic to control the concentration of dissolved oxygen in the field.

### *Thickness of Water Cover*

Increasing the thickness of water cover slows down the rate of dissolved oxygen uptake by submerged tailings through diffusion - by decreasing the dissolved oxygen concentration gradient. Hence, increasing the thickness of water cover is only worthwhile if the water cover can be maintained stagnant (i.e., no aeration or infiltration of the water cover occurs). Measures that can help maintain a stagnant water cover include aquatic plant stabilization, internal dykes, and wave breakers. However, if appreciable degree of aeration occurs throughout the water cover, the benefit of increasing the thickness of the water cover vanishes. In the case where aeration occurs only to a certain depth (i.e., if a dissolved oxygen stratification exists), maintaining a water cover thicker than that depth is a way to ensure a stagnant layer of water near the interface.

### *Infiltration of Water into Tailings*

Infiltration of the overlying water into the submerged tailings is another mechanism to transport dissolved oxygen to sulphides. The faster the infiltration flows, the more oxygen is delivered. Therefore, the downward infiltration should be minimized. To artificially limit infiltration once a tailings impoundment is constructed is usually neither practical nor economical. Infiltration is usually restricted by selecting a tailings containment basin underlain by less permeable formations, such as thick, continuous strata of clays or competent bedrock. Fortunately, the same site selection criteria (of minimizing seepage and ground water flow) is normally practised in tailings management planning.

### *Aeration of Water Cover*

Reducing the degree and depth penetration of aeration is beneficial in reducing oxygen transport to the reactive tailings. As discussed earlier, if the aeration can be limited above a certain depth, a "stagnant" layer can be assured by installing a water cover thicker than the depth of aeration penetration. Failing this (i.e., if the water cover is aerated throughout its entire depth), reducing the degree of aeration can result in a lower dissolved oxygen concentration at the water/tailings interface, which helps reduce the dissolved oxygen flux into submerged tailings.

Aeration of water covers is caused by surface turbulence followed by water mixing and circulation; reduction of aeration thus must address one of these two mechanisms. Measures available include biological support (see discussion below), internal dykes to reduce the aerial extent of water covers, and wave breakers (such as inert waste rock fills in selected areas), and so on.

### *Tailings Resuspension*

Tailings resuspension alone can cause sulphide oxidation that rivals that caused by complete aeration of the water cover; it should thus be minimized. Tailings resuspension is caused by turbulence within the water cover that exceeds a certain critical threshold. All the measures that reduce aeration will likely reduce the tendency for tailings resuspension.

### *Physical Barriers at the Water/Tailings Interface*

Installation of physical barriers at the water/tailings interface, such as sand, inert tailings, or crushed rock layers, is equivalent to “inserting” a “stagnant” layer of water between the reactive tailings and the water cover. This “inserted” stagnant layer of water has a much smaller diffusion coefficient because of the presence of the solid grains (hence the term “diffusion barrier”). For dissolved oxygen to reach reactive tailings, it must diffuse through this barrier. Consequently, the dissolved oxygen uptake by tailings is greatly reduced. Needless to say, the thicker the barrier, the greater the benefit; this benefit however is offset by the cost of placing the barrier.

Another benefit of physical barriers is the complete suppression of tailings resuspension, provided they are thick enough.

### *Chemical/Biological Barriers*

If some organic material is used instead of inert material to form a layer between the reactive tailings and the water cover, a chemical barrier is formed. Ideally, dissolved oxygen diffusing through the barrier is completely consumed by oxidation of the organic material, thereby never having a chance to reach reactive tailings, completely eliminating the oxidation of sulphidic tailings lying underneath. A chemical barrier can be artificially placed using organic wastes such as wood chips, saw dusts, tree barks, manure, sewage sludge, to name just a few. It can also be grown naturally - this brings us to the concept of biologically supported water covers.

### *Biologically Supported Water Cover*

A biologically supported water cover is normally initiated by transplanting aquatic plants into the water cover. Nutrients for growth may be supplemented during the first a few years to help establish the aquatic vegetation. After that, the aquatic plants become self-sustaining without further human intervention; these plants further facilitate the establishment of a healthy biological community. The life cycling of the aquatic biological community provides organic debris to build an organic layer at the water/tailings interface; this interfacial organic layer grows with time as the biological support replenishes itself.

The benefits of a biological support are as follows:

- < The presence of aquatic plants reduces the aeration of the water cover by suppressing both surface turbulence and internal water mixing and circulation;
- < Similarly, the presence of aquatic plants also reduces the possibility of tailings resuspension, first by suppressing internal turbulence within the water cover, then by the presence of ever-growing interfacial organic layer; and
- < The biological support reduces and eventually eliminates the transport of dissolved oxygen into the reactive tailings through the natural growth of an organic chemical barrier between the reactive tailings and the water cover, which behaves as an oxygen sink.

A biological support can be cheaper to install than other physical or chemical barriers; where it is feasible and appropriately installed, it can help create a walk-away solution to reactive tailings disposal, if the water cover alone is insufficient as a walk-away solution. Note that the term “walk-away” here means no need for water quality control measures such as treatment, it does not exclude performing periodic necessary dam maintenance work.

## 5.7 Summary

The range of oxygen fluxes seen in the modelling results suggest a simple water cover alone without additional measures is sufficient to suppress oxidation of sulphides in reactive tailings. Four basic cases which may occur after reactive tailings are disposed off under a shallow, 0.3-m water cover were mathematically modelled based on typical tailings properties and other site conditions found at the Louvicourt Mine. The four cases are stagnant water cover, fully oxygenated and mixed water cover, fully oxygenated and mixed water cover with downward infiltration, and tailings resuspension. The stagnant water cover through which oxygen must diffuse across transports the least amount of oxygen to the submerged tailings, with the flux being on the order of  $3 \text{ g O}_2/\text{m}^2$  of interface/year. Although this is the most desirable condition, to date field data collected in other studies indicated that it is highly questionable that this condition exists in reality, since winds that are almost always present in the field naturally cause mixing, circulation, wave action, and aeration in shallow water bodies. The three other cases are more realistic scenarios, which increase the oxygen flux into the submerged tailings significantly. Modelling results suggest that, compared with the base case of stagnant water cover, mixing/oxygenation of the water cover and tailings resuspension each is capable of increasing the oxygen flux by one order of magnitude, whereas downward infiltration of fully-aerated water can enhance the oxygen flux by a factor of three. The range of oxygen fluxes seen in the modelling results suggest that for most sites, a simple, well-maintained water cover alone without additional measures is sufficient to suppress oxidation of sulphides in reactive tailings while maintaining the discharge from the water cover during wet seasons in compliance. Nevertheless, for exceptional circumstances where this is not achievable, supplemental



measures, such as physical, chemical, and biological barriers/oxygen interceptors, are available to further reduce the oxygen flux and enhance the effectiveness of the water cover.

## 6.0 CONCLUSIONS AND RECOMMENDATIONS

### 6.1 Conclusions

This report documents the results of the NTC part of a MEND-coordinated, multi-participant research project to evaluate the effectiveness of shallow water covers in the prevention of acid mine drainage from reactive sulphidic tailings, using Louvicourt Mine as the experimental site. In this study, various Louvicourt tailings samples were characterized for grain size distribution, quantitative mineralogy, geochemical whole-rock composition, and extended acid-base accounting (ABA). Flow-through cell leach tests were used to investigate the influences of four parameters on metal releases by tailings under simulated submergence. Eight humidity cells containing duplicates of four samples were tested for eighty weeks to determine the rates of sulphide oxidation and acid neutralization. Pre- and post-humidity cell analyses were performed to complete geochemical and mineralogical mass balances and to validate the humidity cell data interpretation. Data generated from these laboratory tests were used to predict field acid generation for a hypothetical field exposure. Mathematical modelling was used to evaluate the effects of four oxygen transport mechanisms on the degree of subaqueous sulphide oxidation.

ABA results indicate that the tailings are potentially net acid-generating. A four-month in-plant monitoring conducted in 1994-1995 showed a variation of sulphide content from 11 to 49%. The sulphides in the tailings are dominated by pyrite, with minor or trace pyrrhotite, sphalerite, and chalcopyrite. Hence upon oxidation of sulphides, metals such as iron, zinc, and copper could potentially be released if the pore water has a low pH. Carbonate mineral contents in samples varied from nearly nil to as high as 24%. The main carbonate minerals are ankerite and siderite, both containing varying amounts of magnesium and manganese. The main silicate neutralising mineral is clinocllore.

Flow-through cell leach experiments with different leachant solutions using the Taguchi design approach suggest the following influence on metal releases: leachant  $\text{Fe}^{2+}$  concentration (strong) > leachant DO level (strong) > leachant pH (medium) > hydraulic gradient (weak). Presence of  $\text{Fe}^{2+}$  in the inflow increases metal releases likely through a one-time ion exchange process. High DO in the inflow promotes Zn releases through oxidation of sulphides whereas low DO promotes the release of Mn. Lower pH favours metal releases probably because of higher solubility of hydroxides, sulphides and carbonates of most metals. The tailings have sufficient buffering capacity to maintain the pore water pH nearly neutral. Mechanisms controlling metal releases include solubility control and dissolution rate control. Overall metal releases are low throughout the experiments except during the initial flush-out of accumulated soluble constituents. Sustained low-pH inflow seems to be able to depress the pH of the pore water only after many pore volumes, causing the release of Mn and Zn.

The humidity cell results show that the Louvicourt tailings have relatively high oxidative reactivity. The oxidation rate of the eight tests ranged 864-2143 (average 1449) mg  $\text{CaCO}_3$

eq/kg/week, and the NP consumption rate ranged 955-2238 (average 1500) mg CaCO<sub>3</sub> eq/kg/week. All samples are potentially net acid-generating, with predicted humidity cell lag times ranging 0.56-2.5 (average 1.2) years.

Predictions based on hypothetical field exposure of the tailings indicate that, for a typical tailings composition as represented by the average of the four samples tested, the lag time before acid generation is 4.5 years. For a worse-than-average case as represented by the sample LVW-3, the lag time reduces to 2.6 years.

Sphalerite oxidation appeared to be accelerated by galvanic effects after the leachate pH dropped below about 3.0. Ankerite contributed fully to the total available NP. Siderite and clinocllore were less reactive and contributed less to the total available NP. Siderite dissolution seemed to be accelerated after onset of acid generation whereas clinocllore dissolution was relatively unaffected by acidification.

A new technique was employed to calculate the dissolution rates of individual neutralizing minerals and sulphide minerals from weekly leachate volume and chemical data. The validity of this technique appears to be acceptable, as the mineralogical mass balances predicted with this technique compare favourably with the mass balances computed from pre- and post-humidity cell solid analysis data that were obtained independently from the leachate chemistry data.

Due to the “non-ideality” of the humidity cell tests, not all particles placed in the cells were accessible for oxidation and neutralization reactions. This was probably attributable to the formation of impermeable particle aggregates as a result of cementation and coating. Methods for correcting for the non-ideality were proposed and demonstrated. It was found that, without agitation, on average only about 37% of the sample mass in the humidity cells was available for oxidation and neutralization reactions. To minimize the deviation of future humidity cell tests from ideality, it is recommended that the test sample be stirred weekly to expose “hidden” particles and that the weekly sample leach be carried out at a greater water to solids ratio and for a longer duration.

Four basic cases which may occur after reactive tailings are disposed of under a shallow, 0.3-m water cover were mathematically modelled based on typical tailings properties and other site conditions found at the Louvicourt Mine. The four cases are stagnant water cover, fully oxygenated and mixed water cover, fully oxygenated and mixed water cover with downward infiltration, and tailings resuspension. The stagnant water cover through which oxygen must diffuse across transports the least amount of oxygen to the submerged tailings, with the flux being on the order of 3 g O<sub>2</sub>/m<sup>2</sup> of interface/year. Although this is the most desirable condition, to date field data collected in other studies indicated that it is highly questionable that this condition exists in reality, since winds that are almost always present in the field naturally cause mixing, circulation, wave action, and aeration in shallow water bodies. The three other cases are more realistic scenarios, which increase the oxygen flux into the submerged tailings significantly. Modelling results suggest that, compared with the base case of stagnant water

cover, mixing/oxygenation of the water cover and tailings resuspension each is capable of increasing the oxygen flux by one order of magnitude, whereas downward infiltration of fully-aerated water can enhance the oxygen flux by a factor of three. The range of oxygen fluxes seen in the modelling results suggest that for most sites, a simple, well-maintained water cover alone without additional measures is sufficient to suppress oxidation of sulphides in reactive tailings while maintaining the discharge from the water cover during wet seasons in compliance. Nevertheless, for exceptional circumstances where this is not achievable, supplemental measures, such as physical, chemical, and biological barriers/oxygen interceptors, are available to further reduce the oxygen flux and enhance the effectiveness of the water cover.

## 6.2 Recommendations

The findings of this laboratory/modelling study should be compared with the results from the field experimental cell study (by INRS-Eau) and the laboratory column study (by Canmet) for consistency and corroboration. Any discrepancies among the three in basic findings should be addressed and ultimately resolved.

Future research opportunities on water covers should be taken advantage of to study factors controlling water cover aeration/mixing and factors controlling resuspension of tailings. The goal of such research should be to establish the capability of quantitatively predicting the degree of aeration and resuspension in shallow water covers from basic information such as tailings properties, meteorological data, and physiography of the site.

## 7.0 CLOSURE

The NTC project team included M. Li (project leader), L. St-Arnaud, K. Shikatani, S. Bouffard, and K. Faubert. This report was written by M. Li and technically reviewed by L. St-Arnaud. L. Bernier (Geoberex) wrote the sections on post-humidity cell solid analyses (Chapter 4.0), which was reviewed by M. Li. K. Wheeland (independent consultant) proof-read the whole document. K. Shikatani, S. Bouffard, and K. Faubert conducted the laboratory tests. Analytical support was provided by the NTC analytical laboratory. External laboratories were also used.

The review comments by D. Riehm (Teck Corporation) on the first version of this report (the milestone report) and by C. Petit (Senes) on the second version are greatly appreciated and have been integrated. We also acknowledge the contribution of J. Kwong (CANMET) and T. Pedersen (University of British Columbia) who did comprehensive reviews of the draft version of the final report. Their comments have been incorporated in the final report by B. Vigneault.

## 8.0 REFERENCES

Coastech Research, 1990. *Acid Mine Drainage Prediction Manual*, MEND Report 1.16.1b.

Crank, J., 1956. *The Mathematics of Diffusion*, 1st edn., Oxford University Press, London, England.

Doepker, R.D. and Drake, P.L., 1991. "Laboratory Study of Submerged Metal-Mine Tailings III: Factors Influencing the Dissolution of Metals," *Proceedings of the Second International Conference on the Abatement of Acidic Drainage*, September 16, 17, and 18, Montreal, Canada, Vol. 1, pp. 139-155.

Domenico, P.A. and Schwartz, F.W., 1990. *Physical and Chemical Hydrogeology*, John Wiley & Sons, New York.

Dryden, A.L.Jr., 1931. "Accuracy in Percentage Representation of Heavy Mineral Frequencies," *National Academy of Science (U.S.) Proceedings*, 17:233-238.

Filion, M.P., Firlotte, F.W., Julien, M.R., and Lacombe, P.F., 1994. "Regulatory Controlled Design - Louvicourt Project - A Case Study," *Proceedings of the Third International Land Reclamation and Mine Drainage Conference and the Third International Conference on the Abatement of Acidic Drainage*, Pittsburgh, PA, USA, April 24-29, pp. 22-31.

Golder Associés Ltée., 1994. *Evaluation of Man-Made Subaqueous Disposal as a Method of Controlling Oxidation of Sulphide Minerals (Phase I)*, SCC File No. 028SQ-23440-3-9321, Contract No. 23440-3-9321/01-SQ, Proposal Submitted to Canmet MSL Division, November.

Golder Associés Ltée., 1994. *Evaluation of Man-Made Subaqueous Disposal as a Method of Controlling Oxidation of Sulphide Minerals (Phase I)*, SCC File No. 028SQ-23440-3-9321, Contract No. 23440-3-9321/01-SQ, Draft Proposal Submitted to Canmet MSL Division, March.

Jambor, J.L., 1994. "Mineralogy of Sulphide-Rich Tailings and Their Oxidation Products," in J.L. Jambor and D.W. Blowes (eds.) *Short Course Handbook on Environmental Geochemistry of Sulphide Mine Wastes*, Waterloo, May.

Jost, W., 1960. *Diffusion in Solids, Liquids, Gases*, 3rd printing with addendum, Academic Press, New York.

Li, M. 2000. "ARD Prediction for Low-Sulphide, Low-Neutralisation Mine Wastes," *Proceedings of ICARD 2000 - 5th International Conference on Acid Rock Drainage*, May 21-24, Denver, Colorado.

Li, M., Catalan, L.J.J., and St-Germain, P., 2000. "Rates of Oxygen Consumption by Sulphidic Tailings under Shallow Water Covers - Field Measurements and Modelling," *Proceedings of ICARD 2000 - 5th International Conference on Acid Rock Drainage*, May 21-24, Denver, Colorado.

Li, M., 1999. "Louvicourt Tailings - Reactivity Assessment and Modelling of Underwater Oxidation Rates", Presentation at *Pre-Conference Short Course - Case Studies on Wet and Dry Covers - at Sudbury '99, Mining and the Environment II*, May 27, Sudbury, Ontario, Canada.

Li, M. and Bernier, L.R., 1999. "Contributions of Carbonates and Silicates to Neutralization Observed in Laboratory Tests and Their Field Implications", *Proceedings of Mining and the Environment II, Sudbury '99 Conference*, Sudbury, Ontario, Canada.

Li, M., 1997. "Factors Influencing Shallow Water Cover Performance," Presentation on *the Water Cover Short Course at the Fourth International Conference on Acid Rock Drainage*, May 31 - June 6, Vancouver, B.C., Canada.

Li, M., St-Arnaud, L. and Aubé, B., 1997. "Considerations in the Use of Shallow Water Covers for Decommissioning Reactive Tailings," *Proceedings of the Fourth International Conference on Acid Rock Drainage*, May 31 - June 6, Vancouver, B.C.

Li, M. and St-Arnaud, L., 1997. "Neutralization Potential Versus Observed Mineral Dissolution in Humidity Cell Tests for Louvicourt Tailings", *Proceedings of the Fourth International Conference on Acid Rock Drainage*, May 31 - June 6, Vancouver, B.C.

Luckner, L. and Schestakow, W.M., 1991. *Migration Processes in the Soil and Ground water Zone*, Lewis Publishers, Chelsea, Michigan.

Morin, K.A. and Hutt, N.M., 1999. "Humidity Cells: How Long? How Many?" *Proceedings of Mining and the Environment II, Sudbury '99 Conference*, September 13 - 17, Sudbury, Ontario, Canada.

Morin, K.A. and Hutt, N.M., 1997. *Environmental Geochemistry of Minesite Drainage: Practical Theory and Case Studies*, Minesite Drainage Assessment Group.

Morin, K., 1996. Personal Communications.

Morin, K., 1993. "Rate of Sulphide Oxidation in Submerged Environments: Implications for Subaqueous Disposal," *Proceedings of the Seventeenth Annual British Columbia Mine Reclamation Symposium*, May 4-7, Port Hardy, B.C.

Noranda Technology Centre, 1996. *Assessment of Reactivity of Louvicourt Tailings*, A Milestone Report Submitted to Noranda Mining and Exploration Inc., Teck Corporation, Aur Resources, and MEND.

Noranda Technology Centre, 1994. *Development and Testing of a Biologically-Supported Water Cover Decommissioning Option for the Louvicourt Tailings*, Proposal submitted to Noranda Minerals, Teck Corporation, Aur Resources and MEND, September.

Sobek, A.A., Shuller, W.A., Freeman, J.R. and Smith, R.M., 1978. *Field and Laboratory Methods Applicable to Overburdens and Minesoils*, EPA Report EPA-600/2-78-054, USEPA, Cincinnati.

SRK (BC) Inc., et. al., 1989. *Draft Acid Rock Drainage Technical Guide*, Vol. 1, Prepared for B.C. AMD Task Force, August.

St-Arnaud, L., 1996. "Progress in the Management of Sulphide Mine Wastes and Acidic Effluents," *CIM Bulletin*, Vol. 89, No. 999, April, pp. 41-42.

St-Arnaud, L., 1994. *Letter to Teck Corporation (M. Fillion)*, Dated June 29.

St-Arnaud, L., 1994. "Water Covers for the Decommissioning of Sulfidic Mine Tailings Impoundments," in *Proceedings of the Third International Conference on the Abatement of Acidic Drainage, April 25-29, Pittsburgh, PA, USA*, Vol. pp.279-287.



## **APPENDIX II-1      ANALYTICAL CERTIFICATES**

- 1      -      B.C. Initial Test and Confirmation Test by Lakefield Research on sample L-1
- 2      -      Extended ABA Tests by NTC on samples LVW-1 to LVW-4
- 3      -      Whole-Rock Analyses by NTC on samples LVW-1 to LVW-4
- 4      -      Whole-Rock Analyses by CRM on sample CRM
- 5      -      TCLP Test by Lakefield Research on sample L-1
- 6      -      Composition of liquid phase of flotation tailings of sample CRM



May 14th, 1993

Mr. Luc St. Arnaud  
Noranda Technology Centre  
240 boulevard Hymus  
Point-Claire, Quebec

Dear Mr. Arnaud:

**Re: Sample L-1 Acid Generation Potential Testing**

LR Reference No. 9341625, Code: 9038

Sample identified as "L-1" was submitted for acid generation potential determination. A preliminary "B.C. Research Initial Test" was conducted on the sample. The test results indicated that Acid Producing Potential was equal to 760 kg H<sub>2</sub>SO<sub>4</sub>/tonne of sample and that Acid Consuming Ability was equal to 25 kg H<sub>2</sub>SO<sub>4</sub>/tonne of sample (as shown in the enclosed test report). The sample showed a net acid producing ability of 735 kg H<sub>2</sub>SO<sub>4</sub>/tonne of sample.

The sample was further evaluated by performing a kinetic prediction test, "B.C. Research Confirmation" test, which is a bacterial oxidation test designed to determine if sulphide-oxidizing bacteria can produce more acid from oxidation of sulphide minerals in a sample that can be consumed by an equal quantity of the sample.

The sample was pre-acidified with 178 kg H<sub>2</sub>SO<sub>4</sub>/tonne (average) to reduce the leachate pH from the initial value of 5.9 to 2.6 and the active culture of bacteria was added, as shown in the enclosed test report. The sample was monitored for the duration of 37 days: the leachate pH slowly declined from 2.5 to 1.8 over the test period and the EMF increased from 400 to 500 mV, which indicates that some Fe<sup>2+</sup>/Fe<sup>3+</sup> oxidation was taking place. However, after the fresh sample was added, the pH of the pulp increased to 4.1 after 24 hours of reaction time and to 5.0, after 48 hours of reaction time.

The test results indicated that the sample has a strong buffering capacity. To further evaluate the rates of depletion of the neutralization capacity, kinetic prediction test such as "Humidity Cell" is recommended. This type of test would provide more detailed information about the rate of and temporal variation in acid generation and leachate water quality.

If you have any questions or comments, please do not hesitate to contact us.

Yours truly

LAKEFIELD RESEARCH



Inna Dymov, P. Eng.  
Project Manager

ID:jm

p.c. - ID  
File

### **The B.C Research Initial test:**

**Sample preparation:** The sample selected must have been taken in such a manner that it is truly representative of the type of mineralization being examined. The bulk sample is systematically reduced in size to provide a representative sample that will pass through a 100 mesh screen. The preparation of the sample can be made at our Lakefield facility for a nominal cost.

**Acid production potential determination:** the pulverized sample is assayed in duplicate for total sulfur using a LECO CS-244 sulfur carbon analyzer. The total sulfur assay value is expressed as kilograms sulfuric acid per tonne of sample, using the calculation %S(total) x 30.6 ( assuming a one to one conversion). This value is called the acid producing potential of the sample.

**Acid consuming titration test:** Duplicate 10 gram portions of the minus 100 mesh sample are suspended in 100 milliliters of deionized water and stirred for approximately 15 minutes. The natural pH of the sample is then recorded and the sample , while stirring , is titrated to pH 3.5 with 1.0Normal sulfuric acid. The addition of acid is repeated approximately every half hour until the pH change over a four hour period is 0.1 pH units or less. The total volume of acid added is recorded an converted to kilograms per tonne of sample. This value is called the Acid Consuming Ability of the sample. The calculation equation is represented below.

$$\text{Acid Consuming Ability(Kg/tonne)} = \frac{\text{ml } 1.0\text{N H}_2\text{SO}_4 \times 0.049\text{g/ml} \times 1000\text{Kg/tonne}}{\text{wt. of sample titrated in grams}}$$

**Interpretation of Results:** If the acid consumption value in Kg of H<sub>2</sub>SO<sub>4</sub> per tonne of sample exceeds the acid producing potential in Kg of H<sub>2</sub>SO<sub>4</sub> per tonne, then the sample will not be a source of acid mine drainage and no additional work is necessary. However, if the acid consumption is less than the acid producing potential, the possibility of acid mine water production exists and the B.C. Research confirmation test should be conducted.

# LAKEFIELD RESEARCH

A Division of Falconbridge Limited

P.O. Bag 4300, 185 Concession St. Lakefield, ON, K0L 2H0

Phone: (705) 652-3341, Facsimile: (705) 652-6365

## B.C Research Initial test Report

Noranda Tech.Centre  
240 boulevard Hymus  
Pointe-Claire  
Quebec  
Mr. Luc St.Arnaud

Date: 03/03/93  
Sample Received: 02/02/93  
No. of Sample: 1  
Our Reference No.: 9341617

Samples submitted show results as follows:

---

Acid Production Potential = %S x 30.6  
Acid Consuming Ability = ml of 1.0 N H<sub>2</sub>SO<sub>4</sub> x 0.049g/ml x 1000 kg/tonne  
-----  
wt. of sample titrated (g)

Sample Name: L-1  
%Sulfur = 24.8  
%Sulfide = 24.3

Acid Production Potential	= 758.88 kg H <sub>2</sub> SO <sub>4</sub> /tonne sample
Acid Consuming Ability (Rep.A)	= 23.955 kg H <sub>2</sub> SO <sub>4</sub> /tonne sample
Acid Consuming Ability (Rep.B)	= 25.67 kg H <sub>2</sub> SO <sub>4</sub> /tonne sample
Net Acid Consuming Ability (Rep.A)	= -734.925 kg H <sub>2</sub> SO <sub>4</sub> /tonne sample
Net Acid Consuming Ability (Rep.B)	= -733.21 kg H <sub>2</sub> SO <sub>4</sub> /tonne sample

Signed: *Dave Hevenor*  
Dave Hevenor  
Chemist

# LAKEFIELD RESEARCH

A DIVISION OF FALCONBRIDGE LIMITED

P.O. Bag 4300, 185 Concession St. Lakefield, ON, K0L 2H0,  
Phone: (705) 652-3341, Facsimile: (705) 652-6365, Telex: 0696-2842

No:1 of 2

## CERTIFICATE OF ANALYSIS

Noranda Tech. Centre  
240 boulevard Hymus  
Point-Claire  
Quebec

Date: May 17 1993  
Sample Received: Feb 22 1993  
No. of Samples: 1  
Our Reference No: 9341625  
Code: 9038

Attention: Mr. Luc St.Arnaud

Samples submitted show results as follows:

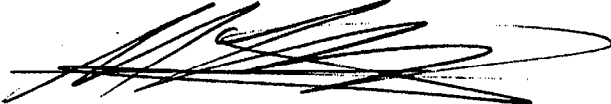
### Biological Confirmation Test

#### Procedure:

The test involves inoculating a pre-acidified (pH 2.0-2.4) pulp containing the test sample with an active culture of bacteria such as *T. ferrooxidans*. The pulp pH is monitored and the test is terminated when oxidation ceases as indicated by the attainment of a stable pH. An equivalent weight to the original sample is then added in two increments after 24 hours after each addition. If the pH is above 3.5 at either point, the sample is classified as a non acid producer. If the final pH remains below 3.5 a potential for the generation of AMD is indicated. Typically the test requires 3 to 4 weeks for completion.

## ANALYTICAL REPORT FOR EXTENDED ACID-BASE ACCOUNTING (ABA)

Norada Technology Centre

Reported by: Michael Li (Please print)Date of Report: 06/26/96Signature: 

Sample No.	Description	Acid-Base Accounting (ABA)					Sulphur Sepciation					Carbon Analysis	
		Paste pH	AP	NP	NNP	NP/AP	S <sub>T</sub>	S(pyr.)	S(pyrh.)	S(sphl.)	S(chlcp.)	TOC	Inorg. CO <sub>2</sub>
	Unit		kg/t*	kg/t*	kg/t*		%	%	%	%	%	%	%
LVW-1	Louvicourt Tails	7.64	475.3	181.5	-294	0.38	15.21	14.43	0.482	0.158	0.141	-	11.8
LVW-2	Louvicourt Tails	7.55	545.3	101.5	-444	0.19	17.45	16.45	0.654	0.237	0.106	-	6.8
LVW-3	Louvicourt Tails	7.60	509.7	75.0	-435	0.15	16.31	15.65	0.359	0.197	0.101	-	5.1
LVW-4	Louvicourt Tails	7.50	486.6	74.0	-413	0.15	15.57	15.16	0.195	0.107	0.112	-	5.6
* kg CaCO <sub>3</sub> equivalent / tonne of sample													

## CENTRE DE TECHNOLOGIE NORANDA

## CERTIFICAT D'ANALYSE/ CERTIFICATE OF ANALYSIS

A/To : S.Bouffard

M.Li

PROJET / PROJECT: V2 1321 021

Ref.: 132119-17-V:Env

Date: 6/06/96

Lab #	I.D.	Description	S
8755	96746	Solide	152111.420 ug/g
8756	96747	Solide	174483.730 ug/g
8757	96748	Solide	163084.720 ug/g
8758	96749	Solide	155725.360 ug/g

Commentaires/ Comments: Par ICP.

Effectué par/ Work by : B. Legault





# AKEFIELD RESEARCH LIMITED

J. Box 4300, 185 Concession St., Lakefield, Ontario, K0L 2H0

phone : 705-652-2038

FAX : 705-652-6441

Centre De Tech Noranda  
10 Hymus Boulevard SW  
Ste. Claire, PQ, H9R 1G5 - Canada

Contact : Peter Krcmery

Lakefield, June 25, 1996

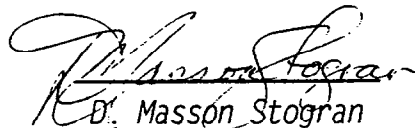
Date Rec. : June 21, 1996  
LR. Ref. : JUN7219.R96  
Reference : ---  
Project : LR 9602987

## CERTIFICATE OF ANALYSIS

No.	Sample ID	CO2 %
6	Analysis Date	25.06.96
7	Analysis Time	13:34
9	96990	11.8
10	96991	6.79
11	96992	5.09
12	96993	5.60

Sample Date: June 19 1996

Sample Received: June 21 1996

  
D. Masson Stogran

A MEMBER OF IAETL CANADA

Accredited by the Standards Council of Canada and CAEAL for specific registered tests.

The analytical results reported herein refer to the samples as received. Reproduction of this analytical report in full or in part is prohibited without prior written approval.

## CENTRE DE TECHNOLOGIE NORANDA

## CERTIFICAT D'ANALYSE/ CERTIFICATE OF ANALYSIS

A/To : M.Li

PROJET / PROJECT: V2 1321 021

Ref.: 132125-14-V:En  
Date: 7/12/96

Lab #	I.D.	Description	Al	As	Ca	Cd	Co
10719	96994 1	LV-1 Solids	27455.240 ug/g	517.450 ug/g	31416.120 ug/g	5.910 ug/g	363.820 ug/g
10720	96995 1	LV-2 Solids	35369.450 ug/g	892.760 ug/g	19220.990 ug/g	13.440 ug/g	231.220 ug/g
10721	96996 1	LV-3 Solids	37748.660 ug/g	770.280 ug/g	14769.820 ug/g	11.790 ug/g	227.440 ug/g
10722	96997 1	LV-4 Solids	39981.220 ug/g	382.350 ug/g	14957.750 ug/g <	2.570 ug/g	282.290 ug/g
10723	96994 2	LV-1 Solids	28386.240 ug/g	501.780 ug/g	33894.900 ug/g	10.780 ug/g	360.550 ug/g
10724	96995 2	LV-2 Solids	30964.860 ug/g	891.770 ug/g	18754.010 ug/g	18.220 ug/g	205.660 ug/g
10725	96996 2	LV-3 Solids	33102.820 ug/g	762.400 ug/g	13225.580 ug/g	14.530 ug/g	198.560 ug/g
10726	96997 2	LV-4 Solids	35276.370 ug/g	453.140 ug/g	11782.320 ug/g	8.120 ug/g	228.230 ug/g

Commentaires/ Comments: Please comments page.

Effectué par/ Work by : B. Legault

MLA

## CENTRE DE TECHNOLOGIE NORANDA

## CERTIFICAT D'ANALYSE/ CERTIFICATE OF ANALYSIS

A/To : M.Li

PROJET / PROJECT: V2 1321 021

Ref.: 132125-14-V:En  
Date: 7/12/96

Lab #	I.D.	Description	Cr	Cu	Fe	K	Mg
10719	96994 1	LV-1 Solids	19.480 ug/g	1410.180 ug/g	224010.380 ug/g	3841.790 ug/g	31425.910 ug/g
10720	96995 1	LV-2 Solids	45.160 ug/g	1111.720 ug/g	224969.970 ug/g	4588.630 ug/g	26982.770 ug/g
10721	96996 1	LV-3 Solids	48.580 ug/g	987.910 ug/g	201510.130 ug/g	5150.000 ug/g	23837.150 ug/g
10722	96997 1	LV-4 Solids	45.880 ug/g	1098.790 ug/g	209609.130 ug/g	5859.510 ug/g	26031.630 ug/g
10723	96994 2	LV-1 Solids	16.840 ug/g	1385.700 ug/g	223361.230 ug/g	3550.900 ug/g	35068.840 ug/g
10724	96995 2	LV-2 Solids	42.930 ug/g	1001.620 ug/g	216401.280 ug/g	3991.650 ug/g	25996.330 ug/g
10725	96996 2	LV-3 Solids	40.150 ug/g	964.310 ug/g	196777.670 ug/g	4960.980 ug/g	21472.320 ug/g
10726	96997 2	LV-4 Solids	33.340 ug/g	1045.760 ug/g	203632.030 ug/g	5555.320 ug/g	22051.020 ug/g

Commentaires/ Comments: Please comments page.

Effectué par/ Work by : B. Legault

## CENTRE DE TECHNOLOGIE NORANDA

## CERTIFICAT D'ANALYSE/ CERTIFICATE OF ANALYSIS

A/To : M.Li

PROJET / PROJECT: V2 1321 021

Ref.: 132125-14-V:Env  
Date: 7/12/96

Lab #	I.D.	Description	Mn	Na	Ni	Pb	S
10719	96994 1	LV-1 Solids	3098.540 ug/g	2773.650 ug/g	53.090 ug/g	136.400 ug/g	151869.300 ug/g
10720	96995 1	LV-2 Solids	1985.190 ug/g	3162.060 ug/g	56.310 ug/g	110.700 ug/g	174234.360 ug/g
10721	96996 1	LV-3 Solids	1532.790 ug/g	3207.340 ug/g	59.680 ug/g	98.580 ug/g	158564.300 ug/g
10722	96997 1	LV-4 Solids	1846.520 ug/g	2482.880 ug/g	65.550 ug/g <	25.720 ug/g	150010.640 ug/g
10723	96994 2	LV-1 Solids	3092.440 ug/g	3115.680 ug/g	29.210 ug/g	175.160 ug/g	145480.230 ug/g
10724	96995 2	LV-2 Solids	1881.610 ug/g	2812.700 ug/g	32.410 ug/g	127.720 ug/g	165333.340 ug/g
10725	96996 2	LV-3 Solids	1390.240 ug/g	3213.840 ug/g	32.740 ug/g	115.580 ug/g	153163.190 ug/g
10726	96997 2	LV-4 Solids	1513.640 ug/g	2603.020 ug/g	25.460 ug/g <	24.080 ug/g	147083.220 ug/g

Commentaires/ Comments: Please comments page.

Effectué par/ Work by : B. Legault

## CENTRE DE TECHNOLOGIE NORANDA

## CERTIFICAT D'ANALYSE/ CERTIFICATE OF ANALYSIS

A/To : M.Li

PROJET / PROJECT: V2 1321 021

Ref.: 132125-14-V:En  
Date: 7/12/96

Lab #	I.D.	Description	Sb	Se	Si	Te	Tl
10719	96994 1	LV-1 Solids <	44.740 ug/g	152.270 ug/g	133416.420 ug/g	46.390 ug/g <	22.370 ug/g
10720	96995 1	LV-2 Solids <	47.570 ug/g	130.660 ug/g	164743.950 ug/g	46.290 ug/g <	23.790 ug/g
10721	96996 1	LV-3 Solids <	44.620 ug/g	117.230 ug/g	187035.060 ug/g	45.550 ug/g <	22.310 ug/g
10722	96997 1	LV-4 Solids <	51.440 ug/g	145.120 ug/g	178086.580 ug/g	36.100 ug/g <	25.720 ug/g
10723	96994 2	LV-1 Solids <	46.640 ug/g	151.770 ug/g		60.260 ug/g <	23.320 ug/g
10724	96995 2	LV-2 Solids <	51.390 ug/g	182.690 ug/g		50.270 ug/g <	25.690 ug/g
10725	96996 2	LV-3 Solids <	47.040 ug/g	154.360 ug/g		40.580 ug/g <	23.520 ug/g
10726	96997 2	LV-4 Solids <	48.170 ug/g	153.920 ug/g		44.530 ug/g <	24.080 ug/g

Commentaires/ Comments: Please comments page.

Effectué par/ Work by : B. Legault

## CERTIFICAT D'ANALYSE/ CERTIFICATE OF ANALYSIS

A/To : M.Li

PROJET / PROJECT: V2 1321 021

Ref.: 132125-14-V:En  
Date: 7/12/96

Lab #	I.D.	Description	Zn
10719	96994 1	LV-1 Solids	3157.440 ug/g
10720	96995 1	LV-2 Solids	4811.680 ug/g
10721	96996 1	LV-3 Solids	4046.390 ug/g
10722	96997 1	LV-4 Solids	2313.590 ug/g
10723	96994 2	LV-1 Solids	3323.370 ug/g
10724	96995 2	LV-2 Solids	4880.380 ug/g
10725	96996 2	LV-3 Solids	3766.710 ug/g
10726	96997 2	LV-4 Solids	1894.480 ug/g

Commentaires/ Comments: Please comments page.

Effectué par/ Work by : B. Legault

**TABLEAU 5.9 Analyse chimique -  
Rejets typiques de flottation**

Solides	
Paramètre <sup>(1)</sup>	%
As	0,16
Ba	0,11
Be	0,0001
Bi	0,008
Ca	1,47
Cd	0,004
Co	0,04
Cr	0,008
Cu	0,60
Fe	22,8
Hg	0,00004
Mg	2,80
Mn	0,3
Mo	<0,01
Na	0,42
Ni	0,006
P	0,07
Pb	0,08
Sb	<0,003
Sc	<0,005
Sn	<0,002
Te	<0,001
Th	<0,001
U	<0,001
Zn	0,92
S (total)	19,5
S <sub>m</sub>	18,2
Au, g/t	0,92
Ag, g/t	19,5
SiO <sub>2</sub>	40

(1) La perte au feu, non mesurée, est estimée à 6-9% (carbonates)

Source : Ressources Atr Inc.

**LAKEFIELD RESEARCH**  
A division of Falconbridge Limited  
Postal Bag 4300, 185 Concession Street,  
Lakefield, ON K0L 2H0 Phone-705-652-3341 / Fax 705-652-6365

Certificate of Analysis

TCLP Leachate

Client: Noranda Technology Centre  
240 Hymus Blvd.  
Pointe Claire, PQ H9R 1G5

Date: April 7, 1993  
Sample Received: Jan. 21, 1993  
No. of Samples: Project 2  
Our Reference No.: 9341625

Attention: Mr. Luc St-Arnaud

Sample Description: L-1

The above sample was subjected to the TCLP leachate procedure. The solution produced gave the following analytical results:

Moisture %	0
100 Dry equivalent gm	100gr
Extraction Fluid #1	-
Initial pH	4.80
Final pH	4.45

Arsenic mg/L	<0.05	Mercury mg/L	<0.001
Silver mg/L	<0.03	Selenium mg/L	<0.01
Barium mg/L	<0.02		
Cadmium mg/L	0.01		
Chromium mg/L	<0.02		
Lead mg/L	<0.05		

Additional:	Copper	<0.02	Fe	0.04
	Zinc	3.75	Mn	2.53
	Al	0.39	Ni	0.04

Signed: 

J. R. Johnston  
Chief Chemist.



**TABEAU 5.13 Analyse chimique-Phase liquide-  
Rejets de flottation**

Paramètre	Procédé avec SO <sub>2</sub> <sup>(1)</sup>	Procédé avec NaCN/ZnSO <sub>4</sub> <sup>(2)</sup>
pH	10,32	11,52
Conductivité (µs/cm)	1 306	1 831
Solides en suspension (mg/l)	2,4	19
Turbidité (UTN)	3,63	4,88
Solides totaux dissous (mg/l)	233	1 330
Dureté totale (mg/l)	730	825
Alcalinité totale (mg/l)	47	120
Sulfate (mg/l)	644	590
Sels sulfureux (equiv. SO <sub>4</sub> ) (mg/l)	406	70
Nitrate (mg/l)	0,73	0,93
Ammoniacque (equiv N de NH <sub>3</sub> et NH <sub>4</sub> ) (mg/l)	1,2	1,35
Phosphore total (mg/l)	0,14	0,26
Phosphore dissous (mg/l)	0,00026	0,00026
Cyanures (total) (mg/l)	0,023	7,94
Métaux totaux (mg/l)		
Ag	<0,005	<0,005
Al	1,35	2,34
As	<0,005	<0,005
Ba	0,03	0,037
Be	<0,01	n.d.
Ca	80	n.d.
Cd	<0,0005	<0,0005
Co	<0,05	n.d.
Cr	<0,05	n.d.
Cu	0,022	11 600 <sup>(3)</sup>
Fe	0,059	0,21
Hg	0,0001	0,0001
Mg	0,54	n.d.
Mn	<0,05	n.d.
Mo	0,07	0,081
Na	9,9	n.d.
Ni	<0,01	0,69
Pb	<0,001	0,013
S	82	n.d.
Sb	<0,005	<0,005
Se	0,2	0,58
Si	0,7	n.d.
Sr	<0,2	n.d.
Te	<0,1	n.d.
Zn	0,013	0,113

(1) Correspond à environ 80% du temps d'opération

(2) Correspond à environ 20% du temps d'opération

(3) Un excès de CuSO<sub>4</sub> est soupçonné lors de l'essai de flottation ayant fourni cet échantillon d'eau

Source : Ressources Aur Inc.

## **APPENDIX II-2      MINERALOGY REPORTS**

- 1      -      Lakefield Report (Note only sample L-1 is relevant to this study.)
- 2      -      CRM Report (a table of mineral contents)
- 3      -      Canmet Report (LVW-1 to LVW-4)

**Project : 8900-596**

March 16, 1993

Nichola Davison

Mineralogist

## **Summary**

The mineralogical investigation of the seven sulphidic tailings samples (labelled L1, PC-1, PC-2, TC5-1, TC5-2, TC6-1 and TC6-2) has been completed. The samples were dominated by pyrite and non-opaque gangue minerals (quartz, chlorite, dolomite and trace other minerals ranging from 50 to 65%). Pyrite was the major sulphide phase and ranged from 29.4% in sample TC6-1 to 46% in sample L1. Minor to trace quantities of sphalerite, chalcopyrite, pyrrhotite, galena, arsenopyrite, covellite, bornite, digenite and marcasite were present. Oxide phases were represented by minor to trace quantities of magnetite, ilmenite, and hematite. Several of the minerals given on the list of requirements were not observed. These included gypsum, ferric hydroxide, malachite, scorodite, calcite, siderite, and zincite.

## **Introduction**

The purpose of the study was to characterize the mineral assemblage and estimate proportions of the contained minerals. A list of the minerals and chemical compounds required for computer modelling (as specified in a similar study for LR Project # 8900-482) was as follows:

pyrite	pyrrhotite
chalcopyrite	arsenopyrite
sphalerite	gypsum
ferric hydroxide	malachite
scorodite	calcite
sericite	siderite
basalumnite	zincite
phosphate	

## Procedures

The study was carried out using a combination of optical microscopy, xray powder diffraction, and quantitative chemical analysis. The procedures are summarized as follows:

1. A portion of each sample was powdered and mounted in an aluminum sample holder and placed in a rotating housing within a Philips diffractometer. The sample was scanned from  $5^{\circ}$  to  $75^{\circ}$  two theta under iron filtered cobalt radiation. The pattern was interpreted using the standard JCPDS data files. The minerals were identified and peak intensities were noted.

An additional portion of each sample was mixed with LiF. The amount of quartz was determined by quantitative xray powder diffraction.

2. Portions of each as-received sample were submitted for quantitative chemical analysis for correlation with the microscopy and XRD interpretation. The samples were analysed for the following:

Cu	Zn	Pb
As	Fe(T)	Fe(%Pyrite)
CaO	P <sub>2</sub> O <sub>5</sub>	S(T)
SO <sub>4</sub>	CO <sub>2</sub>	LOI

3. A portion of each sample was screened at 100, 200, and 400 mesh. The four size fractions were weighed and a material balance was prepared.

4. The screen fractions were prepared as 25mm diameter polished sections for optical microscopy. The polished sections were examined to determine the type and proportion of sulphide phases, and where possible, oxide and gangue minerals. The proportions were determined manually by point counting.

**Results****Size Analysis**

The screen size distribution (wt%) of the samples were as follows:

Fraction	Sample						
	PC-1	PC-2	TC5-1	TC5-2	TC6-1	TC6-2	L1
+100m	41.8	51.6	4.4	21.3	3.3	12.5	0.7
+200m	33.3	28.4	15.8	29.0	19.5	31.1	18.5
+400m	20.2	15.	37.6	27.6	38.0	37.9	39.2
-400m	4.6	4.4	42.1	22.1	39.2	18.4	41.5

**Chemical Analyses**

The quantitative chemical analyses (wt%) are given below:

Analysis	PC-1	PC-2	TC5-1	TC5-2	TC6-1	TC6-2	L1
Cu	0.067	0.075	0.038	0.11	0.064	0.13	0.25
Zn	0.82	0.78	1.29	1.24	1.18	1.08	0.23
Pb	0.15	0.20	0.16	0.17	0.20	0.22	0.03
As	0.16	0.16	0.11	0.18	0.11	0.18	0.11
Fe(T)	18.8	22.1	24.6	23.3	21.8	23.5	28.3
Fe(%Pyrite)	31.0	33.5	32.7	35.5	29.4	38.5	46.0
CaO	0.45	0.66	0.63	0.92	1.37	1.04	1.76
P <sub>2</sub> O <sub>5</sub>	0.026	0.029	0.019	0.030	0.029	0.031	0.068
S(T)	20.0	22.0	19.6	22.3	18.4	23.0	26.5
SO <sub>4</sub>	1.09	3.29	1.16	1.65	1.89	1.51	1.04
CO <sub>2</sub>	1.17	0.73	3.79	1.82	3.36	1.42	6.25
LOI	13.7	18.3	16.9	17.7	15.5	17.1	22.7

**Xray Diffraction**

XRD analyses are given below:

Mineral	PC-1	PC-2	TC5-1	TC5-2	TC6-1	TC6-2	L1
Quartz	major	major	major	major	major	major	major
Pyrite	minor	minor	minor	minor	minor	minor	major
Chlorite	minor	v. minor	minor	minor	minor	minor	major
Sericite	v.minor	v. minor	minor	-	v. minor	v. minor	-
Magnetite	trace	trace	v. minor	v. minor	minor	trace	poss. trace
Ankerite	-	-	trace	trace	trace	trace	minor
Basalumnite	-	poss. minor	-	-	-	-	-

**Petrographic Examination:****L1**

Gangue minerals were abundant . Pyrite was the dominant sulphide mineral and occurred as angular liberated grains, as small rounded inclusions within sulphide, oxide, and gangue, and as a binary phase with chalcopyrite, gangue and other sulphide and oxide grains. Trace chalcopyrite occurred as small inclusions and rims on pyrite grains, binaries with gangue and magnetite, small inclusions within gangue and as rare liberated grains. Chalcopyrite was more abundant in the larger grains (+100 mesh material). Trace sphalerite was present as a binary phase with pyrite, chalcopyrite, magnetite and gangue and as rare liberated grains. Trace pyrrhotite was present as rare liberated grains or binaries with pyrite. No pyrrhotite was observed in +200, +400 and -400 mesh fractions. Trace magnetite was present as tiny inclusions within gangue and as rare liberated grains. Rare hematite was present as an alteration of magnetite. Rare ilmenite was present as fine inclusions within chalcopyrite/gangue binaries. Liberation of pyrite, chalcopyrite, sphalerite, and magnetite grains increased with decreasing particle size.

**PC-1**

Gangue minerals were abundant. Pyrite was the major sulphide phase and occurred as liberated grains, binaries with gangue, and as finely disseminated inclusions within gangue grains. Trace chalcopyrite was present as rare liberated grains, binaries with gangue and pyrite, and as finely disseminated inclusions within gangue, pyrite and sphalerite. Trace sphalerite was present as rare liberated grains, binaries with gangue, and as finely disseminated inclusions within gangue. Trace pyrrhotite was present as liberated grains, binaries with gangue, and binaries with chalcopyrite. Rare covellite and bornite were present as tiny inclusions within chalcopyrite. Trace arsenopyrite, galena and magnetite were present as rare liberated grains and binaries with gangue. Rare ilmenite was present as liberated grains. Liberation of sulphide and oxide minerals increased with decreasing particle size.

**PC-2**

Similar to PC-1. Rare hematite was present as alteration of magnetite. No covellite or bornite were observed.

**TC5-1**

Gangue minerals were abundant. Pyrite was the major sulphide phase and occurred as liberated grains, binaries with gangue, and as finely disseminated inclusions within gangue grains. Trace chalcopyrite was present as rare liberated grains, binaries with gangue, and as finely disseminated inclusions within gangue. Trace sphalerite was present as rare liberated grains, binaries with gangue and fine inclusions within pyrite. Trace pyrrhotite was present as liberated grains, binaries with gangue and magnetite. Trace arsenopyrite was present as binaries with gangue. Trace galena was present as binaries with gangue and rare liberated grains. Trace magnetite were present as rare liberated grains, binaries with gangue and finely disseminated inclusions within gangue.

**TC5-2**

Similar to TC5-1. Rare hematite was present as an alteration of magnetite. Digenite was observed as a single grain in binary association with pyrrhotite. Pyrrhotite was present as binaries with gangue, chalcopyrite, or pyrite, or as liberated grains.

**TC6-1**

Gangue minerals were abundant. Pyrite was the major sulphide phase and occurred as liberated grains, binaries with gangue, and as finely disseminated inclusions within gangue grains. Trace chalcopyrite was present as rare liberated grains, binaries with gangue, pyrite or sphalerite, and as finely disseminated inclusions within gangue. Trace sphalerite was present as rare liberated grains and binaries with gangue, chalcopyrite or pyrite. Trace pyrrhotite was present as liberated grains, binaries with gangue and magnetite. Trace arsenopyrite was present as liberated grains or binaries with gangue. Trace galena was present as binaries with gangue, in complex grains of magnetite/chalcopyrite/gangue and as rare liberated grains. Trace magnetite were present as rare liberated grains and binaries with gangue.

**TC6-2**

Similar to TC6-1. Marcasite was present as rare liberated grains.



The combined chemical, XRD and petrographic data indicate the following mineral assemblages and modal quantities:

Mineral	PC-1 %	PC-2 %	TC5-1 %	TC5-2 %	TC6-1 %	TC6-2 %	L1 %
Pyrite	31.0	33.5	32.7	35.5	29.4	38.5	46.0
Pyrrhotite	0.8	0.3	1.2	1.3	2.4	1.8	<0.1
Chalcopyrite	0.2	0.2	0.1	0.3	0.2	0.4	0.7
Arsenopyrite	0.5	0.4	0.2	0.4	0.3	0.4	0.2
Sphalerite	1.4	1.3	2.2	2.1	2.0	1.8	0.4
Gypsum	-	-	-	-	-	-	-
FeO(OH)	-	-	-	-	-	-	-
Malachite	-	-	-	-	-	-	-
Scorodite	-	-	-	-	-	-	-
Calcite	-	-	-	-	-	-	-
Sericite	v. minor	v. minor	minor	-	v. minor	v. minor	-
Siderite	-	-	-	-	-	-	-
Basalumnite	-	poss. minor	-	-	-	-	-
Zincite	-	-	-	-	-	-	-
P <sub>2</sub> O <sub>5</sub>	0.026	0.029	0.019	0.030	0.029	0.031	0.068
Marcasite	-	-	-	-	-	0.5	-
Covellite	<0.1	-	-	-	-	-	-
Bornite	<0.1	-	-	-	-	-	-
Digenite	-	-	-	<0.1	-	-	-
Galena	0.2	0.2	0.2	0.2	0.2	0.3	<0.1
Magnetite	0.6	1.1	2.8	2.0	1.9	1.0	1.7
Ilmenite	0.2	-	-	-	<0.1	-	<0.1
Hematite	-	<0.1	-	-	-	-	<0.1
Quartz	28.8	21.3	21.2	22.1	17.4	21.1	11.0
Ankerite	-	-	trace	trace	trace	trace	minor
Chlorite	minor	v. minor	minor	minor	minor	minor	major

The deportment of the sulphate and carbonate components was not fully defined. Neither calcite, gypsum nor anhydrite were reported from the XRD patterns. The low CaO concentration and XRD data indicated that carbonate occurred as iron and possible sodium carbonate minerals (ankerite  $(\text{Ca}(\text{Fe},\text{Mg})(\text{CO}_3)_2)$ , possible siderite  $(\text{FeSO}_3)$  and/or thermonatrite  $(\text{Na}_2\text{CO}_3 \cdot \text{H}_2\text{O})$ ). The sulphate was reported as hydrous iron sulphate minerals such as ferroxahydrite  $(\text{FeSO}_4 \cdot 6\text{H}_2\text{O})$  or possible sodium sulphates (thenardite  $\text{Na}_2\text{SO}_4$ ). The high LOI suggests the presence of complex hydrous phases, possibly including clay minerals.

**TABLEAU 5.10** Analyse minéralogique typique  
des résidus

<b>Minéral</b>	<b>%</b>
Pyrite	30-45
Silicates <sup>(1)</sup>	26-53
Carbonates	12-24
Magnétite	1
Chalcopyrite	0,8
Sphalérite	0,6
Pyrrhotine	<2
Hématite	<0,5

(1) Principalement chlorite, plus ou moins altérée

Source : Ressources Aur Inc.

**CARBONATE MINERALOGY OF THE  
LV-SERIES TAILINGS SAMPLES  
FROM THE LOUVICOURT MINE**

**OCTOBER 1996**

**MINING AND MINERAL SCIENCES LABORATORIES  
A.D. Paktunc, J. Wilson, P. Carrière and J.H.G. Flamme**

**Work Performed for:  
NORANDA TECHNOLOGY CENTRE**

**Job No. 51538**

**CONFIDENTIAL**

**MINING AND MINERAL SCIENCES LABORATORIES  
REPORT MMSL 96-068 (CR)**

---

**CANMET** 

## EXECUTIVE SUMMARY

A mineralogical characterization study has been carried out on four tailings samples from the Louvicourt Mine in Québec with the purpose of identifying the carbonate minerals and determining their abundances. The samples were studied by a combination of scanning electron microscopy, X-ray microanalysis, image analysis and X-ray powder diffraction techniques. The tailings samples are fine-grained and consist of silicates, sulphides, carbonates and oxides. The dominant carbonate minerals are ankerite and magnesian siderite. Calcite, dolomite and siderite are trace carbonate phases. All the carbonate minerals display subhedral grain boundaries. There are no apparent morphological differences between ankerite and magnesian siderite grains. Based on standardless microanalysis, the mineral formula of ankerite is estimated to be  $\text{Ca}(\text{Fe}_{0.5}\text{Mg}_{0.4}\text{Mn}_{0.1})(\text{CO}_3)_2$  whereas magnesian siderite has a variable composition from  $\text{Fe}_{0.6}\text{Mg}_{0.3}\text{Mn}_{0.1}\text{CO}_3$  to  $\text{Fe}_{0.7}\text{Mg}_{0.3}\text{CO}_3$ . Ankerite forms about 3 to 15% (by weight) of the samples whereas magnesian siderite abundances range from 6 to 13%. Bulk compositions calculated based on mass balance considerations and measured mineral quantities of this study are in good agreement with the whole rock compositions determined by chemical techniques.

## CONTENTS

<b>EXECUTIVE SUMMARY</b>	<b>i</b>
<b>INTRODUCTION</b>	<b>1</b>
<b>SAMPLE PREPARATION AND METHODOLOGY</b>	<b>1</b>
<b>MINERALOGY</b>	<b>2</b>
<b>MASS BALANCE</b>	<b>4</b>
<b>ACKNOWLEDGEMENTS</b>	<b>5</b>
<b>REFERENCE</b>	<b>6</b>
<b>APPENDIX A - (Figures 1 to 6)</b>	<b>7</b>
<b>APPENDIX B - X-ray Diffractograms</b>	<b>14</b>
<b>APPENDIX C - (Table 4)</b>	<b>19</b>

## TABLES

1. Mineral quantities (wt%) determined by MP-SEM-IPS system	3
2. Mineralogical composition of the samples as determined by XRD	3
3. Comparison of the bulk compositions (wt%) based on mineral quantities, theoretical and approximate mineral compositions, and mass balance calculations (MB) with the measured whole rock compositions (WR)	4
4. Mineral compositions (wt%) used in mass balance calculations	19

## FIGURES

1. LV-1. Note that color (i.e. gray level) distinction between magnesian siderite and ankerite is not apparent on this photomicrograph. Other minerals present in the photomicrograph are aluminosilicates as well as unmarked particles of quartz and carbonates.	8
2. LV-1. Included in a coarse magnesian siderite particle (Mg-sid) are several euhedral Fe oxide grains (white).	9
3. LV-1	10
4. LV-2	11
5. LV-3	12
6. LV-4	13

## INTRODUCTION

Four samples from the Louvicourt Mine tailings were received from Noranda Technology Centre. The samples labeled as LV-1, LV-2, LV-3 and LV-4 consisted of several grams of very fine-grained material kept in small plastic vials. The objectives of this study were to identify carbonate minerals, to quantify their distribution in the samples and to determine the morphological characteristics of the carbonate minerals.

## SAMPLE PREPARATION AND METHODOLOGY

Samples were mounted in araldite and polished sections were prepared using diamond pastes on dry cloth to avoid dissolution of water soluble phases. In order to avoid potential contamination of the samples, lead laps were avoided during polishing. The polished sections were studied by scanning electron microscopy (SEM) and X-ray microanalysis to identify the carbonate minerals. An integrated image analysis system (MP-SEM-IPS) was used in quantifying the distribution of mineral species in the samples. The system consists of a JEOL 733 electron microprobe equipped with two wavelength spectrometers and an energy dispersion spectrometer, interfaced to a Kontron image analyzer (Petruk, 1989). Mineral phases and groups were distinguished based on their gray levels in the backscattered electron image produced by SEM. Gray levels in the backscattered electron image are based on the average atomic number of the material; therefore, they are representative of the chemical composition of the material. Minerals having similar gray levels are discriminated by means of X-ray dot mapping. Because of the gray level overlap of all the silicate and carbonate minerals, X-ray dot mapping was required for the analyses. About 3,000 particles in each polished section were scanned at a magnification of 200x.

The samples were also examined using a Rigaku rotating anode X-ray powder diffractometer for mineral identification. The X-ray diffractograms were collected under

slow conditions using the RIGAKU rotating-anode XRD system, with  $\text{CuK}\alpha$  radiation at 55kV, 180 mA, step-scan  $0.04^\circ$ , scan rate at  $4^\circ$  per minute in  $2\theta$ . This represents scan times of 29 minutes per sample. XRD patterns are given in Appendix B.

## MINERALOGY

The tailings samples are fine-grained and consist of silicates, sulphides, carbonates and oxides (Figures 1 and 2). SEM-EDXA and image analysis study of the tailings samples revealed that the dominant carbonate species are ankerite and magnesian siderite. Calcite, dolomite and siderite are trace carbonate phases. In general, the carbonate minerals display subhedral grain boundaries (Figures 1 to 6 in Appendix A). There are no apparent morphological differences between ankerite and magnesian siderite grains. The carbonate minerals form about 11 to 27% (by weight) of each sample (Table 1). Pyrite, quartz and aluminosilicates (i.e. muscovite and clinocllore) form essentially the remainder. Trace amounts of potassium feldspar, sodic plagioclase, rutile, ilmenite, goethite, pyrrhotite, chalcopyrite, sphalerite, and galena are also present in the samples.

Observations of the EDX spectra suggest that ankerite is relatively uniform in composition. Based on standardless semi-quantitative microanalysis, the composition of ankerite is estimated to be  $\text{Ca}(\text{Fe}_{0.5} \text{Mg}_{0.4} \text{Mn}_{0.1})(\text{CO}_3)_2$ . Magnesian siderite displays a variable composition. Standardless semi-quantitative microanalyses of five magnesian siderite grains suggest that the variation is within  $\text{Fe}_{0.6} \text{Mg}_{0.3} \text{Mn}_{0.1} \text{CO}_3$  and  $\text{Fe}_{0.7} \text{Mg}_{0.3} \text{CO}_3$ .



**Table 1. Mineral quantities (wt%) determined by MP-SEM-IPS system**

	LV-1	LV-2	LV-3	LV-4
Quartz	15.4	23.6	27.0	27.3
Muscovite (K-spar, Na-Plagioclase)	18.0	10.8	5.7	8.7
Clinochlore	8.3	6.4	4.0	8.0
Magnesian siderite	13.0	9.5	6.0	8.8
Ankerite (Calcite)	14.5	7.2	4.8	3.3
Rutile (Ilmenite, Goethite)	tr	1.6	0.9	1.5
Pyrite	29.2	39.9	50.4	41.7
Pyrrhotite	0.6	tr	0.6	0.7
Chalcopyrite	1.0	tr	tr	tr
Sphalerite	tr	1.0	0.6	tr
Galena	tr	tr	tr	tr

tr: < 0.5%; bracketed phases are in lesser quantities.

X-ray powder diffraction analysis indicated that quartz, clinochlore, ankerite, pyrite, muscovite are the dominant minerals in the samples (Table 2). The presence of magnetite and calcic plagioclase in trace amounts in LV-4 is suggested by XRD. There is no matching phase for magnesian siderite in the international powder diffraction database (ICDD); therefore, magnesian siderite does not appear in Table 2. Lines of an unidentified phase, present in all the samples probably belong to magnesian siderite since they are close to those of siderite and ferroan magnesite (see XRD charts in Appendix B).

**Table 2. Mineralogical composition of the samples as determined by XRD**

LV-1	LV-2	LV-3	LV-4
ankerite	quartz	quartz	quartz
quartz	clinocllore	clinocllore	clinocllore
clinocllore	ankerite	ankerite	ankerite
pyrite	pyrite	pyrite	pyrite
muscovite	muscovite	muscovite	muscovite
			Ca-plagioclase
			magnetite

## MASS BALANCE

Bulk compositions of the samples, calculated on the basis of the determined mineral quantities and mass balance considerations, are given in Table 3. These results are in good agreement with the whole rock compositions determined by bulk chemical techniques at the Noranda Technology Centre. Similarities between the calculated and measured values of CaO, MgO, Mn, Fe and CO<sub>2</sub> are especially noteworthy which support the mineralogical compositions of the carbonate species. SiO<sub>2</sub> and Al<sub>2</sub>O<sub>3</sub> values that do not correlate well in LV-3 are probably due to choosing inappropriate mineral compositions for the aluminosilicate minerals.

**Table 3. Comparison of the bulk compositions (wt%) based on mineral quantities, theoretical and approximate mineral compositions, and mass balance calculations (MB) with the measured whole rock compositions (WR)**

	LV-1		LV-2		LV-3		LV-4	
	MB	WR	MB	WR	MB	WR	MB	WR
SiO <sub>2</sub>	26.7	28.6	30.8	35.3	31.0	40.0	34.0	38.1
Al <sub>2</sub> O <sub>3</sub>	6.4	5.2	4.1	6.7	2.3	7.1	3.8	7.6
MgO	5.8	5.5	4.1	4.5	2.6	4.0	4.3	4.3
CaO	4.3	4.4	2.1	2.7	1.4	2.1	1.0	2.1
K <sub>2</sub> O	1.8	0.5	1.1	0.6	0.6	0.6	0.9	0.7
CO <sub>2</sub>	11.6	11.8	7.0	6.8	4.5	5.1	5.0	5.6
Fe	21.1	20.4	23.6	22.5	26.7	20.2	23.5	21.0
Mn	0.3	0.3	0.2	0.2	0.1	0.2	0.1	0.2
Cu	0.4	0.1	0.0	0.1	0.0	0.1	0.0	0.1
S	16.3	15.2	21.5	17.4	27.4	15.9	22.8	15.0

Refer to Appendix C for the mineral compositions used in the mass balance calculations.

## ACKNOWLEDGEMENTS

Mike Beaulne performed the mounting and preparation of polished sections.  
Report was reviewed by Drs. L.J. Cabri, H.F. Steger and R. Lastra.

**REFERENCE**

1. Petruk, W. (1989) The MP-SEM-IPS image analysis system. In: Mineralogical Association of Canada Short Course on Image Analysis Applied to Mineral and Earth Sciences; (Ed. Petruk, W.) pp. 37-42.

## APPENDIX A

### Figures 1 to 6

Backscattered electron images illustrating grain morphologies of the carbonate minerals.

Mg-sid: magnesian siderite; ank: ankerite; cal: calcite; dol: dolomite; sid: siderite;  
Qtz: quartz; Qtz+: composite particle of quartz and other minerals;  
Sil: silicate other than quartz; white grains are essentially pyrite.

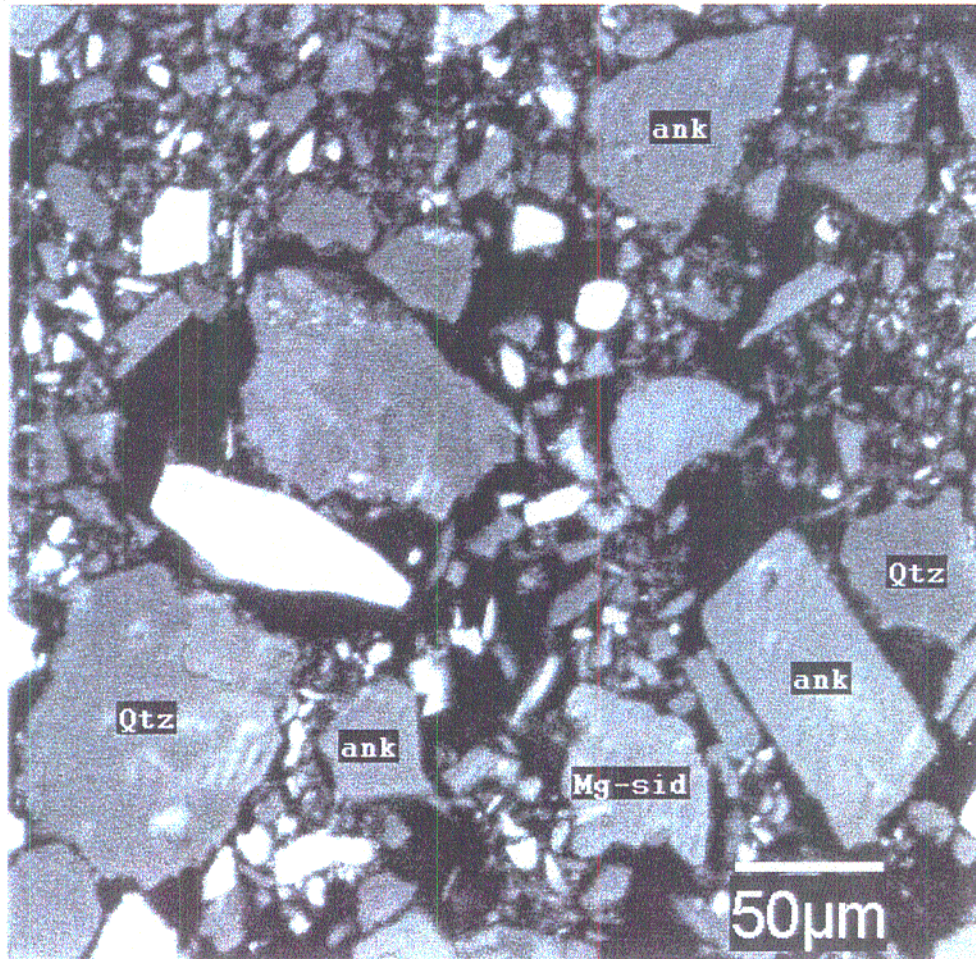


Figure 1. LV-1. Note that color (i.e. gray level) distinction between magnesian siderite and ankerite is not apparent on this photomicrograph. Other minerals present in the photomicrograph are aluminosilicates as well as unmarked particles of quartz and carbonates.



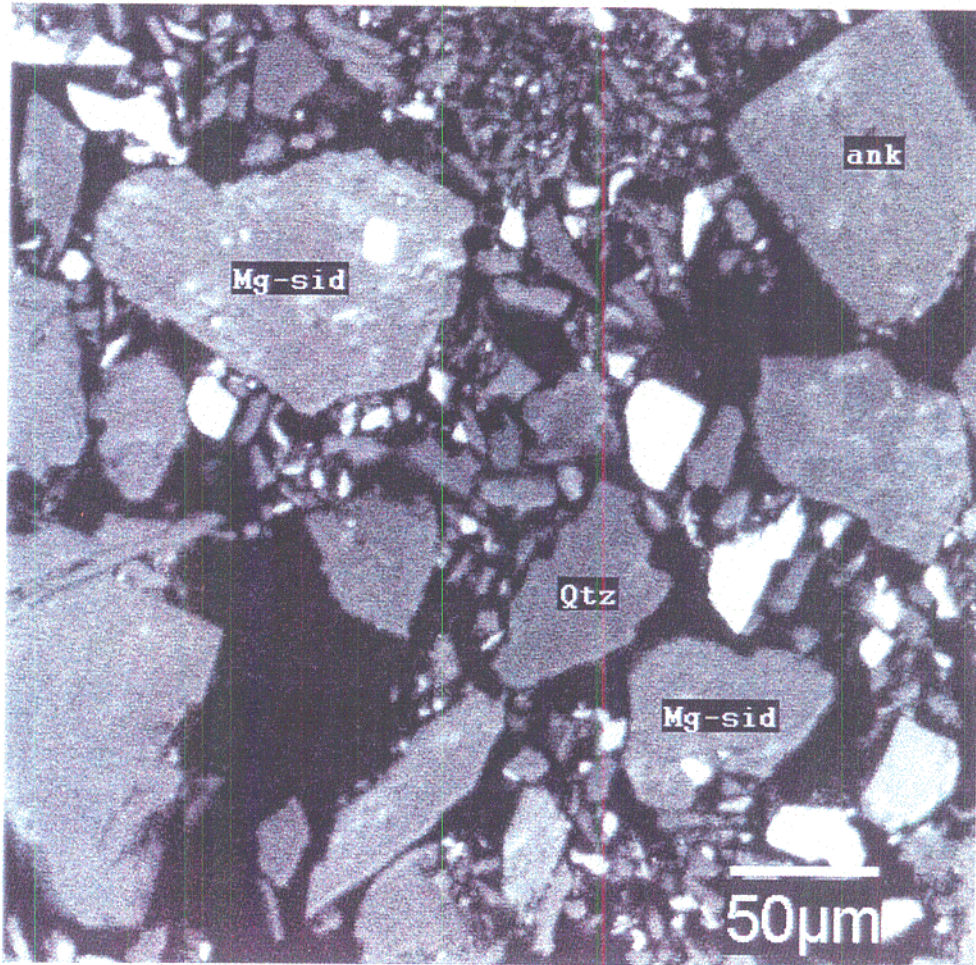


Figure 2. LV-1. Included in a coarse magnesian siderite particle (Mg-sid) are several euhedral Fe oxide grains (white).



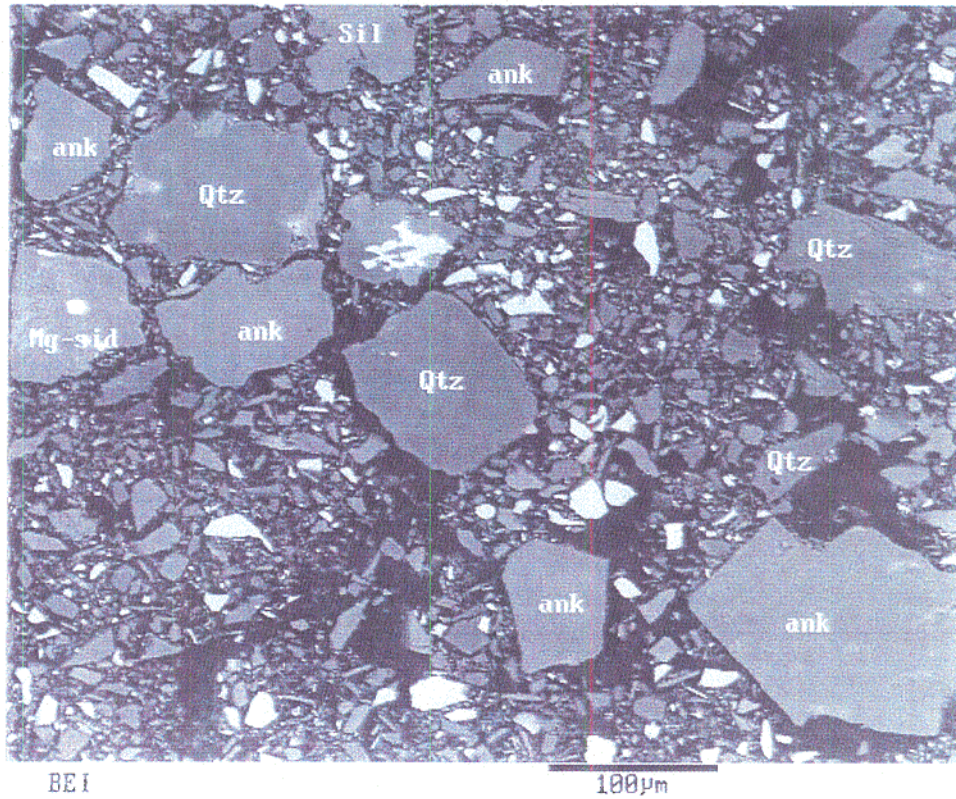
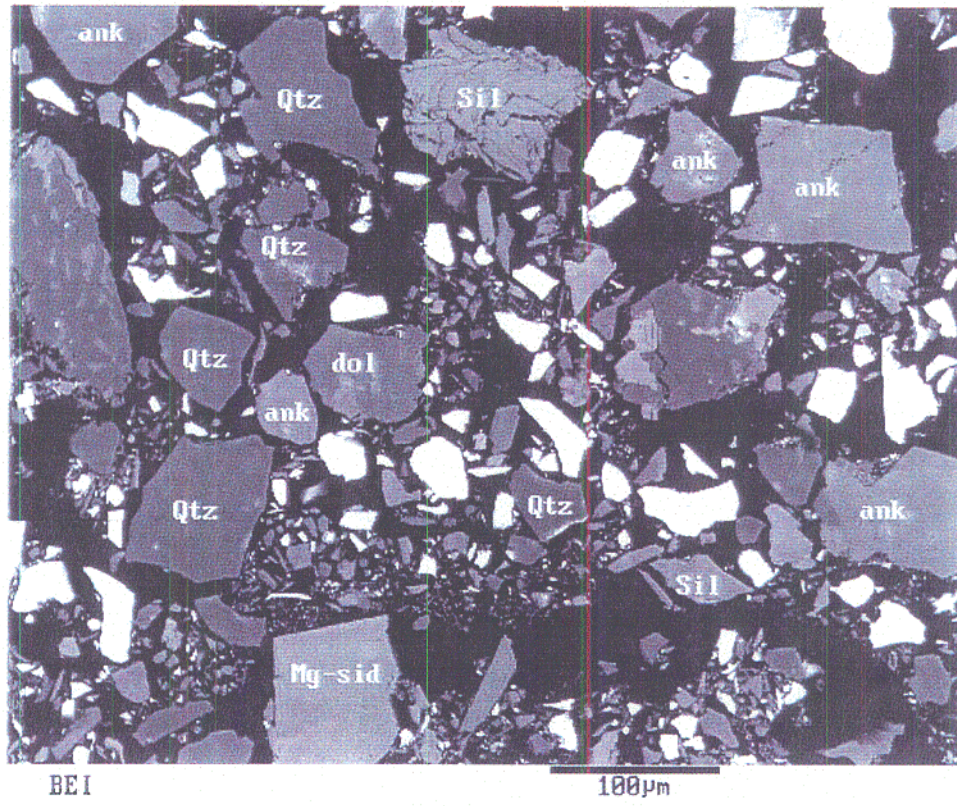


Figure 3. LV-1



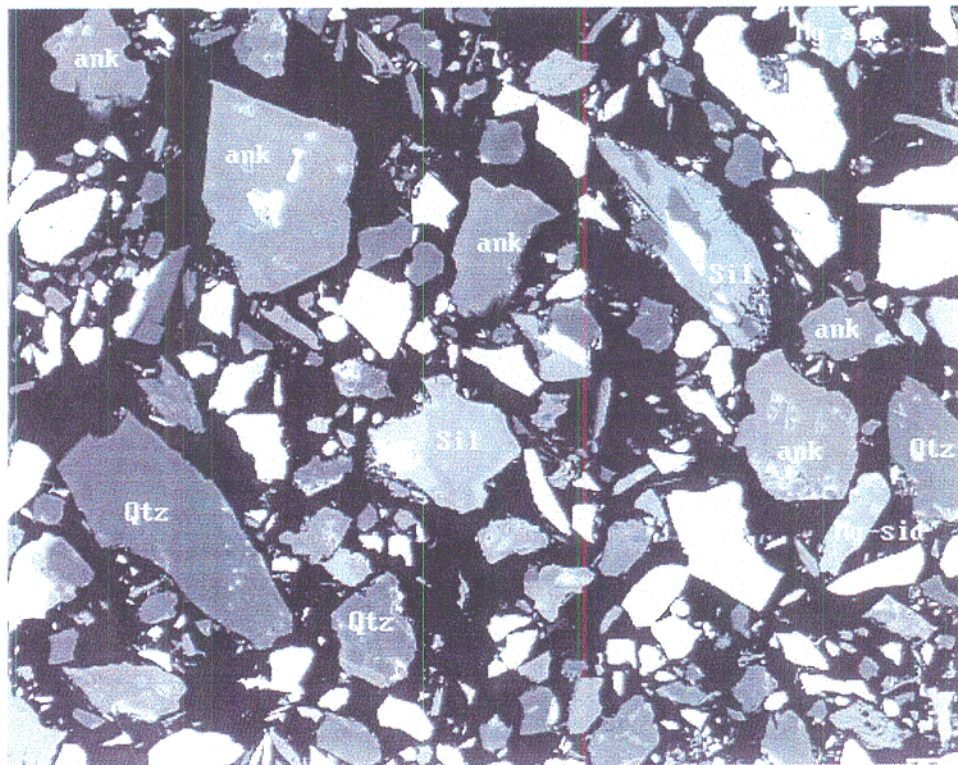
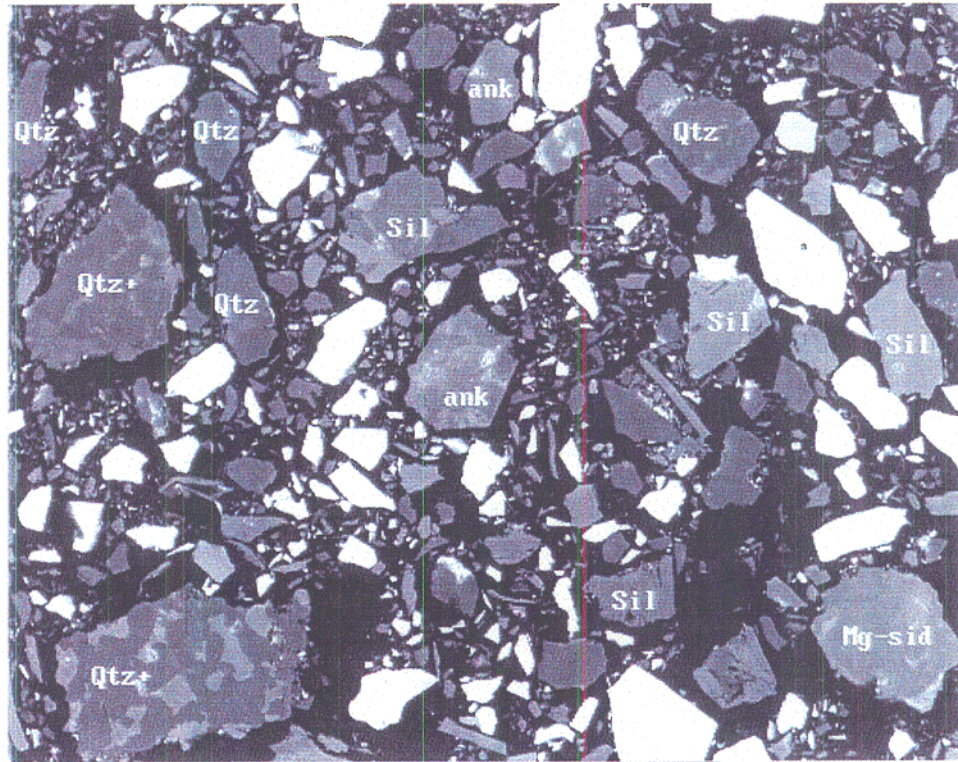


Figure 4. LV-2



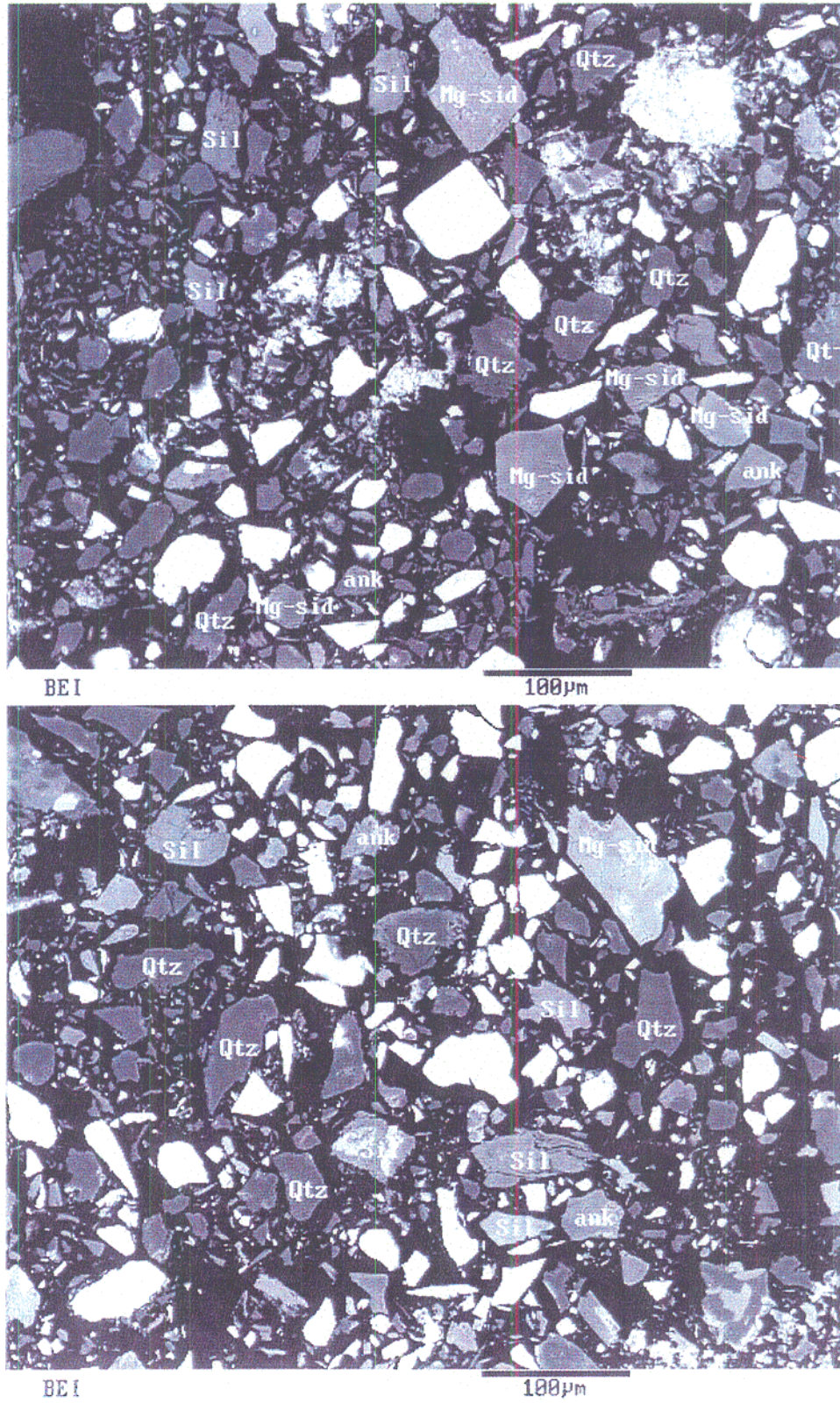


Figure 5. LV-3



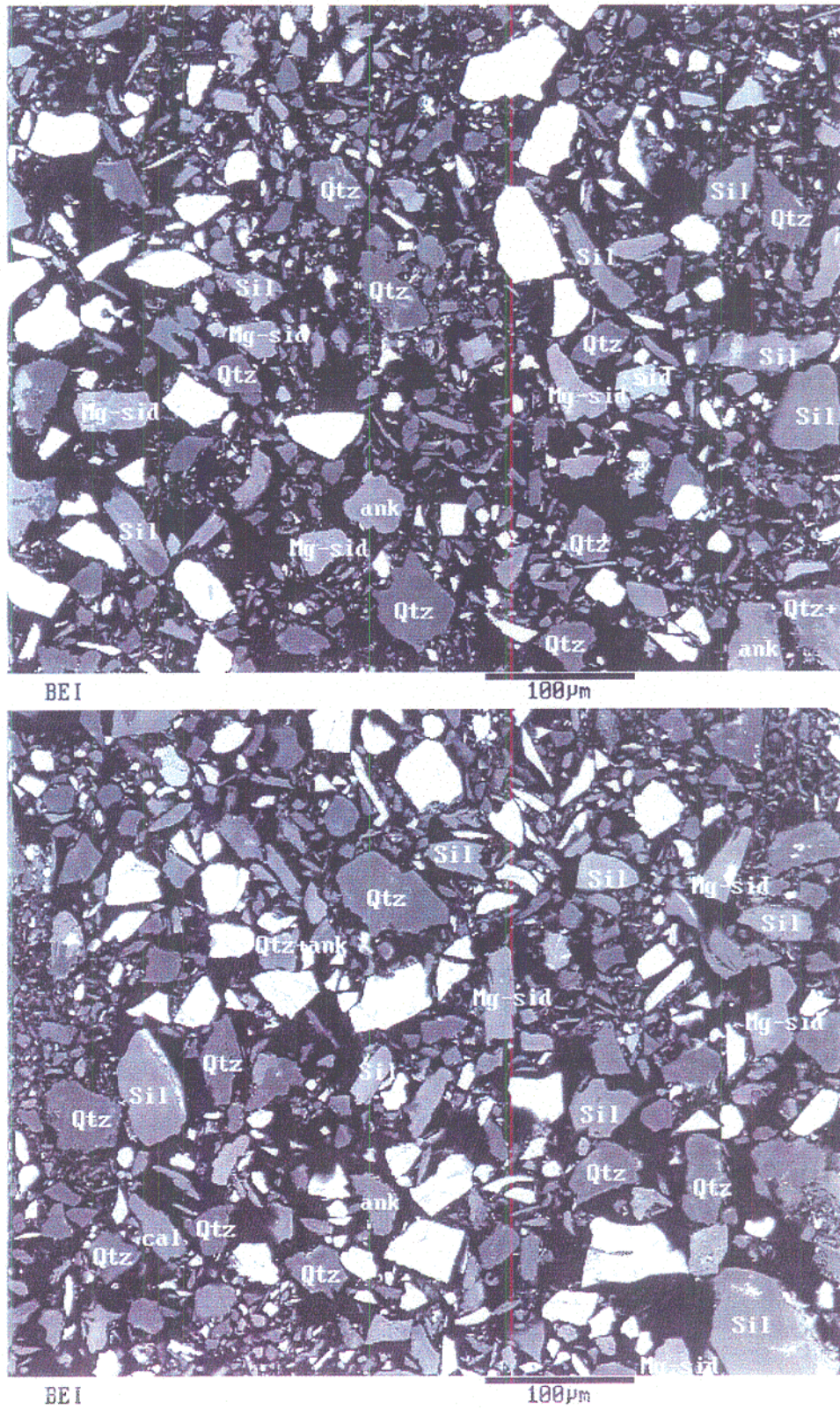


Figure 6. LV-4

## APPENDIX B

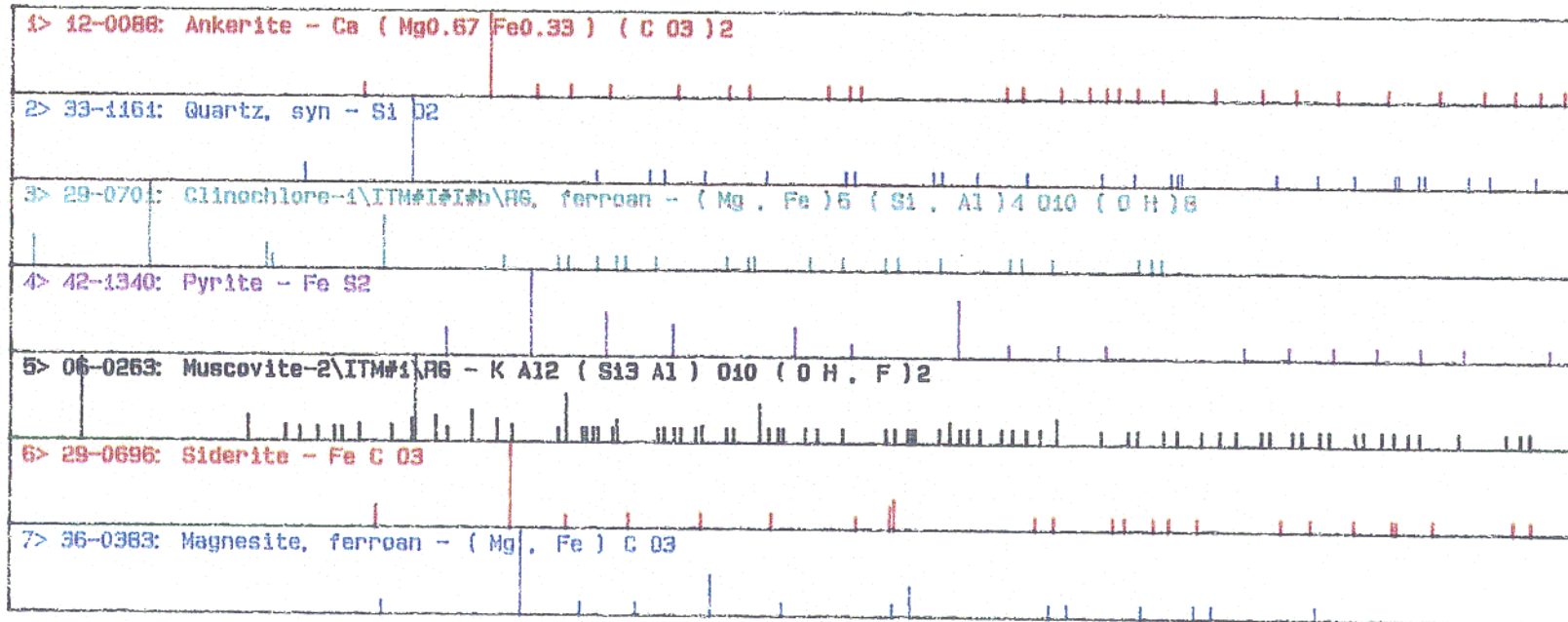
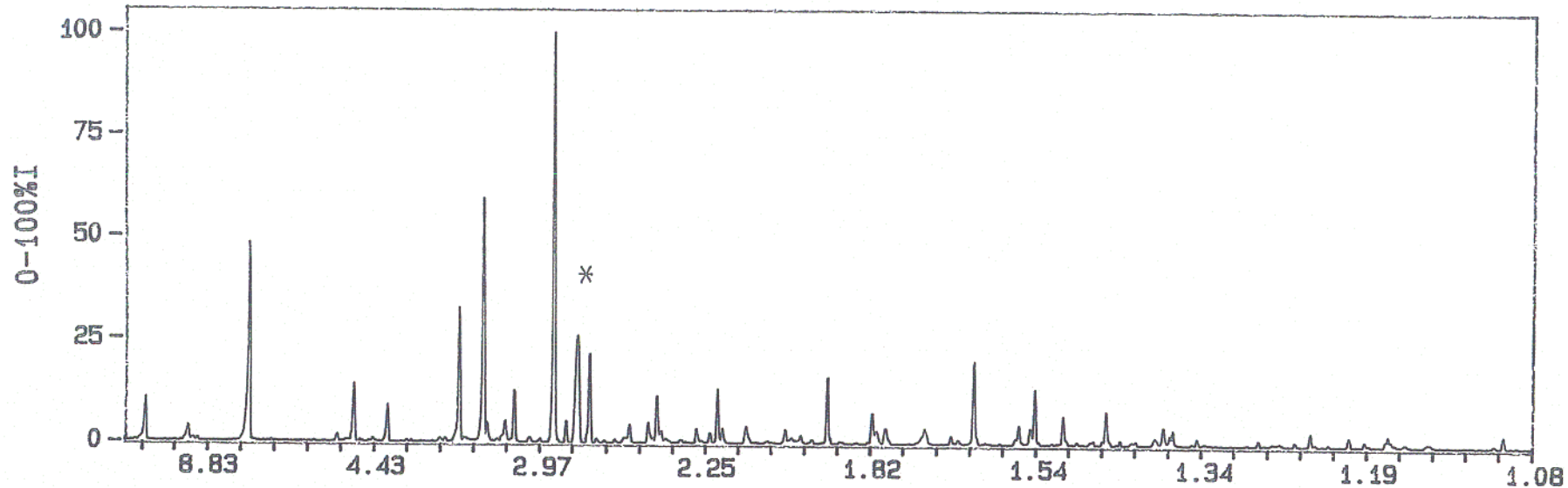
### X-Ray Diffractograms

Asterisk symbol is used to mark the main line of magnesian siderite.

ID: PAKTUNC LV-1, 27-SEP-96@08: 19

File: Z02735.RAW

Scan: 5-90/.04/ 1/#2126, Anode: CU



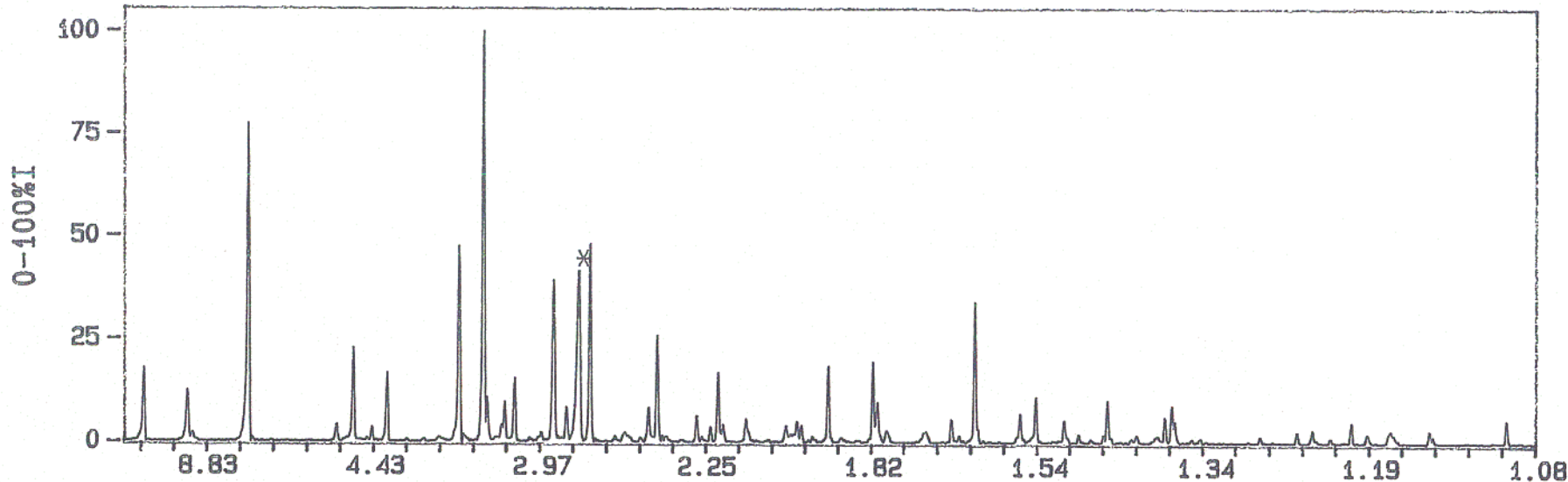
D-Scale



ID: PAKTUNC LV-2, 27-SEP-96@08:19

File: Z02736.RAW

Scan: 5-90/.04/ 1/#2126, Anode: CU



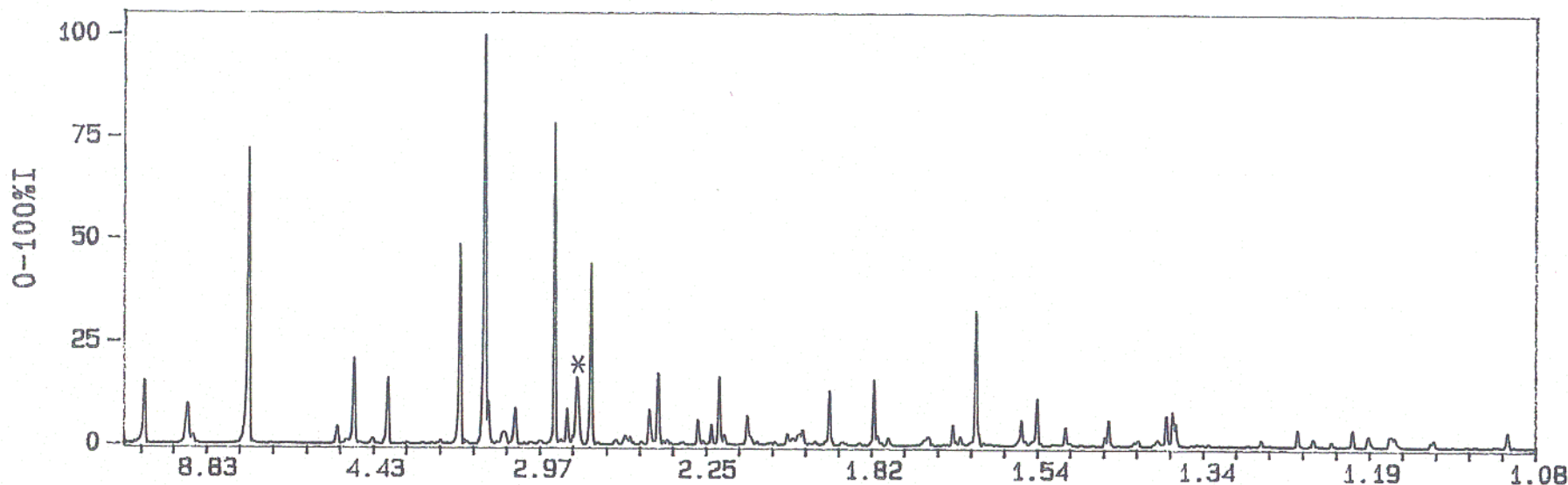
1> 33-1161: Quartz, syn - Si O2
2> 29-070: Clinocllore-1\ITM#I#I#b\RG, ferroan - (Mg, Fe)6 (Si, Al)4 O10 (OH)8
3> 12-0086: Ankerite - Ca (Mg0.67 Fe0.33) (CO3)2
4> 42-1340: Pyrite - Fe S2
5> 06-0263: Muscovite-2\ITM#1\RG - K Al2 (Si3 Al) O10 (OH, F)2
6> 29-0696: Siderite - Fe CO3
7> 36-0383: Magnesite, ferroan - (Mg, Fe) CO3

D-Scale

ID: PAKTUNC LV-3, 27-SEP-96@08: 19

File: Z02737.RAW

Scan: 5-90/.04/ 1/#2126, Anode: CU



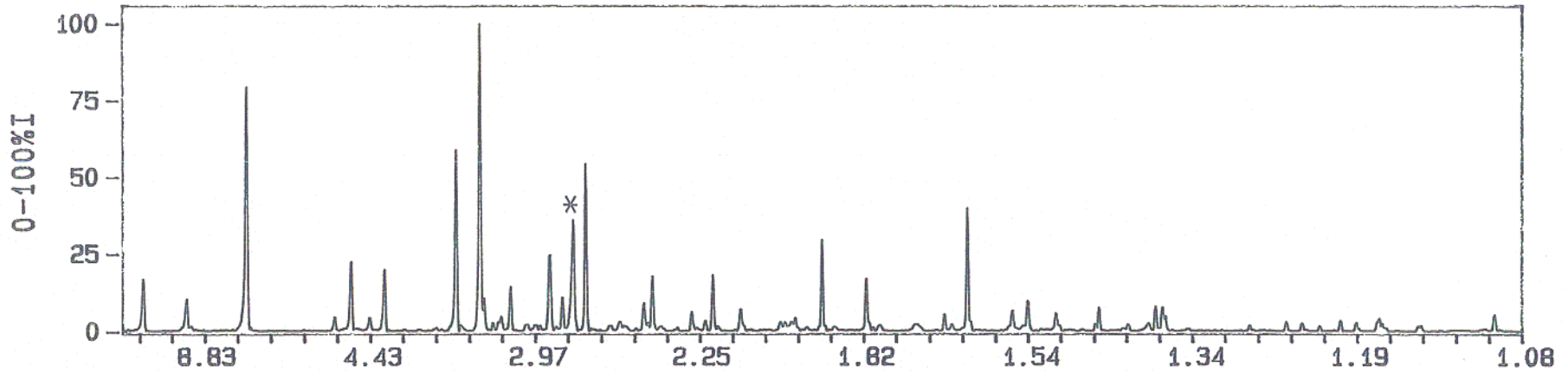
1> 33-1161: Quartz, syn - Si O2
2> 29-0701: Clinocllore-1\ITM#I#I#b\RG, ferroan - ( Mg , Fe ) 6 ( Si , Al ) 4 O10 ( O H ) 8
3> 12-0088: Ankerite - Ca ( Mg0.67 Fe0.33 ) ( C O3 ) 2
4> 42-1340: Pyrite - Fe S2
5> 06-0263: Muscovite-2\ITM#1\RG - K Al2 ( Si3 Al ) O10 ( O H , F ) 2
6> 36-0383: Magnesite, ferroan - ( Mg , Fe ) C O3
7> 29-0696: Siderite - Fe C O3

D-Scale

ID: PAKTUNC LV-4, 27-SEP-96@08: 19

File: Z02738.RAW

Scan: 5-90/.04/ 1/#2126, Anode: CU



1>	33-1161: Quartz, syn - Si O2
2>	29-0701: Clinocllore-1\ITM#I#I#b\RG, ferroan - ( Mg , Fe ) 6 ( Si , Al ) 4 O10 ( O H ) 8
3>	12-0088: Ankerite - Ca ( Mg0.67 Fe0.33 ) ( C O3 ) 2
4>	42-1340: Pyrite - Fe S2
5>	06-0263: Muscovite-2\ITM#1\RG - K Al2 ( Si3 Al ) O10 ( O H , F ) 2
6>	36-0383: Magnesite, ferroan - ( Mg , Fe ) C O3
7>	29-0696: Siderite - Fe C O3
8>	12-0301: Anorthite, ordered - Ca Al2 Si2 O8
9>	19-0629: Magnetite, syn - Fe Fe2 O4

D-Scale



## APPENDIX C

### Mineral Compositions (wt%) Used in Mass Balance Calculations

	SiO <sub>2</sub>	Al <sub>2</sub> O <sub>3</sub>	MgO	CaO	K <sub>2</sub> O	CO <sub>2</sub>	Fe	Mn	Cu	S
Quartz	100									
clinochlore	31	18	37							
Muscovite	48.4	27.2			10		4.7			
Mg-Siderite			13			40	34.6	1.2		
Ankerite			7.1	29.5		44	14.1	1.0		
Pyrite							46			54
Pyrrhotite										36.5
Chalcopyrite									35	35
Sphalerite										26.5

Mineral compositions listed are approximate as they are based on theoretical and/or assumed values. MgO, CaO, Fe and Mn data for ankerite and Mg-siderite are rough estimates based on standardless semi-quantitative energy dispersive X-ray microanalysis.

**APPENDIX II-3**

**IN-PLANT MONITORING DATA OF TAILINGS COMPOSITION VARIATION**

(See the QuattroPro Version 5.0 file "Tail-smp.wb1" included on Diskette 1 attached to this report.)

**APPENDIX III-1      INTERPRETATION OF FLOW-THROUGH CELL LEACH  
TESTS USING TAGUCHI METHODOLOGY**

(See WordPerfect Version 6.1 file "Taguchi.wpd" included on Diskette  
1 attached to this report.)

**APPENDIX IV-1      WEEKLY HUMIDITY CELL LEACHATE CHEMISTRY**

(See the QuattroPro version 6.0 file “Wklydata.wb2”, zipped into “Wklydata.zip”, which is included on Diskette 1 attached to this report. Use a unzip utility, such as WinZip, to unzip the file.)

**APPENDIX IV-2      INTERPRETIVE CALCULATIONS FOR WEEKLY  
HUMIDITY CELL LEACHATE CHEMISTRY**

(See the QuattroPro version 6.0 file "HCinterp.wb2", zipped into "HCinterp.zip", which is included on Diskette 2 attached to this report. Use a unzip utility, such as WinZip, to unzip the file.)

**APPENDIX IV-3 POST-HUMIDITY CELL LEACH DATA**

**Post-Humidity Cell Leach Tests**

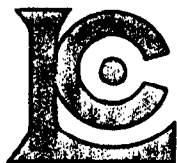
Sample	I.D.	Dry Mass Leached (g)	Vol. of Leachate (mL)	Concentration of Elements (mg/L)												
				Na	Mg	Al	Si	S	K	Ca	Mn	Fe	Cu	Zn	As	Pb
LV1A	972686	11.1397	1472.96	0.11	16.040	<0.2	<5	49.6	0.5	31.370	0.040	0.154	<0.02	0.149	0.030	<0.02
LV2A	972687	12.6067	1480.69	0.11	12.440	<0.2	<5	38.4	0.3	21.430	1.337	0.110	0.0044	3.174	0.034	<0.02
LV3A	972688	11.4750	1481.83	0.08	14.160	9.034	<5	172.0	<0.2	17.240	3.372	91.300	2.7460	6.719	0.039	0.020
LV4A	972689	11.7081	1475.09	0.25	7.932	2.873	<5	40.8	<0.2	6.178	1.289	13.890	1.2000	2.721	0.027	0.060

Sample	I.D.	Dry Mass Leached (g)	Vol. of Leachate (mL)	Residual Elements in mg/kg												
				Na	Mg	Al	Si	S	K	Ca	Mn	Fe	Cu	Zn	As	Pb
LV1A	972686	11.1397	1472.96	14.74	2120.91	N/A	N/A	6558	67.73	4147.94	5.30	20.30	N/A	19.71	4.02	N/A
LV2A	972687	12.6067	1480.69	12.79	1461.11	N/A	N/A	4510	37.78	2517.01	157.03	12.91	0.51	372.79	3.99	N/A
LV3A	972688	11.4750	1481.83	10.92	1828.56	1166.61	N/A	22211	N/A	2226.30	435.44	11790.07	354.61	867.66	4.97	2.52
LV4A	972689	11.7081	1475.09	31.37	999.34	361.97	N/A	5140	N/A	778.36	162.40	1749.99	151.19	342.82	3.45	7.50

Residual Elements in %												
Na	Mg	Al	Si	S	K	Ca	Mn	Fe	Cu	Zn	As	Pb
0.00	0.21	N/A	N/A	0.66	0.01	0.41	0.00	0.00	N/A	0.00	0.00	N/A
0.00	0.15	N/A	N/A	0.45	0.00	0.25	0.02	0.00	0.00	0.04	0.00	N/A
0.00	0.18	0.12	N/A	2.22	N/A	0.22	0.04	1.18	0.04	0.09	0.00	0.00
0.00	0.10	0.04	N/A	0.51	N/A	0.08	0.02	0.17	0.02	0.03	0.00	0.00

**APPENDIX IV-4 POST-HUMIDITY CELL ABA**





# Laboratoires Chemex Ltee.

Essayeurs \* Geochimistes \* Chimistes Analytique

175 Boul. Industriel C.P. 284, Rouyn  
 Quebec, Canada J9X 5C3  
 PHONE: 819-797-1922 FAX: 819-797-0106

To: CENTRE DE TECHNOLOGIE NORANDA

240 BOUL. HYMUS  
 POINTE-CLAIRE, PQ  
 H9R 1G5

A972376

Comments: ATTN: MICHAEL LI

**CERTIFICATE**

**A9723767**

(MHM) - CENTRE DE TECHNOLOGIE NORANDA

Project:  
 P.O. #:

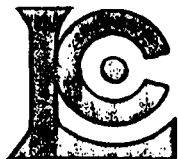
Samples submitted to our lab in Vancouver, BC.  
 This report was printed on 2-JUN-97.

### SAMPLE PREPARATION

CHEMEX CODE	NUMBER SAMPLES	DESCRIPTION
268	22	Assay ring entire sample

### ANALYTICAL PROCEDURES

CHEMEX CODE	NUMBER SAMPLES	DESCRIPTION	METHOD	DETECTION LIMIT	UPPER LIMIT
1119	22	Paste pH	POTENTIOMETER	0.0	14.0
1379	22	Sulfate S %: Acid or H2O leach	GRAVIMETRIC	0.01	100.00
1066	22	S %: HNO3-bromide digestion	GRAVIMETRIC	0.01	100.00
1380	22	S %: Leco furnace	LECO-IR DETECTOR	0.01	100.0
368	22	CO2 %: Inorganic	LECO-GASOMETRIC	0.2	100.0
1117	22	Maximum potential acidity	CALCULATION	1	4000
1118	22	Neutralization potential	TITRATION	-1000	1000
1970	22	Net neutralization potential	CALCULATION	-2000	2000
1971	22	Neutraliz. pot. acidity ratio	CALCULATION	-10.0	1000.0
3731	22	Fizz test		1	10000



# Laboratoires Chemex Ltee.

Essayeurs \* Geochimistes \* Chimistes Analytique

175 Boul. Industriel C.P. 284, Rouyn  
Quebec, Canada J9X 5C3  
PHONE: 819-797-1922 FAX: 819-797-0106

To: CENTRE DE TECHNOLOGIE NORANDA

240 BOUL. HYMUS  
POINTE-CLAIRE, PQ  
H9R 1G5

Project :  
Comments: ATTN: MICHAEL LI

Page Number : 1  
Total Pages : 1  
Certificate Date: 02-JUN-97  
Invoice No. : I9723767  
P.O. Number :  
Account : MHM

## CERTIFICATE OF ANALYSIS A9723767

SAMPLE	PREP CODE	PASTE pH	S % * Sulfate	S % *** Sulfide	S % Total	CO2 % inorg	Max Pot Acid **	Neutral Poten**	Net Neu Poten**	Ratio NP/MPA	Fizz Test
971888	268 --	8.8	0.01	0.18	0.21	0.4	7	46	39	6.57	2
971889	268 --	8.5	0.02	0.70	0.76	2.4	24	45	21	1.88	2
971890	268 --	8.3	0.02	1.28	1.32	0.9	41	34	-7	0.83	2
971891	268 --	8.5	0.02	1.04	1.08	0.9	34	33	-1	0.97	2
971892	268 --	8.4	0.02	0.97	1.04	0.7	33	22	-11	0.67	2
971893	268 --	8.3	0.02	1.83	1.86	0.6	58	32	-26	0.55	2
971894	268 --	8.6	0.01	0.82	0.87	0.5	27	26	-1	0.96	2
971895	268 --	8.5	0.02	1.50	1.57	0.8	49	46	-3	0.94	2
971896	268 --	8.4	0.02	1.23	1.27	0.8	40	30	-10	0.75	2
971897	268 --	8.7	0.02	1.25	1.33	0.9	42	44	2	1.05	2
971898 LV-W-1A	268 --	6.7	0.32	16.40	17.50	7.1	547	83	-464	0.15	2
971899 LV-W-1B	268 --	6.9	0.22	16.45	17.50	9.0	547	33	-514	0.06	1
971900 LV-W-1B	268 --	5.4	0.25	16.49	17.40	2.8	544	28	-516	0.05	1
971901 LV-W-2A	268 --	5.5	0.27	17.42	18.40	1.6	575	22	-553	0.04	1
971902 LV-W-2B	268 --	2.7	1.15	15.23	16.80	0.6	525	-13	-538	-0.02	1
971903 LV-W-3A	268 --	2.7	1.07	14.75	16.40	0.7	513	-16	-529	-0.03	1
971904 LV-W-3B	268 --	2.8	0.90	13.84	15.30	1.2	478	-8	-486	-0.02	1
971905 LV-W-3B	268 --	3.9	0.55	14.37	15.30	1.4	478	4	-474	0.01	1
971906 LV-W-4A	268 --	6.0	0.21	1.00	2.13	< 0.2	67	12	-55	0.18	1
971907 LV-W-4B	268 --	6.1	0.28	0.90	2.17	< 0.2	68	4	-64	0.06	1
971908	268 --	8.7	0.23	0.88	2.35	< 0.2	73	7	-66	0.10	1
971909	268 --	8.6	0.34	0.75	2.29	< 0.2	72	7	-65	0.10	1

NOTE: \* HYDROCHLORIC ACID SOLUBLE SULFATE  
NOTE: \*\* UNITS = KILOGRAMS CaCO3 EQUIVALENT PER METRIC TONNE (Kg/MT)  
NOTE: \*\*\* NITRIC ACID SOLUBLE SULFIDE

CERTIFICATION:

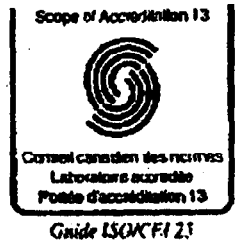
*Said / Lina*

**APPENDIX IV-5 POST-HUMIDITY CELL WHOLE-ROCK GEOCHEMISTRY**

- 1 - NTC Results
- 2 - CRM Results

Lab #	I.D.	Description	S1	As	U1	S2	Cu	U2	S3	Pb	U3	S4	S	U4	S5	Zn	U5	S6	SO4	U6	S7	S°	U7		
8879	972427	Solide		726,87	ug/g		1226,34	ug/g		415,01	ug/g		163298,5	ug/g		3200,91	ug/g		19400	ug/g				7900	ug/g
																			19400	ug/g					
8880	972428	Solide		971,33	ug/g		788,83	ug/g		423,48	ug/g		165878,2	ug/g		5814,48	ug/g		14500	ug/g				3200	ug/g
8881	972429	Solide		705,13	ug/g		778,16	ug/g		237,65	ug/g		135598,2	ug/g		1538,02	ug/g		76000	ug/g				4700	ug/g
8882	972430	Solide		330,91	ug/g		943,98	ug/g		41,75	ug/g		123740,4	ug/g		1231,78	ug/g		23900	ug/g				5900	ug/g

DATE: 97/08/29



A:  
Monsieur Michael G. Li  
Noranda Technology Centre  
240 Hymus Boulevard  
Pointe Claire  
Québec, Canada  
H9R 1G5

Télécopieur : 514-630-9393

Numéro de dossier: 6044  
Numéro de projet : P.O. No 971580  
Numéro de demande: 97 08 13 006

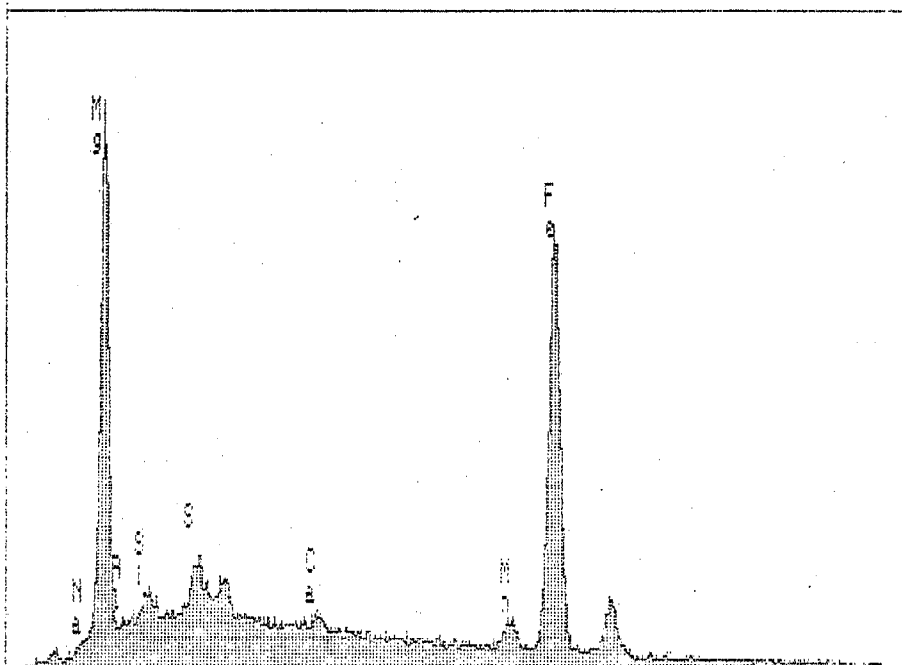
Centre de recherches minérales  
Service du Laboratoire d'analyse  
2700, rue Einstein  
SAINTE-FOY, (Québec), G1P 3W8  
Téléphone : (418) 643-4504  
Télécopieur: (418) 643-6706

	DESIGN: LV-1A	LV-2A	LV-3A	LV-4A
	NO.LAB: 97 006858	97 006859	97 006860	97 006861
* A01 SiO2	25,9 %	37,5 %	39,0 %	38,8 %
* Al2O3	6,37 %	7,86 %	7,56 %	9,26 %
* Fe2O3t	32,8 %	30,1 %	26,7 %	29,6 %
* HgO	5,17 %	3,24 %	2,31 %	3,22 %
* CaO	3,77 %	0,78 %	0,59 %	0,35 %
* Na2O	0,34 %	0,62 %	0,42 %	0,36 %
* K2O	0,53 %	0,65 %	0,75 %	0,76 %
* TiO2	0,35 %	0,41 %	0,48 %	0,50 %
* MnO	0,47 %	0,15 %	0,12 %	0,08 %
* P2O5	0,12 %	0,15 %	0,13 %	0,17 %
* PAF	19,7 %	16,1 %	19,8 %	15,3 %
* B41 S tot	15,5 %	15,7 %	12,7 %	12,1 %
* B45 C tot	2,30 %	0,70 %	0,32 %	0,38 %
* P03 Pulv.F	*	*	*	*
* P05 Pul.BW	*	*	*	*
* REMARQUE 97 006858				
* à 97 006875 Ce certificat (971008) remplace et annule celui émis précédemment.				
* * * * *				

#### **APPENDIX IV-6    POST-HUMIDITY CELL MINERALOGY**

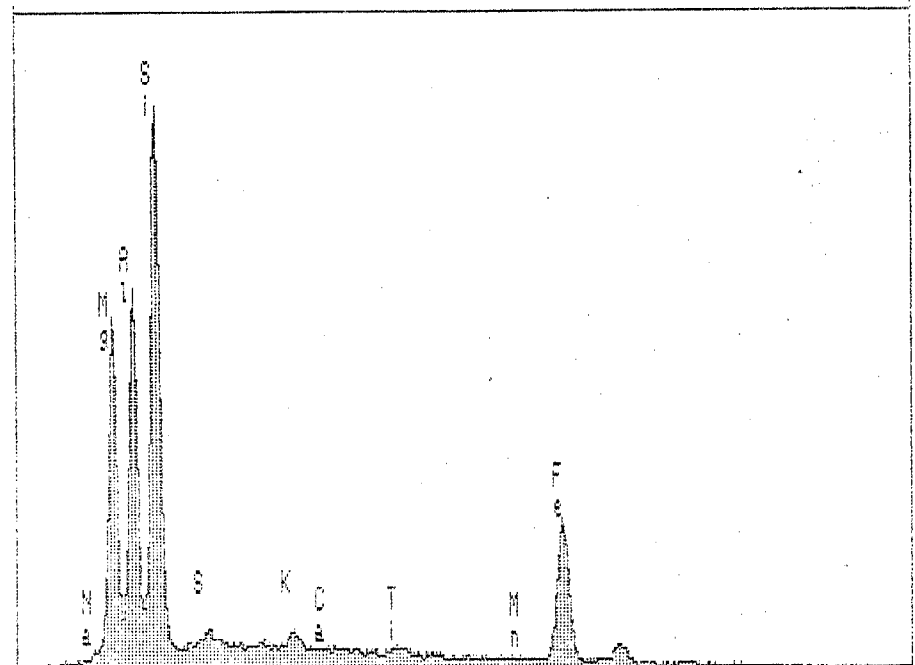
(See the WordPerfect Version 6.1 file "Post-min.wpd" for description of methodology and point-counting results. See the QuattroPro Version 6.0 file "Post-min.wb2" for normative mineralogy calculations. Both files are included on Diskette 2 attached to this report. Hard copies of electron dispersive x-ray spectra (EDS spectra) are attached as follows.)

X-RAY  
 LIVE: 100s Preset: 100s Remaining: 0s  
 DEB: 11% 12% Dead

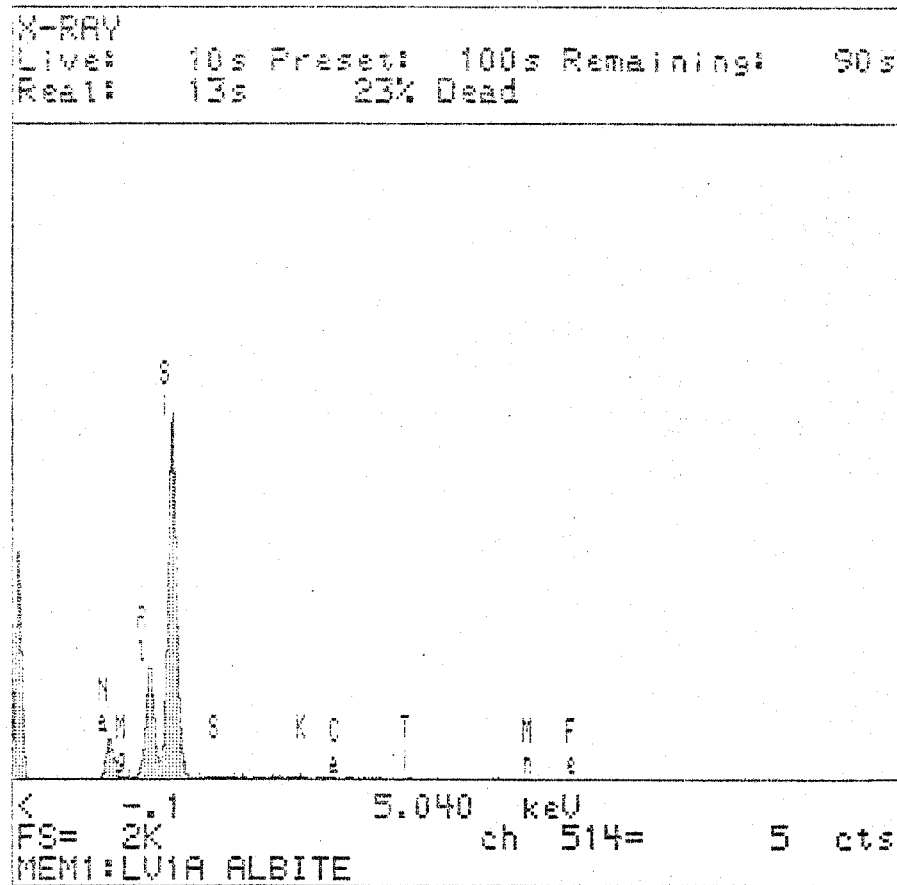
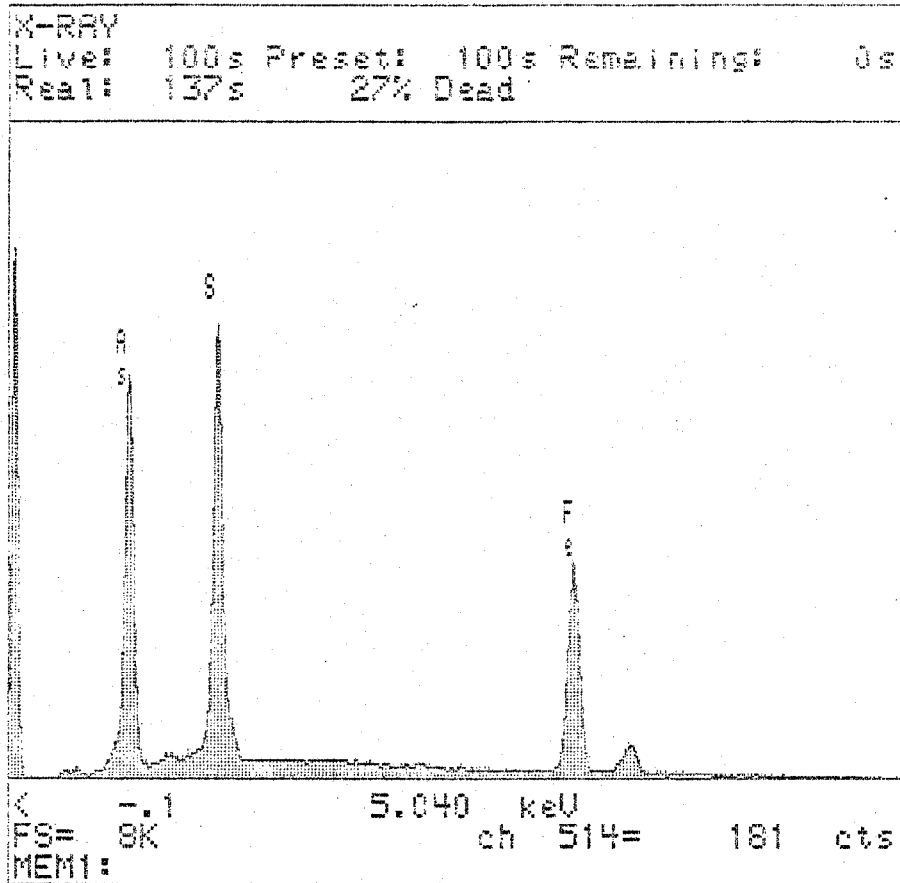


< .2 5.280 keV  
 FS= 2K ch 538= 84 cts  
 MEM1:LV1A MAGNESIAN SIDERITE

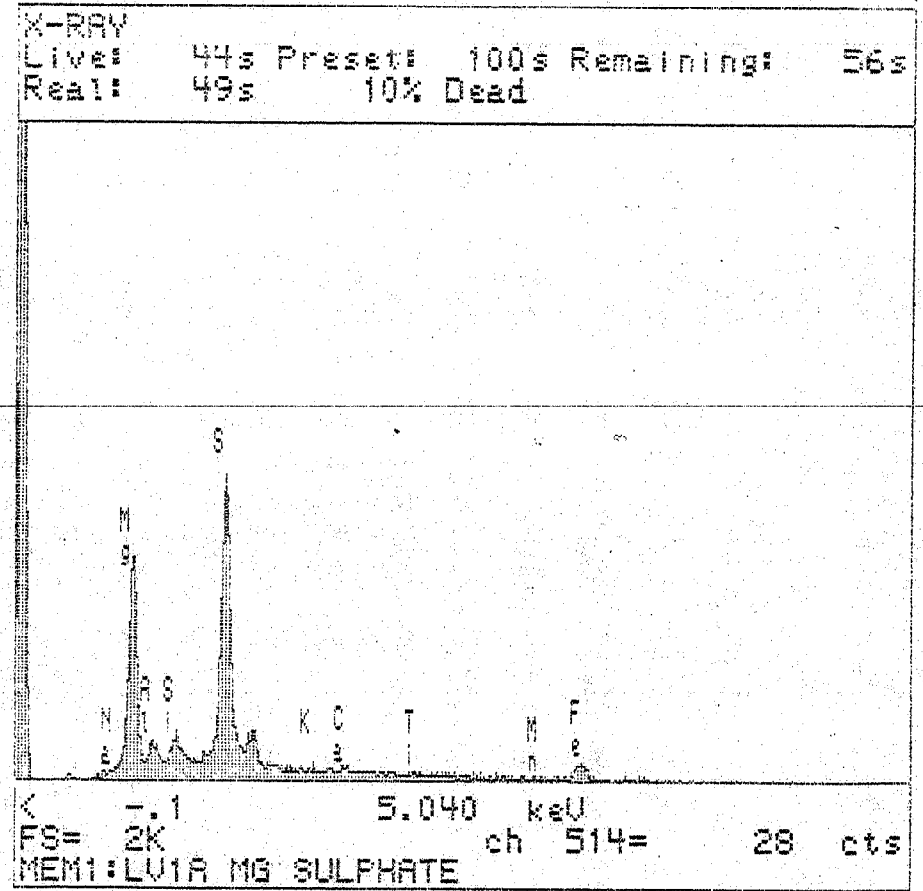
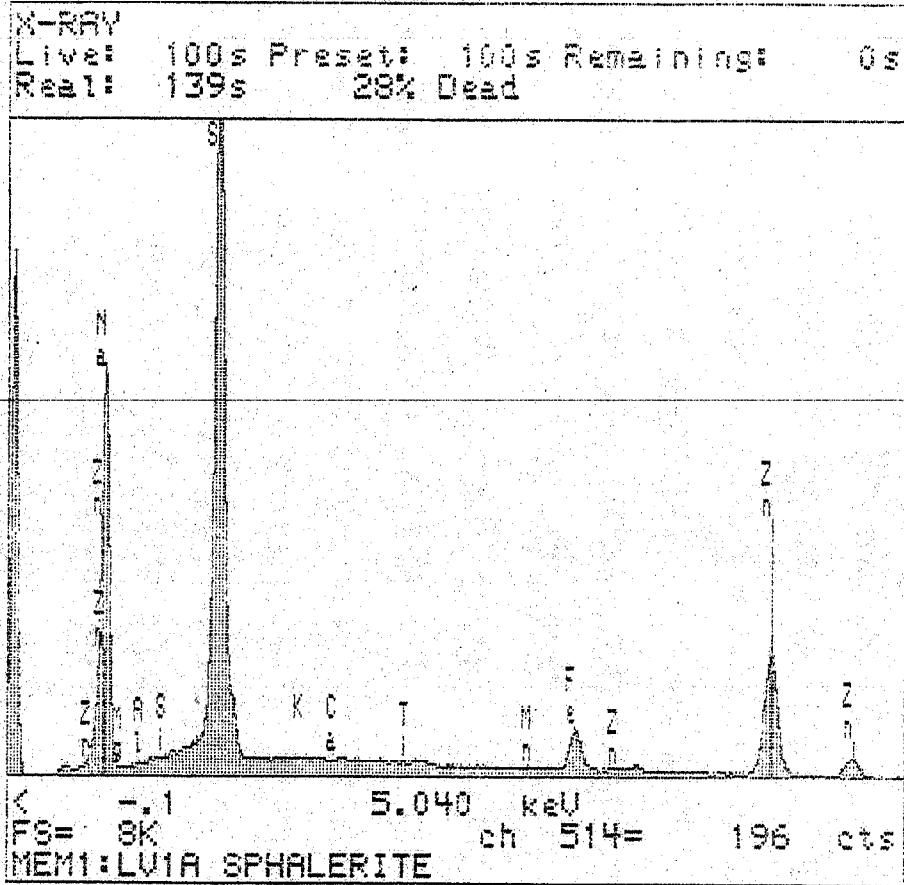
X-RAY  
 LIVE: 100s Preset: 100s Remaining: 0s  
 DEB: 120s 17% Dead



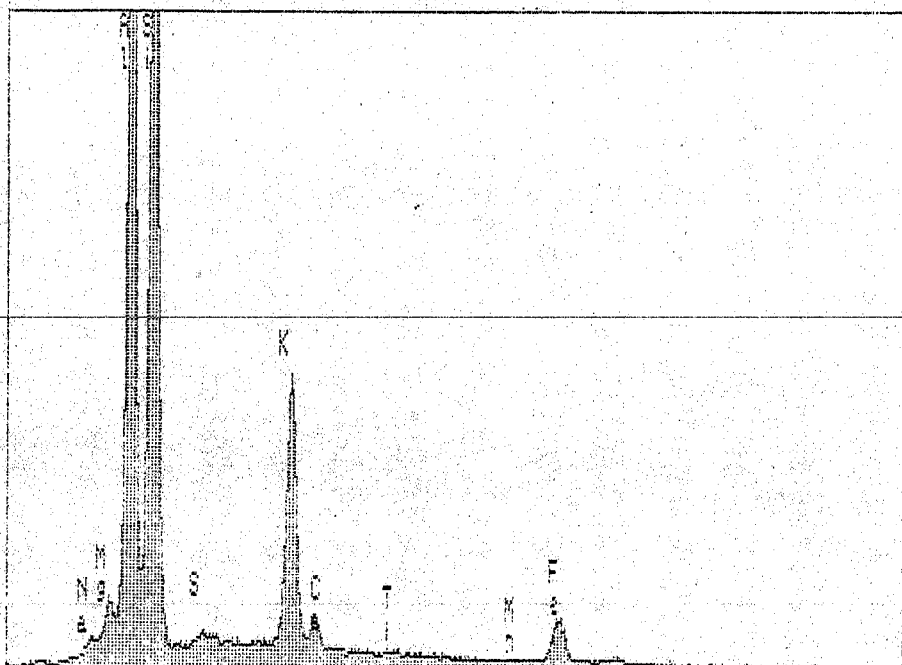
< .2 5.280 keV  
 FS= 4K ch 538= 97 cts  
 MEM1:LV1A MG-CHLORITE





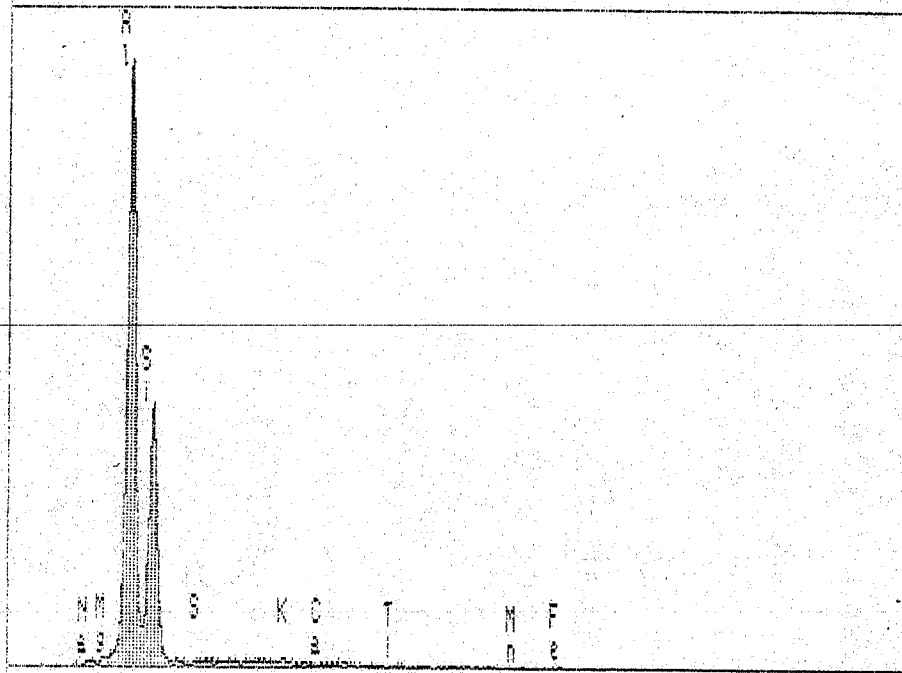


X-RAY  
 Live: 100s Preset: 100s Remaining: 0s  
 Repl: 126s 21% Dead



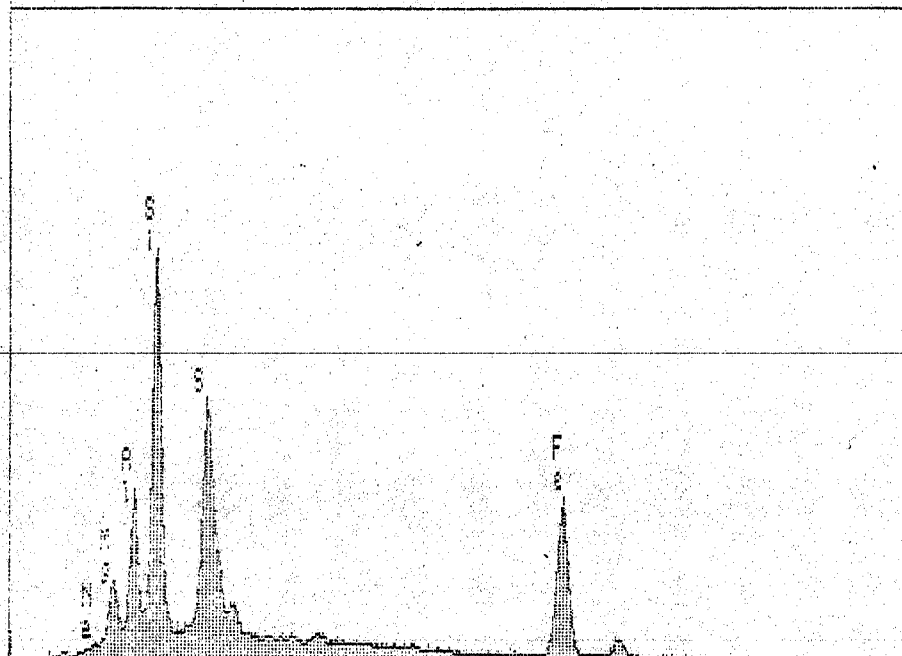
< .1 5.220 keV  
 FS= 4K ch 532= 88 cts  
 MEM1:LV1A MUSCOVITE

X-RAY  
 Live: 17s Preset: 100s Remaining: 83s  
 Repl: 21s 19% Dead



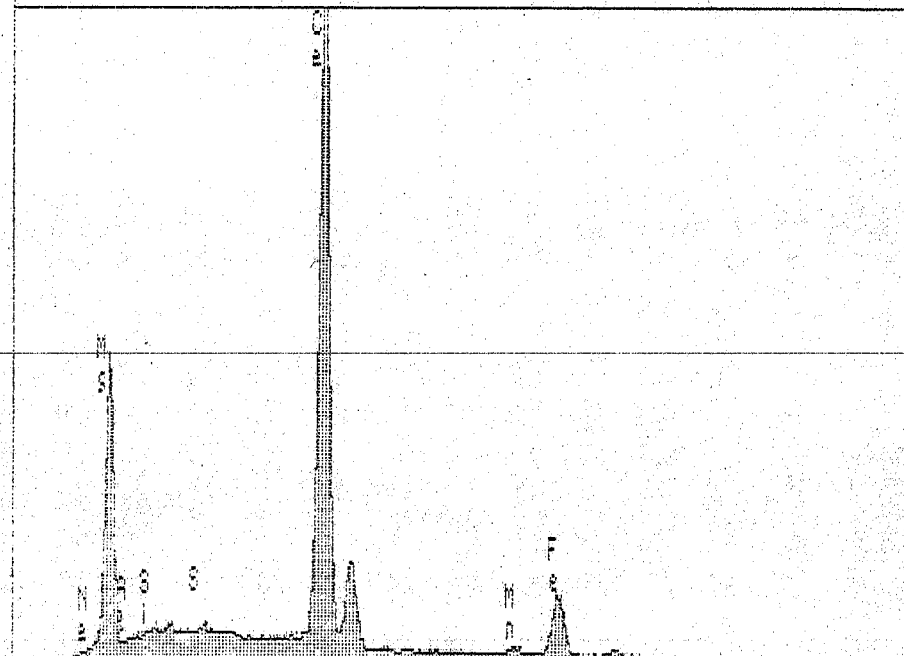
< .1 5.220 keV  
 FS= 2K ch 532= 18 cts  
 MEM1:LV1A ANDALUSITE

X-RAY  
Live: 100s Preset: 100s Remaining: 0s  
Real: 120s 17% Dead



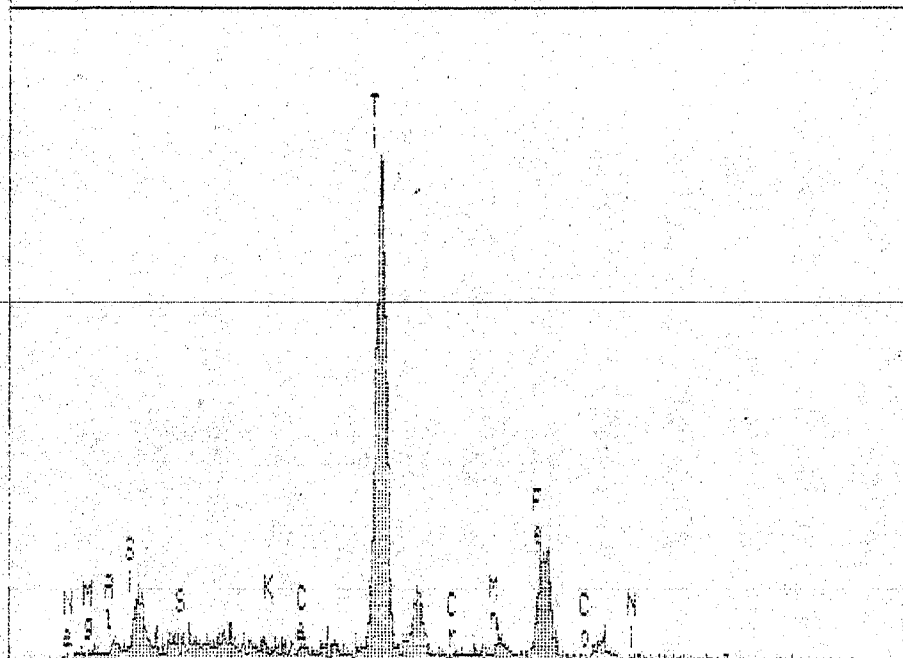
< .1 5.200 keV  
FS= 4K ch 530= 100 cts  
MEM1:LUW-1A

X-RAY  
Live: 100s Preset: 100s Remaining: 0s  
Real: 119s 16% Dead



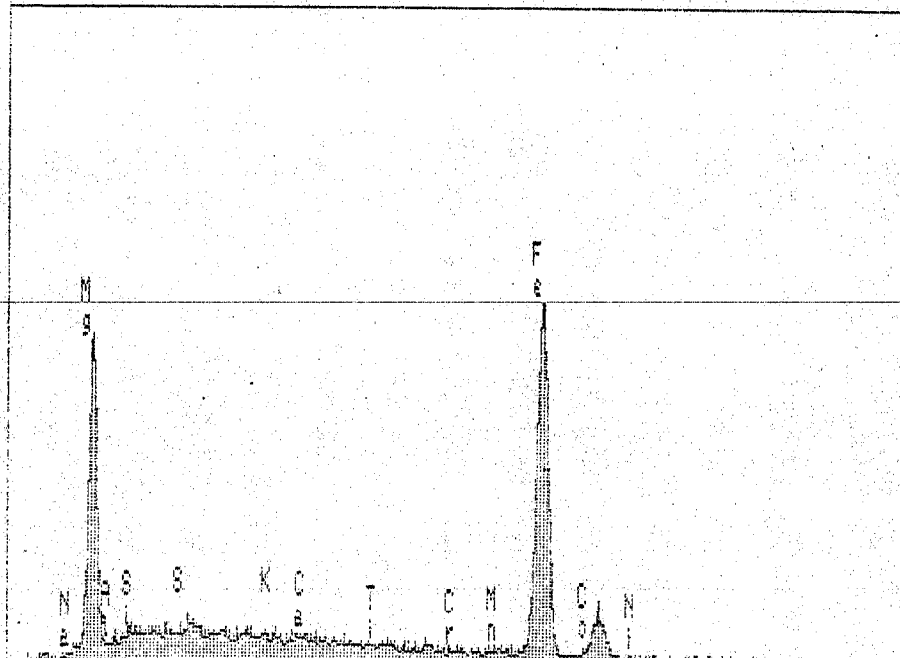
< .2 5.280 keV  
FS= 4K ch 538= 90 cts  
MEM1:LU1A ANKERITIC DOLOMITE

X-RAY  
Live: 11s Preset: 100s Remaining: 89s  
Real: 12s 8% Dead



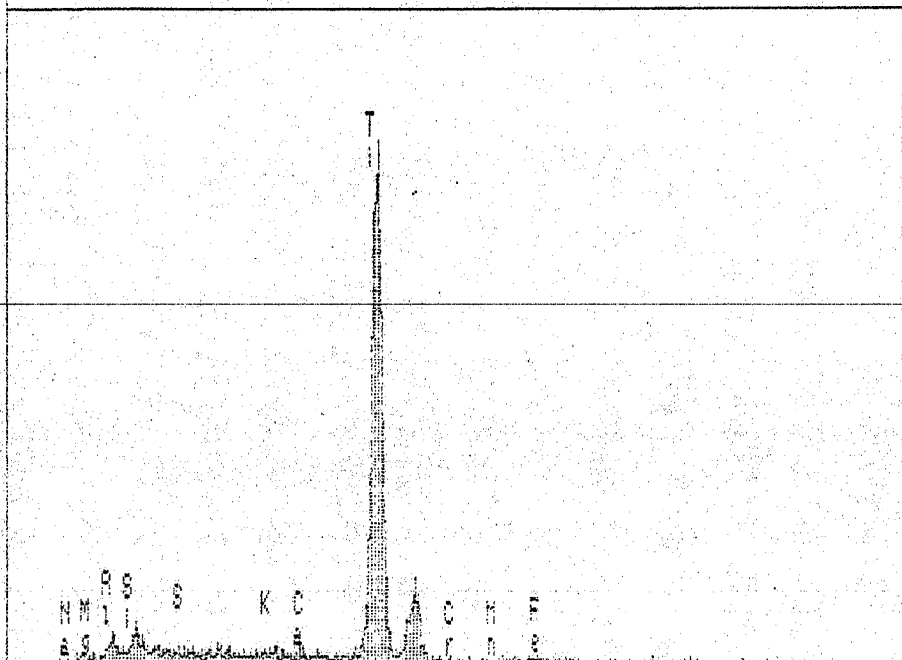
< .3 5.410 keU  
FS=255 ch 551= 5 cts  
MEM1:LU2A ILMENITE

X-RAY  
Live: 100s Preset: 100s Remaining: 0s  
Real: 106s 8% Dead



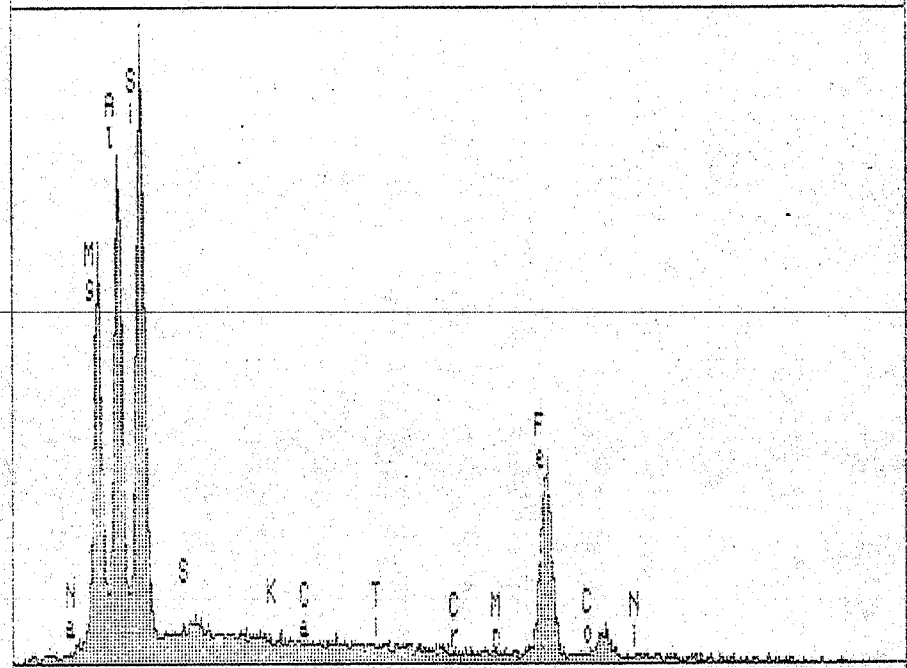
< .3 5.410 keU  
FS= 1K ch 551= 27 cts  
MEM1:LU2A MG-SIDERITE

X-RAY  
 Live: 16s Preset: 100s Remaining: 84s  
 Real: 19s 11% Dead

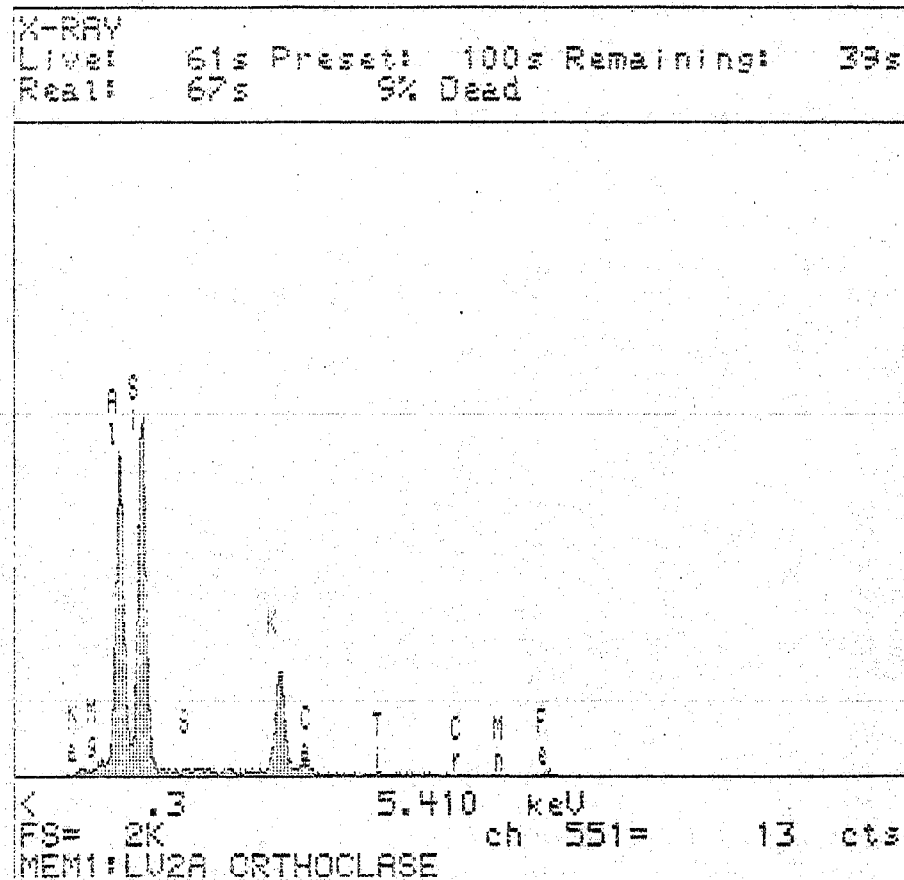
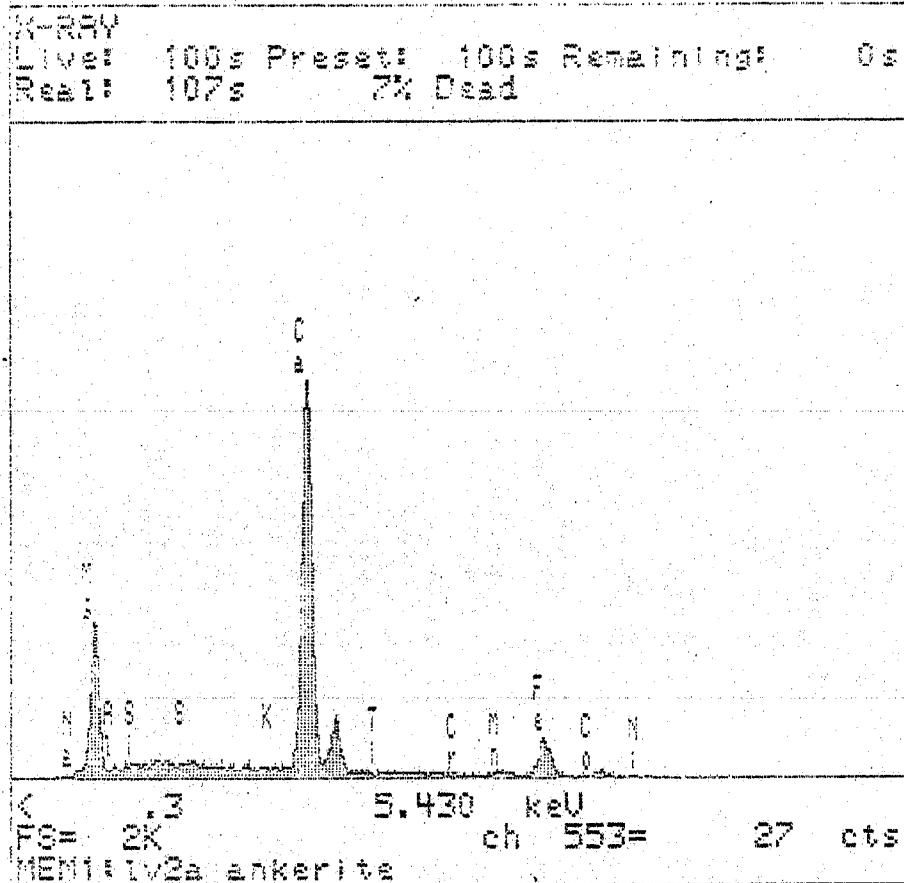


< .3 5.410 keU  
 FS=511 ch 551= 4 cts  
 MEM1:LU2R RUTILE

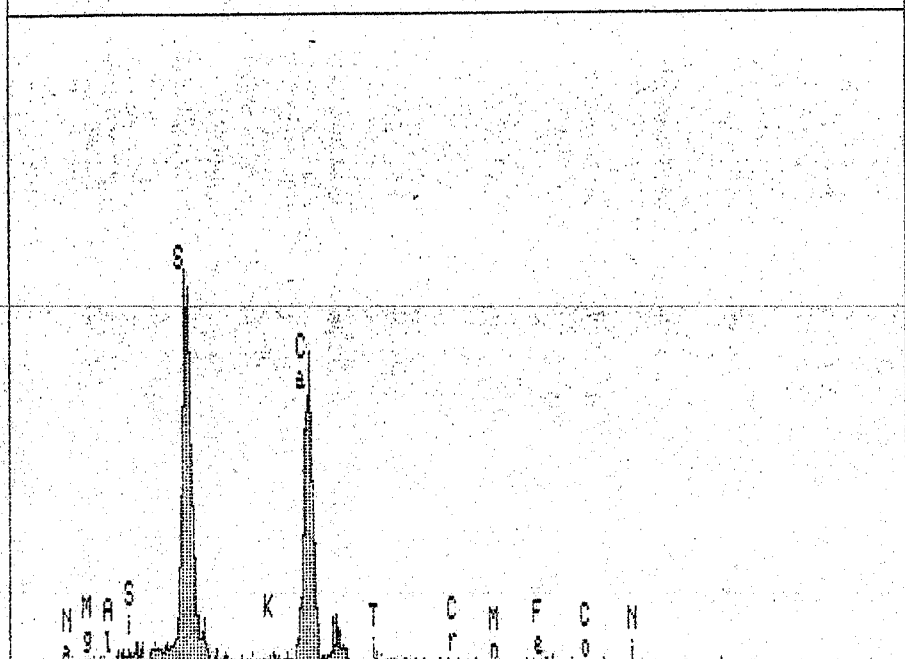
X-RAY  
 Live: 100s Preset: 100s Remaining: 0s  
 Real: 108s 7% Dead



< .3 5.410 keU  
 FS= 1K ch 551= 16 cts  
 MEM1:LU2R CHLORITE

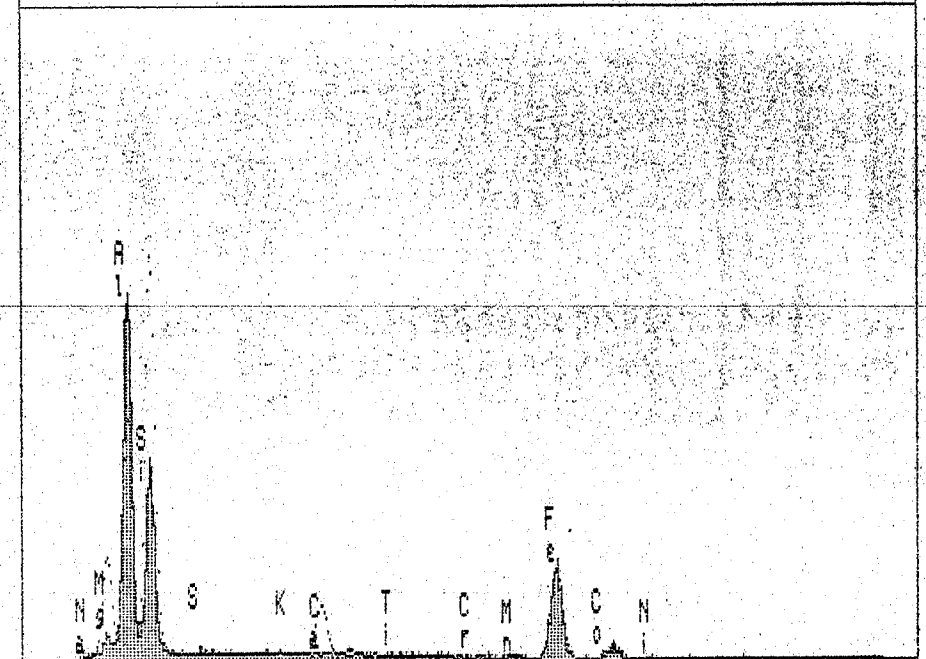


X-RAY  
Live: 6s Preset: 100s Remaining: 94s  
Real: 7s 14% Dead

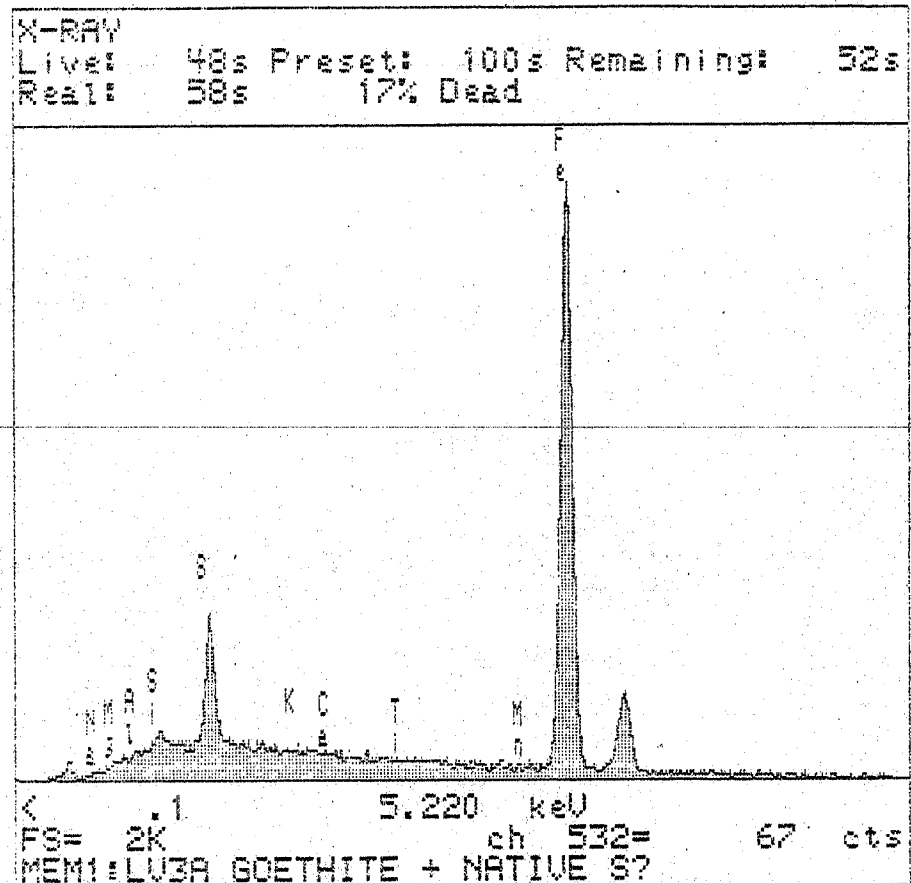
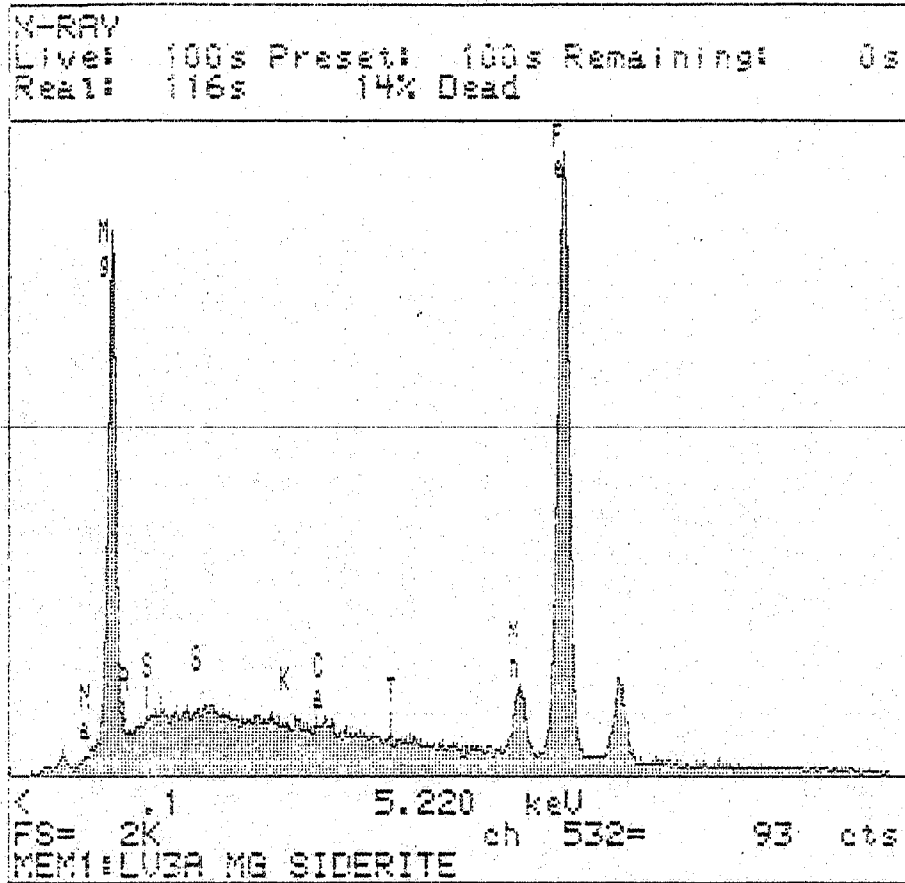


< .3 5.430 keV 3 cts  
FS=255 ch 553=  
MEM1:lv2a gypsum

X-RAY  
Live: 37s Preset: 100s Remaining: 63s  
Real: 40s 8% Dead

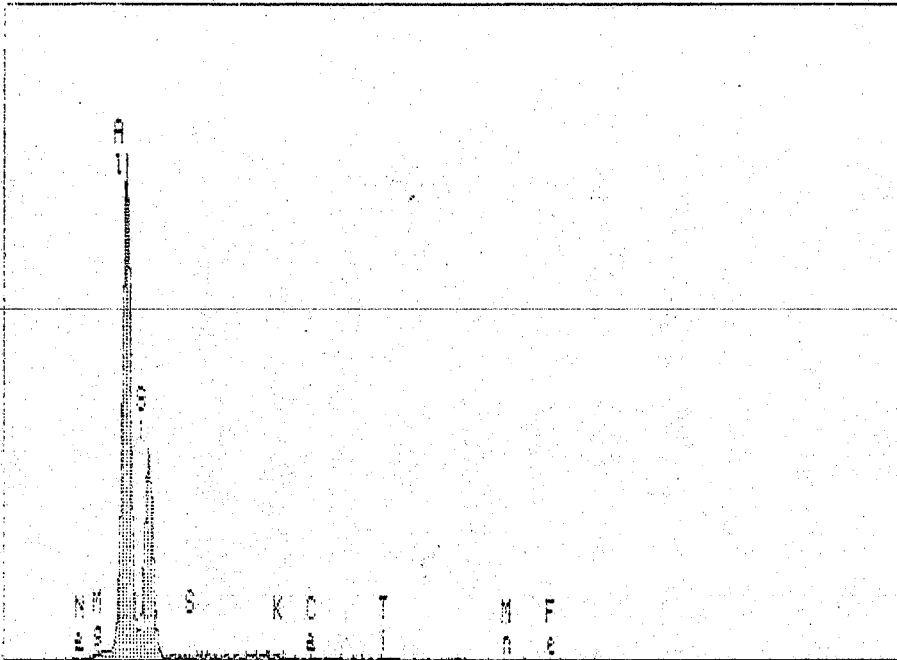


< .3 5.410 keV 13 cts  
FS= 1K ch 551=  
MEM1:LU2A CHLORITOID? /MEM2



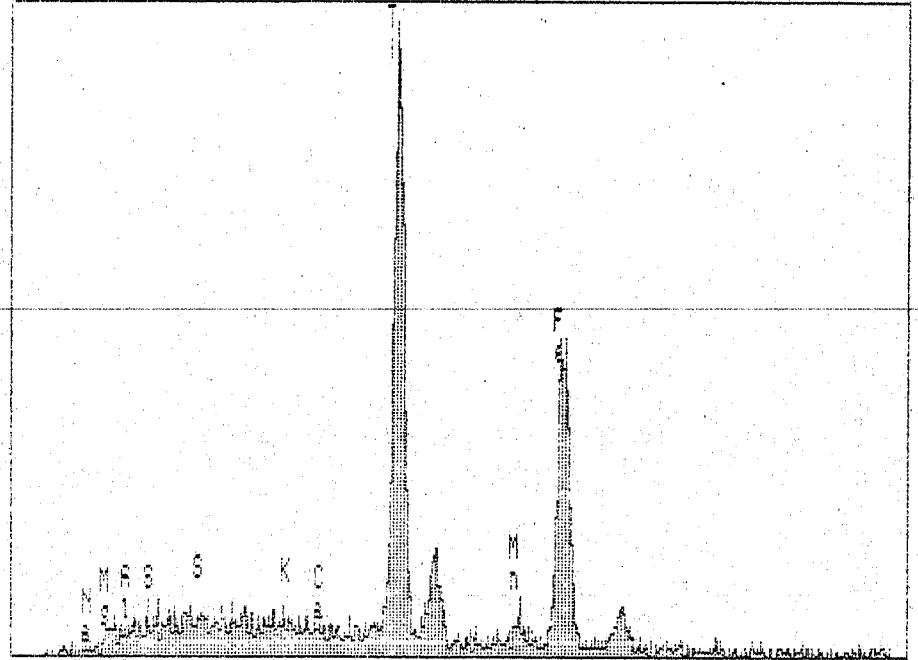


X-RAY  
 Live: 15s Preset: 100s Remaining: 85s  
 Real: 18% 17% Dead



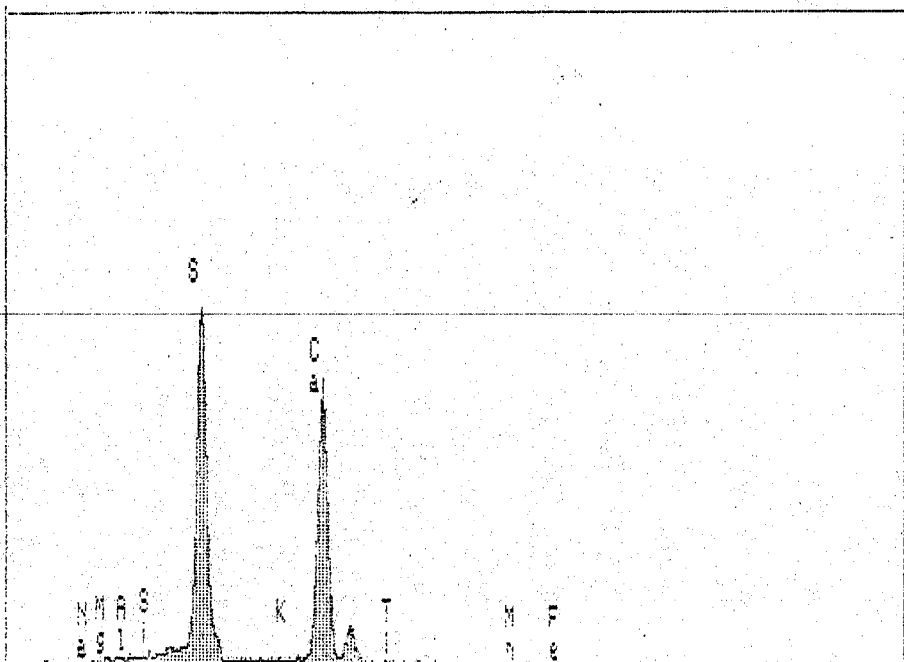
< .1 5.220 keV  
 F9= 2K ch 532= 12 cts  
 MEM1: LU3A ANDALUSITE

X-RAY  
 Live: 4s Preset: 100s Remaining: 96s  
 Real: 5% 20% Dead



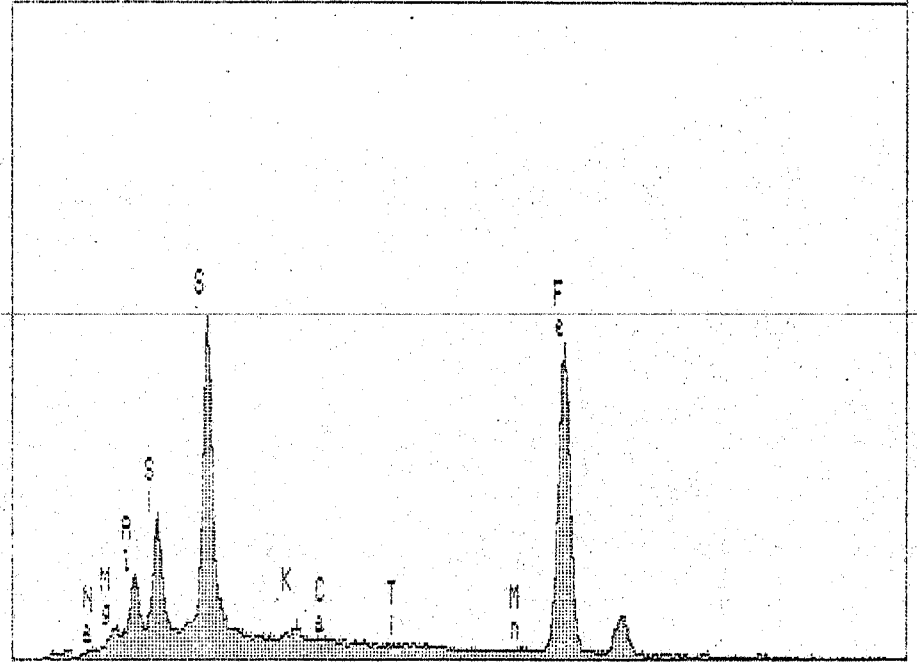
< .1 5.220 keV  
 F9=255 ch 532= 7 cts  
 MEM1: LU3A ILMENITE

X-RAY  
 LIVE: 16s Preset: 100s Remaining: 84s  
 REPT: 21s 24% Dead



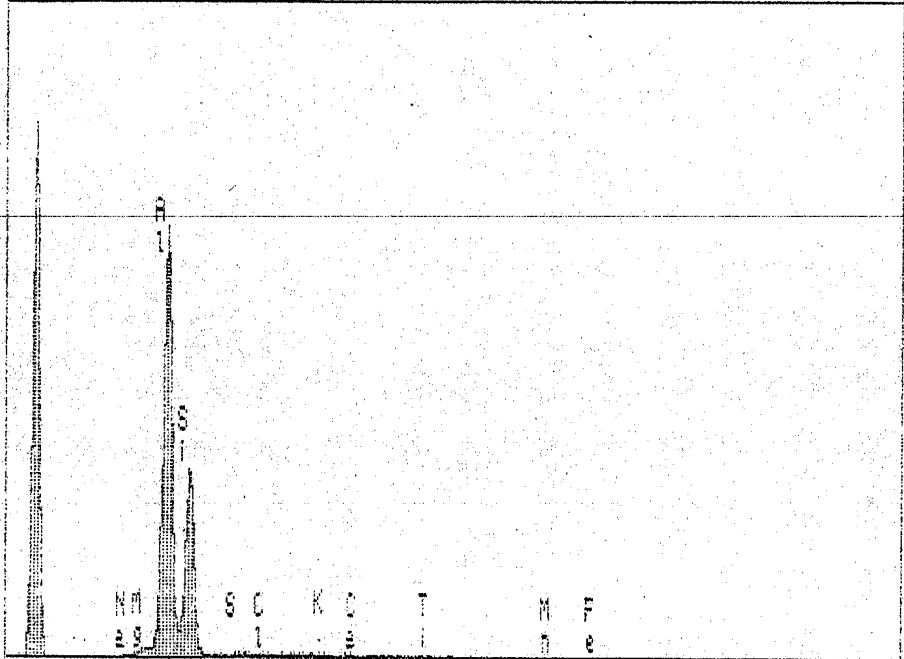
< .1 5.220 keV  
 FS= 2K ch 532= 11 cts  
 MEM1:LU3A GYPSUM

X-RAY  
 LIVE: 27s Preset: 100s Remaining: 13s  
 REPT: 105s 17% Dead



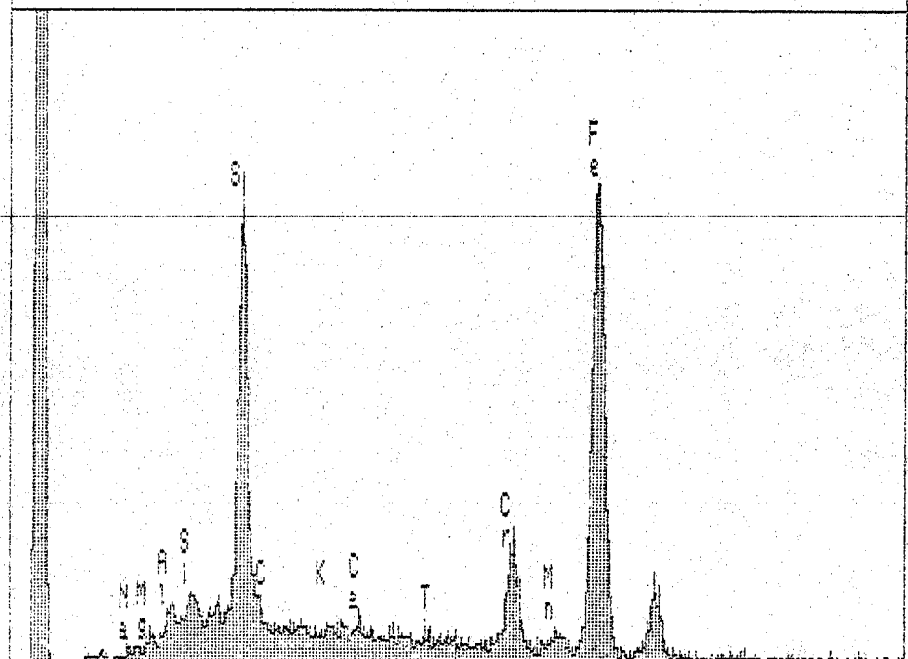
< .1 5.220 keV  
 FS= 4K ch 532= 99 cts  
 MEM1:LU3A FE-SULFATE + ILLITE?

X-RAY  
 Live: 24s Preset: 100s Remaining: 76s  
 Real: 27s 11% Dead

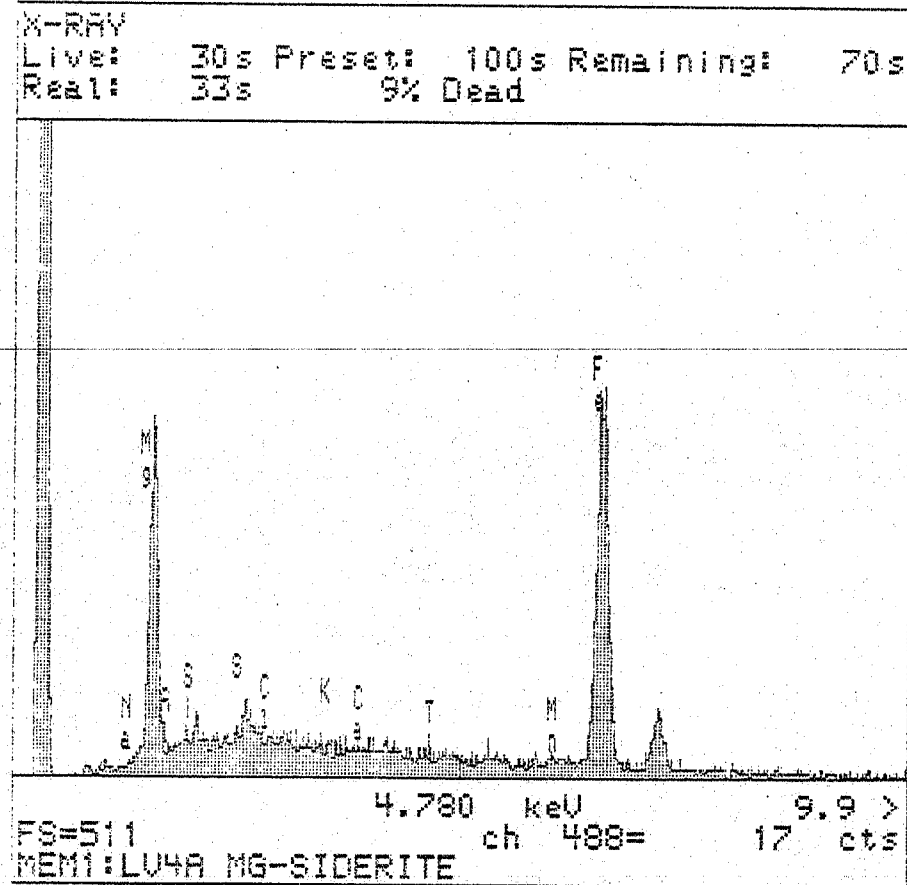
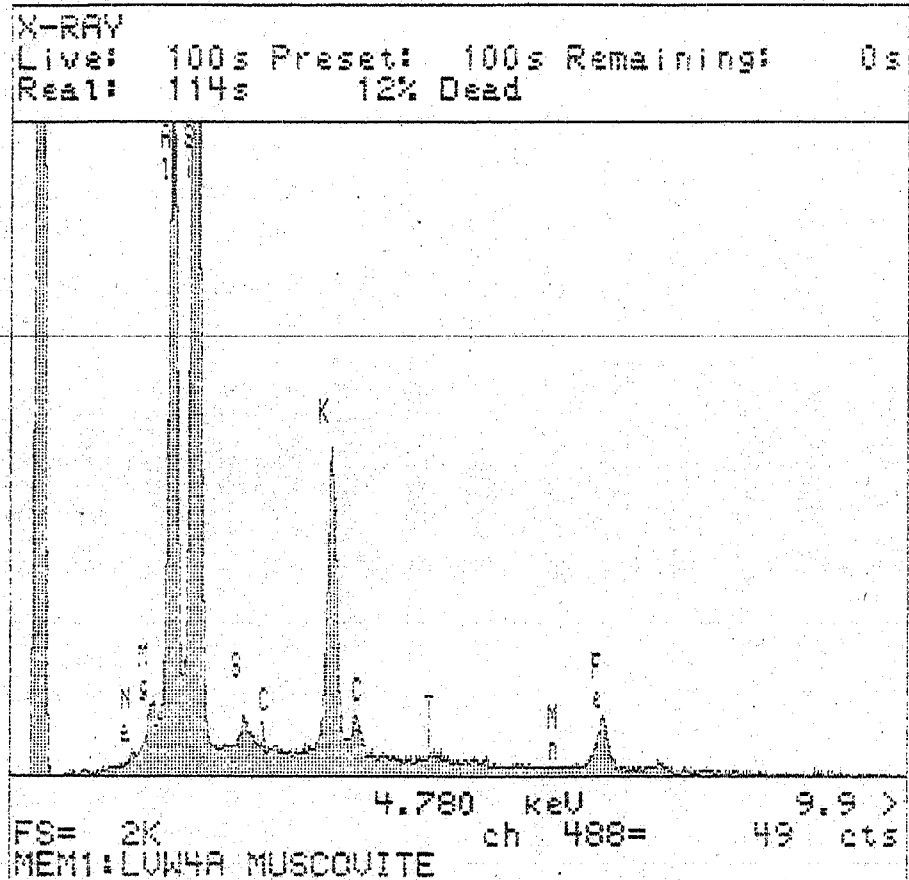


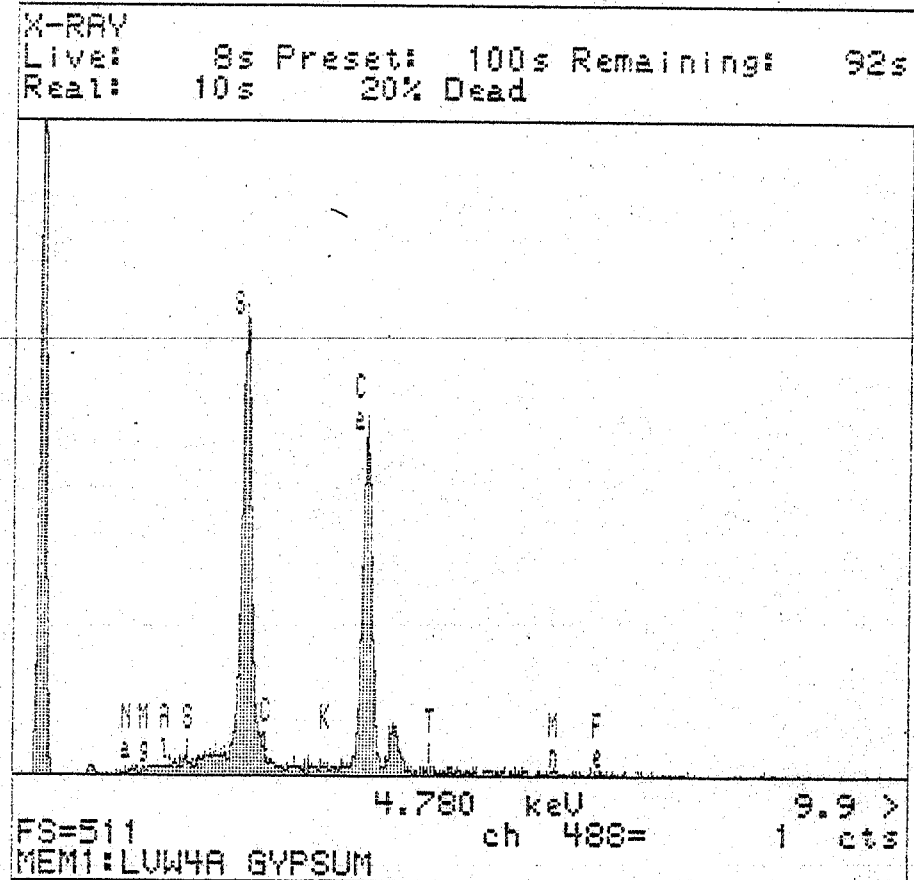
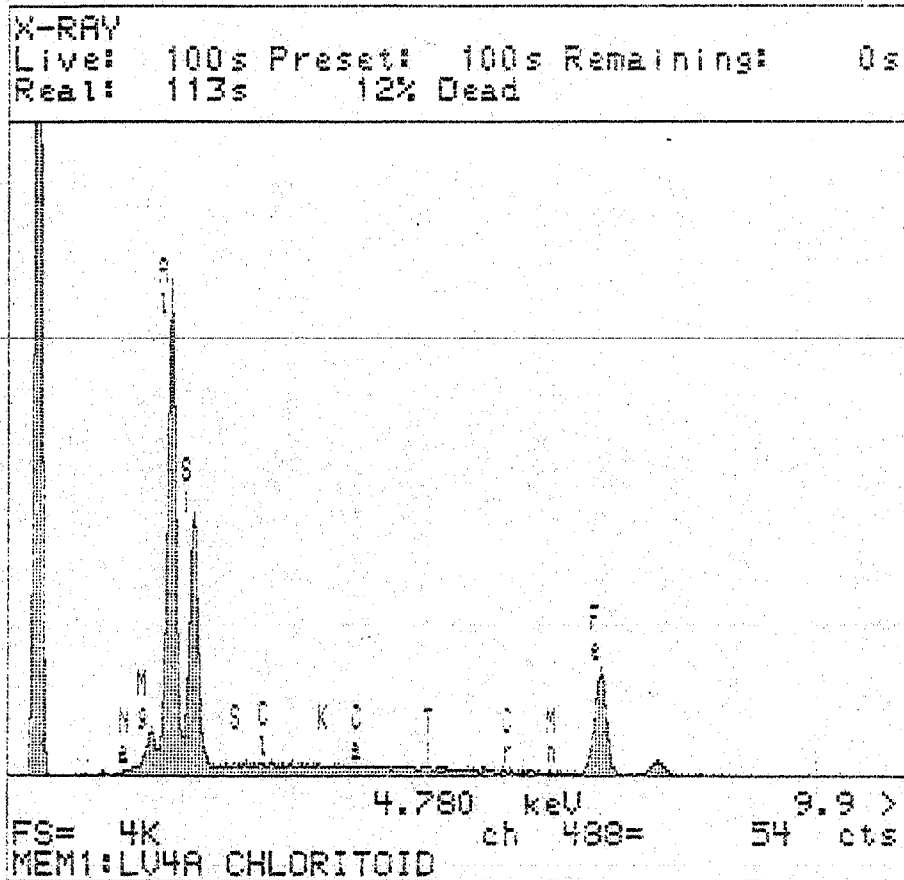
FS= 2K 4.780 keV 9.9 >  
 MEM1:LV4A ANDALUSITE ch 488= 12 cts

X-RAY  
 Live: 29s Preset: 100s Remaining: 71s  
 Real: 33s 12% Dead



FS=511 4.780 keV 9.9 >  
 MEM1:LV4A ??? ch 488= 31 cts





**APPENDIX IV-7      POST-HUMIDITY CELL GEOCHEMICAL MASS BALANCE  
CALCULATIONS**

(Data are presented in two QuattroPro Version 6.0 files: "Chem-bal.wb2" and "Mol-chem.wb2", both of which are included on Diskette 2 attached to this report. The former shows the calculations for chemical balance and the latter shows the calculations for molar balance.)

**APPENDIX IV-8    POST-HUMIDITY CELL MINERALOGICAL MASS BAL-  
ANCE CALCULATIONS**

(Data are presented in two QuattroPro Version 6.0 files: "Post-min.wb2" and "Norm-min.wb2", both of which are included on Diskette 2 attached to this report. The former shows the calculations for unadjusted mineralogical balance and the latter shows the calculations for adjusted mineralogical balance.)

**APPENDIX V-1      30-YEAR HISTORIC WEATHER RECORDS AT THE VAL  
D'OR METEOROLOGICAL STATION**

(See the text file "Weather.txt" included on Diskette 2 attached to this report.)